



THIRD EDITION



Includes CD-ROM

Introduction to **POLYMER VISCOELASTICITY**

MONTGOMERY T. SHAW

WILLIAM J. MACKNIGHT

Introduction to Polymer Viscoelasticity

Introduction to Polymer Viscoelasticity

Third Edition

**Montgomery T. Shaw
William J. MacKnight**



A JOHN WILEY & SONS, INC., PUBLICATION

Copyright © 2005 by John Wiley & Sons, Inc. All rights reserved.

Published by John Wiley & Sons, Inc., Hoboken, New Jersey.
Published simultaneously in Canada.

No part of this publication may be reproduced, stored in a retrieval system, or transmitted in any form or by any means, electronic, mechanical, photocopying, recording, scanning, or otherwise, except as permitted under Section 107 or 108 of the 1976 United States Copyright Act, without either the prior written permission of the Publisher, or authorization through payment of the appropriate per-copy fee to the Copyright Clearance Center, Inc., 222 Rosewood Drive, Danvers, MA 01923, (978) 750-8400, fax (978) 750-4470, or on the web at www.copyright.com. Requests to the Publisher for permission should be addressed to the Permissions Department, John Wiley & Sons, Inc., 111 River Street, Hoboken, NJ 07030, (201) 748-6011, fax (201) 748-6008, or online at <http://www.wiley.com/go/permission>.

Limit of Liability/Disclaimer of Warranty: While the publisher and author have used their best efforts in preparing this book, they make no representations or warranties with respect to the accuracy or completeness of the contents of this book and specifically disclaim any implied warranties of merchantability or fitness for a particular purpose. No warranty may be created or extended by sales representatives or written sales materials. The advice and strategies contained herein may not be suitable for your situation. You should consult with a professional where appropriate. Neither the publisher nor author shall be liable for any loss of profit or any other commercial damages, including but not limited to special, incidental, consequential, or other damages.

For general information on our other products and services or for technical support, please contact our Customer Care Department within the United States at (800) 762-2974, outside the United States at (317) 572-3993 or fax (317) 572-4002.

Wiley also publishes its books in a variety of electronic formats. Some content that appears in print may not be available in electronic format. For information about Wiley products, visit our web site at www.wiley.com.

Library of Congress Cataloging-in-Publication Data is available.

ISBN 13: 978-0-471-74045-2

ISBN 10: 0-471-74045-4

Printed in the United States of America

10 9 8 7 6 5 4 3 2 1

*To A. V. Tobolsky, who first introduced us to the mysteries
of polymer viscoelasticity and to the art of scientific
research.*

Preface to the Third Edition

More than 20 years have passed since the publication of the 2nd Edition of “Introduction to Polymer Viscoelasticity.” Although many of the fundamental aspects of the field remain unchanged, there have been a number of significant developments. Many have to do with instrumentation and the revolution in data collection and analysis, which in no small part has been due to the advent of the personal computer and the associated progression of instrumentation of all types.

In recognition of these changes, we have included descriptions of newer techniques for studying molecular motion along with updated descriptions of the classical experimental methods. An example of the latter is a new appendix that describes in more detail the advantages and disadvantages of the various geometries commonly used for measuring mechanical response. Included are tables with the working equations for these geometries. Those familiar with the earlier editions will also notice an increased emphasis on shear properties, which is an understandable response to the wide availability of instruments that can measure viscoelastic properties in simple shear. We have also, where possible, changed nomenclature to follow the recommendations of the Society of Rheology, and updated all the figures to increase readability and consistency.

Inexpensive computation hardware along with accessible software has impacted not only the acquisition of viscoelastic data, but also its interpretation. In the spirit of these changes, the 3rd Edition features many examples and problems that involve numerical modeling and analysis. To relieve the student

of the drudgery of data entry, a CD with data files for most numerical problems has been included.

The authors' experience has shown that by far the most effective way to master the material in the text is to work as many problems as possible, hence the increased emphasis on this aspect in the 3rd Edition. The problems range from relatively straightforward use of an equation included in the book, to far more challenging problems requiring detailed analysis and/or numerical methods. Some of these would even be suitable for term projects. Problems requiring the use of the computer are clearly marked, as are open-ended problems that have no one "correct" answer. This type of problem, which is required in many undergraduate curricula, provides the student with an opportunity to search, assume, approximate and innovate. As in past editions, answers to many of the problems are provided in an appendix. These answers form an important part of the book, and contain in some cases more details concerning the subject phenomena.

New topics have been introduced such as interfacial polarization, thermally stimulated currents (TSC), impedance spectroscopy for highly conducting polymers, Nuclear Magnetic Resonance (NMR) relaxation techniques, and the physical relaxation of elastomers. Because impedance spectroscopy has not been used extensively as a tool for examining polymer motion, this short section is included more to explain the similarities and differences between this spectroscopy and the related dielectric spectroscopy. On the other hand, NMR techniques have undergone rapid development in the last few decades, not only in fields such as imaging and high resolution studies of the structures of biological macromolecules, but also as a tool for studying the relaxation behavior of polymers, particularly in identifying the molecular motions responsible for a given relaxation process. While the new section describing NMR techniques is necessarily introductory, we have attempted to compare its capabilities with dielectric and mechanical spectroscopy in a direct fashion.

As for other changes, we have with considerable trepidation moved the description of deformation in materials from one to three dimensions. Perhaps the main impetus for doing this was to simplify the rather complex explanation in previous editions of the relationship between tensile and shear properties. As an admitted expense, we now have double-subscripted variables in several sections. However, we have refrained from including nonlinear strain theory, which should properly be left for more advanced courses.

It is always a difficult task to select material appropriate for inclusion and exclusion in an introductory text of modest size and cost. Because of the discussion of the topics mentioned above and a somewhat expanded treatment of the phenomenology of viscoelasticity, it was felt appropriate to eliminate the chapter on chemical stress relaxation. In its place, a discussion of this topic has

been included in the chapter entitled Transitions and Relaxations in Polymers; and, of course, in several problems at the end of this chapter.

Professor Aklonis did not participate in the preparation of the 3rd Edition, but, as was the case with Professor Shen in the 2nd Edition, his influence is clearly present and it is a pleasure for us to acknowledge it.

Many individuals and organizations have been involved with the assembly of the 3rd edition. We wish to thank Ms. Jennifer Chudy and Mr. Alvin A Altamirano for help with data entry and equation editing; Dr. Mark Poliks, Dr. Lou Madsen and Prof. Marcel Utz for critically reviewing the NMR section, Mr. Antonio Senador for checking several problem solutions and Mr. Gerald Ling who provided assistance with the challenging task of finding authors of classical publications for courtesy permission to reproduce figures. We especially want to acknowledge the patience displayed by our spouses, Maripaz N. Shaw and Carol B. MacKnight, as the endured though this lengthy project.

Errors in the text are, of course, the sole responsibility of the authors. It is to be hoped that we have recognized and corrected at least some of the errors in the 2nd Edition, (many of which were pointed out to us by friends and colleagues) and have refrained from introducing a significant number of new ones in the 3rd Edition.

M. T. SHAW
W. J. MACKNIGHT

*Storrs, Connecticut
Amherst, Massachusetts
December 2004*

Preface to the Second Edition

In the decade since the first edition of *Introduction to Polymer Viscoelasticity* appeared, we have noted a number of significant scientific developments. We also suffered a personal tragedy with the death of Professor M. C. Shen.

Among the major developments are a new approach to long-range relaxational motions known as the theory of reptation, and the further elucidation of the kinetic theory of rubber elasticity. In this second edition, we have attempted to take account of some of these developments on a level consistent with the introductory nature of the text. We have also added an entirely new chapter on dielectric relaxation, a technique now widely used to investigate molecular motions in polar polymers. Finally, we have tried to strengthen and clarify several other sections as well as eliminate errors or inconsistencies in the first edition that have been pointed out to us by colleagues and students.

Both of us felt very deeply the untimely death of Professor Shen, as did many others who valued his friendship and respected his scientific prowess. He made important and lasting contributions to such diverse areas as rubber elasticity theory, the understanding of mechanical properties of block copolymers, and plasma polymerization, to name but a few. His collaboration in the preparation of the second edition was sorely missed, but we feel that his influence remains clear and we are proud to acknowledge it.

We wish to thank Dr. Richard M. Neumann, who read the manuscript critically, and Ms. Teresa M. Wilder, who drew many of the figures. We are

also indebted to Dr. Neumann and Professor L. L. Chapoy for furnishing some of the new problems contained in this edition.

Once again we accept sole responsibility for any errors in the text, be they old ones remaining from the first edition or new ones that may appear in the second.

J. J. AKLONIS
W. J. MACKNIGHT

*Los Angeles, California
Amherst, Massachusetts
December 1982*

Preface to the First Edition

The viscoelastic response of polymeric materials is a subject which has undergone extensive development over the past twenty years and still accounts for a major portion of the research effort expended. It is not difficult to understand the reason for this emphasis in view of the vast quantities of polymeric substances which find applications as engineering plastics and the still greater volume which are utilized as elastomers. The central importance of the time and temperature dependence of the mechanical properties of polymers lies in the large magnitudes of these dependencies when compared to other structural materials such as metals. Thus an understanding of viscoelastic behavior is fundamental for the proper utilization of polymers.

Viscoelasticity is a subject of great complexity fraught with conceptual difficulties. It is possible to distinguish two basic approaches to the subject which we shall designate as the continuum mechanical approach and the molecular approach. The former attempts to describe the viscoelastic behavior of a body by means of a mathematical schema which is not concerned with the molecular structure of the body, while the latter attempts to deduce bulk viscoelastic properties from molecular architecture. The continuum mechanical approach has proven to be very successful in treating a large number of problems and is of very great importance. However, it is not our intention to treat this approach rigorously in this text. Rather, we shall be concerned with the molecular approach and attempt to present a basic foundation upon which the reader can build. The fundamental difficulty encountered with the molecular approach lies in the fact that polymeric materials are large molecules

of very complex structures. These structures are too complex, even if they were known in sufficient detail which, in general, they are not, to lend themselves to mathematical analysis. It is therefore necessary to resort to simplified structural models, and the results deduced from these are limited by the validity of the models adopted.

Several excellent treatments of molecular viscoelasticity are available. (See the references of Chapter 1.) The book by Professor Ferry, in particular, is an exhaustive and complete exposition. The question may then be asked, why the necessity for still another text and one restricted to bulk amorphous polymers, at that? Such a question must send each of the authors scurrying in quest of an "apologia pro vita sua." The answer to the question lies in the use of the word "introduction" in the title. What we have attempted to do is to provide a detailed grounding in the fundamental concepts. This means, for example, that all derivations have been presented in great detail, that concepts and models have been presented with particular attention to assumptions, simplifications, and limitations, and that problems have been provided at the end of each chapter to illustrate points in the text. The level of mathematical difficulty is such that the average baccalaureate chemist should be able to readily grasp it. Where more advanced mathematical techniques are required, such as transform techniques, the necessary methods are developed in the text.

Having attempted to delineate what this book is, it may be well to remind the reader what it is not. First of all, it is not a complete treatment -lacking among other topics discussions of crystalline polymers, solution behavior, melt rheology, and ultimate properties. It is also not written from the continuum mechanics approach and thus is not mathematically sophisticated. Finally, it is not a primer of polymer science. Familiarity with the basic concepts of the field is presumed.

The authors' first acquaintance with the literature of viscoelastic behavior in polymers evoked a response much like that experienced by neophytes in the literary arts on a first reading of *Finnegan's Wake*, by James Joyce. It is immediately apparent that one is in the presence of a great work, but somehow it will be necessary to master the language before appreciation, let alone understanding, may be achieved. Recognizing the nature of the problem, Joycean scholars came to the rescue with works of analysis to provide a skeleton key to *Finnegan's Wake*. Proper utilization of this skeleton key will open the door to an understanding of that forbidding masterwork. It was thus our intent to provide a similar skeleton key to the literature of molecular viscoelasticity. How well we have succeeded must be left to the judgment of our readers.

We are grateful to the students at our respective institutions who have suffered our attempts to present the material in this text in coherent form at various stages of development. Their criticisms and suggestions have led to

significant improvements. We are also grateful to Mrs. William Jackson, who translated many rough sketches into finished drawings. It is hardly to be expected that a work of this nature could be free from errors. We have attempted to eliminate as many as possible but, of course, bear full responsibility for those remaining.

JOHN J. AKLONIS
WILLIAM J. MACKNIGHT
MITCHEL SHEN

Los Angeles, California

Contents

1. Introduction	1
Suggested Reading, 6	
2. Phenomenological Treatment of Viscoelasticity	7
A. Elastic Modulus, 7	
B. Transient Experiments, 19	
C. Dynamic Experiments, 23	
D. Boltzmann Superposition Principle, 27	
E. Relationship Between the Creep Compliance and the Stress Relaxation Modulus, 32	
F. Relationship Between Static and Dynamic Properties, 33	
Appendix 1. Connecting Creep Compliance and Stress Relaxation Modulus Using Laplace Transforms, 35	
Appendix 2. Borel's Theorem, 38	
Appendix 3. Geometries for the Measurement of Viscoelastic Functions, 38	
1. Axial Geometries, 38	
2. Rotational Geometries, 42	
Problems, 46	
References, 50	
3. Viscoelastic Models	51

A.	Mechanical Elements, 51	
1.	Maxwell Model, 53	
2.	Voigt Model, 59	
3.	Generalized Maxwell Model, 61	
4.	Voigt-Kelvin Model, 64	
B.	Distributions of Relaxation and Retardation Times, 66	
C.	Molecular Theories, 69	
D.	Application of Flexible-Chain Models to Solutions, 78	
E.	The Zimm Modification, 79	
F.	Extension to Bulk Polymer, 82	
G.	Reptation, 93	
	Appendix: Manipulation of the Rouse Matrix, 97	
	Problems, 102	
	References, 105	
4.	Time-Temperature Correspondence	107
A.	Four Regions of Viscoelastic Behavior, 107	
B.	Time-Temperature Superposition, 114	
C.	Master Curves, 117	
D.	The WLF Equation, 119	
E.	Molecular Interpretation of Viscoelastic Response, 124	
	Problems, 125	
	References, 128	
5.	Transitions and Relaxation in Polymers	129
A.	Phenomenology of the Glass Transition, 129	
B.	Theories of the Glass Transition, 132	
1.	Free-Volume Theory, 133	
2.	Thermodynamic Theory, 137	
3.	Kinetic Theories, 141	
C.	Structural Parameters Affecting the Glass Transition, 145	
D.	Relaxations in the Glassy State, 151	
E.	Relaxation Processes in Networks, 154	
1	Physical Relaxation, 154	
2.	Chemical Processes, 156	
	Problems, 159	
	References, 163	

6. Elasticity of Rubbery Networks	165
A. Thermodynamic Treatment, 166	
B. Statistical Treatment, 172	
1. Derivation, 172	
2. Energy Contribution, 183	
C. Phenomenological Treatment, 187	
D. Factors Affecting Rubber Elasticity, 190	
1. Effect of Degree of Crosslinking, 190	
2. Effect of Swelling, 192	
3. Effect of Fillers, 195	
4. Effect of Strain-Induced Crystallization, 198	
Appendix 1. Statistics of a Polymer Chain, 199	
Appendix 2. Equation of State for a Polymer Chain, 206	
Problems, 208	
References, 211	
7. Dielectric and NMR Methods	213
A. Dielectric Methods, 213	
1. Phenomenology, 214	
2. Molecular Interpretation of Dielectric Constant, 220	
3. Interfacial Polarization, 227	
4. Application to Polymers, 229	
5. Experimental Methods, 231	
6. Application of Dielectric Relaxation to Polymethyl Methacrylate, 235	
7. Comparisons Between Mechanical and Dielectric Relaxation for Polymers, 236	
B. Nuclear Magnetic Resonance Methods, 237	
Problems, 243	
References, 244	
Answers to Problems	247
List of Major Symbols	293
List of Files on CD	301
Author Index	305
Subject Index	308

1

Introduction

The subject matter of this book is the response that polymers exhibit when they are subjected to external forces of various kinds. Almost without exception, polymers belong to a class of substances known as viscoelastic bodies. As the name implies, these materials respond to external forces in a manner intermediate between the behavior of an elastic solid and a viscous liquid. To set the stage for what follows, it is necessary to describe in very general terms the types of force to which the viscoelastic bodies are subjected.

Consider first the motion of a rigid body in space. This motion can be thought of as consisting of translational and rotational components. If no forces act on the body, it will maintain its original state of motion indefinitely in accordance with Newton's first law of motion. However, if a single force or a set of forces whose vector sum is nonzero act on the body, it will experience acceleration or a change in its state of motion. Consider, however, the case where the vector sum of forces acting on the body is zero and the body experiences no change in either its translational or rotational component of motion. In such a condition, the body is said to be stressed. If the requirement of rigidity is removed, the body will in general undergo a deformation as a result of the application of these balanced forces. If this occurs, the body is said to be strained. It is the relationship between stress and strain that is our main concern. Depending on the types of stress and strain applied to a body, it is possible to use these quantities to define new quantities—material properties—that ultimately relate to the chemical and physical structure of the body. These material properties are called moduli. To understand the physical meaning of the modulus of a solid, consider the following simple experiment.

2 INTRODUCTION

Suppose we have a piece of rubber (e.g., polyisobutylene), $\frac{1}{2}$ cm $\times \frac{1}{2}$ cm $\times 4$ cm, and a piece of plastic (e.g., polystyrene) of the same dimensions. The experiment to be performed consists of suspending a weight (applying a force) of, say 1 kg, from each sample as shown in Figure 1-1.

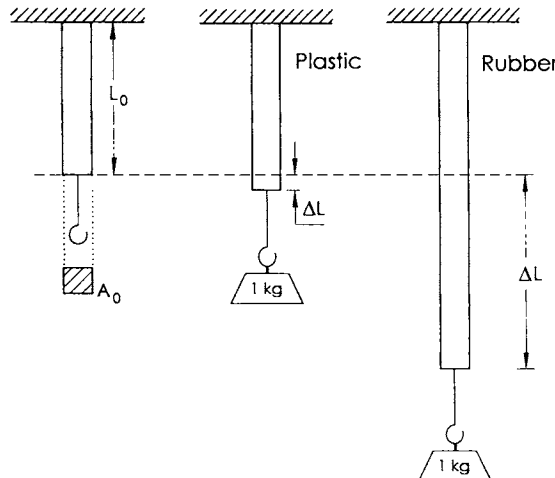


Figure 1-1. Deformation of samples made from plastic vs. rubber. As a reference, the undeformed shape for both samples is shown on the left.

As is obvious, the deformation of the rubber will be much greater than that of the plastic. Using this experiment we can define a spring constant k as the applied force F divided by the change in length ΔL

$$k = F / \Delta L \quad (1-1)$$

and use this number to compare the samples. However, to obtain a measure that is independent of the sample size, i.e., a material property, as opposed to a sample property, we must divide the applied force by the initial cross-sectional area A_0 and divide the ΔL by the initial sample length L_0 . Then the modulus M is:

$$M = \frac{F / A_0}{\Delta L / L_0} \quad (1-2)$$

Since ΔL is much larger for the rubber than for the plastic, from equation (1-2) it is clear that the modulus of the rubber is much lower than the modulus of the plastic. Thus the particular modulus defined in equation (1-2) specifies the resistance of a material to elongation at small deformations and is called the Young's modulus. It is normally given the symbol E . (See www.rheology.org for suggestions on standard nomenclature for viscoelastic quantities.)

Further experimentation, however, reveals that the situation is more complicated than is initially apparent. If, for example, one were to carry out the test on the rubber at liquid nitrogen temperature, one would find that this "rubber" undergoes a much smaller elongation than with the same force at room temperature. In fact, the extension would be so small as to be comparable to the extension exhibited by the plastic at room temperature. A more dramatic demonstration of this effect is obtained by immersing a rubber ball in liquid nitrogen for several minutes. The cold ball, when bounced, no longer has the characteristic properties of a rubbery object but, instead, is indistinguishable from a hard sphere made of plastic.

On the other hand, if the piece of plastic is heated in an oven to 130 °C and then subjected to the modulus measurement, it is found that a much larger elongation, comparable to the elongation of the rubber at room temperature, results.

These simple experiments indicate that the modulus of a polymeric material is not invariant, but is a function of temperature, that is, $M=M(T)$.

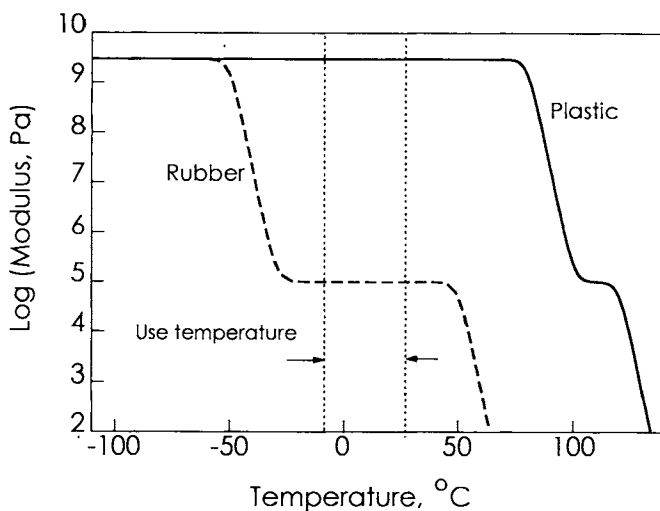


Figure 1-2. Schematic of the modulus vs. temperature behavior for a rubber and a plastic over a broad temperature range.

An investigation of the temperature dependence of the modulus of our two samples is now possible. At temperature T_1 we measure the modulus as before, then increase the temperature to T_2 , and so on. Schematic data from such an experiment are plotted in Figure 1-2. The temperature dependence of the modulus is so great that it must be plotted on a logarithmic scale. (This large variation in modulus presents experimental problems that will be treated subsequently.) The region between the vertical dashed lines represents normal-use temperatures and, consistent with the opening experiment, we find that in

4 INTRODUCTION

this range the plastic has a high modulus while the rubber has a relatively low modulus. Upon cooling, the modulus of the rubber rises markedly, by as much as four orders of magnitude, indicating that the rubber at lower temperatures behaves like a plastic. Another drastic change in modulus for the rubber is evidenced at higher temperatures; here the material is becoming softer, as indicated by further decreases in modulus. This behavior is discussed in detail in Chapter 4. The modulus-temperature behavior for the plastic is seen to be quite similar to that of the rubber except that the changes occur at higher temperatures, resulting in the high modulus observed at room temperature. At 135°C it is clear that the modulus of this material is that of a rubber, agreeing with the results of one of the earlier "experiments" in this discussion.

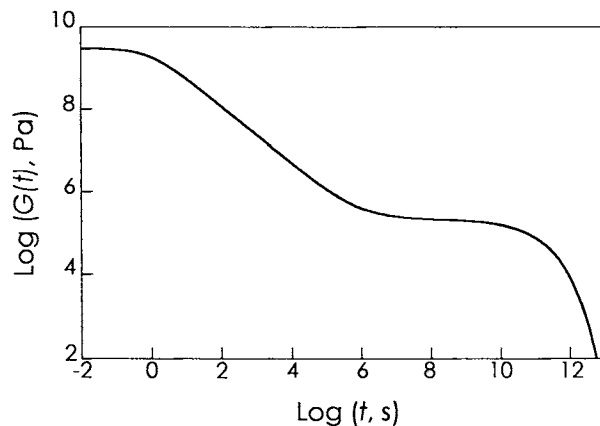


Figure 1-3. Schematic modulus-time curve for a polymer at constant temperature.

One more type of deformational experiment remains to be discussed. Consider a material like pitch or tar, which is used as a roof coating and is applied at elevated temperatures. Our test is similar to the standard experiment done above, utilizing the same size sample at room temperature. First we suspend the 1-kg weight from the sample and observe the small resultant extension. According to equation (1-2), the modulus calculated is high. However, if the sample is left suspended in this vertical position for several hours, the result is a considerable elongation of the sample. Now application of equation (1-2) gives a very low value for the modulus. Thus the modulus measurement on the short time-scale of a few seconds resulted in a high value while the modulus measurement on the longer time-scale of hours resulted in a low modulus. This apparent discrepancy is accounted for by realizing that the modulus is a function of time as well as temperature; this has been found to be the case generally for polymeric systems. Strictly then, the measurements spoken of earlier in this chapter and depicted schematically in Figure 1-2 should have some time associated with each modulus value. (Time represents

the duration between the application of the force and the measurement of the extension.) It is convenient to pick the same constant time for all measurements, so one might consider the constant time-factor in Figure 1-2 to be 10 seconds.

As is evident from the above discussion, it should be possible to measure the behavior of a material as a function of time at constant temperature. A schematic modulus-time behavior is shown in Figure 1-3. The modulus is seen to fall from its initial high value by about three orders of magnitude to a modulus indicative of a rubber and, after evidencing a plateau, fall again. The ordinate here is $\log t$; at the chosen temperature an experiment lasting for 1 to 30 minutes would characterize this material as a plastic. However, in an experiment lasting 10^8 minutes (200 years), the material would "look like" an elastomer. Longer measurements would correspond to still softer materials. Methods for obtaining curves of the type shown in Figure 1-3 are discussed in Chapter 4, as well as methods of converting from modulus-time behavior to modulus-temperature behavior and vice versa.

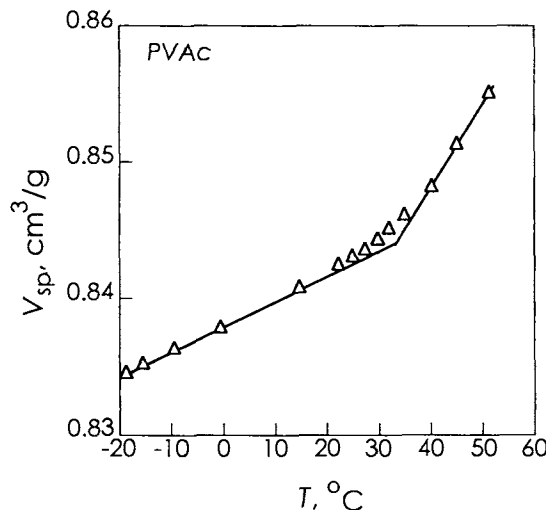


Figure 1-4. Specific-volume data for poly(vinyl acetate) used to determine its T_g .

Another experiment is often carried out in laboratories dealing with the physical properties of polymers. This is the determination of the temperature at which the material properties change from those of a plastic to those of a rubber. This temperature is known as the glass transition temperature and is a characteristic property of each substance. In Figure 1-2, for example, it is clear that at about 100°C, the modulus of the plastic exhibits a steep decrease. Careful analysis of the curve in this region, however, indicates no abrupt change in modulus but rather a smoothly varying change. From this experiment, it would seem that the glass transition occurs over a range of

6 INTRODUCTION

temperatures rather than at a single temperature. Experimentally, it has been found that the coefficient of expansion of a substance undergoes a more abrupt change in the region of the glass transition. The temperature at this change, in fact, is defined as the glass transition temperature T_g . An example of the data obtained in the determination of a glass transition temperature by this method is presented in Figure 1-4. The volume of a sample is measured as a function of temperature using a dilatometer, care being taken to change the temperature slowly and at an essentially constant rate. The temperature where there is a change in slope (due to a discontinuity in the coefficient of expansion) is taken as T_g . In the example shown in Figure 1-4, T_g is about 34 °C.

SUGGESTED READING

- Alfrey, T.,** *Mechanical Behavior of High Polymers*, Interscience, New York, 1948.
- Bueche, F.,** *Physical Properties of Polymers*, Interscience, New York, 1962.
- Christensen, R. M.,** *Theory of Viscoelasticity, an Introduction*, Academic Press, New York, 1971.
- Eirich, F. R., Ed.,** *Rheology, Theory and Applications*, Vol. 1, Academic Press, New York, 1956.
- Ferry, J. D.,** *Viscoelastic Properties of Polymers*, 3rd ed., Wiley, New York, 1990.
- Findley, W. N.,** *Creep and Relaxation of Nonlinear Viscoelastic Materials with Introduction to Linear Viscoelasticity*, North-Holland Publishing Co., Amsterdam, 1976.
- McCrumb, N. G., B. E. Read, and G. Williams,** *Anelastic and Dielectric Effects in Polymeric Solids*, Wiley, New York, 1967.
- Middleman, S.,** *The Flow of High Polymers*, Interscience, New York, 1968.
- Nielsen, L. E. and R. F. Landel,** *Mechanical Properties of Polymers and Composites*, Marcel-Dekker, New York, 1994.
- Pipkin, A. C.,** *Lectures on Viscoelasticity Theory*, Applied Mathematical Sciences, Vol. 7, Springer-Verlag, New York, 1972.
- Schwarzl, F. R.,** "Viscoelasticity," in *Encyclopedia of Polymer Science and Engineering*, Vol. 17, (H. F. Mark, N. M. Bikales, C. G. Overberger, G. Menges and J. I. Kroschwitz, eds.) Wiley-Interscience, New York, 1989, pp. 587-665.
- Timoshenko, S., and J. N. Goodier,** *Theory of Elasticity*, McGraw-Hill, New York, 1951.
- Tobolsky, A. V.,** *Properties and Structure of Polymers*, Wiley, New York, 1960.
- Tobolsky, A. V., and H. F. Mark, Eds.** *Polymer Science and Materials*, Wiley, New York, 1971.
- Treloar, L. R. G.,** *The Physics of Rubber Elasticity*, Clarendon Press, Oxford, 1975.
- Tschoegl, N.,** *The Phenomenological Theory of Linear Viscoelastic Behavior: An Introduction*, Springer-Verlag, New York, 1989.
- Ward, I. M.,** *Mechanical Properties of Solid Polymers*, Wiley, New York, 1971.
- www.rheology.org is the web site of the Society of Rheology. It gives current information on many aspects of the deformation and flow of materials.

2

Phenomenological Treatment of Viscoelasticity

To place the concepts discussed in the Introduction on a more quantitative basis, and to understand better some of the added complications that arise from the time dependence of the modulus, several methods commonly used to make physical measurements on polymeric systems are described in this chapter. First, however, it is necessary to define rigorously the parameters to be derived from the experimental data in terms of the type of deformation applied to the sample.*

A. ELASTIC MODULUS

Perhaps the simplest deformation that can be applied to a sample is uniaxial tension or compression, shown in Figure 2-1a. This is the type of deformation mentioned in the Introduction. However, our previous concept of force is

* In this context, both stress and strain are defined considering very small deformations. Under these conditions, the properties of the material are strictly constant and second-order effects (nonlinearities) are negligible. For example, to effect large shear strains, it is necessary to apply stresses to the material other than the obvious shear stress. While nonlinear effects are important, they are beyond the scope of this book, and the reader is advised to consult more advanced texts.

8 PHENOMENOLOGICAL TREATMENT OF VISCOELASTICITY

modified slightly in this more quantitative discussion to become the stress defined as

$$\sigma_E = \frac{F}{A} = \frac{F}{YZ} \quad (2-1)$$

where the subscript E represents uniaxial extension and the other symbols are defined in the figure. Stress, denoted in general by the symbol σ , has the units of dynes/cm² (dynes per square centimeter), lb_f/in.² (psi), or N/m² (Newtons per square meter). Current international convention prescribes the latter, which is named the Pascal (after Blaise Pascal, 1623–1662). Pa is the abbreviation for the Pascal. Note that static definitions are being considered here, that is, the parameters do not vary with time. These initial considerations will shortly be generalized to time-dependent functions.

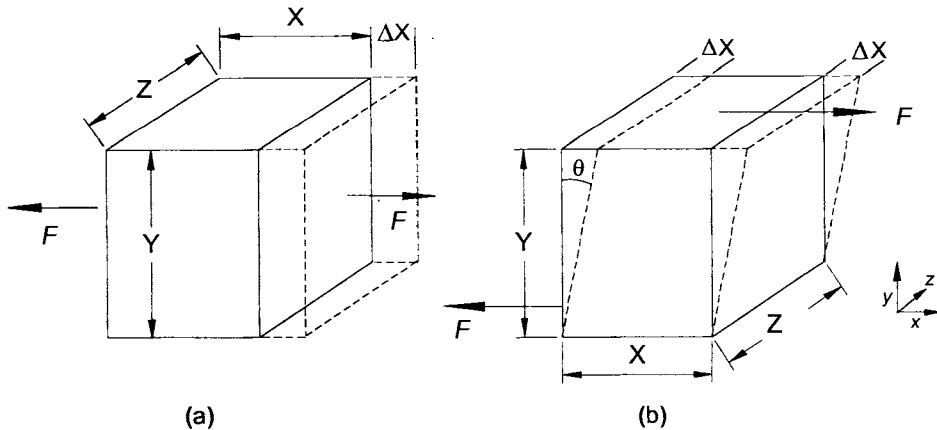


Figure 2-1. Tension (a) and shear (b) of a three-dimensional sample subjected to very small deformations.

The application of a tensile stress to a real body will result in a corresponding extensional deformation as illustrated in Figure 2-1a. The fractional extension is defined as the tensile strain. Thus, ε , the tensile strain resulting from the application of a uniaxial stress, is given as

$$\varepsilon = \frac{\Delta X}{X} \quad (2-2)$$

and it is clear from this expression that ε is dimensionless. For the static situation, the tensile modulus E and the tensile compliance D are defined by equation (2-3)

$$E = \frac{\sigma_E}{\epsilon} = \frac{1}{D} \quad (2-3)$$

Again it must be emphasized that this discussion is strictly limited to time-independent phenomena.

The second type of deformation is illustrated in Figure 2-1b and is called simple shear. The application of the force F in the x direction will result in the shearing displacement shown by the dashed lines. Here the stress σ , is

$$\sigma = \frac{F}{XY} \quad (2-4)$$

where, by convention, no subscript is used. The shear strain γ is given as

$$\gamma = \frac{\Delta X}{Y} = \tan \theta \quad (2-5)$$

where θ is the angle shown and is related to $\Delta X/Y$ by simple trigonometry. Note that there are no displacements at all in either the y direction or the z direction for simple shear.[†] The shear modulus G and the shear compliance J are defined using the relationship

$$G = \frac{\sigma}{\gamma} = \frac{1}{J} \quad (2-6)$$

Note that the choice of the coordinate symbols (x , y , z) for the directions parallel to the X , Y and Z sides, respectively, is arbitrary. In this regard, we should again remind ourselves that real pieces of material are three-dimensional. The three-dimensional aspect of a material means that both the *location* and *direction* of the forces on the sample's surfaces must be taken into account. As stated in the Introduction we must balance the forces in all directions on the sample, and similarly balance all the moments. Otherwise, the sample will start to accelerate, which would make the measurements difficult indeed!

For example, consider the shearing of a cube. Our simple picture is as shown in Figure 2-1b, but let us think about how this might actually be done in the laboratory.

[†] The x , y and z direction are often referred to as the flow, gradient and neutral direction, respectively. The z direction is also known as the vorticity axis. Indeed, round particles suspended in a sheared fluid will tend to rotate around the z axis.

10 PHENOMENOLOGICAL TREATMENT OF VISCOELASTICITY

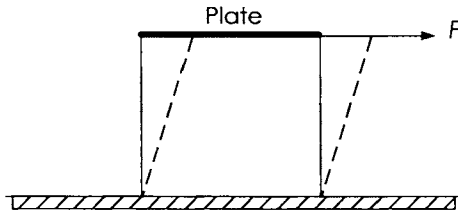


Figure 2-2. Forcing a sample to shear by fastening it to a solid surface and pulling a plate adhered to its top surface.

Suppose the sample is glued to a solid platform and sheared by a force applied to a movable plate glued similarly to the top surface, as illustrated in Figure 2-2. While this appears to be a simple application of two balanced forces, the table and plate are actually doing more; they are applying a torque or moment to the sample. To understand this, consider the sample as a free body for a moment, as shown in Figure 2-3.

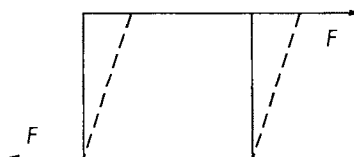


Figure 2-3. Forces applied to the sample to cause shear will also lead to rotation.

It should be clear from this drawing that the forces, while balanced in the x , y and z directions, are not aligned, and the sample will rotate. This twist can be opposed by application of a counteracting twist, or moment, to either the top or bottom plate (or both). But as far as the sample is concerned, this counteracting moment is equivalent to placing a second pair of forces on the sample as shown in Figure 2-4. Now all forces and moments are in balance.

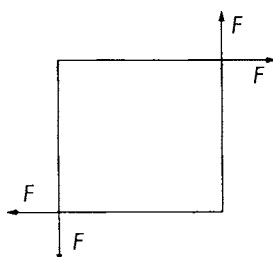


Figure 2-4. Rotation of the sample can be stopped by applying another pair of forces.

Note the apparent symmetry of the arrangement in Figure 2-4 about the diagonal. Simple shear, however, does not have such symmetry. Although this discrepancy is not important at low strains, it is evident that at larger deformations, there must be a slight difference in the "plates" through which

the forces are applied to the vertical sides: they must be able to stretch effortlessly to allow the sample volume to be preserved. (Compare the length of the slanted dotted lines in Figure 2-3 with that of the original vertical lines.) Clearly such “virtual clamps” would be extremely hard to make, but they do help us to visualize how the external forces can, in principle, be applied to sample to make it deform according to our definition of the deformation, in this case simple shear. In addition, in general, it may be necessary to apply a force to the top and bottom plates to force the sample thickness to stay the same. The apparently straightforward “simple shear” has turned out to be quite complicated!

A somewhat simpler example of the virtual clamp is the one used to stretch a sample. For uniaxial extension, the situation is as depicted in Figure 2-5.

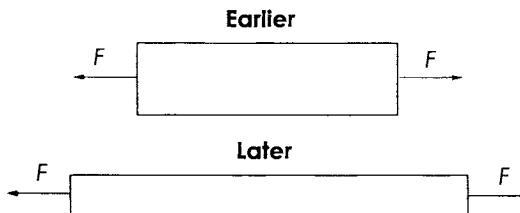


Figure 2-5. To keep the volume of the sample constant during stretching, the sample must become thinner.

Note that the sample has elongated in the stretch direction; but, to preserve volume, has had to thin. The “clamps” at the ends also had to shrink to accommodate this motion and avoid distortion of the sample. In practice, of course, this can't be done, so an “end correction” must be applied unless the sample is very long and thin. Alternatively, one can visualize the virtual clamps as a transverse line of material points well removed from the physical clamps.

One might ask what has pinched the sides together, as there is no external force acting on these surfaces. Surprisingly, the answer is pressure; a negative pressure inside the sample has drawn in the sides. Interestingly, one can alternatively apply pressure or forces to the sides of a sample and effect the same deformation. For example, Griswold et al.¹³ accomplished this by winding rubber bands around a piece of polyethylene. Children do this by wrapping their hand around a cylinder of soft clay, and squeezing; the clay elongates.

We can see most easily how pressure works by introducing the concept of material stress, as opposed to the total or applied stress to the sample. Material stress can be regarded as the stress produced by the deformation of the material; it always *opposes* the deformation. The force applied to the clamps must be

12 PHENOMENOLOGICAL TREATMENT OF VISCOELASTICITY

strong enough to counteract both the material stress and any pressure, just as when an inflated rubber balloon is squeezed, both the gas pressure and the stretching of the rubber oppose the force applied.

Considering the tension experiment, we designate the direction of stretch as the x direction and the force causing this as F_x . This is also the direction of the normal to the plane to which the force is applied (the virtual clamp); its area will be designated A_x . The stress on this face is given by

$$\sigma_{xx} = \frac{F_x}{A_x} \quad (2-7)$$

where the double subscript on σ reminds us of both the force direction (x) and the area normal (also x in this example). This is the total stress; it's what's actually applied to the sample by a clamp. As mentioned earlier, the material stress (sometimes called extra or deviatoric stress[†]) is what the material produces as a reaction to its deformation. We designate this as τ_{xx} . The two may or may not be equal as we can see by examining the virtual clamp. Remember that the virtual clamp does not bend, but shrinks or expands freely in both directions and applies the tensile force uniformly to the material it contacts.

Examining the virtual clamp for a moment, we have the following free-body diagram for the clamp:

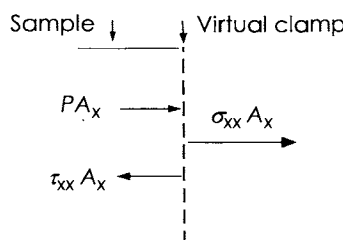


Figure 2-6. Free-body force diagram for the clamp used to stretch a sample.

The force balance includes *three* contributions: (1) $\sigma_{xx}A_x$ due to the applied force or the total stress σ_{xx} times the clamp area A_{xx} , (2) $\tau_{xx}A_x$ due to the material resisting the deformation, and (3) the pressure P in the sample, again multiplied by the clamp area to give force. Because the clamp area is common to all, we can write the equation:

[†] The technical difference between “deviatoric” and “extra” stress, and correspondingly the differences between the pressure in equation (2-9) and the thermodynamic pressure are important for describing compressible materials at large strains. By restricting the discussion to small strains and incompressible materials, we can avoid these complications.

$$\tau_{xx} = \sigma_{xx} + P \quad (2-8)$$

or, on rearranging

$$\sigma_{xx} = \tau_{xx} - P \quad (2-9)$$

The pressure is written as if it were positive. But this is not always the case. If P is negative, the value of the total stress σ_{xx} required to sustain the deformation will be *larger* than the stress created by the deformation of the material, τ_{xx} . This is one reason why the tensile modulus is larger than the shear modulus. But how can this relationship be firmed up? We can do this by examining the *sides* of the sample.

The equation relating total, material and pressure stresses will work for any clamp, including one placed on the sides of the sample, as shown in Figure 2-7.

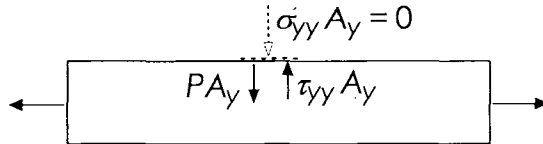


Figure 2-7. Free-body diagram of a virtual clamp pasted to the side of the sample..

First of all, the material-generated force $\tau_{yy} A_y$ must act outward on the "clamp" because the material is being compressed, which it resists. Except for the small contribution of atmospheric pressure (which we will neglect), the external force $\sigma_{yy} A_y$ applied to this virtual clamp is zero. The force sum now shows that the pressure-generated force PA_y must be negative, i.e., the pressure is negative. In equation form, we write:

$$\sigma_{yy} = \tau_{yy} - P = 0 \quad (2-10)$$

Thus

$$P = \tau_{yy} \quad (2-11)$$

Because τ_{yy} is compressive, or negative, the value of P is negative, as we surmised. (In common English, the sides are being pulled in by the negative pressure.) Equation (2-11) can be substituted into equation (2-9) to yield

$$\sigma_{xx} = \tau_{xx} - \tau_{yy} \quad (2-12)$$

or, more generally,

$$\sigma_{ii} - \sigma_{jj} = \tau_{ii} - \tau_{jj} \quad (2-13)$$

14 PHENOMENOLOGICAL TREATMENT OF VISCOELASTICITY

where i and j denote any of the three coordinate directions. Now it remains to connect the stresses with the deformations.

As we have seen, the connection between stress and strain in a material is the modulus as given by equations (2-3) and (2-6). We can combine both of these equations into one, called Hooke's law, which will apply for the material-generated stress due to any deformation, as written in equation (2-14).

$$\tau_{ij} = G\gamma_{ij} \quad (2-14)$$

Here τ_{ij} is the material-generated stress, G is the shear modulus and γ_{ij} is the general deformation, which we still need to define. Applying equation (2-14) gives

$$\sigma_{xx} = G(\gamma_{xx} - \gamma_{yy}) \quad (2-15)$$

Equation (2-14) requires that the deformation γ_{ij} be defined so that it is consistent with the shear strain in a shear experiment, and is independent of whole-body rotations or displacements. As mentioned in Chapter 1, whole-body motions simply move or rotate the sample without deforming it. Referring to the shear experiment, we can see that the ij correspond to y and x ; that is the plate on which the force is applied has a normal in the y direction, while the force is the x direction. Thus we might guess that the expression for γ_{yx} should be

$$\gamma_{yx} = \frac{\partial u_x}{\partial y} \quad (2-16)$$

where u_x are displacements in the x direction (designated as ΔX in Figure 2-1). Unfortunately, while close, this is not general enough, because a rotation of the cube will produce a value of the displacement gradient *even though the sample is not deformed*. To correct for this, the following form is used:

$$\gamma_{yx} = \frac{\partial u_x}{\partial y} + \frac{\partial u_y}{\partial x} \quad (2-17)$$

and, in general,

$$\gamma_{ij} = \frac{\partial u_j}{\partial x_i} + \frac{\partial u_i}{\partial x_j} \quad (2-18)$$

where in shear, $x_1 = x$, $x_2 = y$ and $x_3 = z$.[§] The numeric subscript convention is widely used and is more convenient if matrix notation is needed. Also, as a point of interest for the mathematically inclined, it can be shown that for very small deformations, the form in equation (2-18) is unique, i.e., there are no other choices.

Returning to the tensile sample and applying this form in a consistent fashion gives:

$$\gamma_{xx} = \frac{\partial u_x}{\partial x} + \frac{\partial u_x}{\partial x} = 2 \frac{\partial u_x}{\partial x} = 2\epsilon \quad (2-19)$$

where ϵ is the tensile strain. Similarly,

$$\gamma_{yy} = \frac{\partial u_y}{\partial y} + \frac{\partial u_y}{\partial y} = 2 \frac{\partial u_y}{\partial y} = -\epsilon \quad (2-20)$$

for small strains in order to keep the volume constant (but see discussion under Poisson ratio). Thus the applied tensile stress becomes

$$\sigma_{xx} = G(\gamma_{xx} - \gamma_{yy}) = G[2\epsilon - (-\epsilon)] = 3G\epsilon \quad (2-21)$$

Using the definition of tensile modulus from equation (2-3) gives the relationship:

$$\sigma_E \equiv E\epsilon = \sigma_{xx} \quad (2-22)$$

On comparing equation (2-21) and equation (2-22) we see that

$$E = 3G \quad (2-23)$$

Note that we have assumed that the deformations are small and the sample does not change volume.

To avoid problems with pressure that might be applied to the outside of the sample, it is customary to define the extensional stress σ_E in terms of the difference between the two applied stresses, thus

$$\sigma_E \equiv \sigma_{xx} - \sigma_{yy} \quad (2-24)$$

When σ_{yy} is very small or zero, σ_E is just the stress applied to the ends of the sample via the clamps. However, if the stretch is accomplished by squeezing

[§] Some authors choose to define strain with a factor of $1/2$ on the right-hand side. This removes a factor of two from the expressions in tension, e.g., in equation (2-20), but introduces a factor of two in expressions for shear stress.

16 PHENOMENOLOGICAL TREATMENT OF VISCOELASTICITY

on the sides, then σ_{yy} is a negative number (equal to the squeezing pressure) and σ_{xx} is zero. σ_E remains the same, which is quite appropriate.

In the case of tension, the stresses on the tensile sample are parallel to what is referred to as the principal directions, and one can then use the shorthand

$$\sigma_{xx} = \sigma_x \quad \text{and} \quad \sigma_{yy} = \sigma_y \quad (2-25)$$

They are thus referred to a “principal stresses.”

A comment about nomenclature is in order because the student will discover different conventions. As hinted at above, for Cartesian coordinates there is a natural tendency to connect the (x, y, z) directions with direction vectors (x_1, x_2, x_3) used in general expressions such as equation (2-18). To convert to numerals, changes such as listed below are needed:

$$\begin{aligned}\sigma_x &= \sigma_1 \\ \sigma_y &= \sigma_2 \\ \sigma_z &= \sigma_3 \\ \sigma_{xx} &= \sigma_{11} \\ \sigma_{xy} &= \sigma_{12}\end{aligned}\quad (2-26)$$

The decision to connect x to 1 is arbitrary; the z direction could as well be assigned the number 1. Conventionally, the subscript 1 is associated with the direction of principal motion or displacement, but again this is arbitrary. Also, there is a convention with respect to the sign of the tensile stress that is applied to the sample [e.g., equation (2-14)]; it could as well be called positive if the sample were compressed from the ends, rather than pulled. The latter in fact has the advantage that the sense (compression) is the same as externally applied pressure. The disadvantage is that expressions such as equation (2-14) would carry negative signs. Of lesser importance is the convention used for the order of subscripts for shear, i.e., $\sigma_{12} = F_1/A_2$ or $\sigma_{21} = F_1/A_2$, as $\sigma_{12} = \sigma_{21}$ in most cases. Thus the student should be aware of these differences, and ask the following three questions: (1) What is the sign convention for tensile stress; (2) What is the subscript for the principal direction of flow and (3) What is the definition of the strain [e.g., equation (2-18)]? Finally, the reader should note the subscript order for shear flows.

Example 2-1:

Calculate the pressure required to inflate a thin-walled spherical balloon made from a Hookian elastic material.

The equation describing the Hookian material is

$$\tau_y \approx G\gamma_y \quad (2-14)$$

with

$$\gamma_y = \frac{\partial u_j}{\partial x_i} + \frac{\partial u_i}{\partial x_j} \quad (2-18)$$

If the balloon has an initial radius of R_0 and a thickness of δ_0 , then the thickness at any state of inflation will be

$$\delta = \delta_0 R_0^2 / R^2 \quad (a)$$

to preserve material volume. A force balance between the two hemispheres reveals that

$$\pi R^2 P = \sigma_{ss} 2\pi R \delta \quad (b)$$

where P is the pressure in the balloon and σ_{ss} is the stress applied by the material of one hemisphere on the material of the other. Combining equations (a) and (b) and solving for P gives

$$P = 2\delta\sigma_{ss} / R = 2\delta_0\sigma_{ss}R_0^2 / R^3 \quad (c)$$

Now it remains to find the total "applied" stress σ_{ss} . Our strategy is to calculate the material-generated stress τ_{ss} , which we can connect to the balloon's growing radius using equation (2-14). To do this, we first need to relate the strain to the balloon radius (or thickness). If the curvature of the balloon surface is ignored, the deformation is similar to a flat sheet being stretched biaxially, with the amount of stretch being proportional to the balloon circumference (and radius). Thus, at small strains, the displacement gradient is $\partial u / \partial x_i = \partial u / \partial x_j = du_i / dx = \Delta R / R_0 = R / R_0 - 1$. Therefore, via equation (2-18),

$$\gamma_{ss} = 2 \frac{R - R_0}{R_0} = 2 \left(\frac{R}{R_0} - 1 \right) \quad (d)$$

at low strains. Assigning the subscript z for the thickness direction, and remembering that the volume of the material is constant, gives

$$\gamma_{zz} = -4(R / R_0 - 1) \quad (e)$$

18 PHENOMENOLOGICAL TREATMENT OF VISCOELASTICITY

again for low strains. Note that γ_{xx} is negative, corresponding to thinning of the balloon as it inflates. The material-generated stresses τ_{xx} and τ_{yy} are obtained using equation (2-14), and the difference between them will be $\sigma_{xx} - \sigma_{yy}$. With σ_{yy} there is a slight problem because the inside of the balloon has pressure, whereas the outside does not. Suffice it to say that with thin balloons, this contribution is negligible and

$$\sigma_{yy} = G(\gamma_{yy} - \gamma_{xx}) = 6G\left(\frac{R}{R_0} - 1\right) \quad (f)$$

Using equation (2-29) to get the pressure gives finally

$$P = 12G\varepsilon\delta_0 / R_0(1 + \varepsilon)^3 \quad (g)$$

where ε is used in place of $R/R_0 - 1$. The interesting prediction of this equation is that the pressure will rise at first, and then fall starting at $\varepsilon = 1/2$. Although a pressure maximum is indeed observed, we should be acutely aware that strains this large are well beyond the limits of the Hookean elastic model of equations (2-14) and (2-18).

The important lesson from this example is that we can determine the shear modulus of a material by deforming it in an experiment that looks nothing like the picture of simple shear in Figure 2-2. This is an illustration of the advantage of the full consideration of the three-dimensional character of deformation.

The applications of Hooke's law [equations (2-14) and (2-18)] discussed above have assumed that the volume of the material is invariant with strain during a tensile deformation. However, because the pressure is not zero, this may not be the case, and the strains in each direction must be known to account for this. By measuring the actual transverse (γ_{yy}) and longitudinal (γ_{xx}) strains, one can define the ratio of these two strains as a material property. This is called Poisson's ratio μ , and is defined as:

$$\mu \equiv -\gamma_{yy} / \gamma_{xx} \quad (2-27)$$

where the γ_{ii} are defined in (2-18) in terms of the displacement gradients. If we still assume Hookean behavior under these circumstances, then we find the following relationships between E and G and D and J :

$$E = 2(1 + \mu)G \quad \text{and} \quad J = 2(1 + \mu)D \quad (2-28)$$

In terms of volume changes, Poisson's ratio is given by the equivalent relationship

$$\mu = \frac{1}{2} \left[1 - \left(\frac{1}{V} \right) \frac{dV}{d\epsilon} \right] \quad (2-29)$$

where $\epsilon = \gamma_{xx}/2$, i.e., the displacement gradient in the stretch direction. Experimentally, μ is quite close to 0.5 for a rubber but is lower, in the range of 0.2 to 0.3, for some plastics and still lower for certain heterogeneous materials. In fact, one can make heterogeneous anisotropic materials that *expand* in thickness when pulled! One is shown in Figure 2-8.

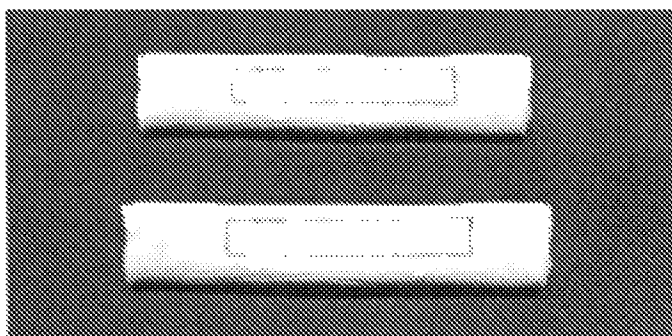


Figure 2-8. This gasket material exhibits a slightly negative Poisson ratio. On pulling, the square marked on the sample increased in width from 7.1 to 7.6 mm, or about 7%. The thickness direction (not shown) expanded even more. The length of the square increased ~10%. Thus, Poisson's ratio is about $-0.07/0.1 = -0.7$.

B. TRANSIENT EXPERIMENTS

Consideration of the time dependence of relaxation phenomena adds additional complications. The value of a measured modulus or compliance will very definitely depend on the exact manner in which the experiment is carried out.

As an example, consider the following experiments. First, a polymer is subjected to a constant uniaxial stress σ_1 , for one hour; this perturbation results in some measurable strain, say ϵ (1 hour). In a second experiment, however, an identical sample is subjected to sufficient stress to result in the same strain ϵ (1 hour) immediately upon application of the stress. Then the stress is decreased so that the strain remains constant at ϵ (1 hour). The value of the stress after 1 hour in the second experiment is defined as σ_2 . In general, σ_1 and σ_2 will not be the same, the stress σ_2 associated with the constant strain experiment being lower. However, since the strains are the same, the two "modulus" values

20 PHENOMENOLOGICAL TREATMENT OF VISCOELASTICITY

calculated from equation (2-3) are different. Consequently one must explicitly state the method in which a parameter is to be measured in its definition. Fortunately, most parameters obtained from different experiments will suffice to define all the others² if the strains are small. Some of these transformations will be treated later in this chapter.

The two experiments just described are, respectively, creep and stress relaxation, both in tension. Figure 2-9, shows a crude form of a creep experiment in shear. In such an experiment the sample is subjected to constant shear stress σ_0 and its shear strain γ is measured as a function of time. The shear creep compliance $J(t)$ resulting from such an experiment is:

$$J(t) = \frac{\gamma(t)}{\sigma_0} \quad (2-30)$$

The corresponding experiment in extension results in the tensile creep compliance $D(t)$ defined by

$$D(t) = \frac{\varepsilon(t)}{\sigma_{E,0}} \quad (2-31)$$

where $\sigma_{E,0}$ is the constant tensile stress applied to the sample and $\varepsilon(t)$ is the observed tensile strain.

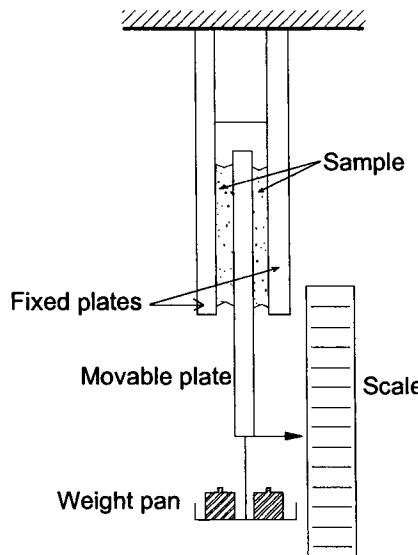


Figure 2-9. A simple apparatus to measure shear creep.

To run the experiment shown in Figure 2-9, the sample and the fixtures (plates) should be placed into a constant temperature environment where the sample

and fixtures are allowed to come to thermal equilibrium. During this time the movable plate is locked in place to eliminate stress from the sample. When the sample and fixtures are at thermal equilibrium, the appropriate weights are placed on the weight pan and the movable plate is unlocked. The experimenter must then record the position of the weight pan using the scale and the corresponding time. It should be clear that the shear strain $\gamma(t)$ as a function of time is easily calculated from these data and knowledge of the sample dimensions using equation (2-5). The force exerted by the total weight of the pan, weights and clamp is used to calculate the constant shear stress. With this information in hand, the shear creep compliance $J(t)$ can be calculated using equation (2-30). It must be emphasized that this experimental setup is among the crudest imaginable and will give correspondingly imprecise results unless considerable refinement is made. Commercial instruments are now readily available that apply the shearing force using a low-inertia, low-friction, constant-torque motor, rather than weights. For more details, the student may refer to the manufacturers' web sites.⁷

Another common type of transient experiment, called stress relaxation, may be considered. Here, the strain is maintained constant and the stress is measured as a function of time. A schematic of a simple stress-relaxation apparatus is shown in Figure 2-10. The sample, in the form of a strip, is first attached to the upper clamp and the signal produced by the load cell is recorded; this corresponds to zero stress applied to the sample. Next the lower clamp is attached and the latch is locked. The sample is heated to the temperature desired and thermal equilibrium established. (Usually the sample's temperature is raised to about 10 degrees above the test temperature or to a temperature above the glass temperature to allow possible "frozen-in" strains to relax before approach to the test temperature is established.) Adjustments are made with the threaded lower clamp to compensate for thermal expansion of the sample. At the start of the experiment, the strain is introduced by releasing the latch and allowing the strong spring to stretch the sample until the stop is reached. A recorder monitors the signal from the load cell; this can be converted to force by subtracting the zero signal and multiplying by a constant derived from the signal produced by known weights attached to the upper clamp. From these data, application of equations (2-7), (2-19) and (2-22) and the definition of the tensile relaxation modulus $E(t)$ from equation (2-32)

$$E(t) \equiv \frac{\sigma_E(t)}{\varepsilon_0} \quad (2-32)$$

22 PHENOMENOLOGICAL TREATMENT OF VISCOELASTICITY

gives the desired result. In contrast to the creep experiment, the tensile strain ε_0 is held constant. (The strain varies minutely during the measurement because of the flexibility of the frame, clamps and load cell.)

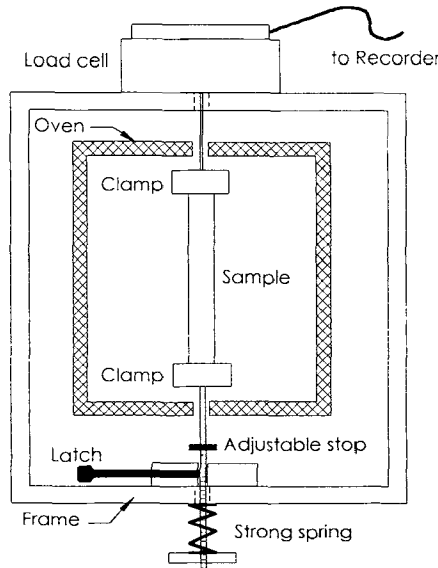


Figure 2-10. A simple apparatus to measure tensile stress relaxation. The spring must be strong enough to stretch the sample very quickly.

Similarly, a shear stress relaxation experiment would measure $G(t)$, the shear stress relaxation modulus

$$G(t) \equiv \frac{\sigma_{21}(t)}{\gamma_0} \quad (2-33)$$

with γ_0 being the constant shear strain.

Equations of the form of (2-3) and (2-6) relating moduli and compliances are no longer applicable to our new time-dependent functions, since

$$E(t) = \frac{\sigma_E(t)}{\varepsilon_0} \neq \frac{\sigma_{E,0}}{\varepsilon(t)} = \frac{1}{D(t)} \quad (2-34)$$

as was discussed in the example mentioned earlier in this section.

Similarly, other moduli and compliances can be defined and they are not, in general, equal to the functions defined above.** Remember that $G(t)$ and $E(t)$ can only be measured directly from constant-strain experiments, while $J(t)$ and

** Examples include the time-dependent modulus from stress-strain experiments, and the constant-force creep compliance.^{2,11}

$D(t)$ can only be measured directly from constant-stress experiments. Conversions from other experiments are often troublesome and can easily lead to considerable error.

C. DYNAMIC EXPERIMENTS

In addition to creep and stress relaxation experiments, another type of measurement is quite common. Here the stress or strain, instead of being a step function, is an oscillatory function with an angular frequency ω . The standard unit of ω is radians per second (rad/s).^{††} Dynamic modulus values measured using such perturbations are functions of ω rather than time. The problem of putting dynamic experiments on a quantitative level is only slightly more difficult than is the case with step-deformation experiments.

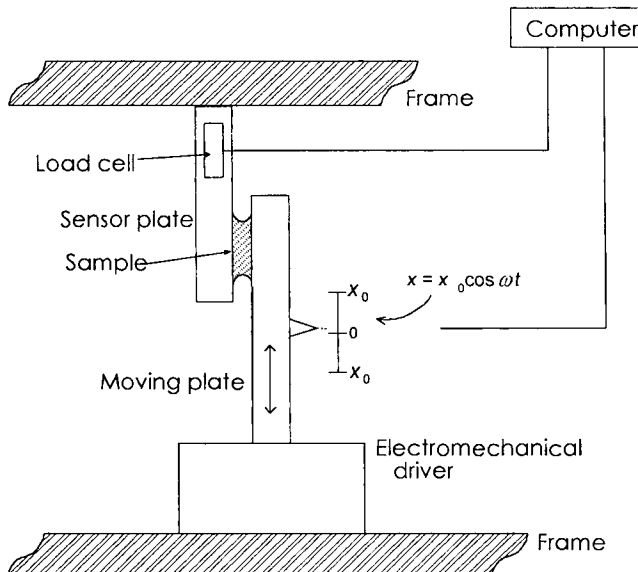


Figure 2-11. Schematic of a dynamic experiment in shear. The electromechanical driver provides a sinusoidal motion of fixed frequency and amplitude.

To become familiar with the dynamic experiment, we will begin by considering the simple apparatus depicted in Figure 2-11. The key part of this apparatus is the electromechanical driver, which provides a vertical motion that is sinusoidal in nature and of fixed amplitude and frequency. In early instruments, the driver was essentially a loudspeaker coil that was driven by a sinusoidal voltage from a signal generator. More modern instruments use a

^{††} Frequency in cycles per second (Hz) and in radians per second (rad/s) are related by the equation $\omega = 2\pi f$.

linear servomotor. The experiment can also be done by twisting a rod or disk in a sinusoidal pattern as shown in Figure (2-12). Another essential part of the apparatus is the device that detects the position of the driven plate. Early instruments simply assumed that the clamp moved in synchrony with the electrical signal supplied to the driver. Modern instruments detect the position separately, using an optical encoder, for example. (An optical encoder is simply a very fine pattern on a transparent substrate that moves through a light beam. A photocell counts the number of interrupts, and thus the position of the encoder pattern. Many computer mice use such devices.) The third key part of the instrument is the load cell, which measures the force sustained by the sample as a result of the moving plate. It must be calibrated carefully.

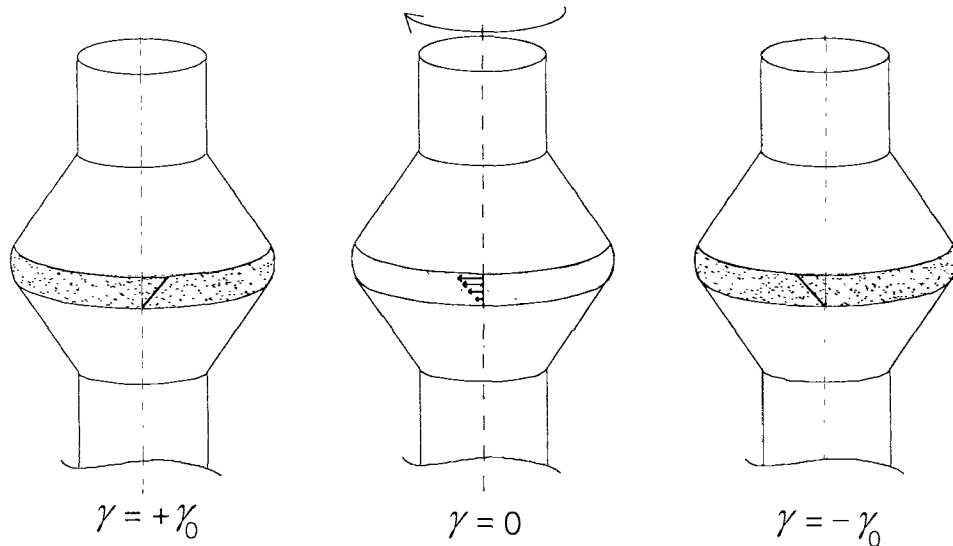


Figure 2-12. Dynamic experiment in shear wherein the disk-shaped sample is twisted sinusoidally. The line in the shaded sample depicts a line of material points, showing the shearing of the sample from right to left. In some designs, one plate is connected to a servomotor that produces the sinusoidal motion while the other plate is connected to the load cell. Other manufacturers use one plate for both functions, with the other solidly fastened to the frame of the machine.

On running the experiment, the motion of the driven plate and the force on the load cell are recorded with a computer. These two signals are then compared in two ways: The first comparison is the phase difference between the two. The phase can be regarded as an angle if one considers the complete cycle to take place over an angle of 2π corresponding to a complete circle. The phase angle is given the symbol δ . For a perfectly elastic substance, the two signals will be exactly in phase and $\delta = 0$. The second comparison is the amplitude ratio of the two signals. The force amplitude, along with the proper

geometric quantities as shown in equation (2-4), will give the stress amplitude, σ_0 (not to be confused with that in equation (2-30)). The motion detector, along with the thickness of the sample between the plates, will give the amplitude of the shear strain γ_0 (not to be confused with γ_0 in equation (2-33)). The ratio of these two would be a modulus, but this modulus is not customarily used. Instead, the following quantities are defined:

$$G' = (\sigma_0 / \gamma_0) \cos \delta \quad (2-35)$$

and

$$G'' = (\sigma_0 / \gamma_0) \sin \delta \quad (2-36)$$

A depiction of the origin of these definitions is provided by Figure 2-13, which shows graphically the nature of the two sinusoidal signals vs. time. For this example, the strain, which is fixed by the instrument, is given by the equation

$$\gamma(t) = \gamma_0 \sin \omega t \quad (2-37)$$

while the resulting stress is given by:

$$\sigma(t) = \sigma_0 \sin(\omega t + \delta) \quad (2-38)$$

G' is simply the stress (termed σ') measured at the maximum strain divided by the strain amplitude γ_0 , which is the strain reached at $\omega t = \pi/2$. On the other hand, G'' is the stress (termed σ'') at zero strain (i.e., the strain at $\omega t = 0$) divided by γ_0 . In spite of the fact that the strain is zero, the stress, in general, will not be zero. According to Figure 2-13, the stresses at these two points can be calculated from equation (2-38) on substituting $\omega t = \pi/2$ and $\omega t = 0$, respectively. The latter gives directly $\sigma' = \sigma_0 \sin \delta$, while the former gives $\sigma'' = \sigma_0 \sin(\pi/2 + \delta) = \sigma_0 [\sin(\pi/2) \cos \delta + \cos(\pi/2) \sin \delta] = \sigma_0 \cos \delta$. These two results complete the demonstration of the correspondence of equations (2-35) and (2-36) with the stress values shown in Figure 2-13.

The physical meaning of the material properties G' and G'' can be sought by referring again to Figure 2-13. From this figure it is clear that the rate of strain is a maximum when the strain passes through zero because a sine wave has its maximum rate of change at this point. Thus, the stress at zero strain, σ'' is the result of the sample responding to *strain rate* as would a purely viscous material. As the strain reaches its peak at $\omega t = \pi/2$, the strain rate approaches zero. The sample at this point must therefore be responding only to strain, as would an elastic material.

26 PHENOMENOLOGICAL TREATMENT OF VISCOELASTICITY

For the dynamic experiment, most will agree that the stress response resulting from perfect sinusoidal strain input is likely to be sinusoidal and have the same frequency. However, it is far from obvious that the response will always be this simple. In fact, with real materials a perfectly sinusoidal stress response is achieved only at vanishingly low values of strain, γ_0 . The response at higher strain will still be periodic, but will be mixed with higher frequency components.^{††} The relative amplitude of these components will increase with strain level.

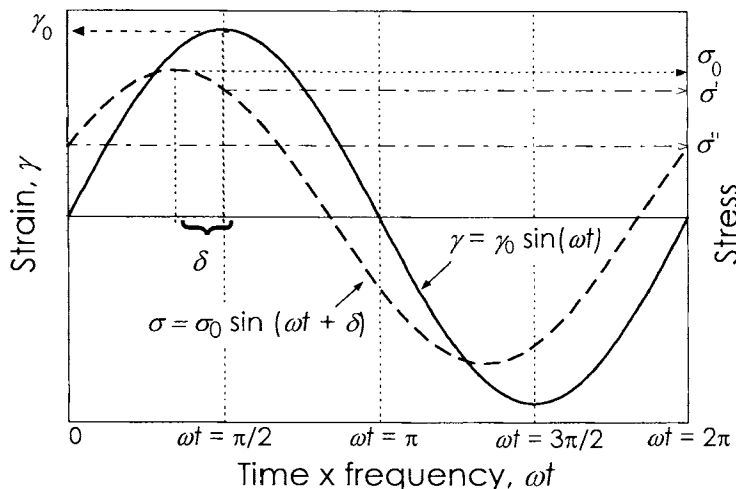


Figure 2-13. The response of a sample to a sinusoidal shear strain $\gamma(t)$ is a sinusoidal shear stress $\sigma(t)$ that leads the strain by a phase angle δ . Arrows show the physical meaning of the stresses σ' and σ'' corresponding to the elastic or in-phase component G' of the dynamic shear modulus and the viscous, out-of-phase or loss component G'' , i.e., $G' = \sigma'/\gamma_0$ and $G'' = \sigma''/\gamma_0$.

One widely used quantity, $\tan \delta$, remains to be defined. Simple trigonometric relationships reveal the following equalities:

$$\tan \delta = \frac{\sigma''}{\sigma'} = \frac{G''}{G'} \quad (2-39)$$

where $\tan \delta$ is often called the loss tangent. Parameters with one prime are called storage functions and those with two primes loss functions. This has to do with the fact that in-phase stress and strain results in elastically stored energy; however the component of stress that is out of phase with the strain

^{††} The response of complex materials, e.g., block copolymers, may not even be periodic, as the oscillatory deformation can lead to transient changes in the properties of the material. Eventually, of course, the response should become strictly periodic as the material transforms to its new structure, although some have reported chaotic behavior.

results in the viscous dissipation of energy, which simply heats the sample (Problem 2-4). Thus $\tan \delta$ is the ratio of lost energy to stored energy.

In the above considerations, a sinusoidal shear strain is applied to the sample. It should be clear that a sinusoidal shear *stress* could also be applied resulting in corresponding compliance functions J' and J'' . The former results from the deformation in phase with the stress, while the latter corresponds to the out-of-phase deformation. The value of $\tan \delta$ remains the same, as can be seen from the curves in Figure 2-13, where we can easily imagine the stress as the applied variable and strain as the measured variable. Tensile stress is equally applicable and definitions of $E'(\omega)$, $E''(\omega)$, $D''(\omega)$, $D'(\omega)$, etc. are completely analogous to the derived shear parameters. At a given frequency, the value of $\tan \delta$ is always the same for any of these quantities, i.e., $\tan \delta = E''/E' = D''/D'$.

The nomenclature of complex moduli and compliances is also often used. Here the out-of-phase component is made the imaginary part of a complex parameter; thus the complex shear modulus G^* and the complex shear compliance J^* are defined as

$$\begin{aligned} G^* &= G' + iG'' \\ J^* &= 1/G^* = J' - iJ'' \end{aligned} \quad (2-40)$$

The difference in sign on the imaginary term results from the fact that the stress leads the strain, while the strain lags the stress; see Figure 2-13. The use of complex numbers to represent the functions has no particular physical significance, although some mathematical manipulations become significantly easier.

D. BOLTZMANN SUPERPOSITION PRINCIPLE

The Boltzmann superposition principle is one of the simplest but most powerful principles of polymer physics.² We have previously defined the shear creep compliance as relating the stress and strain in a creep experiment.^{§§} Solving equation (2-6) for strain gives

$$\gamma(t) = \sigma_0 J(t). \quad (2-41)$$

^{§§} The development here will be done for shear, and σ_{21} will be referred to simply as σ without a subscript. All arguments presented concerning shear variables are completely applicable to tensile parameters also.

28 PHENOMENOLOGICAL TREATMENT OF VISCOELASTICITY

The stress σ_0 is applied instantaneously at time equal to zero. One might, however, imagine an experiment where a stress σ_1 is applied, not at $t = 0$, but at some other arbitrary time, perhaps s_1 . For this experiment equation (2-41) would become

$$\begin{aligned}\gamma(t) &= \sigma_1 J(t - s_1) & t \geq s_1 \\ \gamma(t) &= 0 & t < s_1.\end{aligned}\quad (2-42)$$

Consider now the application of two stress increments σ_0 and σ_1 at the times $t = 0$ and $t = s_1$ respectively. The Boltzmann superposition principle asserts that the two stresses act independently and the resultant strains add linearly. This situation is illustrated in Figure 2-14. Thus

$$\gamma(t) = \sigma_0 J(t) + \sigma_1 J(t - s_1) \quad (2-43)$$

or for a more general experiment consisting of discrete stress increments $\sigma_1, \sigma_2, \sigma_3, \dots, \sigma_n$ applied at times $t = s_1, s_2, s_3, \dots, s_n$

$$\gamma(t) = \sum_{i=1}^n \sigma_i J(t - s_i). \quad (2-44)$$

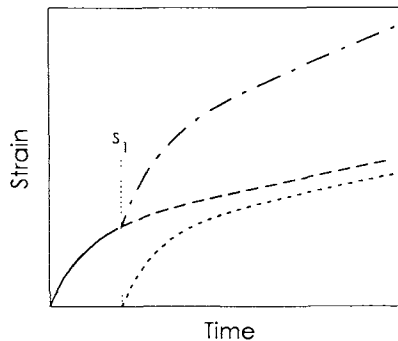


Figure 2-14. Linear addition of strains resulting from sequentially applied stresses.

The summation of the individual σ_i 's would represent the total stress so that in considering a continuous stress application, $\sigma(s)$, the increment of applied stress is just the derivative of $\sigma(s)$ times the increment of time ds . Replacing the summation by an integration results in

$$\gamma(t) = \int_{-\infty}^t \frac{\partial \sigma(s)}{\partial s} J(t - s) ds. \quad (2-45)$$

Note that in this equation t has become the *fixed* time of the observation of the strain; and, for the purposes of integration, can be regarded as a constant. The stress history is accounted for in terms of the dummy integration variable s . The lower limit of integration is taken as $-\infty$, because the complete stress history contributes to the observed strain. The upper limit is t , the time of observation of the strain, because stresses applied after t can have no effect on the observed strain.

In a completely analogous manner, one may derive an expression relating the stress $\sigma(t)$ to the strain in a sample that has experienced some continuous strain history given by the function $\gamma(t)$:

$$\sigma(t) = \int'_{-\infty} \frac{\partial \gamma(s)}{\partial s} G(t-s) ds \quad (2-46)$$

Equations (2-45) and (2-46) are often given in an alternative form, which we will now derive. Integrating equation (2-45) by parts

$$\int u dv = uv - \int v du \quad (2-47)$$

where

$$\begin{aligned} v &= \sigma(s) & dv &= \frac{\partial \sigma(s)}{\partial s} ds \\ u &= J(t-s) & du &= \frac{\partial J(t-s)}{\partial s} ds \end{aligned}$$

one obtains

$$\gamma(t) = J(t-s)\sigma(s)|'_{-\infty} - \int'_{-\infty} \sigma(s) \frac{\partial J(t-s)}{\partial s} ds \quad (2-48)$$

We assume that $\sigma(-\infty)$ is equal to zero; that is, the sample was initially unstressed. Setting $t-s$ equal to a , a new variable, and observing new limits of integration due to this variable change, gives

$$\gamma(t) = J(0)\sigma(t) + \int_0^\infty \sigma(t-a) \frac{\partial J(a)}{\partial a} da \quad (2-49)$$

In an analogous manner, equation (2-46) becomes

$$\sigma(t) = G(0)\gamma(t) + \int_0^\infty \gamma(t-a) \frac{\partial G(a)}{\partial a} da \quad (2-50)$$

30 PHENOMENOLOGICAL TREATMENT OF VISCOELASTICITY

Example 2. Consider a material with a creep compliance given by the function

$$J(t) = J_r + \frac{t}{\eta} \quad (a)$$

where J_r represents the recoverable deformation and η is the viscosity. Using the Boltzmann superposition principle, calculate the strain $\gamma(t)$ when this body is subjected to the linear stress function $\sigma(t)$ shown in Figure 2-15; (i) at times during the loading and (ii) at times after the loading has ceased, i.e., $t > t_1$.

i. For $0 < t < t_1$, the stress history in terms of the integration variable s , is

$$-\infty \leq s \leq 0 \quad \sigma(s) = 0$$

$$0 \leq s \leq t_1 \quad \sigma(s) = ks$$

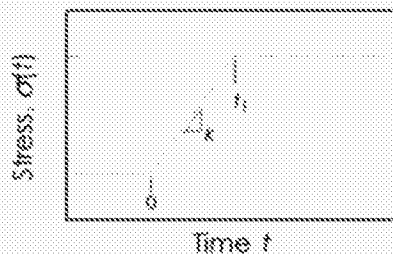


Figure 2-15. Stress history used in calculations.

Making use of equation (2-45), one has

$$\gamma(t) = \int_0^t k \left(J_r + \frac{t-s}{\eta} \right) ds. \quad (b)$$

Carrying out this simple integration (remembering that t is constant for the purposes of integration) leads to

$$\gamma(t) = ktJ_r + \frac{kt^2}{2\eta} \quad (c)$$

Recalling that kt is just the total applied stress at the time t yields

$$\gamma(t) = \sigma(t) \left(J_r + \frac{t}{2\eta} \right) \quad (d)$$

Equation (d) then gives an expression for the strain at time t in a body whose creep compliance is given by equation (a) when it is subjected to a linear

loading pattern starting at time zero. Note that t must fall in the stressing period, i.e., $0 \leq t \leq t_1$.

ii. We now calculate the strain after the stress addition has stopped. Again we can summarize the stressing history in terms of the integration variable s :

$$-\infty \leq s \leq 0 \quad \sigma(s) = 0$$

$$0 \leq s \leq t_1 \quad \sigma(s) = ks$$

$$t_1 \leq s \leq t \quad \sigma(s) = kt_1$$

On splitting the integral of equation (2-45) into the three zones corresponding to the above history, we see that only the one for the zones, $0 < s < t_1$, is nonzero. It becomes:

$$\gamma(t) = \int_0^t k \left[J_s + \frac{t-s}{\eta} \right] ds \quad (e)$$

Note the difference between equations (e) and (b), the latter has as its limit t_1 instead of t . Again, this is a simple integration, which gives the result:

$$\gamma(t) = \sigma(t_1) \left[J_t + \frac{(t-t_1)+t_1/2}{\eta} \right] \quad (f)$$

At $t = t_1$, both equations (d) and (f) yield the same result, as they indeed must.

It is informative to carry out part (ii) of this example using the alternative form of equation (2-45), that is, equation (2-49). One must use the new variable in the integral so that the strain history is introduced in terms of this transformed variable rather than in terms of the normal laboratory time. Writing equation (2-49) for part (ii) of the example gives

$$\gamma(t) = J(0)\sigma(t) + \int \sigma(t-a) \frac{\partial J(a)}{\partial a} da \quad (g)$$

Recalling the stress history described above, there was no stress imposed between the time $s = -\infty$ and time $s = 0$. However, in terms of the variable $a = t - s$, this corresponds to $a = +\infty$ and $a = t$. This is a consequence of the variable change used to derive equation (2-49). Application of this equation without changing variables will necessarily lead to an incorrect result. Completing the stress summary in the usual way:

$$-\infty \leq s \leq 0 \quad \sigma(s) = 0 \quad \infty \geq a \geq t$$

32 PHENOMENOLOGICAL TREATMENT OF VISCOELASTICITY

$$\begin{aligned} 0 \leq s \leq t_1 & \quad \sigma(s) = ks \quad t \geq a \geq t - t_1 \\ t_1 \leq s \leq t & \quad \sigma(a) = kt_1 \quad t - t_1 \geq a \geq 0 \end{aligned}$$

From equation (a)

$$\frac{\partial J(a)}{\partial a} = \frac{1}{\eta}. \quad (b)$$

Again we divide the integral into three parts corresponding to the strain history above: $0 \rightarrow t - t_1$, $t - t_1 \rightarrow t$ and finally $t \rightarrow \infty$. The latter is zero because the stress is zero. Substituting equation (b) and the strain history into equation (g) yields

$$\gamma(t) = J_1 \sigma(t_1) + \int_{t-t_1}^t \frac{kt}{\eta} da + \int_{t-t_1}^t \frac{k}{\eta}(t-a)da. \quad (g)$$

Integration and cancellation gives (f) as indeed it must.

Any of equations (2-45), (2-46), (2-49), or (2-50) is sufficient as a statement of the Boltzmann superposition principle for linear viscoelastic response of a material. Often in particular applications, however, it is more convenient to use one form than another. All can be extended to three dimensions by using the same forms with the strains given by equation (2-18). Thus, for example, equation (2-46) becomes:

$$\sigma_{ij}(t) = \int_{-\infty}^t \frac{\partial \gamma_{ij}(s)}{\partial s} G(t-s) ds, \quad (2-46a)$$

The reader should remember that the use of the definition of strain given in equation (2-18) means that this result applies only to small deformations. For example, equation (2-46a) fails to predict that one must apply a normal stress to the plates to constrain the displacements to the x_1 direction. The failure is evident on realizing that development of a normal stress σ_{22} would require a displacement in the x_2 direction (i.e., normal to the plates), which is not present.

E. RELATIONSHIP BETWEEN THE CREEP COMPLIANCE AND THE STRESS RELAXATION MODULUS

One of the direct consequences of the Boltzmann superposition principle is that there is a relationship between the stress relaxation modulus and the creep compliance. We have already seen that when dealing with time-independent

functions, the compliance and the modulus are simply the reciprocals of each other. This simple relationship no longer holds in the time-dependent case. For materials describable by the Boltzmann superposition principle, the general solution is

$$t = \int_0^t G(s) J(t-s) ds \quad (2-51)$$

This relationship is derived using Laplace transforms in Appendix I. Figure 2-16 illustrates the relationship between G and J for a particular material; it can be readily seen that the shapes of these two curves are markedly different, i.e., $J(t) \neq G(t)$.

F. RELATIONSHIPS BETWEEN STATIC AND DYNAMIC PROPERTIES

Still another relationship between experimental parameters is a direct consequence of the Boltzmann superposition principle. We will derive the equations relating the shear stress relaxation modulus $G(t)$ to the in-phase and out-of-phase dynamic shear moduli $G'(\omega)$ and $G''(\omega)$ starting from equation (2-46)

$$\sigma(t) = \int_{-\infty}^t \frac{\partial \gamma(s)}{\partial s} G(t-s) ds \quad (2-46)$$

A simple variable change setting $a = t - s$ yields

$$\sigma(t) = - \int_0^\infty \frac{\partial \gamma(t-a)}{\partial a} G(a) da \quad (2-52)$$

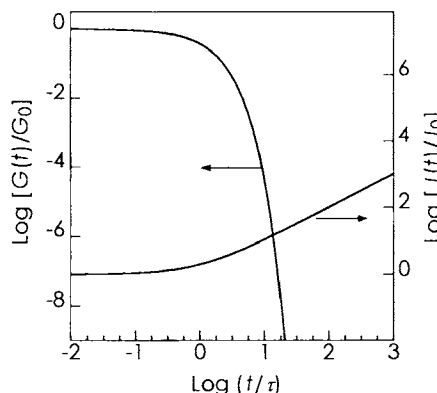


Figure 2-16. An example of the relationship between creep compliance and a stress relaxation modulus. On a log-log plot, the two would be mirror images if reciprocally related.

Consider the application of a sinusoidal strain, which may be represented by

$$\gamma(t) = \gamma_0 \sin \omega t \quad (2-37)$$

where γ_0 is the maximum amplitude of the strain. The phase of the strain is arbitrarily set at zero, which can be done without loss of generality, and will simplify the development. Equation (2-37) applies, of course, for any time, including $t - a$; thus

$$\gamma(t - a) = \gamma_0 \sin[\omega(t - a)] = \gamma_0 \sin \omega t \cos \omega a - \gamma_0 \cos \omega t \sin \omega a \quad (2-53)$$

Differentiation of this result with respect to the variable a gives

$$\frac{\partial \gamma(t - a)}{\partial a} = -\gamma_0 \omega (\sin \omega t \sin \omega a + \cos \omega t \cos \omega a) \quad (2-54)$$

which is just what we need for the integrand of equation (2-52). Substitution of equation (2-54) into equation (2-26) and simplification gives

$$\sigma(t)/\gamma_0 = \sin \omega t \int_0^\infty \omega G(a) \sin \omega a da + \cos \omega t \int_0^\infty \omega G(a) \cos \omega a da \quad (2-55)$$

Thus we have two integrals—one that is modified by $\sin \omega t$, the other by $\cos \omega t$. Due to the way in which we phased the strain in equation (2-37), the stress corresponding to G' will occur at $\omega t = \pi/2$, at which point $\sin \omega t = 1$ and $\cos \omega t = 0$ (see Figure 2-13). Thus

$$G'(\omega) = \omega \int_0^\infty G(a) \sin \omega a da \quad (2-56)$$

from the remaining first term. On the other hand, the stress corresponding to G'' will occur at $\omega t = 0$, at which point $\sin \omega t = 0$ and $\cos \omega t = 1$. Thus

$$G''(\omega) = \omega \int_0^\infty G(a) \cos \omega a da \quad (2-57)$$

from the remaining second term of equation (2-55). Note that the choice of the symbol for the integration variable, in this case a , is completely arbitrary. Also in this section we have tacitly assumed that $G(t)$ approaches zero at long times. If this is not true, as is the case with a crosslinked polymer, one may introduce the function $G(t) - G_e$ where G_e represents the equilibrium shear modulus. It is clear that this difference does indeed become zero at long times.

It is apparent that equation (2-56) and equation (2-57) embody a Fourier sine and cosine transformation of $G(t)$; thus normal Fourier transform⁸ methods

permit the inversion of these relations to give the static modulus as a function of the dynamic properties. This is a specific example illustrative of the method by which one may relate static and dynamic properties. Listings of other results may be found in texts such as Ferry.² In more general terms, it can be stated that the Boltzmann superposition principle, written in terms of a single material function, $G(t)$, can be used to derive all other for linear viscoelastic properties. In practice, however, these transforms are often mathematically very challenging and prone to numerical error. One example is the conversion of $G(t)$ to $J(t)$, which is derived analytically in Appendix 1 and illustrated by problems 6 and 14 at the end of this chapter.

APPENDIX 1: CONNECTING CREEP COMPLIANCE AND STRESS RELAXATION MODULUS USING LAPLACE TRANSFORMS

At sufficiently low strains, the Boltzmann superposition principle allows us to express moduli and compliances in terms of one another even in the time-dependent case. We will derive these relationships directly from equations (2-45) and (2-46) with the aid of Laplace transforms. A short introduction or review of Laplace transform techniques will be presented first.

Transform techniques in general are remarkably useful mathematical tools. The manner in which a transform operates is to take a problem in equation form from one space, where its solution is difficult, to another space where, it is hoped, the solution will be simpler. The solution in transform space is then transformed back into the original space to yield the answer to the problem.

The Laplace transform of a function $F(t)$ is denoted $f(p)$ or $L(F(t))$ and is defined as

$$f(p) \equiv L(F(t)) \equiv \int_0^{\infty} e^{-pt} F(t) dt \quad (a)$$

However, to see how the transform technique works, it is instructive to apply it to several simple examples that will also be needed later. Many of these basic relationships are listed in tables of Laplace transforms.

Our first example is the calculation of the Laplace transform of the function

$$F(t) = at \quad (b)$$

where a is a constant. Substitution into equation (a) gives

$$L(at) = \int_0^{\infty} e^{-pt} at dt \quad (c)$$

36 PHENOMENOLOGICAL TREATMENT OF VISCOELASTICITY

which, upon integration, yields

$$L(at) = \frac{a}{p^2} \quad (d)$$

Thus it is clear that

$$L(t) = \frac{1}{p^2} \quad L(aF(t)) = aL(F(t)) \quad (e)$$

Next, consider the Laplace transform of the function $F(t-a)$, where $F(x) = 0$ for $x < 0$. Again, substitution into equation (a) gives

$$L(F(t-a)) = \int_0^\infty e^{-pt} F(t-a) dt \quad (f)$$

Now letting $t - a = x$, one has

$$L(F(t-a)) = e^{-ap} \int_0^\infty e^{-xp} F(x) dx = e^{-ap} L(F(t)) \quad (g)$$

Lastly, consider the transform of $F'(t)$. Proceeding as above,

$$L(F'(t)) = \int_0^\infty e^{-pt} F'(t) dt \quad (h)$$

Integration by parts yields

$$L(F'(t)) = e^{-pt} F(t)|_0^\infty + p \int_0^\infty e^{-pt} F(t) dt \quad (i)$$

The second term is just the definition of the Laplace transform of $F(t)$ times p ; evaluation of the first term at the limits of integration gives

$$L(F'(t)) = -F(0) + pL(F(t)) \quad (j)$$

It is clear that this expression is very helpful, allowing one to find the transform of the derivative of a function from knowledge of the function itself; it is not necessary to know the derivative of the function explicitly.

One additional result is needed, and it is derived in Appendix 2 of this chapter. This is Borel's theorem, which states:

$$L\left(\int_0^t F_1(t-s)F_2(s) ds\right) = L(F_1(t))L(F_2(t)) \quad (k)$$

Using these results, we can now derive the relationship between the creep compliance and the stress relaxation modulus.

The Laplace transform of equation (2-45) yields

$$L(\gamma(t)) = J(0)L(\sigma(t)) + \int_0^\infty e^{-pt} \int_0^\infty \sigma(t-a) \frac{\partial J(a)}{\partial a} da dt \quad (l)$$

or

$$L(\gamma(t)) = J(0)L(\sigma(t)) + \int_0^\infty \frac{\partial J(a)}{\partial a} \int_0^\infty e^{-pt} \sigma(t-a) dt da \quad (m)$$

Making use of the result derived in equation (g) gives

$$L(\gamma(t)) = J(0)L(\sigma(t)) + \left[\int_0^\infty e^{-ap} \frac{\partial J(a)}{\partial a} da \right] L(\sigma(t)) \quad (n)$$

The term enclosed in brackets, however, is nothing except the Laplace transform of the derivative of $J(t)$. Thus we may apply the result obtained in equation (j) to get

$$L(\gamma(t)) = J(0)L(\sigma(t)) + L(\sigma(t)) [pL(J(t)) - J(0)] = pL(\sigma(t))L(J(t)) \quad (o)$$

Next, transform equation (2-50) into Laplace space in the same manner to obtain

$$L(\sigma(t)) = G(0)L(\gamma(t)) + L(\gamma(t)) [pL(G(t)) - G(0)] = pL(\gamma(t))L(G(t)) \quad (p)$$

Equations (o) and (p) give

$$\frac{1}{p^2} = L[G(t)]L[J(t)] \quad (q)$$

This is the solution of the problem in transform space. We have a direct relationship between the transforms of the compliance and the modulus. This solution must now be returned to real space. Making use of Borel's theorem, equation (k), and the result derived in equation (e) gives the final result:

$$t = \int_0^t G(s)J(t-s)ds \quad (2-51)$$

This *convolution integral* expresses the relationship between the creep compliance and the stress relaxation modulus. It is exact and depends only on the applicability of the Boltzmann superposition principle.

38 PHENOMENOLOGICAL TREATMENT OF VISCOELASTICITY

These equations are used to convert a modulus to compliance in problem 6 of this chapter. The results of this calculation are depicted in Figure 2-16. In dealing with experimental results, the modulus is often available only as a set of discrete data gathered over a finite time interval. In this case, the transformation to a similar set of predicted creep data is a difficult numerical problem that can result in substantial errors.^{8,9} Commercial software packages are available that can do this and other "integral" transforms, but these should all be used with caution. A simplified example is suggested in problem 14.

APPENDIX 2: BOREL'S THEOREM

Consider the two functions $F_1(t)$ and $F_2(t)$ whose Laplace transforms are given as $f_1(p)$ and $f_2(p)$ respectively. Then the product

$$f_1(p)f_2(p) = \int_0^\infty F_1(T)e^{-pT} \int_0^\infty e^{-pt} F_2(t)dt dT \quad (a)$$

if

$$F_2(t) = 0 \quad t < 0 \quad (b)$$

However, application of equation (g) in Appendix 1 yields

$$f_1(p)f_2(p) = \int_0^\infty F_1(T) \int_0^\infty e^{-pt} F_2(t-T)dt dT \quad (c)$$

Upon rearrangement we get

$$f_1(p)f_2(p) = \int_0^\infty e^{-pt} \int_0^\infty F_2(T)F_2(t-T)dt dT \quad (d)$$

Applying condition (b) yields the desired result

$$f_1(p)f_2(p) = L \left[\int_0^\infty F_1(T)F_2(t-T)dt \right] \quad (e)$$

APPENDIX 3: GEOMETRIES FOR THE MEASUREMENT OF VISCOELASTIC FUNCTIONS

1. Axial Geometries

The geometries commonly used for measurements in instruments generating a linear or axial motion are listed in Table 2-1. With the exception of the shear sandwich, all require a solid sample. The drawings and associated formula

apply to the step-strain stress relaxation test wherein the sample is subjected to an instantaneous small displacement Δx . For a dynamic experiment, the Δx should be replaced by the amplitude of the oscillatory displacement, while the force should be replaced by the amplitude of the oscillatory force. Introduction of the phase angle will then give the real and imaginary components of the complex modulus. For example, for simple tension

$$E = \frac{L}{wd} \left(\frac{F}{\Delta x} \right) \rightarrow |E^*| = \frac{L}{wd} \left(\frac{F_{mag}}{\Delta x_{mag}} \right) \quad (a)$$

and

$$E' = |E^*| \cos \delta \quad (b)$$

$$E'' = |E^*| \sin \delta \quad (c)$$

where $|E^*|$ is the magnitude of the complex dynamic modulus.

Simple extension or compression of a rod or strip serves to define the Young's modulus. While straightforward in appearance, this geometry has experimental difficulties that may require several precautions and corrections. For example, the tensile sample may be difficult to grip without inducing locally high stresses or slippage. Thus, careful work requires that the deformation ϵ be measured separately from the motion of the grips that apply the force to the sample. Often deformation is measured with an optical gauge or a clip-on extensometer. Another approach is to use samples of different lengths and extrapolate the observed moduli to infinite length. At nonambient temperatures, variation of temperature along a long sample may be difficult to eliminate. As with most axial geometries, it is necessary to provide a preload of the sample for dynamic measurements to prevent buckling.

For stiff specimens, conveniently large displacements can be realized by using a bending mode. Shown in Table 2-1 are several bending geometries, all of which have certain advantages. Before discussing these, it should be pointed out that the bending of sample results in a spatially nonuniform stress. The highest stress is at the concave and convex surfaces of the specimen, while it is zero at the centroid of the cross-section. This means that the outside layers of the sample have a disproportionately large effect on the resulting modulus. While this is not an issue with perfectly homogeneous samples, it is common for molded specimens to have a skin that is quite different from the core. A skin effect can be used to advantage to examine, say, degradation of the outside surface.

In choosing among the bending modes, the important factors are the stiffness and size of the specimen and the amount of displacement that is needed to produce a workable force signal. If the sample is short and thick, it is probably best to choose the single cantilever geometry, because it will give the most displacement for the least force.*** At the other extreme is the double cantilever, which consequently would be the most appropriate for thinner and/or more flexible samples. For the latter, it is important to note that the geometry is over determined if both of the clamps are rigidly fixed to the instrument frame. While this is not an issue at very low displacements, it should be corrected for at higher displacements. It also should be recognized that all the bending modes subject the sample to shear as well as bending. (The center part of the 4-point bending mode is pure bending, but the ends are subjected to shear.) Shearing of the sample leads to artificially low modulus values, although the effect is negligible if the sample thickness and displacements are low relative to the length of the sample. Corrections for shear are also available.

As mentioned the 4-point bending experiment is special in that the center section is subjected to pure bending that is constant along this section. As the bottom surface of material in this section is under the greatest tensile stress, the sample is likely to fail somewhere in this region. Thus the 4-point geometry can provide a method of testing the ultimate mechanical properties of uniform brittle materials as well as a method for measuring the modulus. This combination is difficult to achieve in other geometries.

On examination of the bending formulas, it should be apparent that the accuracy of the modulus is highly dependent on the accuracy of the samples length and thickness measurements. A 3% error in either of these dimensions will give a 10% error in the modulus. Interestingly, the strong influence of the length measurement is alleviated by the bending geometry shown in Table 2-2.

The shear sandwich is widely used for generating shearing motion in soft or even fluid samples. Clearly the amount of strain is limited, and this geometry is thus not generally suitable for gaining information on the steady-state flow properties of fluids, although it useful for transient measurements that approach the steady state. It is highly important that the flat plates be strictly parallel, as misaligned plates will generate very high squeezing forces that lead to artificially high modulus values. With fluids, the gap should be small enough to hold the fluid in place by capillary forces.

The compression mode has been used successfully for soft samples that can be accurately made with strictly parallel faces on the top and bottom of the

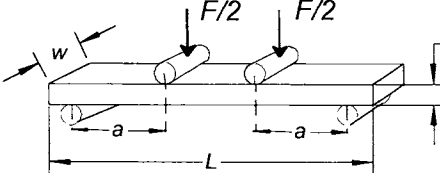
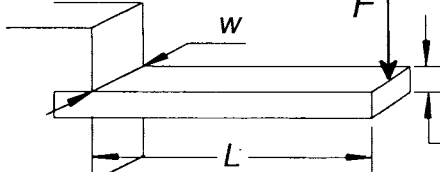
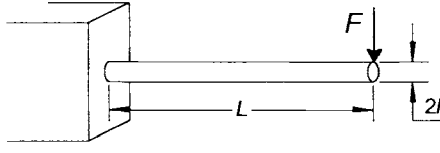
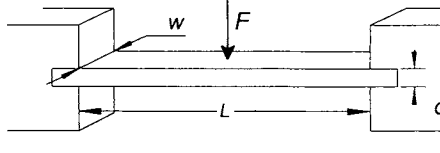
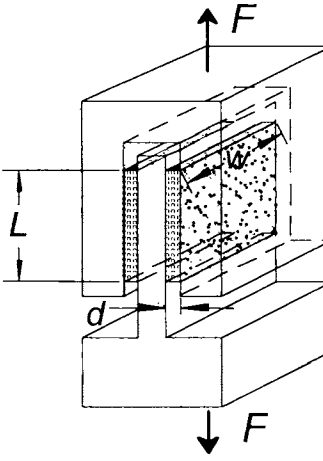
*** Samples of low length/height ratio may deform considerably due to shear, invalidating the results obtained with the equations that assume bending is the major source of deformation.

sample. To prevent buckling, the sample must have a modest height relative to its width. The penalty for this condition is that the state of the boundary at the sample/plate interface has an extraordinarily large influence on the measured modulus value. Not only must the faces be smooth and parallel, but also they must be either treated to eliminate slip, or to induce complete slip. The former can be realized by using an adhesive, selecting one that does not influence the properties of the sample, or roughened surfaces. Complete slip requires very smooth surfaces treated to reduce the coefficient of friction. For example, Teflon®-coated plates used in conjunction with a compatible lubricant have found to be effective.¹⁰

Table 2-1 Test Geometries for Instruments that Generate Axial (Linear) Motion

Simple extension		$E = \frac{L}{wd} \left(\frac{F}{\Delta x} \right)$ $\varepsilon = \frac{\Delta x}{L}$
Compression		$E = \frac{L}{\pi R^2} \left(\frac{F}{\Delta x} \right)$ for complete slip $\varepsilon = \frac{-\Delta x}{L}$
3-point bending		$E = \frac{L^3}{4wd^3} \left(\frac{F}{\Delta x} \right)$ $\varepsilon_{\max} = 6 \frac{d}{L} \left(\frac{\Delta x}{L} \right)$

42 PHENOMENOLOGICAL TREATMENT OF VISCOELASTICITY

4-point bending		$E = \frac{a^2(3L - 4a)}{wd^3} \left(\frac{F}{\Delta x}\right)$ $\varepsilon_{\max} = 3 \frac{d}{a(2 - 4a/L)} \left(\frac{\Delta x}{L}\right)$
Single cantilever (Slab)		$E = \frac{4L^3}{wd^3} \left(\frac{F}{\Delta x}\right)$ $\varepsilon_{\max} = \frac{3}{2} \frac{d}{L} \left(\frac{\Delta x}{L}\right)$
Single cantilever (Rod)		$E = \frac{4L^3}{3\pi R^4} \left(\frac{F}{\Delta x}\right)$ $\varepsilon_{\max} = 3 \frac{R}{L} \left(\frac{\Delta x}{L}\right)$
Double cantilever		$E = \frac{L^3}{16wd^3} \left(\frac{F}{\Delta x}\right)$ $\varepsilon_{\max} = 12 \frac{d}{L} \left(\frac{\Delta x}{L}\right)$
Shear sandwich		$G = \frac{d}{2wL} \left(\frac{F}{\Delta x}\right)$ $\gamma = \frac{\Delta x}{d}$

2. Rotational Geometries

The test geometries listed in Table 2-2 are those commonly used for instruments that can apply rotary motion, either in the form of a controlled torque or a controlled amount of rotation. The listed examples can as a set handle samples from stiff viscoelastic solids to freely flowing liquids. All are

suitable for low-strain transient or dynamic experiments, whereas the parallel-plate, cone and plate and concentric rotating cylinders can also be used for steady shearing measurements as well. Rotation does not lend itself easily to the application of tensile or compressive deformations, but one example—the bending geometry—can provide a direct measure of Young's modulus.

Solid viscoelastic samples can be tested in shear using rods or strips that are twisted by the instrument. The torque, M , is then directly proportional to the shear modulus and amount of twist Ω (in radians) with a proportionality factor that is purely dependent upon the geometry of the sample. Note that unlike the bending of bars and rods, the geometric factor is only linearly dependent on the sample length. However, the dependence on the sample thickness is exactly the same. This provides the experimentalist with an opportunity for measuring Poisson's ratio by dividing the obtained Young's modulus from bending by the shear modulus from twisting the exact same sample. This will result in cancellation of errors in the sample thickness (but not length). For example, with rods, the ratio of the two is:

$$\frac{E/G}{G} = \frac{\frac{4L^3}{3\pi R^4} \left(\frac{F}{\Delta x} \right)}{\frac{2ML}{\pi R^4 \Omega}} = \frac{2}{3} \frac{\Omega L}{\Delta x} \frac{FL}{M} = 2(1 + \nu), \quad (d)$$

where ν is Poisson's ratio. Note that the radius of the sample no longer appears. Implied by this cancellation is the concomitant cancellation of slight radial material variations.

Twisting of bars or strips has been studied throughout the years because of its practical importance. Normally bars and strips are also the simplest sample to fabricate. The formulas given are for very small amounts of twist, and with no axial load. Clamps that cannot move at all in the axial direction may exert significant axial loads on the sample once the twist is applied. Depending upon the properties of the sample, this can increase the apparent torque significantly and result in an excessively high modulus. Corrections are available. Interestingly, while the maximum strain on twisting a cylindrical rod is at the outer surface, the outer corners of a twisted bar or strip have no strain at all.

Flex tests on rotational equipment can be run on the geometry indicated in Table 2-2. While this fixture may not be provided with commercial instruments, it is easy to build. The remarkable aspect of this geometry for flex testing is that the length of the sample enters only to the first power instead of the third power of the usual flex test. This means that one can be a bit less fastidious about the length and still get good results. The sample's width and thickness still enter in the same fashion, however.

44 PHENOMENOLOGICAL TREATMENT OF VISCOELASTICITY

The plate-plate, cone and plate and Couette geometries are appropriate for very soft solids, e.g., gels or viscoelastic liquids. The selection between these depends on several factors, including the consistency of the sample and the amount of sample available. Of the three, the Couette geometry requires the most sample and is the hardest to load, but is the most sensitive for low stiffness samples and has the lowest dependence on the spatial dimensions of the fixture. It has the additional feature that the highest stress is uniquely at the surface of the inner cylinder. The plate-plate or parallel plate (disc) geometry requires the smallest amount of material, as the gap can be made indefinitely thin. For example, a 0.05-mm gap with 25-mm-diameter plates requires only 25 mm³ of sample (about 25 mg). However, the modulus depends heavily (4th power) on the radius of the sample, which means that the sample must be very carefully prepared. In contrast, the cone and plate result depends only on the 3rd power. The additional advantage of the cone and plate geometry is that the deformation in the sample is spatially uniform. Although this is important only for nonlinear properties of the materials, it implies that the results may be less sensitive to slight nonlinearities found at workable angles of twist. In the plate-plate geometry, the highest strain and stress are at the outside edge where the influence of any nonlinearity in the sample is magnified for two reasons: (1) the area of sample for a fixed differential radial amount is greatest and (2) the lever arm for this outside ring is greatest. In spite of these drawbacks, the parallel plate fixtures are perhaps the most popular for linear viscoelastic measurements because they are easy to load, gap and clean, inexpensive to make (disposable plates are available), and the flat surfaces are convenient for optical or dielectric measurements. A first-order correction for nonlinear effects is provided in the table.

Links to representative suppliers of commercial equipment, both axial and rotational are listed at www.rheology.org.⁷

Table 2-2. Geometries for Instruments that Generate Rotational Motion

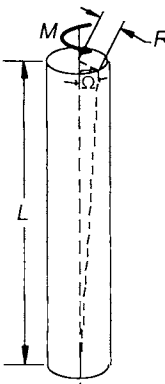
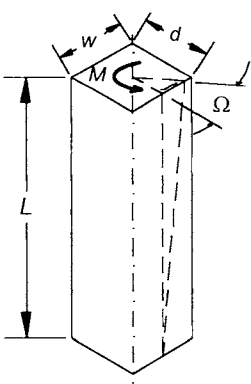
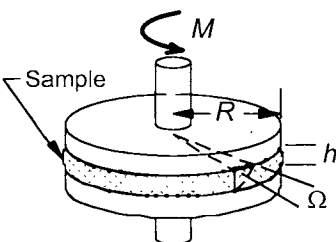
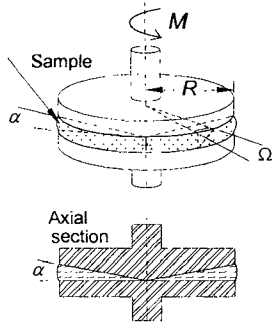
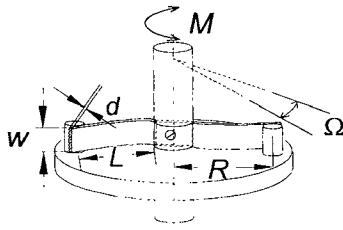
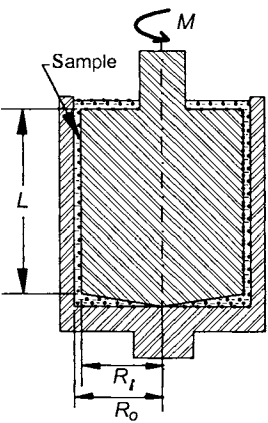
Rod		$G = \frac{2ML}{\pi R^4 \Omega}$ $\gamma_{\max} = R\Omega / L$ <p>(For $G(\gamma)$, a good approximation is to assign the modulus given above to a strain of $3R\Omega/4L$ instead of γ_{\max}).¹¹</p>
Bar or strip		$G = \frac{ML}{\Omega w d^3 \frac{1}{3} (1 - 0.63d/w)}$ $\gamma_{\max} = d\Omega / L$ <p>An elastic formula to higher order has been reported:¹²</p> $G = \frac{ML}{\Omega w d^3 \frac{1}{3} \left[(1 - 0.63 \left(\frac{d}{w} \right)) + \frac{1}{120} \frac{E w^3}{G d L^2} \Omega^2 \right]}$
Parallel plates (aka: plate-plate, parallel disks)		$G = \frac{2Mh}{\pi R^4 \Omega}$ $\gamma_{\max} = R\Omega / h$ $\eta = \frac{2Mh}{\pi R^4 \omega} \text{ for steady shear at angular velocity } \omega = d\Omega/dt,$ <p>(see "Rod" for approximation to nonlinear properties)</p>

Table 2-2. (Continued)

Cone and Plate		$G = \frac{3M\alpha}{2\pi R^3 \Omega}$ $\gamma = \Omega/\alpha$
Bending		$E = \frac{2L}{wd^3} \left(\frac{M}{\Omega} \right)$ $\varepsilon_{\max} = \frac{3d}{2L} \Omega$
Cup and Bob (aka: Couette, circular Couette)		$G = \frac{M}{4\pi L \Omega} \left[\frac{1}{R_i^2} - \frac{1}{R_o^2} \right]$ $\gamma = 2\Omega \left[1 - \frac{R_i^2}{R_o^2} \right]$ <p>Ω = amount of twist, rad</p> <p>(Does not include small contribution from bottom or top surfaces.)</p>

PROBLEMS

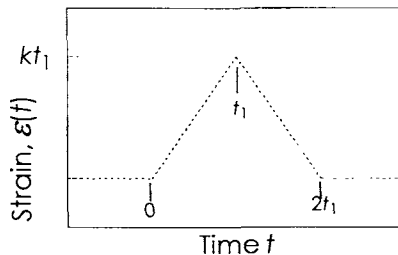
1. Calculate the weight needed to bring about a 0.40-cm shearing displacement ΔX , of a viscoelastic cube 2 cm on a side after 10^{-4} , 10^{-2} , 10^0 , 10^4 , and 10^6 seconds. The time-dependent shear compliance is

$$J(t) = \left(10^{-9} + \frac{t}{10^9} \right) \text{ Pa}^{-1}$$

2. Make a table expressing J' , J'' , $\tan \delta$, $|J^*|$, $|G^*|$, G' and G'' in terms of (a) G' and G'' , (b) J' , J'' , (c) $|G^*|$ and $\tan \delta$, and (d) $|J^*|$ and $\tan \delta$.
3. Calculate the stress at time t longer than $2t_1$ in a body with a relaxation modulus given by

$$E(t) = E_1 e^{-t/\tau_1} + E_2 e^{-t/\tau_2}$$

when the body is subjected to the strain history depicted in the drawing below.



4. By considering a sinusoidal stress applied to a viscoelastic body, show that in-phase strain results in conservation of energy (work) whereas out-of-phase strain results in energy dissipation.

5. Show that

$$J(t) = \frac{\sin m\pi}{m\pi} \frac{1}{G(t)}$$

if $\log J(t) = \log A + m \log t$. Note $\Gamma(n) = \pi / \sin(n\pi)$, where $\Gamma(n)$ is the gamma function defined as

$$\int_0^\infty x^{n-1} e^{-x} dx \equiv \Gamma(n) \quad \text{and} \quad \Gamma(n) = (n-1)! \quad \text{for } n > 0$$

6. Calculate the creep compliance for a body whose stress relaxation modulus is given by

$$G(t) = G_0 e^{-t/\tau}$$

7. Calculate $G'(\omega)$ and $G''(\omega)$ for a body whose stress relaxation modulus is given by the expression

$$G(t) = G_0 e^{-t/\tau}$$

8. The strain in a dynamic shear experiment may be represented as

$$\gamma^* = \gamma_0 e^{i\omega t}$$

48 PHENOMENOLOGICAL TREATMENT OF VISCOELASTICITY

Since, in general, the stress will lead the strain, the corresponding function for the stress is

$$\sigma^* = \sigma_0 e^{i(\omega t + \delta)}$$

Obtain expressions for $G'(\omega)$ and $G''(\omega)$ using this formalism.

9. The behavior of viscoelastic materials subjected to oscillatory perturbations may also be treated by generalizing the concept of viscosity (rather than modulus) and separating it into in-phase and out-of-phase components. Thus Newton's law for viscous fluids in shear, defined in equation (3-4) in Chapter 3, Section A, becomes

$$\sigma^* = \eta^* \frac{d\gamma^*}{dt}$$

where $\eta^* = \eta' - i\eta''$. Here η' measures energy dissipation, and η'' measures stored energy. In this formalism, show that

$$\eta'(\omega) = \frac{G''(\omega)}{\omega} \quad \text{and} \quad \eta''(\omega) = \frac{G'(\omega)}{\omega}$$

10. Show that the form of the Boltzmann principle given in equation (2-45) reverts to the defining equation for the shear creep compliance, equation (2-9), when a sample, initially at rest, is subjected to an instantaneous increment of stress at $t = 0$, which is thereafter held constant.

It may be helpful to note that the Dirac delta function $\delta(a)$ can be defined as

$$f(x) = \int_{-\infty}^{\infty} \delta(x - x') f(x') dx'$$

That is, it has unit area when $a = 0$ and is zero everywhere else.

11. Stress-strain curves are often measured by monitoring the tensile stress as a sample, originally at rest, is subjected to a constant tensile strain *rate* starting at $t = 0$. Show that, at any subsequent time during the constant-strain-rate period, the slope of the stress-strain curve is the tensile stress relaxation modulus:

$$E(t) = \frac{d\sigma_E}{d\varepsilon}$$

12. Suppose that a material with a tensile stress relaxation modulus given as

$$E(t) = E_0 e^{-t/\tau}$$

is used in an ordinary stress relaxation experiment starting at $t = 0$ and employing a constant strain ε_0 . At some later time, t' , the stress is suddenly removed. Show that the strain at times greater than t' is

$$\varepsilon(t) = \varepsilon_0 \left(1 - e^{-(t-t')/\tau} \right)$$

13. (Computer) The approximation

$$G(t) \approx G'(\omega) - 0.566G''(\omega/2) + 0.203G''(\omega)$$

with $\omega = 1/t$ has been proposed for converting dynamic data to stress-relaxation modulus.¹³ Quantify the error incurred through the use of this approximation for the relaxation modulus

$$G(t) = G_0 e^{-t/\tau}$$

14. (Computer) Using a spread sheet with numerical integration and differentiation capabilities, attempt to convert discrete creep data created using the equation

$$J(t) = \left(10^{-9} + \frac{t}{10^9} \right) \text{ Pa}^{-1}$$

to the corresponding stress relaxation modulus data. Check your result against the analytical prediction. (*Hint:* Divide the integral of equation (2-51) into small steps and, starting with the first step over a range Δt , use the trapazoidal rule to integrate this step. Repeat with the next step to establish a pattern. Then set up a spread sheet with J_i and $\Delta J_i = J_i - J_{i-1}$. Starting at $G_0 = G(0) = 1/J_0$, calculate G_1 , etc.)

15. (a) Show that the shear strain in the parallel-plate geometry (Table 2-2) is given by $\gamma(r) = r\Omega/h$. (b) Develop the expression for the torque M , given the shear modulus G . (c) If $G = G(\gamma)$, develop an integral expression for the torque. (c) Show that Gauss's moment integration formula (see p. 921, *Handbook of Mathematical Functions*¹⁴) will give the approximation listed in Table 2-2 under "Rod."

16. Tensile machines often operate at constant velocity, which means that the length of a sample of initial length L_0 long will follow the program $L = L_0 + vt$, where v is the crosshead velocity. Develop an expression for the error in the Young's modulus as derived from the initial slope of the stress-strain curve from such a machine assuming a viscoelastic material with a relaxation modulus given by $E = E_0 \exp(-t/\tau)$.

17. Design a continuous two-dimensional structure that will, on stretching, expand in the transverse direction, as depicted in Figure 2-8.

18. The infinitesimal material elements in the sharp corners of a solid rectangular bar are not strained when the bar is twisted by a small amount. Where then, is the location of the material elements that experience the highest shear strain γ_{\max} ? (*Hint:* Examine the equation in Table 2-2 for twisting of bars.)

19. (Computer) The following exercises use the dynamic modulus (G' and G'') data in file PMMA45.TXT in the CD.

- (a) Plot the data using log-log and linear-linear scales, and comment on the appearance of each.

50 PHENOMENOLOGICAL TREATMENT OF VISCOELASTICITY

(b) Calculate and plot the magnitude of the complex viscosity $|\eta^*|$ as a function of frequency using log-log scales. Estimate the zero-shear-rate viscosity η_0 where $\eta_0 = |\eta^*|(\omega \rightarrow 0)$.

(c) Create a Cole-Cole plot using this data (see index).

REFERENCES

1. L. Malvern, *Introduction to the Mechanics of a Continuous Medium*, Prentice-Hall, New York, 1969.
2. J. D. Ferry, *Viscoelastic Properties of Polymers*, 3rd ed., Wiley, New York, 1980.
3. A. V. Tobolsky, *Properties and Structure of Polymers*, Wiley, New York, 1960.
4. F. R. Schwarzl, "Viscoelasticity," in *Encyclopedia of Polymer Science and Engineering*, Vol. 17, (H. F. Mark, N. M. Bikales, C. G. Overberger, G. Menges and J. I. Kroschwitz, eds.) Wiley-Interscience, New York, 1989, pp. 587-665.
5. N. W. Tschoegl *The Phenomenological Theory of Linear Viscoelastic Behavior: An Introduction*, Springer-Verlag, New York, 1989.
6. P. D. Griswold, R. S. Porter, R. J. Farris, C. R. Desper, *Polym. Eng. Sci.*, **18**, 537 (1978).
7. See, for example, atsrheosystems.com; bohlinusa.com; brookfieldengineering.com; goettfert.com; haake.de; rheosci.com; tainst.com; paarphysica.com; reologicainstruments. com. The website rheology.org may have links to other sources.
8. S. Goldman, *Transformation Calculus and Electrical Transients*, Prentice-Hall, New York, 1949.
9. I. L. Hopkins and R. W. Hamming *J. Appl. Phys.*, **28**, 906 (1957).
10. E. B. Bagley and D. D. Christianson, *J. Rheol.* **32**, 555-573 (1988).
11. G. V. Gordon and M. Shaw, *Computer Programs for Rheologists*, Hanser Publishers, Munich, 1994, pp. 149-187.
12. Y. Inoue, and Y. Kopabatake, *Kolloid Z.* **159** 18 (1958).
13. F. R. Schwarzl, in *Deformation and Fracture of High Polymers*, H. H. Kausch, J. A. Hassell and R. I. Jaffee, eds, Plenum Press, New York, 1973, pp. 47-70.
14. M. Abramowitz and I. A. Stegun, Eds., *Handbook of Mathematical Functions with Formulas, Graphs and Mathematical Tables*, Dover, New York, 1972.

3

Viscoelastic Models

The phenomenological theory of linear viscoelasticity developed in Chapter 2 is completely independent of the structural details of the material being deformed. The material could be anything that is uniform and isotropic, be it a polymer, metal, biological tissue, or clay. As our focus is polymers, it is desirable to consider the representation of linear viscoelastic processes by certain model systems in order to gain greater insight into relaxation behavior and eventually its relationship to structure. In this chapter we consider two broad classes of models. The first consists of the so-called "mechanical analogs." These are combinations of elements, usually springs and dashpots, that more or less faithfully reproduce the qualitative aspects of the viscoelastic response of real systems. The second group is composed of the molecular theories. Here a fairly reasonable representation of a polymer molecule is assumed and the motion of such a molecule in a viscous medium is deduced. In this case the viscoelastic behavior is predicted on the basis of molecular parameters. It will be demonstrated that the two classes of models are equivalent in many respects.

A. MECHANICAL ELEMENTS

We return to the tensile elongation experiment described in the Introduction and Chapter 2. The simplest mechanical model that has some of the gross physical behavior exhibited by bodies subject to uniaxial elongation is a pure Hookean spring (Figure 3-1a). This body is purely elastic and all inertial effects are neglected. If a Hookean spring is stretched by a fixed amount, it will produce a force that is proportional to the stretch. By analogy, if a

52 VISCOELASTIC MODELS

Hookean elastic material is subjected to an instantaneous strain ε_0 , it will produce instantaneously a stress σ_0 related to by the equation

$$\sigma_0 = E\varepsilon_0 \quad (3-1)$$

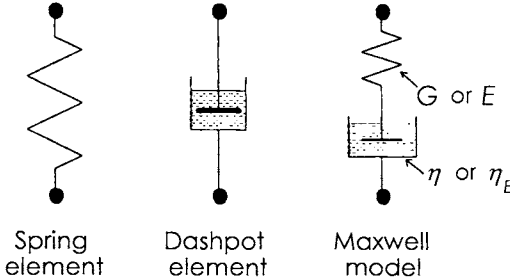


Figure 3-1. Spring, dashpot, and Maxwell model. In subsequent depictions of the dashpot, the "fluid" will be removed for simplicity.

The proportionality constant, E , is the Young's modulus with which we are already acquainted. The instantaneous strain application is assumed to produce no oscillation, only a constant stress. Note that the comparison of the Hookean spring with the Hookean elastic solid is useful only as a mathematical analogy; we don't expect, for example, to shear the coil spring depicted in Figure 3-1, although we can certainly shear a three-dimensional Hookean elastic solid. While no actual substances obey Hooke's law exactly, some materials, such as steel and glass, follow Hooke's law very closely at low values of stress and strain. All real materials have inertial effects, and most have at least slight time dependence, which Hooke's law does not address.

The dominant characteristic of fluids, on the other hand, is not their elasticity, but rather their viscosity. The equation of motion for simple linear viscous flow is Newton's law

$$\tau_{ij} = \eta \left(\frac{dv_i}{dx_j} + \frac{dv_j}{dx_i} \right) \quad (3-2a)$$

$$\sigma_{21} = \tau_{21} = \eta \frac{dv_1}{dx_2} = \eta \dot{\gamma} \quad (3-2b)$$

$$\sigma_{11} - \sigma_{22} = 3\eta \frac{dv_1}{dx_1} \quad \text{or} \quad \sigma_E = \eta_E \frac{d\varepsilon}{dt} = \eta_E \dot{\varepsilon} \quad (3-2c)$$

where the general three-dimensional form in (3-2a) is analogous to equations (2-14) and (2-18) for Hooke's law but with displacement u_i replaced by

velocity v_i . The symbol η stands for the shear viscosity, and is constant for Newtonian fluids. The variant in equation (3-2b) is for simple shear, and introduces the symbol $\dot{\gamma}$ for shear rate. Equation (3-2c) shows the form for simple extension, and defines the extensional viscosity η_E . Clearly $\eta_E = 3\eta$, and for the same reason that $E = 3G$. At low strains, the tensile strain ε is the same as for Hooke's law, equations (2-2) and (2-19). On the other hand, to maintain the relationship $\dot{\varepsilon} = dv_1/dx_1$ at higher strains, we must redefine strain as $\varepsilon = \ln(L/L_0)$, where L is the length of the specimen and L_0 is its initial length. This is referred to as the Hencky strain. At low strains, the two are equivalent (see Problem 16).

The mechanical analog of equation (3-2) is the dashpot element (Figure 3-1). This is merely a leaky piston in a cylinder filled with a liquid of viscosity η for shear or η_E for extension. (Remember, the details of geometry, etc. are not important; we are looking only for qualitative behavior by analogy. Thus we will use the models of Figure 3-1 for both extensional and shear properties.) Integration of equation (3-2b) for constant shear stress σ_0 , yields

$$\gamma(t) = \frac{\sigma_0}{\eta} t \quad (3-3)$$

Thus, subjecting the dashpot to a stress of $10\sigma_0$ for time t produces the same strain as a stress of σ_0 applied for a time $10t$.

The general expression for rate of deformation that is analogous to equation (2-17) for deformation is not surprisingly

$$\dot{\gamma}_{ij} = \frac{dv_i}{dx_j} + \frac{dv_j}{dx_i} \quad (3-4)$$

Some conventions based on equation (3-4) include the use of $\dot{\gamma} = \dot{\gamma}_{21} = dv_1/dv_2$ for shear rate, and the symbol $\dot{\varepsilon} = dv_1/dx_1$ for rate of extension. Note that $\dot{\varepsilon} \neq \dot{\gamma}_{11}$.

1. Maxwell Model

The mechanical response of viscoelastic bodies such as polymers is poorly represented by either the spring or the dashpot. J. C. Maxwell suggested that a better approximation would result from a series combination of the spring and dashpot elements. Such a model, called a Maxwell element, is shown on the right in Figure 3-1. In describing tensile response with the Maxwell element, E , the instantaneous tensile modulus, characterizes the response of the spring while η_E , the viscosity of the liquid in the dashpot, defines the viscous

54 VISCOELASTIC MODELS

behavior. The ratio of η_E to E or η to G defines a time constant τ in the following manner

$$\eta_E = \tau E \quad \text{or} \quad \eta = \tau G \quad (3-5)$$

The time constant τ is often called the relaxation time of the element. The equation of motion of the Maxwell model is

$$\frac{d\varepsilon}{dt} = \frac{1}{E} \frac{d\sigma_E}{dt} + \frac{\sigma_E}{\eta_E} \quad \text{or} \quad \frac{d\gamma}{dt} = \frac{1}{G} \frac{d\sigma}{dt} + \frac{\sigma}{\eta} \quad (3-6)$$

where σ_E is used for the tensile stress and σ without a subscript stands for the shear stress. Equation (3-6) is merely a linear combination of the deformation rates of the perfectly elastic behavior as stated in the time derivative of Hooke's law (first term on right side) and perfectly viscous behavior as stated in Newton's law (second term on right side).

We will now solve this differential equation subject to several sets of experimental boundary conditions. Extensional deformations will be used in these examples, but they could also be done equally well for shear.

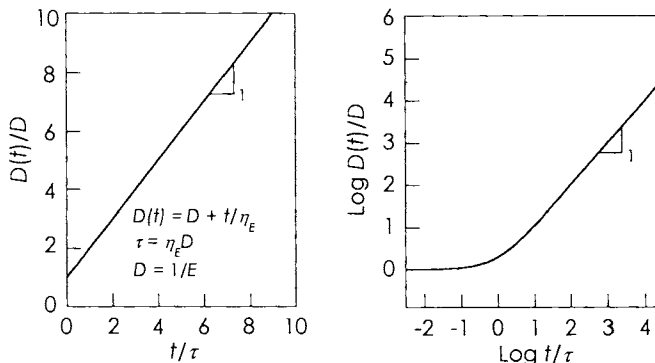


Figure 3-2. Creep response of a Maxwell body displayed using linear (left) and log-log (right) scales.

Creep Experiment. The model is subjected to an instantaneous tensile stress $\sigma_{E,0}$, which is then held constant. Thus equation (3-6) becomes

$$\frac{d\varepsilon}{dt} = \frac{\sigma_{E,0}}{\eta_E} \quad (3-7)$$

since $d\sigma_E/dt$ is zero. Integration of equation (3-7) from time 0 to some time t yields, after division by σ_0 ,

$$\frac{\varepsilon(t)}{\sigma_{E,0}} = \frac{\varepsilon_0}{\sigma_{E,0}} + \frac{t}{\eta_E} \quad (3-8)$$

One notices that $\varepsilon_0/\sigma_{E,0}$ is just the instantaneous response of the Hookean spring, and from equation (3-1) it is seen to be equal to the reciprocal of E . From the results of Chapter 2, Section A, we have

$$D = \frac{1}{E} = \frac{\varepsilon_0}{\sigma_{E,0}} \quad (3-9)$$

where D is the tensile compliance of the spring unit of the model.

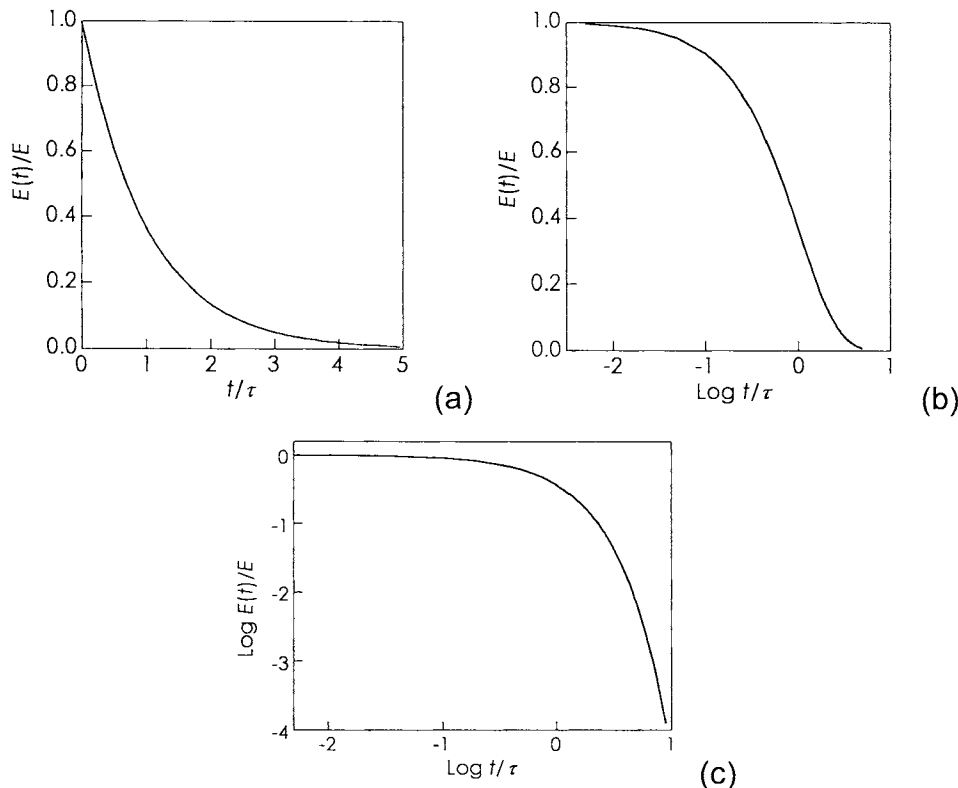


Figure 3-3. Maxwell body behavior using stress relaxation conditions: (a) linear plot, (b) linear-log plot, and (c) log-log plot.

Also from the results of Chapter 2, Section A, it is clear that the left side of equation (3-8) is simply the tensile creep compliance, $D(t)$. Thus the response of the Maxwell model to a creep experiment is

$$D(t) = D + \frac{t}{\eta_E} \quad (3-10)$$

This is illustrated in Figure 3-2. Note that the compliance of the Maxwell model increases without limit as time goes on, a behavior characteristic of a viscoelastic fluid.

Stress Relaxation Experiment. In a stress relaxation experiment, one strains the sample instantaneously to some strain ε_0 and studies the stress $\sigma_E(t)$ necessary to maintain this constant strain (Chapter 2, Section C). The instantaneous strain will be realized only in the spring element. The dashpot will gradually relax so that the stress decreases as a function of time.

After the strain application, $d\varepsilon/dt$ is zero so equation (3-6) becomes, in light of equation (3-5),

$$\frac{d\sigma_E}{\sigma_E} = -\frac{dt}{\tau} \quad (3-11)$$

This expression is easily integrated from $\sigma_{E,0}$ at time 0 to $\sigma(t)$ at time t to give

$$\ln \sigma_E(t) = \ln \sigma_{E,0} - \frac{t}{\tau} \quad (3-12)$$

Exponentiation and division by ε_0 yields

$$\frac{\sigma_E(t)}{\varepsilon_0} = \frac{\sigma_{E,0}}{\varepsilon_0} e^{-t/\tau} \quad (3-13)$$

Here again, $\sigma_{E,0}/\varepsilon_0$ is the modulus of the spring, E , and the left side of equation (3-13) is $E(t)$, the tensile stress relaxation modulus.

$$E(t) = E e^{-t/\tau} \quad (3-14)$$

Note that the stress relaxation behavior is exponential in time. Now the value of a model is evident: we learn that the mark of a viscoelastic fluid in a stress-relaxation experiment is exponential decay of the stress.

Figures 3-3 illustrate the behavior of the Maxwell model in a stress-relaxation experiment. Note that these functions have been plotted on log scales as well as the usual rectilinear scales. At times considerably shorter than the relaxation time of the spring/dashpot combination, the element behaves as if it were a spring alone. At times very long compared to the relaxation time of the dashpot, the model behaves as if it were a dashpot alone, that is, the stress

decays to zero. At times comparable to the relaxation time, the response involves both the spring and the dashpot.

Dynamic Experiments. We will now consider the response of a Maxwell element subjected to a sinusoidal stress, as in a controlled-stress dynamic mechanical analyzer. In such a case the strain will also be sinusoidal but out of phase with the stress by the angle δ , as discussed in Chapter 2. Thus

$$\sigma_E(t) = \sigma_{E,0} e^{i\omega t} \quad (3-15)$$

where $\sigma_{E,0}$ is the amplitude of the stress and ω is the frequency (rad/s). Substitution into equation (3-6) yields

$$\frac{d\varepsilon(t)}{dt} = \frac{\sigma_{E,0}}{E} i\omega e^{i\omega t} + \frac{\sigma_{E,0}}{\eta_E} e^{i\omega t} \quad (3-16)$$

which is easily integrated using the limits of $\varepsilon(t_1)$ at t_1 and $\varepsilon(t_2)$ at t_2 . (Note that ε_0 is not necessarily zero because the stress and strain are not in phase.)

$$\varepsilon(t_2) - \varepsilon(t_1) = \frac{\sigma_{E,0}}{E} (e^{i\omega t_2} - e^{i\omega t_1}) + \frac{\sigma_{E,0}}{\eta_E i\omega} (e^{i\omega t_2} - e^{i\omega t_1}) \quad (3-17)$$

Division of the strain increment by the stress increment yields:

$$\frac{\varepsilon(t_2) - \varepsilon(t_1)}{\sigma_E(t_2) - \sigma_E(t_1)} = D^* = D - i \frac{D}{\tau\omega} \quad (3-18)$$

where D^* is the complex tensile compliance defined as $D^* = D' - iD''$ and $D = 1/E$. Thus in terms of storage and loss compliances (Chapter 2),

$$D' = D \quad \text{and} \quad D'' = \frac{D}{\tau\omega} = \frac{1}{\eta_E \omega} \quad (3-19)$$

From this point, the calculation of the complex tensile modulus, E^* , is straightforward. From Chapter 2, Section C, it will be remembered that E^* is the reciprocal of D^* , so we have

$$E^* = \frac{1}{D - iD/\tau\omega} = \frac{\tau\omega E}{\tau\omega - i} \quad (3-20)$$

Use of the complex conjugate gives

58 VISCOELASTIC MODELS

$$E^* = \frac{E\tau^2\omega^2}{1+\omega^2\tau^2} + \frac{i\tau\omega E}{1+\omega^2\tau^2} = E' + iE'' \quad (3-21)$$

so

$$E' = \frac{E\tau^2\omega^2}{1+\omega^2\tau^2} \quad (3-22)$$

and

$$E'' = \frac{E\tau\omega}{1+\omega^2\tau^2} \quad (3-23)$$

The tangent of the phase angle between the stress and strain was shown to be (Chapter 2, Section C):

$$\tan \delta = \frac{E''}{E'} \quad (3-24)$$

giving

$$\tan \delta = \frac{1}{\tau\omega} \quad (3-25)$$

for a Maxwell body. Figure 3-4 represents the frequency dependence of E' and E'' for a Maxwell element.

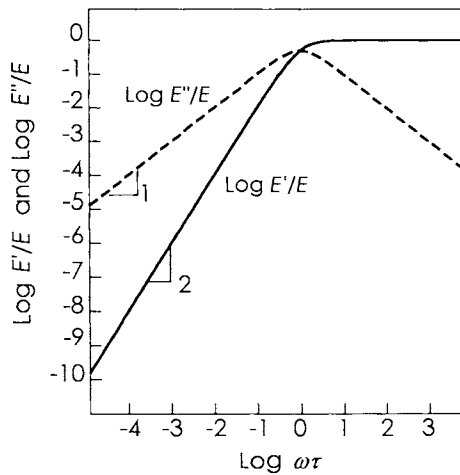


Figure 3-4. Log-log plots of $E'(\omega)/E$ and $E''(\omega)/E$ versus $\omega\tau$ for a Maxwell model.

Again, we can see that the use of the mechanical analog has given us important information: a viscoelastic fluid will show, at sufficiently low

frequency, E' behavior with frequency that is quadratic (slope of 2 on the log-log graph of Figure 3-4) and E'' behavior that is linear (slope of 1 on the log-log graph of Figure 3-4).

2. Voigt Element

Another simple element, the Voigt model, has been used frequently in connection with viscoelastic behavior. The Voigt model (Figure 3-5) consists of the same fundamental elements as the Maxwell model, except here the spring and dashpot are in parallel instead of being in series. Because of this arrangement, the Voigt model represents in the simplest possible form a viscoelastic *solid*. The constraint on the model is that the strain must be the same in both elements. The stress then must be the sum of the stresses in the two individual elements. Thus the fundamental equation of motion for the Voigt element is

$$\sigma_E(t) = \varepsilon(t)E + \eta_E \frac{d\varepsilon(t)}{dt} \quad \text{or} \quad \sigma(t) = \gamma(t)G + \eta \frac{d\gamma(t)}{dt} \quad (3-26)$$

for extension or shear, respectively. This model is usually used in considering creep experiments since, as will be seen shortly, it cannot easily be applied to a stress relaxation experiment. For the Voigt element we will use shear for our development instead of extension.

Creep Experiment. As the stress is a constant in a creep experiment, one has

$$\frac{d\gamma(t)}{dt} + \frac{\gamma(t)}{\tau} = \frac{\sigma_0}{\eta} \quad (3-27)$$

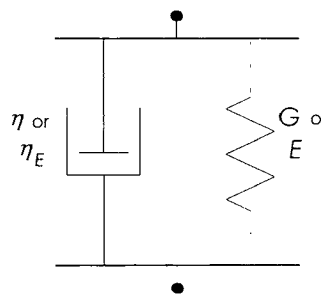


Figure 3-5. Voigt model.

which is a linear differential equation that can be made exact and then integrated using the integrating factor $e^{t/\tau}$. Integration between the limits $\gamma = 0$ and $\gamma = \gamma(t)$ yields

$$\int_{\gamma(0)}^{\gamma(t)} d[\gamma(t') e^{t'/\tau}] = \frac{\sigma_0}{\eta} \int_0^t e^{t'/\tau} dt' \quad (3-28)$$

giving

$$\gamma(t) e^{t/\tau} = \frac{\sigma_0}{G} (e^{t/\tau} - 1) \quad (3-29)$$

Simplification gives

$$\frac{\gamma(t)}{\sigma_0} = J(t) = J(1 - e^{-t/\tau}) \quad (3-30)$$

where $J(t)$ is the creep compliance in shear and $J = 1/G$. G is associated with the spring in the model (Figure 3-5).

Stress Relaxation. With constant strain, the equation of motion of the Voigt element reduces to Hooke's law with

$$G(t) = G \quad (3-31)$$

In spite of this promising result, it is clear that true stress relaxation is an impossible experiment, as the dashpot would develop an indefinitely high force with the input of a step change of strain.

Table 3-1. Behavior in Extension of Simple Viscoelastic Models in Various Experiments.^a

Experiment	Maxwell Element	Voigt Element
Creep	$D(t) = D + t/\eta_E$	$D(t) = D(1 - e^{-t/\tau})$
Stress relaxation	$E(t) = Ee^{-t/\tau}$	—
Dynamic	$D' = D$ $D'' = 1/\eta_E \omega$ $E' = E\omega^2 \tau^2 / (1 + \omega^2 \tau^2)$ $E'' = E\omega \tau / (1 + \omega^2 \tau^2)$	$D' = D/(1 + \omega^2 \tau^2)$ $D'' = D\omega \tau / (1 + \omega^2 \tau^2)$ $E' = E$ $E'' = \omega \eta_E$
Stress growth (transient) ^b	$\eta_E^+(t) = E\tau(1 - e^{-t/\tau})$	$\eta_E^+(t) = Et + \eta_E$

^a For both models the spring element has properties $E = 1/D$; the dashpot $\eta_E = E\tau$.

^b The symbol η_E^+ signifies the tensile stress σ_E^+ divided by the constant strain rate $\dot{\epsilon}$. See www.rheology.org for standard nomenclature.

The application of sinusoidal stress and strain is similar to that for a Maxwell body. The results are summarized in Table 3-1 along with the previously derived results for a Maxwell element. Figure 3-6 displays the frequency dependence of D' and D'' for the Voigt element in tension. The response in shear would be identical with J replacing D .

The response of both the Maxwell and Voigt models to several kinds of deformation experiments are much simpler than those of real polymer systems according to the results presented in Chapters 2 and 4. In particular, whereas most linear polymers of sufficiently high molecular weight have at least two

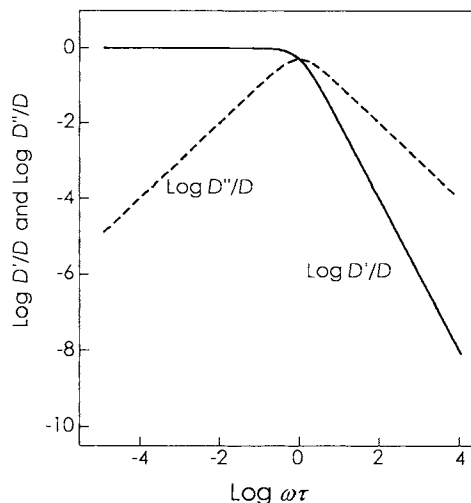


Figure 3-6. Frequency dependence of the complex dynamic compliance for the Voigt model.

major transitions (glass to rubber and rubber to liquid), these models exhibit only one transition under all conditions. Upon closer examination, it is also apparent that the decay of modulus exhibited by a Maxwell model at times slightly greater than τ is much more rapid than the corresponding modulus decay exhibited by real polymers in either transition region. Thus these simple models, while providing qualitative guidance, do not provide good quantitative representations of the observed viscoelastic behavior of real polymers.

To overcome these deficiencies, models have been proposed that consist of combinations of Maxwell and Voigt elements. Although an infinite number of such combinations is possible, we will consider only two here. The treatments of other such models are completely analogous.

3. Generalized Maxwell Model

This widely used model consists of an arbitrary number of Maxwell elements connected in parallel, as shown in Figure 3-7.

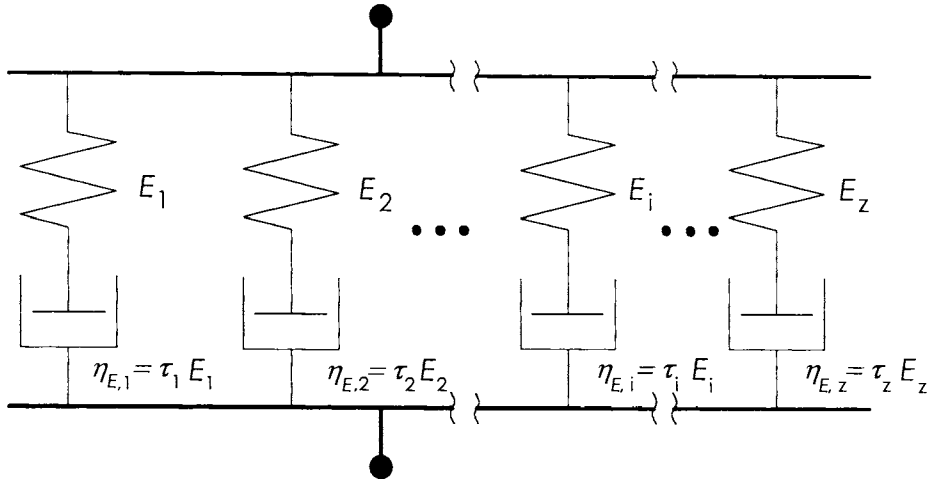


Figure 3-7. Generalized Maxwell model.

Consider a generalized Maxwell model with z elements subjected to a stress relaxation experiment. The strain in each element is characterized by a spring constant E_i and a viscosity $\eta_{E,i}$; thus each τ_i is determined. In all of the individual elements, the strain is the same and the total stress σ_E is the summation of the individual stresses experienced by each element. One can then write:

$$\begin{aligned}
 \frac{d\varepsilon(t)}{dt} &= 0 = \frac{1}{E_1} \frac{d\sigma_{E,1}}{dt} + \frac{\sigma_{E,1}}{\eta_{E,1}} \\
 &= \frac{1}{E_2} \frac{d\sigma_{E,2}}{dt} + \frac{\sigma_{E,2}}{\eta_{E,2}} \\
 &= \frac{1}{E_n} \frac{d\sigma_{E,n}}{dt} + \frac{\sigma_{E,n}}{\eta_n} \\
 &= \frac{1}{E_z} \frac{d\sigma_{E,z}}{dt} + \frac{\sigma_{E,z}}{\eta_{E,z}}
 \end{aligned} \tag{3-32}$$

$$\sigma_E = \sigma_{E,1} + \sigma_{E,2} + \sigma_{E,3} + \dots + \sigma_{E,n} + \dots + \sigma_{E,z} \tag{3-33}$$

Integration of equation (3-32) gives the partial stresses $\sigma_{E,i}$, which can then be substituted into equation (3-33) to calculate the total stress. When the total stress is divided by the constant strain, ε_0 , the stress relaxation modulus results:

$$\begin{aligned}
 E(t) &= \frac{\sigma_E(t)}{\varepsilon_0} = \frac{\sigma_{E,1}(0)}{\varepsilon_0} e^{-t/\tau_1} + \frac{\sigma_{E,2}(0)}{\varepsilon_0} e^{-t/\tau_2} \\
 &+ \dots + \frac{\sigma_{E,n}(0)}{\varepsilon_0} e^{-t/\tau_n} + \dots + \frac{\sigma_{E,z}(0)}{\varepsilon_0} e^{-t/\tau_z} \\
 &= \sum_{i=1}^z E_i e^{-t/\tau_i} \tag{3-34}
 \end{aligned}$$

where $\sigma_{E,n}(0)$ is the stress on the n th element at zero time ($t = 0$). Thus we see, as expected, that the total modulus is the summation of the responses of the individual elements.

The flexibility of this model in reproducing real viscoelastic behavior can be easily demonstrated. Consider a two-element model with parameters

$$E_1 = 3 \times 10^9 \text{ Pa}; \quad \tau_1 = 1 \text{ min} \quad \text{and} \quad E_2 = 5 \times 10^5 \text{ Pa}; \quad \tau_2 = 10^3 \text{ min}$$

Its behavior (Figure 3-8) reproduces the two transitions observed in real polymers. It is possible to replace one of the Maxwell elements in the generalized Maxwell model with a spring. The stress would decay to a finite value in such a model rather than zero and would approximate the behavior of crosslinked polymers.

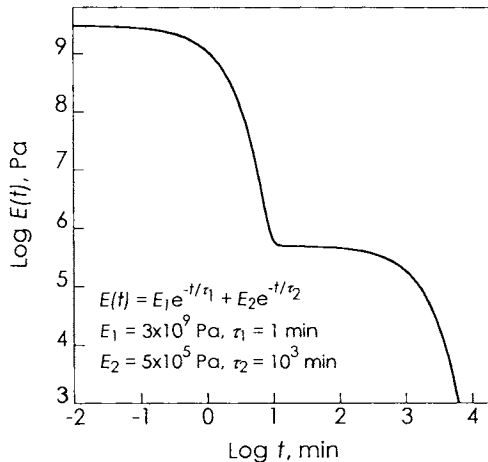


Figure 3-8. Behavior of a two-component generalized Maxwell model in stress relaxation.

Treatments similar to those used in equations (3-32) and (3-33) can be applied to the generalized Maxwell model undergoing sinusoidal stress or strain

64 VISCOELASTIC MODELS

to calculate the complex modulus. The results are given in Table 3-2. Expressions for the complex compliance are not simple functions.

4. Voigt-Kelvin Model

The Voigt-Kelvin model is a generalization of the Voigt element that results from connecting Voigt elements in series (Figure 3-9). Here the compliance functions are easily calculated, while the modulus functions are rather complicated. The results are summarized in Table 3-2; a sample calculation is provided below.

Table 3-2. Behavior of Generalized Maxwell and Voigt-Kelvin Models in Various Experiments

Experiment	Generalized Maxwell Model ^a	Voigt-Kelvin Model
Creep	$D(t) = \sum_{i=1}^z D_i(1 + t/\tau_i)$	$D(t) = \sum_{i=1}^z D_i(1 - e^{-t/\tau_i})$
Stress relaxation	$E(t) = \sum_{i=1}^z E_i e^{-t/\tau_i}$	Not applicable
Dynamic	$E' = \sum_{i=1}^z \frac{E_i \omega^2 \tau_i^2}{1 + \omega^2 \tau_i^2}$ $E'' = \sum_{i=1}^z \frac{E_i \omega \tau_i}{1 + \omega^2 \tau_i^2}$	$D' = \sum_{i=1}^z \frac{D_i}{1 + \omega^2 \tau_i^2}$ $D'' = \sum_{i=1}^z \frac{D_i \omega \tau_i}{1 + \omega^2 \tau_i^2}$
Stress growth (transient) ^b	$\eta_E^+(t) = \sum_{i=1}^z \eta_{E,i}(1 - e^{-t/\tau_i})$	—

^a Also known as the Maxwell-Wiechert model.

^b The symbol η_E^+ signifies the tensile stress σ_E^+ divided by the strain rate $\dot{\varepsilon}$. (See www.rheology.org for standard nomenclature.)

Here we derive expressions for D' and D'' of a Voigt-Kelvin model consisting of z elements assuming a sinusoidal strain application. Applying equation (3-22) to the Voigt-Kelvin model experiencing a strain in the j th element given by

$$\varepsilon_j(t) = \varepsilon_{0,j} e^{i\omega t} \quad (3-35)$$

results in the set of equations

$$\sigma(t) = E_j \varepsilon_{0,j} e^{i\omega t} + \eta_{E,j} i\omega \varepsilon_{0,j} e^{i\omega t} \quad \text{for } j = 1 \text{ to } z \quad (3-36)$$

$$\varepsilon(t) = \sum_{j=1}^z \varepsilon_j(t) \quad (3-37)$$

Solving equations (3-36) and (3-37) for the strain in the j th element gives

$$\varepsilon_j(t) = \varepsilon_{0,j} e^{i\omega t} = \frac{\sigma_E(t)}{E_j + \eta_{E,j} i\omega} \quad (3-38)$$

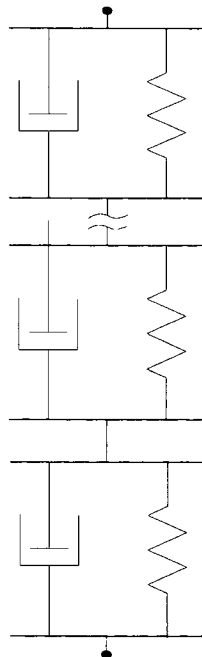


Figure 3-9. Voigt-Kelvin model.

which, when substituted into equation (3-37) and simplified, results in

$$\frac{\varepsilon(t)}{\sigma_E(t)} = D^* = \sum_{j=1}^z \frac{1}{E_j + \eta_{E,j} i\omega} = \sum_{j=1}^z \frac{D_j}{1 + \omega^2 \tau_j^2} - i \sum_{j=1}^z \frac{D_j \omega \tau_j}{1 + \omega^2 \tau_j^2} \quad (3-39)$$

It is clear that an inversion of this equation will not yield a simple result.

B. DISTRIBUTIONS OF RELAXATION AND RETARDATION TIMES

The pertinent parameters used in a generalized Maxwell model can be easily presented in graphical form as shown in Figure 3-10. Here three spring constants (10^{10} , 10^8 , and 10^6) are associated with relaxation times (10^2 , 10^4 , and 10^5 respectively). Clearly the stress relaxation modulus for this particular generalized Maxwell model could be easily calculated using equation (3-34).

In considering systems where there are very many Maxwell elements employed in the model, that is, z in equation (3-34) is large, it is often convenient to replace the summation in the equation by an integration. Thus:

$$E(t) = \int_0^\infty E_D(\tau) e^{-t/\tau} d\tau \quad (3-40)$$

The various E_i 's are replaced by a continuous function, $E_D(\tau)$, of the relaxation time where this function is called a distribution of relaxation times. Note that the dimensions of the variable $E_D(\tau)$ and E_i are not the same nor is $E(\tau)$ a modulus; instead it is akin to a probability density. The variable τ has dimensions of time. The physical interpretation is as follows: $E(\tau)d\tau$ is the fraction of the total relaxation modulus that has relaxation times between τ and $\tau + d\tau$. In addition to the distribution $E(\tau)$, one often encounters $H(\tau)$, which is defined as

$$H(\tau) = \tau E(\tau) \quad (3-41)$$

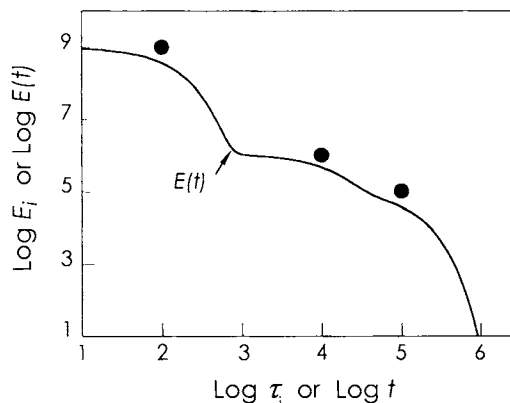


Figure 3-10. Discrete distribution of relaxation times and associated partial modulus values. The continuous line represents the stress relaxation modulus based on this distribution.

Note that $H(\tau)$ has the dimensions of modulus (e.g., units of Pa). In terms of $H(\tau)$, equation (3-40) becomes

$$E(t) = \int_0^{\infty} \frac{H(\tau)}{\tau} e^{-t/\tau} d\tau = \int_{-\infty}^{+\infty} H(\tau) e^{-t/\tau} d\ln\tau \quad (3-42)$$

where the integral on the right is done over $\ln \tau$, as opposed to τ .

Consider calculating the modulus for the distribution of relaxation times given in Figure 3-11. Mathematically $H(\tau)$ can be written as

$$\begin{aligned} H(\tau) &= 0 & \log \tau < 0 \\ H(\tau) &= k\tau^{-1} & 0 < \log \tau < 1 \\ H(\tau) &= 0 & \log \tau > 1 \end{aligned} \quad (3-43)$$

With this $H(\tau)$, equation (3-42) becomes:

$$E(t) = \frac{k}{t} (e^{-(t/10)} - e^{-t}) \quad (3-44)$$

This function is also plotted in Figure 3-11;

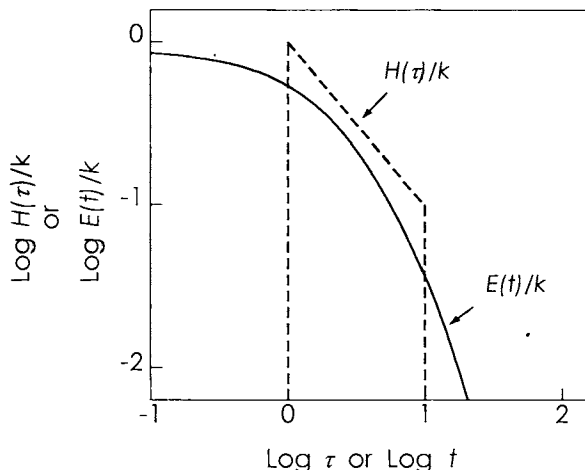


Figure 3-11. Continuous distribution of relaxation times expressed as $H(\tau)$ and the corresponding tensile stress relaxation modulus $E(t)$.

In addition, dynamic modulus functions can be calculated via this distribution function; $E'(\omega)$, for example, is given as

$$E'(\omega) = \int_{\ln \tau = -\infty}^{\ln \tau = \infty} H(\tau) \frac{\omega^2 \tau^2}{1 + \omega^2 \tau^2} d\ln \tau \quad (3-45)$$

A similar method is used to consider compliance functions. Here, however, the distribution of retardation times $L(\tau)$, defined as

$$J(t) = \int_{\ln \tau = -\infty}^{\ln \tau = \infty} L(\tau) (1 - e^{-t/\tau}) d \ln \tau \quad (3-46)$$

is used. Although $H(\tau)$ and $L(\tau)$ are related, their exact quantitative relationship is quite complicated; the interested reader should consult sources such as Ferry¹ or Gross.² Mathematical methods for extracting distribution functions from experimental modulus or compliance data are also given by these authors, and are available commercially³ as well in the form of freeware (e.g., Contin³). In addition, see Problem 10 at the end of this chapter.

Distributions of relaxation times for real polymer systems are slightly more complex than that shown in Figure 3-11. Tobolsky has suggested, for example, that the stress relaxation modulus of NBS polyisobutylene shown in Figure 3-12 can be thought to arise from a distribution of relaxation times that is composed of a “box and a wedge.” This composite is shown in Figure 3-12, and can be expressed as

$$\begin{aligned} H(\tau) &= M / \tau^{1/2} & \tau_1 < \tau < \tau_2 \\ H(\tau) &= E_0 & \tau_3 < \tau < \tau_m \end{aligned} \quad (3-47)$$

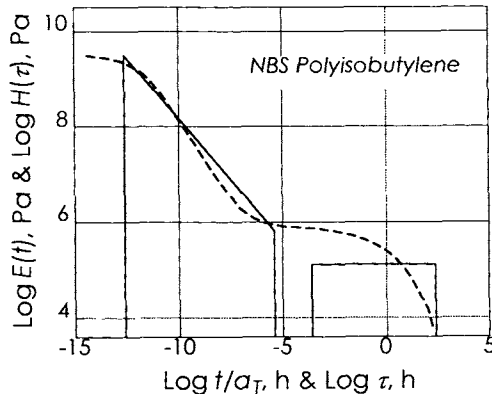


Figure 3-12. Stress relaxation master curve for N.B.S. polyisobutylene at 25°C (dotted line) and corresponding box-and-wedge distribution (solid lines). [Adapted from A. V. Tobolsky, *Properties and Structure of Polymers*, p. 128 and 151, by permission of John Wiley & Sons, Inc.]

In this particular case, Tobolsky gives the pertinent parameters the following values:

$$\begin{aligned} M &= 8.9 \times 10^3 \text{ Pa s}^{1/2} & E_0 &= 7.2 \times 10^5 \text{ Pa} \\ \tau_1 &= 10^{-12.5} \text{ s} & \tau_2 &= 10^{-5.4} \text{ s} \\ \tau_3 &= 9.65 \times 10^{-26} M_w^{3.30} \text{ s} \end{aligned} \quad (3-48)$$

$$\tau_m = 1.06 \times 10^{-20} M_w^{3.30} \text{ s}$$

Clearly the wedge is independent of molecular weight and gives rise to the primary transition. The box portion of the spectrum generates the rubbery plateau and rubbery flow regions of the master curve. As discussed in Chapter 4, Section A, these regions are strong functions of the molecular weight and molecular weight distribution, and the box portion of the spectrum mirrors this fact in the dependence of τ_3 and τ_m on the weight-average molecular weight M_w .

C. MOLECULAR THEORIES

Having discussed the viscoelastic responses of simple mechanical models, we may now consider molecular theories. In this treatment it will be shown that the results of molecular theories can, in fact, be couched in terms of the mechanical models already presented. The molecular theories predict the distribution of relaxation times and partial moduli associated with each relaxation time (τ_i 's and E_i 's for all i 's), which we treated as unknowns or parameters in the previous discussion. Thus, although molecular theories are not based on mechanical models, the results of these treatments may be presented in terms of the parameters of these models. Since, as we have already shown, it is possible to develop expressions giving the viscoelastic responses of the models to various types of deformations, the predictions of the molecular theories are obtainable through the known responses of these models.

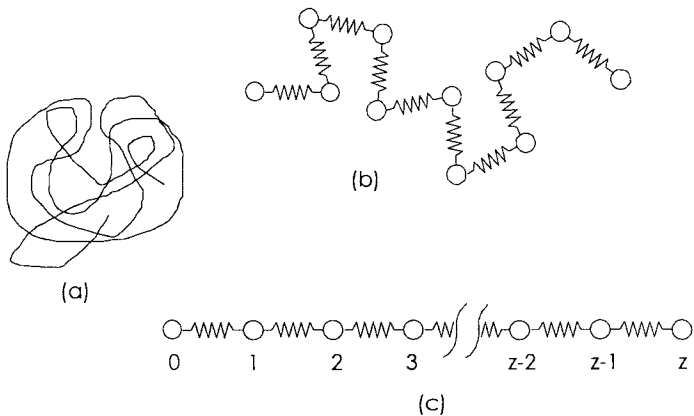


Figure 3-13. Bead-and-spring representation of a real polymer molecule in dilute solution.

Although far from being rigorous, a presentation of some of the salient points of the Rouse theory⁴ will be attempted using the method of Peticolas.⁵ The conclusions reached in this section are more or less applicable to the

70 VISCOELASTIC MODELS

theories presented by Rouse,⁴ Bueche,⁶ and Zimm,⁷ among others. The aim of this treatment is to present assumptions upon which the Rouse theory is based and to outline the results. Mathematical rigor is not attempted in this introductory treatment. For a complete or perhaps accurate understanding of the field, the reader *must* consult the original papers.^{4,6,7}

On examining the treatment of the isolated polymer chain in Appendix 2 of Chapter 6, one realizes that a long, freely orienting molecule behaves like a Hookean entropy spring (Figure 3-13a.). Manipulation of equation (j) in Appendix 2 of Chapter 6 shows that the restoring force on this spring upon stretching by some amount ΔX is given by

$$f = \frac{3kT}{r^2} \Delta X \quad (3-49)$$

The molecular theory subdivides the polymer molecule into subunits or submolecules just long enough so that the end-to-end distribution of each of these subunits is Gaussian. This is done so that equation (3-49) is applicable to each submolecule. Our picture of the molecule then becomes much like Figure 3-13b. The volume of the submolecule is concentrated at the beads, which are held together by the Hookean springs. Since we will be considering the response of the system to a unidirectional perturbation in the x direction, a spring oriented exactly perpendicular to the x direction will not contribute to the stress acting in the x direction. This holds also for any component of an oblique spring not in the x direction. Figure 3-14 indicates the deformations allowed for springs in different configurations relative to the perturbing function. It should be clear that an “effective spring constant” in the x direction will now allow us to portray our system as a one-dimensional chain (Figure 3-13c). This linearization of the problem is in no way restrictive. It arises because the polymer chain is linear and because the deformation considered is a unidirectional one. The only interactions in the model are those of adjacent submolecules with one another.

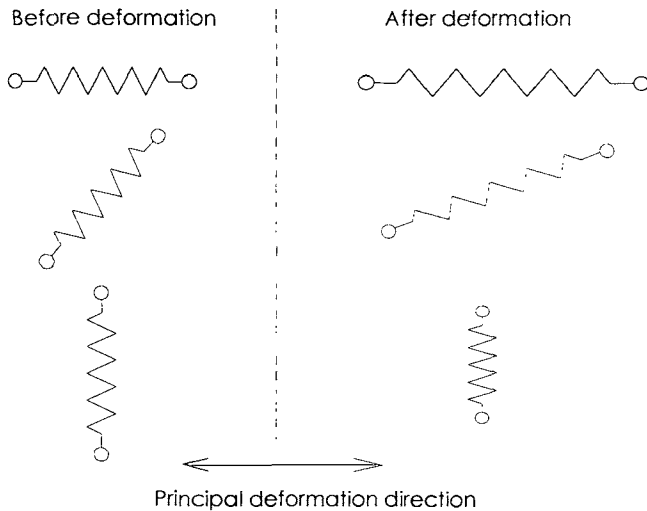


Figure 3-14. Motions of submolecules with varying orientations in a medium subjected to a uniform extensional deformation. A polymer chain will contain many submolecules.

Having proceeded this far, we are now in a position to write the equation of motion for our linear bead-and-spring model. To do this we divide the polymer molecule into z submolecules so that there are z springs and $z + 1$ beads. We now introduce a unidirectional deformation. The restoring force on each of the beads is given by:

$$\begin{aligned}
 f_{0x} &= \frac{-3kT}{a^2}(X_0 - X_1) \\
 f_{1x} &= \frac{-3kT}{a^2}(-X_0 + 2X_1 - X_2) \\
 f_{ix} &= \frac{-3kT}{a^2}(-X_{i-1} + 2X_i - X_{i+1}) \quad 1 \leq i \leq z-1 \\
 f_{zx} &= \frac{-3kT}{a^2}(-X_{z-1} + X_z)
 \end{aligned} \tag{3-50}$$

In this set of equations f_{ix} is the force on the i th bead in the x direction, X_i is the amount by which bead i has been displaced from its equilibrium position, and a^2 is the mean square end-to-end distance of the submolecule. The form of the equation results from the fact that the x -directed force on the i th bead reflects the difference between the x -directed forces on the i th and $i + 1$ st segments. An additional force acts on the molecule due to the viscous nature of the medium in which it is immersed. Under the assumption that the beads

move in the manner of spheres through a viscous solvent, the drag force on each bead is

$$f_{ix} = \rho_s \frac{dX_i}{dt} = \rho_s \dot{X}_i \quad (3-51)$$

where ρ_s is the segmental friction factor. Under the further assumption that the forces arising from the acceleration of the beads are small, the elastic forces given in equation (3-50) and the viscous forces given in equation (3-51) must balance. This allows us to write:

$$\begin{aligned} \rho_s \dot{X}_0 &= \frac{-3kT}{a^2} (-X_0 + X_1) \\ \rho_s \dot{X}_i &= \frac{-3kT}{a^2} (-X_{i-1} + 2X_i - X_{i+1}) \quad 1 \leq i \leq z-1 \\ \rho_s \dot{X}_z &= \frac{-3kT}{a^2} (-X_{z-1} + X_z) \end{aligned} \quad (3-52)$$

This set of linear first-order differential equations may be represented in matrix notation as:

$$[\dot{X}] = -B[A][X] \quad (3-53)$$

where

$$[\dot{X}] = \begin{bmatrix} \dot{X}_0 \\ \dot{X}_1 \\ \vdots \\ \dot{X}_z \end{bmatrix} \quad [X] = \begin{bmatrix} X_0 \\ X_1 \\ \vdots \\ X_z \end{bmatrix} \quad (3-54)$$

$[A]$ is the square $(z + 1) \times (z + 1)$ matrix

$$[A] = \begin{bmatrix} 1 & -1 & 0 & . & . & . & . & . \\ -1 & 2 & -1 & 0 & . & . & . & . \\ 0 & -1 & 2 & -1 & 0 & . & . & . \\ 0 & 0 & . & . & . & . & . & . \\ 0 & 0 & . & . & . & -1 & 2 & -1 \\ . & . & . & . & . & 0 & -1 & 1 \end{bmatrix} \quad (3-55)$$

which gives the coefficients for the equations (3-52), while B is the composite constant $3kT/a^2\rho_s$.

Equation (3-52) represents the total physical content of our model. From here on, we will be concerned with mathematical methods that allow us to solve this apparently complicated set of equations. The main problem arising in any attempted solution of these differential equations results from coupling of the motions of the beads. Thus X_i is not a function of the position of the i th bead itself, but is directly dependent on the position of the adjacent beads. This rather standard problem is effectively treated using the techniques of normal coordinates. We will define a new set of coordinates, q_i , made up of a linear combination of the X 's. Thus these new coordinates will be defined as

$$q_i = \sum_j Q_{ij} X_j \quad (3-56)$$

or, in matrix notation:

$$[q] = [Q][X] \quad (3-57)$$

In this equation, $[q]$ and $[X]$ are column matrices and $[Q]$ is a $(z + 1)$ by $(z + 1)$ square array. It remains for us to define $[Q]$ in such a way that it will lead to the solution of equation (3-52). To do this, we wish to be able to express every equation in the set in terms of the normal coordinate and its time derivative alone. In matrix notation we formally write:

$$[\dot{q}] = -B[\Lambda][q] \quad (3-58)$$

where $[\Lambda]$, unlike $[A]$, is diagonal. Now, for example, the j th equation in this set reads

$$\dot{q}_j = -B\lambda_j q_j \quad (3-59)$$

Since only the j th normal coordinate and its time derivative appear in equation (3-59), direct integration yields the time dependence of the motion of this coordinate. Clearly, it is in general difficult to have any "feel" for what motion each normal coordinate represents since it has a complicated dependence on *all* of the real coordinates. Nevertheless, the sum of the motions of all of the normal coordinates is identically equal to the sum of the motions of all of the real coordinates because one is just a linear transform of the other [equation (3-56)].

Thus, to proceed mathematically, we must transform equation (3-52) into equation (3-58), which is done by diagonalizing the matrix $[A]$. There exists another matrix $[Q]$ such that

$$[Q^{-1}][A][Q] = [\Lambda] \quad (3-60)$$

Also

$$[Q^{-1}][Q] = [I] \quad (3-61)$$

In this equation $[I]$ is a diagonal matrix with all nonzero elements = 1. Operation by $[Q^{-1}]$ from the left on equation (3-52) leads to

$$[Q^{-1}][\dot{X}] = -B[Q^{-1}][A][Q][Q^{-1}][X] \quad (3-62)$$

If we now set

$$[Q^{-1}][\dot{X}] = [\dot{q}] \quad [Q^{-1}][X] = [q] \quad (3-63)$$

our problem is solved, since equation (3-62) becomes

$$[\dot{q}] = -B[\Lambda][q] \quad (3-64)$$

It must be reemphasized that the exact nature of $[Q^{-1}]$ is not necessary to the physical solution of our problem. Because the normal-coordinate approach merely represents a linear transformation of the real coordinates, the motion of the polymer represented by all the q_i 's will be identical to the motion of the polymer represented by all the x_i 's. Our problem thus becomes the rather simple one of finding a diagonal representation of the $(z + 1) \times (z + 1)$ matrix $[\Lambda]$.^{*} This rather well known result (a similar form applies in the treatment of a vibrating string, among others) is derived in the appendix at the end of this chapter, and is merely stated here:

$$\lambda_p = 4 \sin^2 \left(\frac{p\pi}{2(z+1)} \right) \quad (3-65)$$

where p goes from 1 to z . Thus the diagonal matrix $[\Lambda]$ is

^{*} Note that $[A]$ was a $(z + 1) \times (z + 1)$ square matrix while $[\Lambda]$ is a $z \times z$. This difference in order represents the fact that while translation of the total molecule is expressed in $[A]$, it is not built into $[\Lambda]$. This causes no complication.

$$[\Lambda] = \begin{bmatrix} \lambda_1 & 0 & 0 & \cdot & \cdot & \cdot \\ 0 & \lambda_2 & 0 & \cdot & \cdot & \cdot \\ 0 & 0 & \lambda_3 & \cdot & \cdot & \cdot \\ \cdot & \cdot & \cdot & \lambda_{z-1} & & 0 \\ \cdot & \cdot & \cdot & 0 & & \lambda_z \end{bmatrix} \quad (3-66)$$

and

$$\dot{q}_p = -B\lambda_p q_p \quad (3-67)$$

which can be directly integrated to give

$$q_p(t) = q_p(0)e^{-Bt\lambda_p} = q_p(0)e^{-t/\tau_p} \quad (3-68)$$

$$\tau_p = \frac{1}{B\lambda_p} \quad p = 1 \text{ to } z$$

Here $q_p(0)$ is the value of the normal coordinate at time zero, that is, at the application of a perturbation, and $q_p(t)$ is the value of the coordinate at time t . We see that the coordinate response is exponential and the system response is just the sum total of all the coordinate responses.

As mentioned above, however, the exact nature of the normal coordinate in terms of the real coordinates is not easily perceived. Likewise, the exact nature of the real perturbation is not easily visualized in terms of perturbation to the normal coordinates. Thus to carry out our calculation exactly, we would have to transform the perturbation into the normal-coordinate framework. This is exactly the technique used by Bueche.⁶ The perturbation, that is, the boundary condition, used to solve equation (3-67) was that every normal coordinate was instantaneously displaced to the position of $q_i(0)$ at time zero and then no additional forces were put on the system. This perturbation corresponds neither to creep nor to stress relaxation. Although boundary conditions corresponding to these real experiments are more complicated in terms of normal coordinates,⁶ it can be shown² that the relaxation times that arise in a stress-relaxation experiment are just one-half as large as those calculated above. Thus, from here on τ_p will be used to denote a relaxation time and is given by

$$\tau_p = \frac{1}{2B\lambda_p} = \frac{1}{8B \sin^2 \left(\frac{p\pi}{2(z+1)} \right)} \quad (3-69)$$

Now one may associate these relaxation times with the relaxation times of a generalized Maxwell model. Thus the stress relaxation behavior for the bead-and-spring model is given as

$$E(t) = \sum_{p=1}^z E_p e^{-t/\tau_p} \quad (3-70)$$

where the individual τ_p 's are given in equation (3-69).

It remains to define the individual E_p 's; here one normally relies on the kinetic theory of rubber elasticity as applied to the submolecules. Once again,

$$f = \frac{3kT}{a^2} \Delta x \quad (3-49)$$

is the elastic force experienced by each spring if the ends are perturbed some amount Δx . Consider, however, that we have N polymer molecules per unit volume and the average cross-sectional area of each is b^2 . Thus the stress experienced by each spring should be given as

$$\sigma_E = \frac{f}{b^2} = \frac{3kT}{a^2 b^2} \Delta x \quad (3-71)$$

The instantaneous tensile modulus is just the stress divided by the strain, so

$$E(0) = \frac{\sigma_E}{\varepsilon} = \frac{3kT}{ab^2} \quad (3-72)$$

The denominator of the right side of this equation is merely the volume occupied per submolecule, given as

$$ab^2 = \frac{1}{Nz} \quad (3-73)$$

Here N is the polymer concentration in molecules per unit volume. Substitution of equation (3-73) into (3-72) yields

$$E(0) = 3NkTz \quad (3-74)$$

Clearly, however, the short-time limit of equation (3-70) is just

$$E(0) = \sum_{p=1}^z E_p \quad (3-75)$$

Now one usually assumes that all of the individual E_p 's are equal and given as

$$E_p = 3NkT \quad (3-76)$$

so that equations (3-74) and (3-75) are consistent. Since we have the τ_p 's and E_p 's of the generalized Maxwell model we may immediately write, for example,

$$E'(\omega) = 3NkT \sum_{p=1}^z \frac{\omega^2 \tau_p^2}{1 + \omega^2 \tau_p^2} \quad (3-77)$$

Note that the choice of the tensile modulus is arbitrary; the shear modulus could have been calculated. In this case the factor of 3 would be absent. Remember that the variable N represents the number of chains per unit volume. Alternatively, equation (3-77) can be written:

$$E'(\omega) = \frac{3cRT}{M} \sum_{p=1}^z \frac{\omega^2 \tau_p^2}{1 + \omega^2 \tau_p^2} \quad (3-78)$$

where c is the more familiar mass concentration of polymer (e.g., kg/m³), R is the gas constant (e.g., 8.3145 J/mol K) and M is the molecular weight of the polymer (e.g., kg/mol).

Example 3-1. Calculate the modulus E_p for each Rouse mode assuming a 10% solution of polymer of molecular weight 100 kDa.

For a 10% solution, $c \approx 100 \text{ kg/m}^3$, assuming a solution density of about 1000 kg/m³. A molecular weight of 100 kDa is the same as 100,000 g/mol or 100 kg/mol. Thus in SI units, $M = 100 \text{ kg/mol}$. The modulus according to equation (3-76) is then

$$\begin{aligned} E_p &= 3NkT = 3cRT/M \\ &= 3 \times 100 \text{ kg/m}^3 \times 8.31434 \text{ J/mol K} \times 298 \text{ K} / 100 \text{ kg/mol} \\ &\approx 7400 \text{ J/m}^3 = 7.4 \text{ kPa} \end{aligned}$$

This value is reasonable for solutions of this concentration.

D. APPLICATIONS OF FLEXIBLE-CHAIN MODELS TO SOLUTIONS

As we are primarily concerned with the viscoelastic nature of bulk materials in this introductory text, we will not dwell on the application of these ideas to solutions; however, considering that the model has been derived for the case of a dilute solution, it is of interest to examine briefly its agreement with the observed viscoelastic response of solutions. First it must be recognized that neither a^2 , the mean square end-to-end distance of the submolecule nor ρ , the segmental friction factor, may be easily evaluated. Thus a method of eliminating them from our equations would be helpful. The solution viscosity in excess of the solvent viscosity can be thought of as arising from the dissolved polymer and since our polymer behavior has been cast into the generalized Maxwell framework, this excess viscosity is just the sum of the viscosity of each of the elements in the model.

$$\eta - \eta_s = \sum_{p=1}^z G_p \tau_p \quad (3-79)$$

where η is the shear viscosity of the solution, η_s is the shear viscosity of the solvent, and G_p is the shear modulus (one third of E_p for incompressible fluids). Combining equation (3-79) with (3-69), (3-76), with the definition $B = 3kT/a^2\rho_s$ yields

$$\eta - \eta_s = NkT \sum_{p=1}^z \frac{1}{2B\lambda_p} = \frac{ca^2\rho_s}{24} \sum_{p=1}^z \frac{1}{\sin^2\{p\pi/[2(z+1)]\}} \quad (3-80)$$

Now for small values of X ,

$$\sin X \approx X \quad (3-81)$$

and since this expression is in the denominator of each term in the sum in equation (3-80), where the smallest arguments of the sine function will contribute most, we may write

$$\sum_{p=1}^z \frac{1}{\sin^2\{p\pi/[2(z+1)]\}} \approx \sum_{p=1}^z \frac{4(z+1)^2}{p^2\pi^2} = \frac{4(z+1)^2}{\pi^2} \sum_{p=1}^z \frac{1}{p^2} \quad (3-82)$$

This summation is well known, and for large values of z it is equal to $\pi^2/6$. Furthermore, for large values of z , 1 is small compared to z so that substitution of equation (3-82) into equation (3-80) yields

$$\eta - \eta_s \approx \frac{Na^2 \rho_s z^2}{36} \quad (3-83)$$

Applying the same arguments to equation (3-69), remembering that $B = 3kT/a^2\rho_s$, yields

$$\tau_p = \frac{a^2 \rho_s z^2}{6\pi^2 k T p^2} \quad \text{for } p < z \quad (3-84)$$

Combination of equation (3-83) and equation (3-84) gives

$$\tau_p = \frac{6(\eta - \eta_s)}{NkT\pi^2 p^2} \quad (3-85)$$

where the excess viscosity $\eta - \eta_s$ and concentration of the solution are known or are easily measured. Recalling that $c = MN/N_A$, where c is the mass concentration, M is molecular weight and N_A is Avogadro's number, gives the convenient form

$$\tau_p = \frac{6M(\eta - \eta_s)}{cRT\pi^2 p^2} \quad (3-86)$$

Rouse and Sittel⁸ have investigated the applicability of the theory to real systems, in particular, dilute solutions of polystyrene in the good solvent toluene. Their results are reproduced in Figure 3-15. The agreement between theory and experiment is excellent. However, in a sense a certain amount of "curve fitting" is involved, since the friction factors and a^2 have been adjusted to fit the data through the method outlined in deriving equation (3-84).

E. THE ZIMM MODIFICATION

Consideration of another major modification that has been applied to the flexible chain model seems pertinent at this point. It has long been appreciated that the velocity field of the solvent would be perturbed deep inside a coiled polymer molecule. It is clear that this effect is not considered in the above treatment because the viscous drag is given as $\rho_s X_i$ in equation (3-51) irrespective of whether X_i happens to be inside the coiled molecule or on its surface. Thus one might expect the Rouse formulation to be most applicable to polymer-solvent systems in which the elongated conformations of polymer chains predominate. For such conformations, there would be little shielding of one part of a molecule by another part of the same molecule. This is the case in

Figure 3-15, where toluene, a good solvent for polystyrene, would favor extended conformations. Balanced against this is the assumption of the model that the Gaussian distribution function holds (see Chapter 6, Appendix 2 for details). This is not the case in a solvent that favors extended conformations. Thus, the agreement shown in Figure 3-15 is probably fortuitous.

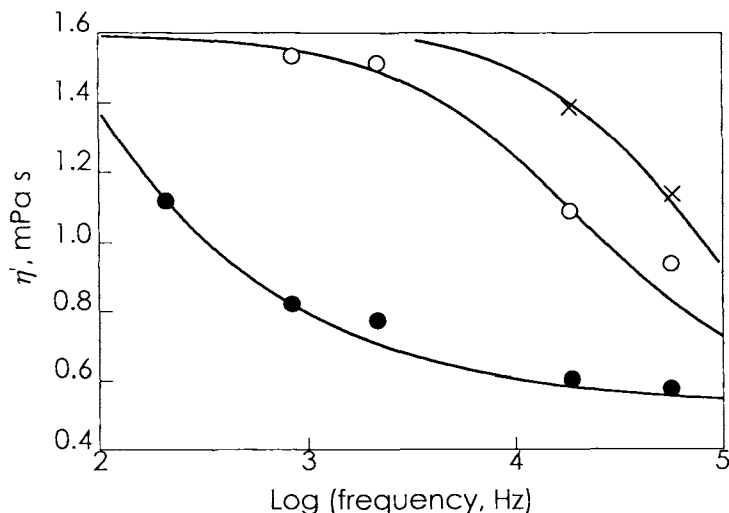


Figure 3-15. Experimental observation (PS in toluene at 30.3 °C) and prediction of the Rouse theory. The molecular weights (kDa) and concentrations (kg/m³) from left to right are: 6200, 1.44; 520, 8.9; and 253, 14.6. [After P. E. Rouse and K. Sittel, *J. Appl. Phys.*, **24**, 690 (1954)]

Zimm⁷ has developed a theory that treats such "hydrodynamic shielding" and although we will not go into detail, it is helpful to examine the results of this calculation. The main difference between the Rouse and Zimm treatments occurs in the relaxation times, not in the partial modulus values. The relaxation times according to the Zimm treatment are

$$\tau_p = \frac{1.71(\eta - \eta_s)}{NkTK_p} \quad (3-87)$$

where the K_p are constants: $K_1 = 4.04$, $K_2 = 12.79$, $K_3 = 24.2$, and so on.

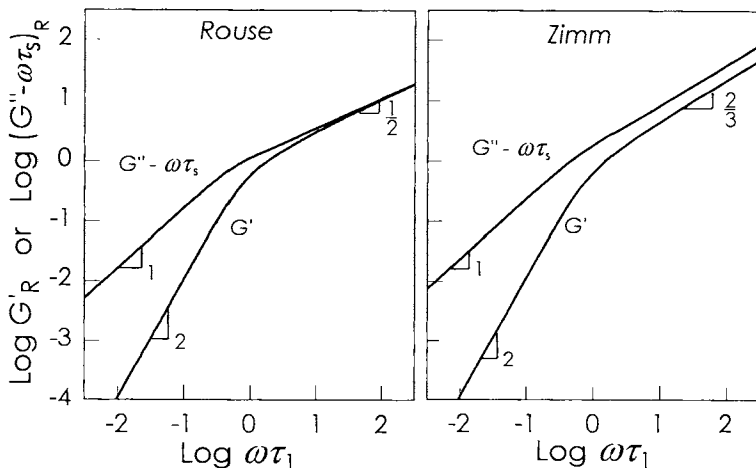


Figure 3-16. Predictions of the Rouse and Zimm theories. [After J. D. Ferry et al., *J. Phys. Chem.*, **66**, 536 (1962). Reprinted by permission of the American Chemical Society.]

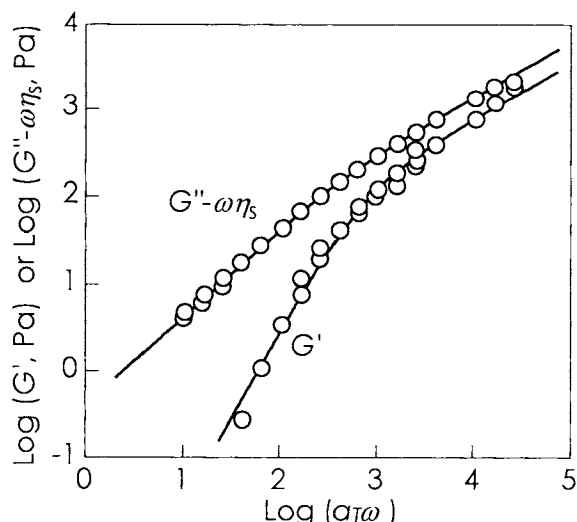


Figure 3-17. Experimental results for polystyrene in Arochlor® compared with predictions according to the Zimm theory. [After J. D. Ferry et al., *J. Phys. Chem.*, **66**, 536 (1962). Reprinted by permission of the American Chemical Society.]

In Figure 3-16 we have compared the prediction of the Rouse and Zimm theories.¹ The limiting values of the slopes of plots of $\log G'$ versus $\log \omega$ at large ω are one-half for the Rouse treatment and two-thirds for the Zimm treatment. This arises from the different distributions of relaxation times in the Rouse and Zimm theories. In Figure 3-17 the results of DeMallie⁹ for the

system of polystyrene in Arochlor® are presented.[§] Arochlor®, a rather poor solvent for polystyrene, yields a predominance of tightly coiled polymer conformations where hydrodynamic shielding would be expected to be most important. The remarkable agreement between theory and experiment shown by Figures 3-16 and 3-17 illustrates the validity of the bead-and-spring model for the viscoelastic behavior of polymer solutions.

F. EXTENSION TO BULK POLYMER

Returning to our major concern, bulk polymeric behavior, we may ask if we should expect the bead-and-spring model to be applicable at all. The equations of motion, equation (3-52), were written on the premise that the beads encountered viscous drag by virtue of their immersion in a solvent with viscosity η_s . No solvent is present in the bulk case, and it would thus appear that equation (3-51) should not apply to this situation. However, the functional form of the viscous drag term [the left side of equation (3-52)] merely states that the solvent medium exerts the same drag on each bead regardless of the bead's position. Substituting an ensemble of bead-spring polymer molecules for the solvent can preserve this functional form. This procedure has the effect of changing the numerical value of the segmental friction factor, ρ_s , but leaving the form of the left side of equation (3-52) unchanged. The right side of equation (3-52), representing the restoring force resulting from the perturbation of a submolecule, is an intramolecular property, at least to a first approximation, and thus would not be expected to change drastically with the substitution of additional polymer for solvent. Therefore equation (3-52) is still applicable to the bulk polymer with the appropriate changes in numerical values for such parameters as ρ_s and a^2 . The usual normal coordinate analysis again leads directly to equation (3-69) for the distribution of the z relaxation times. The partial modulus remains NkT where N is the number of polymer chains per unit volume of bulk polymeric material. An analysis equivalent to that given in equations (3-79) through (3-85) yields the relationship:

$$\tau_p = \frac{6\eta}{NkT\pi^2 p^2} = \frac{6\eta M}{\rho RT\pi^2 p^2} \quad (3-88)$$

where η represents the steady-flow shear viscosity of the bulk polymer and ρ is the mass density. Again, this is for high z . The time-dependent shear stress relaxation modulus would thus be given as

[§] Arochlor® is the trademark for a series of chlorinated biphenyls, which are no longer widely available due to health and environmental concerns.

$$G(t) = NkT \sum_{p=1}^z e^{-t/\tau_p} = \frac{\rho RT}{M} \sum_{p=1}^z e^{-t/\tau_p} \quad (3-89)$$

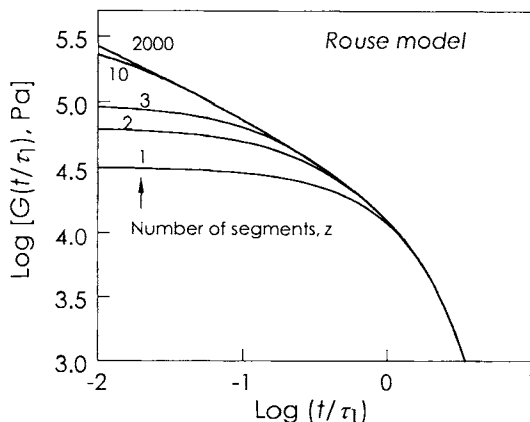


Figure 3-18. Rouse theory in the rubbery plateau and flow regions. Varying numbers of segments considered. Note increasing region of power-law behavior (slope = $-1/2$) as the number of segments is increased.

A plot of $\log G(t/\tau_1)$ versus $\log(t/\tau_1)$ is shown in Figure 3-18. We have assumed that $N = 6 \times 10^{18}$ molecules/cm³, which corresponds roughly to a molecular weight of 10^5 and a density of 1 g/cm³; NkT , the modulus associated with each relaxation time, is then 3.2×10^4 Pa at 385 K. The number of terms in the summation of equation (3-89), or equivalently, the number of submolecules in the polymer molecule, z , is not determined. We have plotted $G(t)$ for several values of z . It should be clear that $z = 1$ is just the Maxwell body behavior. As z increases, the Rouse theory predicts that the relaxation profile, while still approaching exponential behavior at long times, becomes increasingly power law (straight line on the plot shown) at lower frequencies. The slope has the same magnitude, $1/2$, as that for the components of the complex dynamic modulus. Power-law behavior denotes an indefinitely broad and continuous spectrum of relaxation processes, placing the material at the boundary between a solid and a liquid. If the relaxation is truly power law over all frequencies, then all viscoelastic properties will also be power law.

Quite disappointing, however, is the comparison of the curves in this figure with those presented in Chapters 2, 4 and 5 that show the observed experimental response of bulk polymers. Experimentally, high-molecular-weight polymers exhibit two major transitions while the bead-and-spring model predicts only one, albeit with a broadened time response relative to a Maxwell model.

Ferry, Landel, and Williams¹⁰ have suggested a simple but appealing explanation for this apparent shortcoming of the theory and, moreover, have put

forth a modification of the theory that "predicts" two transitions as observed experimentally. In describing their treatment, let us introduce some of the considerations regarding the molecular mechanisms giving rise to these transitions; these are explained in greater detail in Chapter 4, Section A. The behavior in the rubbery region is due mainly to the long-range translational motions of an entangled rubbery mass. The molecular motion responsible for the behavior observed in the primary transition region, however, is of a much shorter range, involving perhaps only a handful of monomer units.

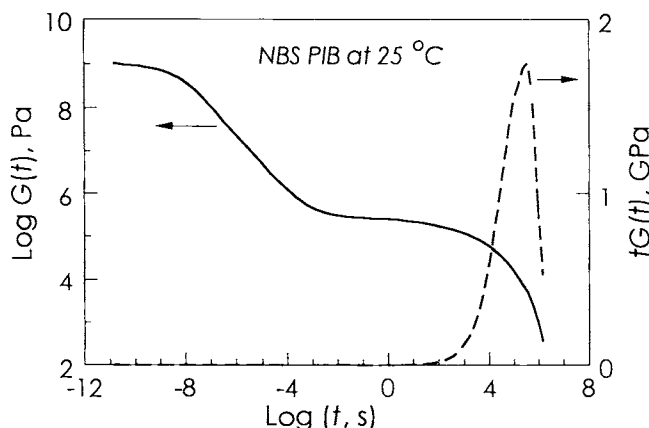


Figure 3-19. Calculations of the viscosity from the stress relaxation master curve for NBS PIB at 25 °C (see Figure 3-12) via equation (3-89), showing the important contribution to the integral from the long-time data and the negligible contribution from the short-time modes in the glassy region.

Consider now the segmental friction factor ρ_s used in equation (3-52). If the motion of submolecule j is part of a coordinated long-range type of motion, we would expect the friction factor to reflect the entangled nature of the system, since for a long-range motion to take place, entanglements must be unraveled. Conversely, in short-range motions, entanglements should play only a diminishingly small role; the friction factor would be expected to correspond to that of the same chemical species without entanglements (low-molecular-weight polymer). Thus Ferry, Landel, and Williams argued that one should expect two independent friction factors to be operative. One of these reflects the viscous drag experienced by a submolecule taking part in short-range uncoordinated motions with short relaxation times, and the other is indicative of the viscous drag experienced by a submolecule taking part in long-range coordinated motions with long relaxation times.

We now ask which of the two friction factors has been used in the expression for τ_p equation (3-88). The segmental friction factor ρ_s has been eliminated from this expression through its dependence on η , the steady-state

shear viscosity. Our question becomes, then, what molecular motion does η depend upon? Quite possibly it could reflect all motions of the polymer molecules, but fortunately for this discussion, it is rather simple to show that only long-range coordinated motions contributed substantially to η . To do this, we borrow from Chapter 4 equation (4-7):

$$\eta = \int_0^\infty G(t)dt \quad (4-7)$$

where we are now calculating a shear viscosity. (See problem 3-8 for the demonstration of this equation.) A simple transformation yields

$$\eta = \int_{-\infty}^\infty tG(t)d\ln t \quad (3-90)$$

In Figure 3-19 is plotted the integrand of this integral along with a typically reduced master curve of a high-molecular-weight polymer. It is evident that the only significant contribution to the area comprising η comes from the long-time portion of the master curve, clearly indicating that the above statement concerning long-range motions as being the primary contribution to η is correct.

The friction factor operative for the short-range motions may be thought of as being obtained from measurements on polymers where entanglements are not present and the only contribution to all physical properties, η included, comes from short-range motions. Such a polymer is just one of low molecular weight where entanglements are not possible because the chains are too short. The critical molecular weight for the onset of entanglements varies strongly with the structure of the polymer. For example the critical molecular weight is about 30,000 for polystyrene and only about 3000 for polybutadiene. To account for behavior both above and below the critical entanglement length, Ferry, Landel, and Williams postulate one friction factor $\rho_{s,0}$, operative at relaxation times shorter than some critical relaxation time τ_c and another, ρ_s , operative at longer relaxation times:

$$\begin{aligned} \tau_p &= \frac{\rho_{s,0}a^2z^2}{6\pi^2 k T p^2} & \tau_p < \tau_c \\ \tau_p &= \frac{\rho_s a^2 z^2}{6\pi^2 k T p^2} & \tau_p \geq \tau_c \end{aligned} \quad (3-91)$$

Moreover, they postulated a relationship ρ/ρ_0 as

$$\log \frac{\rho_s}{\rho_{s,0}} = 2.4 \log \frac{M}{M_c} \quad (3-92)$$

where M_c is the critical molecular weight for the onset of entanglement. We see that they postulate a friction factor ρ_s which varies as molecular weight to the 2.4 power, unlike $\rho_{s,0}$ which is not a function of molecular weight. If we associate the long modes ($\tau_p \geq \tau_c$) with the rubbery-flow region, then the number of modes for this region is $\sqrt{\tau_1/\tau_c}$. The distribution of relaxation times given in equation (3-84) was used to calculate the stress-relaxation modulus curve shown in Figure 3-20, and it is clear that the gross features of the relaxation of a real polymer are reproduced. However, to generate this curve, it was

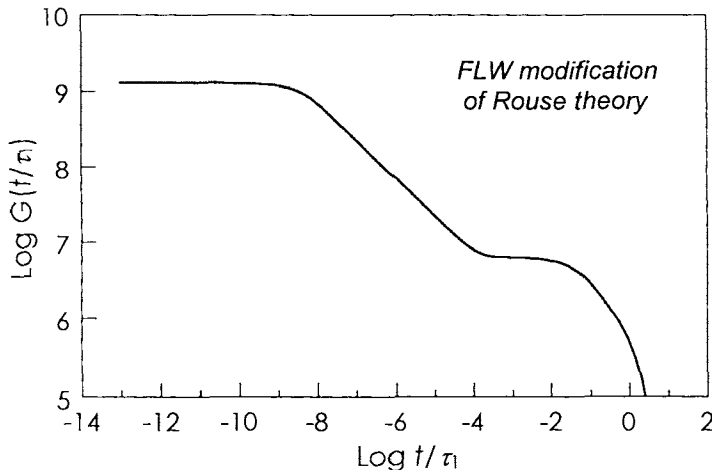


Figure 3-20. Two transitions predicted using the Ferry, Landel, and Williams⁸ modification of the Rouse theory. The parameters required to get this result are quite extreme; see text.

necessary to assume unrealistic physical parameters. Before tackling this problem, let us examine the origin of the 2.4 in equation (3-92).

Remembering that the viscosity of a generalized Maxwell model is just the sum of the viscosities of the individual Maxwell elements will help shed light on the 2.4 factor in equation (3-92). We have already noted that all of the viscosity of a high-molecular-weight polymer derives from long-range translational motion of the polymer, that is, from motions with $\tau_p > \tau_c$ or where the friction factor ρ_s is operative. Thus we may write

$$\eta = \sum_{p=1}^z G_p \tau_p \quad \tau_p > \tau_c \quad (3-93)$$

and

$$\eta = \frac{NkT\rho_s a^2 z^2}{6\pi^2 kT} \sum_{p=1}^{p_c} \frac{1}{p^2} \quad (3-94)$$

where p_c is defined as

$$p_c = \sqrt{\frac{\tau_1}{\tau_c}} \quad (3-95)$$

If p_c is greater than five, for example, the summation is relatively insensitive to changes in p_c and essentially may be considered as a constant. Examination of each variable in equation (3-94) with respect to molecular-weight dependence reveals

$$\eta \propto M^{3.4} \quad (3-96)$$

since N , the number density of chains is inversely proportional to molecular weight; z , the number of submolecules per polymer molecule, is directly proportional; and the friction factor ρ_s , it has been pointed out, varies as the 2.4 power of molecular weight. All the other terms are independent of molecular weight. Realizing that equation (3-96) is an established experimental fact for high-molecular-weight materials makes clear the choice of 2.4 in equation (3-92). There is no direct way of deriving this value from this theory.

As mentioned above, there are several shortcomings of the Ferry, Landel, and Williams modification of the Rouse theory that must be kept in mind. Although these considerations indicate that the modification does not strictly account for all observations, it must be appreciated that this was a major step in making a degree of theoretical sense out of a large amount of sometimes confusing experimental data.

The argument of Williams¹¹ is perhaps the most serious blow to the Ferry–Landel–Williams work. Williams examined the short-time limit of equation (3-89) and observed that

$$G(0) = NkT \sum_{p=1}^z (1) = zNkT \quad (3-97)$$

He pointed out that this relationship is true no matter what value of the friction factor is used, because the exponential of $(0/\tau_p)$ is always 1.0. The limiting value of the modulus at short times is clearly predicted from equation (3-97). Experimentally, $G(0)$ is found to be in the neighborhood of 3 GPa for most polymers (Chapter 4). If we consider, for example, a polymer of molecular

weight 150,000 and a density of 1.5 g/cm³, the value for NkT at 300 K turns out to be about 2.5×10^4 Pa.

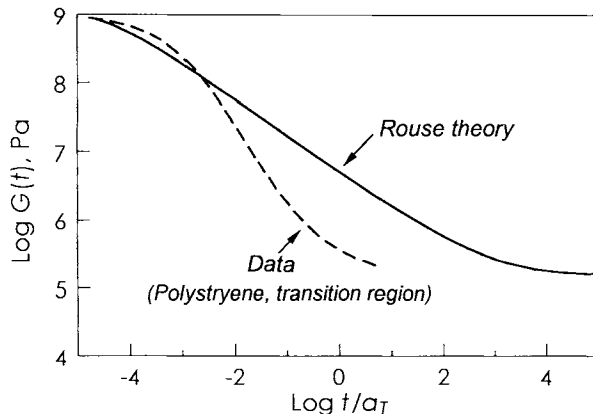


Figure 3-21. Comparison between master curve of polystyrene and predictions of the modified Rouse theory in the primary transition region.

What, then, is the value of z ? One should recall that a submolecule was defined as the shortest unit of a chain whose end-to-end distance is Gaussian. Clearly, this would not be true of a monomeric or dimeric submolecule due to internal constraints on molecular geometry. Williams decided that the smallest unit he could accept for a submolecule was composed of five monomer units. If we let our polymer be polystyrene, whose monomer molecular weight is 100, we have 1500 monomer units per chain, or 300 submolecules per polymer chain. Using equation (3-97)

$$G(0) = 300 \times (2.5 \times 10^4 \text{ Pa}) = 7.5 \times 10^6 \text{ Pa} \quad (3-98)$$

which is about two orders of magnitude smaller than the experimentally determined value. A reasonable explanation for this shortcoming is the use of NkT as a partial modulus for all chain motion. This value, while clearly applicable to rubberlike systems, is not so clearly applicable to deformations of the glassy state. Tobolsky and DuPré¹² have pointed out that the equations of motion [equation (3-52)] can be written and solved for chain units much smaller than the submolecule while employing a partial modulus more realistic for the types of molecular motion expected in the glassy state. Thus a Ferry–Landel–Williams type of modification is still feasible in spite of Williams' objection.

Another major discrepancy between theory and experiment is exemplified in Figure 3-21. In this figure, the predicted relaxation according to the Rouse theory is compared with an experimental result for polystyrene in the primary transition region. It is clear that polystyrene undergoes its glass-to-rubber

transition much more sharply than is predicted by flexible chain theories, which predict a slope of $-1/2$ in this region for a log-log plot. Many other polymers, in contrast to this, obey the flexible-chain theory result rather closely. Polyisobutylene is one notable example. The discrepancy noted in the case of polystyrene is important, however, as we shall show. The question arises: What molecular factors contribute to the discrepancy in the case of polystyrene? To explore this question, we use the maximum slope of the stress relaxation master curve in the glass-to-rubber transition region as a criterion for agreement between theory and experiment. Values of this slope measured experimentally for several polymers are listed in Table 3-3.

Table 3-3. Transition Region Slope for Several Polymers¹³

Polymer	Slope
Poly(vinyl chloride)	-0.6
Polyisobutylene	-0.7
Poly(ethylene terephthalate)	-0.9
Polycarbonate	-1.2
Polystyrene	-1.5

The starting point is the theoretical expression for the relaxation modulus taken from the fundamental Rouse formulation given in equation (3-89). The relaxation times are those given in equation (3-91), except we are concerned for this demonstration only with the transition region where short-range motions dominate, i.e., $\tau_p < \tau_c$. Let us define a fictitious relaxation time τ_L such that

$$\tau_L = \frac{\rho_0 a^2 z^2}{6\pi^2 kT} \quad (3-99)$$

where τ_L would be the maximum relaxation time τ_1 if one were not forced to change friction factors from $\rho_{s,0}$ to ρ_s for the long relaxation times. For all $\tau_p < \tau_c$ one may then write

$$\tau_p = \frac{\tau_L}{p^2} \quad (3-100)$$

and equation (3-89) is modified to become

$$G(t) = G \sum_{p=p_c}^z e^{-tp^2/\tau_L} \quad (3-101)$$

90 VISCOELASTIC MODELS

where G , the partial modulus associated with each relaxation, may or may not be NkT but is the same for all short-range molecular motions. Similarly, z is the number of molecular units considered per chain and is not necessarily the usual number of submolecules. It is argued now that for relatively large values of p , say $p > 5$, the summation may be replaced by an integration to yield

$$\frac{G(t)}{G} = \int_{p_c}^z e^{-tp^2/\tau_L} dp \quad (3-102)$$

Letting

$$X = \frac{tp^2}{\tau_L}$$

$$\frac{G(t)}{G} = \frac{1}{2} \left(\frac{\tau_L}{t} \right)^{1/2} \int_{tp_c^2/\tau_L}^{tz^2/\tau_L} X^{-1/2} e^{-X} dX \quad (3-103)$$

Although this integral cannot be carried out analytically, it is proportional to the incomplete gamma function $P(a, x) = \gamma(a, x)/\Gamma(a)$, where $\Gamma(a)$ is the complete gamma function.^{14,15} Thus

$$\int_0^x u^{a-1} e^{-u} du = \gamma(a, x) = P(a, x)\Gamma(a) \quad (3-104)$$

As $a = 1/2$ in this case, $\Gamma(a) = \Gamma(1/2) = \sqrt{\pi}$. Thus

$$\frac{G(t)}{G} = \frac{1}{2} \sqrt{\pi} (t/\tau_L)^{-1/2} [P(1/2, z^2 t/\tau_L) - P(1/2, p_c^2 t/\tau_L)] \quad (3-105)$$

An important aspect of this equation is the behavior of $P(1/2, x)$, which rapidly varies between 0 and 1 near $x = a$. Thus, if z and p_c are sufficiently different, there exists a range of t/τ_L that gives a value of almost exactly 1.0 for the quantity in the square brackets. In this range, then, $G(t)$ is controlled exclusively by the $t^{1/2}$ term, giving the characteristic $-1/2$ slope on log-log scales. The advent of the incomplete gamma function is incidental. Recall that the $t^{1/2}$ term resulted from the substitution of $X = tp^2/\tau_L$ to simplify the integral in Eq. (3-100). Thus the important and fundamental feature of the Rouse formulation is the $1/p^2$ dependence of the relaxation times, which leads to the $-1/2$ slope. The function $G(t)/G(0)$ has been plotted in Figure 3-22, and for times between τ_L/z^2 and τ_L/p_c^2 it is clear that the slope of $\log G(t)$ versus $\log t$ is $-1/2$, as expected.

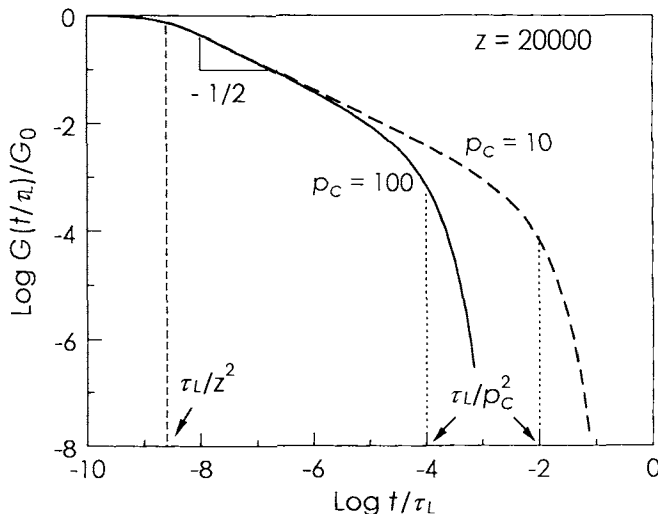


Figure 3-22. Relaxation in the primary transition region considering varying numbers of relaxing elements. The elements in the transition region in each case is $z - p_c$.

Tobolsky¹⁶ has suggested that the response of a highly coupled system would be more like that experimentally observed for polystyrene and has suggested ways to solve the equations generated from these considerations. Instead of considering the response of a linear chain, he treats the assembly of molecules as a network that is coupled, via springs, in two and three dimensions. This treatment is considered beyond the scope of an introductory book; interested readers are referred to the original papers.^{12,13,16,17}

Advancement of these historical treatments has taken many routes. One fresh approach was to abandon the normal-mode approach altogether for the rubbery-flow region and to treat relaxation in this region as a diffusion process. This approach, called reptation, is described below. It focuses principally on the motions at longer times and assigns Rouse-like relaxation to shorter times. For description of relaxation in the glassy region, there has been some recent development in justifying the “stretched exponential” form

$$G(t) = G_0 \exp[-(t/\tau)^\beta] \quad (3-106)$$

in terms of molecular motions in the glass.¹⁸ This equation is also known as the KWW (Kohlrausch; Williams and Watts) equation as was first used by Kohlrausch¹⁹ in 1876 to describe the relaxation of inorganic glasses. The shape of the KWW equation is compared with the Maxwell model in Figure 3-23.[†]

[†] For $\beta < 1$, the KWW function has an unusual behavior as time t approaches zero in that the relaxation rate $-dG(t)/dt$ becomes infinite, while the slope on a log-log plot such as Figure 3-23 becomes zero.

The KWW model has found use in describing the results of dynamic simulations of a glass using a partially filled cubic lattice construct (e.g., Okun et al.²⁰). Relaxation in the glass occurs, according to this model, by hopping of segments from filled to open sites in the lattice. As the glass is cooled, the segments become longer, and the probability of a neighboring open site becomes rapidly lower. The result of this analysis is a Rouse spectrum wherein the normal-mode relaxation follows the KWW form instead of single exponential. As the mode number index p increases (lower relaxation times), the value of β decreases; that is, the relaxation process covers a wider time frame. Thus

$$G(t) = G \sum_{p=p_g}^z \exp[-(tp^2 / \tau_L)^{\beta(p)}] \quad (3-107)$$

where $\beta(p)$ is the mode-dependent exponent. The form of $\beta(p)$ is not given explicitly by the theory.

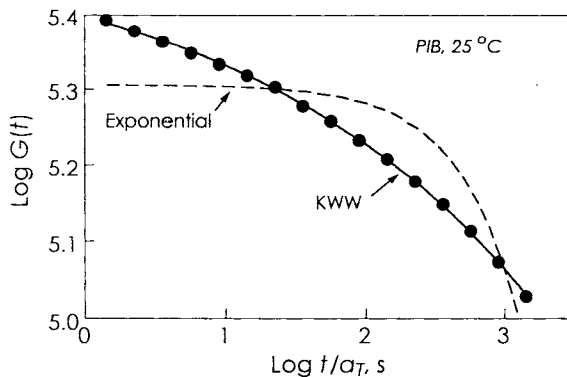


Figure 3-23. Comparison of the relaxation behavior of the empirical KWW expression of equation (3-104) with data for PIB in the rubbery flow region. Data: NBS PIB; see Ferry¹ for a table of these data. Copies of the data are also in the CD (PIB-Rel-1.TXT and PIB-Rel-2.TXT).

Relaxation processes in the crosslinked rubbery state are generally small in magnitude but nonetheless of great practical importance. Heating in cyclically deformed elastomers is an often-undesirable outcome of these processes. While the high-frequency relaxation processes in elastomers undoubtedly involves Rouse-like motions of segments of the network chains, the low-frequency relaxation is assignable to reptation (see section G) of dangling chain ends. Curro and Pincus²¹ showed that reptation of the dangling ends by path retracement (diffusion by doubling back along its own contour) will produce a relaxation of the form

$$G(t) = G(\infty)[1 - (t/\tau)^{-m}] \quad (3-108)$$

where $G(\infty)$ is the equilibrium modulus, τ is a characteristic time and m is a positive constant that depends on the crosslink density of the network (see Chapter 6 for a description of network topology). This relationship was postulated earlier by Chasset and Thirion,²² but purely as a convenient empiricism for describing their data. Typically m is around 0.1, indicating that the relaxation process is extremely broad. Clearly equation (3-108) is not valid except at $t \gg \tau$.

G. REPTATION

Although theories of the Rouse–Bueche–Zimm type have been very successful in rationalizing the behavior of polymeric systems from a molecular point of view, another class of theories is presently commanding the most attention. These theories treat the motion of polymer molecules in terms of reptation, a reptile-like diffusive motion of each polymer molecule through a matrix formed by its neighbors.[†] To a considerable extent, this new approach has overcome some of the most important shortcomings of the normal-mode theories, which we will outline next.²³

As mentioned above, it is not clear that the concept of random- or ideal-chain elasticity is an appropriate assumption for modeling the dynamics of high-molecular-weight polymeric solids. In equation (3-97), for example, it is clear that the maximum value of the modulus predicted by the normal mode theories is much smaller than that observed experimentally. Even in solution, it may not be correct to use the spring constant associated with an ideal chain.²³ Also, the complications arising from hydrodynamic screening, which Zimm has considered for the case of dilute solutions, have been essentially ignored. Finally, in the normal-mode theories no direct account is taken of interchain interactions; it is tacitly assumed that one chain may pass through other chains to execute its normal-mode motion as if the latter were not present, that is, as if they were phantom chains (Chapter 6, Section B). The only role of these chains is to present a uniform viscous continuum in which the beads of the chain can move freely. Clearly, the influence of entanglements becomes difficult to visualize in this picture. In addition, the normal-mode theories provide no guidance on the role of more complicated chain architectures such as branches.

[†] The word “reptation” was created by De Gennes in 1971 (see De Gennes²³). The term “tube model” is used to describe complete theories that incorporate Rouse and reptation motions within a tube-like constraint of the surrounding polymer chains.

The reptation model, on the other hand, recognizes such impediments to chain motion. In Figure 3-24a a single chain is shown along with randomly placed dots that represent fixed obstacles to the chain motion. The reptation model suggests that the chain must move through this obstacle course in a worm-like fashion as relaxation occurs.

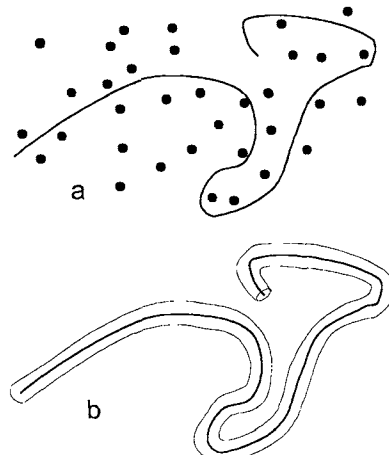


Figure 3-24. Reptation model view of a polymer chain: (a) with obstacles (dots); (b) in a tube.

Exact calculations based on this model are complex. Nevertheless, it is relatively easy to develop certain "scaling laws" that relate how various macroscopic properties might depend on molecular properties. We will briefly sketch the development of such a scaling law for viscosity and chain length (or molecular weight) based on the reptation model.^{23,24}

For convenience, motion of the chain through the set of obstacles of Figure 3-24a may be thought of as the motion of a chain constrained to move in a tube as shown in Figure 3-24b. The maximum relaxation time, τ_{\max} , can be associated with the time necessary for the molecule to diffuse out of the constraining tube. This is so because the contour of the original tube would be influenced by external stresses applied to the system, and these would be totally relaxed when the molecule was no longer contained in the tube. Thus the problem becomes one of calculating diffusion times of polymer molecules in tubes.

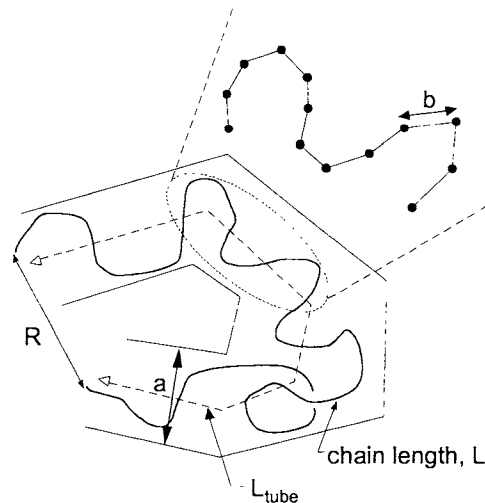
According to De Gennes,²³ this may be done as follows: First, apply a steady force f to the chain and observe its velocity v in the tube. Under these circumstances the mobility, μ_{tube} , of the molecule in the tube is defined as

$$v = \mu_{\text{tube}} f \quad (3-109)$$

Let n be the number of monomer units per molecule. To obtain the *same* velocity v_c with molecules of various contour lengths, that is with various values of n , the force must be directly proportional to n . Thus, equation (3-109) may be rewritten:

$$\frac{v_c}{\mu_{\text{tube}}} = f \propto n \quad \mu_{\text{tube}} = \frac{\mu_1}{n} \quad (3-110)$$

where μ_1 is independent of chain length. Knowing the molecular mobility allows one to calculate the diffusion constant through the Nernst-Einstein equation²⁵:



$$b \ll a \ll R \ll L_{\text{tube}} \ll L$$

Figure 3-25. Tube model with definitions of important length scales. [Adapted from R. G. Larson, T. Sridhar, L. G. Leal, G. H. McKinley, A. E. Likhtman and T. C. B. McLeish, *J. Rheol.*, **47**, 809 (2003), with permission.]

$$a = kT\mu_{\text{tube}} = \frac{kT\mu_1}{n} = \frac{a_1}{n} \quad (3-111)$$

where k is Boltzmann's constant and where a_1 is also independent of chain length. From the study of diffusion, it is well known²⁶ that

$$D = \frac{x^2}{2t} \quad (3-112)$$

where x is the average distance a molecule moves in time t in a medium of diffusion constant D . The direct combination of equations (3-111) and (3-112) gives

$$\tau_{\max} \propto \frac{L_{\text{tube}}^2}{a} = \frac{L_{\text{tube}}^2 n}{a_1} \propto n^3 \quad (3-113)$$

where the diffusion time has been identified with the maximum relaxation time and the diffusion distance with the tube length L_{tube} (Figure 3-25). Clearly, the tube length is directly proportional to the polymer chain length and thus the maximum relaxation time is predicted to depend on chain length to the third power.

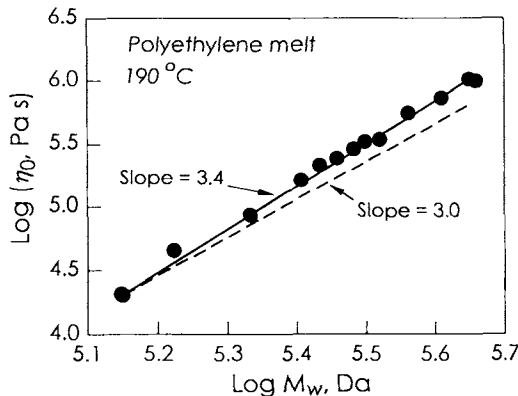


Figure 3-26. The molecular-weight dependence of the viscosities of a series of polyethylene melts. It can be seen that the slope of 3 predicted by equation (3-115) falls short, while a slope of 3.4 is virtually perfect. (Data from various sources.)

The viscosity associated with this reptating motion may now be calculated as

$$\eta = \tau G \quad (3-114)$$

In the elementary reptation model, the modulus G depends on distance between obstacles and is, therefore, not chain length dependent. Thus, the chain length dependence of η and τ_{\max} are predicted to be the same, that is,

$$\eta \propto n^3 \quad (3-115)$$

Equation (3-115) is an example of a scaling law in that it indicates how viscosity should depend on or "scale with" chain length and, therefore, molecular weight. It is perhaps a bit surprising that this equation can be derived so simply, considering the complicated picture of chain motion

suggested by the reptation model. It is known from experiment that the viscosity of polymer melts actually varies as about the 3.4 power of molecular weight (equation 3-96), as shown in Figure 3-26. The polymer must be above a critical molecular weight, which is related to that for entanglement.

Within the context of the tube model of entanglement melts and solutions, more complex motions are possible at shorter times. In addition there are additional phenomena at long times. For the latter, it is clearly unrealistic to expect the constraints of the tube to remain in place indefinitely. The process of removal of constraints is termed "constraint release." This results in the effective widening of the tube, referred to as "tube enlargement." A quantitative description of by des Cloizeaux²⁷ has been termed "double reptation" because the tube walls are reptating away from the chain at the same time the chain is reptating out of the tube. This becomes exceedingly important in considering mixtures of different molecular weights, and states, in essence, that the large molecules slow down the relaxation of the small molecules, while the small molecules speed up the relaxation of the large ones. The form of the relaxation is

$$G(t) = G_0 \left(\sum_{i=1}^N w_i \sqrt{F(t; M_i)} \right)^2 \quad (3-116)$$

where w_i are the weight fractions of the components, and F are the reduced relaxation functions $G(t)/G(0)$ of the components.

At times less than τ_{max} there are rapid motions within the tube that are thought to be Rouse-like.

APPENDIX: MANIPULATION OF THE ROUSE MATRIX

Equation (3-65), which will be derived in this appendix, represents the eigenvalues used in diagonalizing the matrix $[A]$ of equation (3-53)

$$[\dot{X}] = -B[A][X] \quad (3-53)$$

where $[A]$ is a square matrix of order $(z + 1)$.

$$[A] = \begin{bmatrix} 1 & -1 & 0 & . & . & . & . & . & . \\ -1 & 2 & -1 & 0 & . & . & . & . & . \\ 0 & -1 & 2 & -1 & 0 & . & . & . & . \\ 0 & 0 & . & . & . & . & . & . & . \\ 0 & 0 & . & . & . & -1 & 2 & -1 & 1 \\ . & . & . & . & . & 0 & -1 & 1 & . \end{bmatrix} \quad (a)$$

First transform $[A]$ into a form that will be easier to treat. To do this, note that

$$[A] = [C^T][C] \quad (b)$$

where $[C]$ is also a matrix of order $z \times (z + 1)$ and has the form

$$[C] = \begin{bmatrix} 1 & -1 & 0 & 0 & . & . & . \\ 0 & 1 & -1 & 0 & . & . & . \\ 0 & 0 & 1 & -1 & . & . & . \\ . & . & . & . & 1 & -1 & 0 \\ . & . & . & . & 0 & 1 & -1 \end{bmatrix} \quad (c)$$

and

$$[C^T] = \begin{bmatrix} 1 & 0 & 0 & 0 & . & . & . \\ -1 & 1 & 0 & 0 & . & . & . \\ 0 & -1 & 1 & 0 & . & . & . \\ . & . & . & . & . & . & . \\ . & . & . & . & -1 & 1 & . \\ . & . & . & . & 0 & -1 & . \end{bmatrix} \quad (d)$$

Thus, equation (3-53) can be written as

$$[\dot{X}] = -B[C^T][C][X] \quad (e)$$

Now premultiply both sides of this equation by $[C]$:

$$\begin{aligned} [C][\dot{X}] &= -B[C][C^T][C][X] \\ &= -B[R][C][X] \end{aligned} \quad (f)$$

where $[R]$ is called the Rouse matrix,

$$[R] = \begin{bmatrix} 2 & -1 & 0 & 0 & \cdot & \cdot & \cdot & \cdot \\ -1 & 2 & -1 & 0 & \cdot & \cdot & \cdot & \cdot \\ 0 & -1 & 2 & 1 & \cdot & \cdot & \cdot & \cdot \\ \cdot & \cdot \\ \cdot & \cdot & \cdot & \cdot & -1 & 2 & -1 & 0 \\ \cdot & \cdot & \cdot & \cdot & 0 & -1 & 2 & -1 \\ \cdot & \cdot & \cdot & \cdot & 0 & 0 & -1 & 2 \end{bmatrix} \quad (g)$$

which is a $z \times z$ square matrix. (See footnote near equation (3-65) for a discussion of matrix order.) The Rouse $[R]$ matrix can now be diagonalized by the approach mentioned in the text:

$$[\varphi^{-1}][R][\varphi] = [\Lambda] \quad (h)$$

Operation by $[\varphi^{-1}]$ from the left on equation (b) gives

$$[\varphi^{-1}][C][\dot{X}] = -B[\varphi^{-1}][R][\varphi][\varphi^{-1}][C][X] \quad (i)$$

In the above equation we took advantage of the fact that $[\varphi^{-1}][\varphi] = [I]$, similar to that shown in equation (3-61). Now define normal coordinates

$$[q] = [\varphi^{-1}][C][X] \quad (j)$$

and

$$[\dot{q}] = [\varphi^{-1}][C][\dot{X}] \quad (k)$$

which are slightly different from equation (3-63). This is done strictly for mathematical convenience and has no consequence in the final solution. Equation (i) can thus be recast as

$$[\dot{q}] = -B[\Lambda][q] \quad (3-64)$$

where $[q]$ and $[\dot{q}]$ are column matrices and $[\Lambda]$ is a diagonal matrix.

Now diagonalize $[R]$ by rewriting equation (h) as

$$[R][\varphi] = [\varphi][\Lambda] \quad (l)$$

Equation (1) requires that the corresponding elements in the matrices on both sides must be equal after the multiplication has been carried out. Thus, for each value of Λ_{ii} , we obtain a set of linear equations as follows (the reader may wish to verify them for a 3×3 matrix):

$$\begin{aligned}
 & (2 - \lambda)\varphi_{11} - \varphi_{12} = 0 \\
 & -\varphi_{21} + (2 - \lambda)\varphi_{22} - \varphi_{23} = 0 \\
 & -\varphi_{32} + (2 - \lambda)\varphi_{33} - \varphi_{34} = 0 \\
 & \dots \\
 & -\varphi_{z,z-1} + (2 - \lambda)\varphi_{zz} = 0
 \end{aligned} \tag{m}$$

where φ_{ij} is the ij th term in $[\varphi]$.

To solve the set of equations given above, we note that they all have the same form:

$$-\varphi_{m-1} + (2 - \lambda)\varphi_m - \varphi_{m+1} = 0 \quad (n)$$

with the condition that

$$\varphi_0 = \varphi_{z+1} = 0 \quad (o)$$

Equation (n) can be treated and solved as a difference equation. In operator notation it is just

$$[-E^{-1} + (2 - \lambda) - E] \varphi_m = 0 \quad (p)$$

where the operator E displaces a function in the positive direction and E^{-1} in the negative direction, that is,

$$E\varphi_m = \varphi_{m+1}$$

$$E^{-1}\varphi_m = \varphi_{m-1}$$

Now to solve equation (p), assume that the solution has the following form:

$$\varphi_m = \beta e^{m\alpha} \quad (q)$$

where β is a constant and α is a function to be determined. Insertion of equation (q) into (p) results in

$$\beta e^{m\alpha}[-e^{-\alpha} + (2 - \lambda) - e^{\alpha}] = 0 \quad (\text{r})$$

For equation (m) to yield nontrivial results, it is necessary that

$$-e^{-\alpha} + (2 - \lambda) - e^{\alpha} = 0$$

or

$$\frac{2 - \lambda}{2} = \frac{e^{\alpha} + e^{-\alpha}}{2} = \cosh \alpha \quad (s)$$

Equation (s) is satisfied by two values of α , namely $+\alpha$ and $-\alpha$, since $\cosh(+\alpha) = \cosh(-\alpha)$. Thus, the solution to the difference equation also must be satisfied by two functions (βe^{+ma} and βe^{-ma}). The general solution is then just

$$\varphi_m = P_1 \beta e^{+ma} + P_2 \beta e^{-ma} \quad (t)$$

where P_1 and P_2 are constants. Since

$$\sinh x = \frac{e^x - e^{-x}}{2}$$

and

$$\cosh x = \frac{e^x + e^{-x}}{2}$$

we can have the following equivalent general solution:

$$\varphi_m = M_1 \sinh(m\alpha) + M_2 \cosh(m\alpha) \quad (u)$$

where the M 's are constants. For $m = 0$, equation (o), the boundary condition, demands

$$\varphi_0 = 0 = M_2 \quad (v)$$

and

$$\varphi_m = 0 = \sinh(z + 1) \quad (w)$$

since M_1 is a constant. But the value of the hyperbolic sine is zero if the argument is an integral multiple of $(i\pi)$, where $i = \sqrt{-1}$. Therefore,

$$\alpha = \frac{ip\pi}{z + 1} \quad p = 1, 2, 3, \dots, z \quad (x)$$

Combination of equations (x) and (s) finally gives the desired result:

$$\begin{aligned}
 \lambda_p &= 2 - 2 \cosh \frac{ip\pi}{z-1} \\
 &= 2 \left(1 - \cos \frac{p\pi}{z+1} \right) \\
 &= 4 \sin^2 \left(\frac{p\pi}{2(z+1)} \right)
 \end{aligned} \tag{3-65}$$

where $p = 1, 2, 3, \dots, z$.

PROBLEMS

1. Calculate the slope of the curve in Figure 3-3c and its limiting value at reduced times t/τ much greater than 1.
2. Develop expressions for the complex modulus and compliance for a Maxwell body
 - (a) From the stress relaxation modulus of the body using the phenomenological theory of Chapter 2.
 - (b) From the equation of the Maxwell model equation (3-6) assuming a sinusoidal strain application.
3. Develop expressions for D' , D'' , E' , and E'' for a Voigt element
 - (a) From equation (3-31) using the phenomenological relationships of Chapter 2.
 - (b) From the equation of motion of the Voigt element, equation (3-26), assuming a sinusoidal stress application. (Notice the appearance of a transient term when the boundary condition $\varepsilon(0) = 0$ is used.)
4. Derive an expression for the complex modulus of a generalized Maxwell model subjected to a sinusoidal strain. Show that the complex compliance is not obtainable as a simple analytical function.
5. Derive an expression for the complex modulus of z Maxwell elements in series assuming a sinusoidal strain application.
6. Bueche⁶ has shown that the flexible bead-and-spring model leads to the following expression for the creep compliance of an undiluted polymer:

$$D(t) = \frac{8}{3NkT\pi^2} \sum \frac{1}{p^2} (1 - e^{-t/\tau_p})$$

where $p = 1, 3, 5, \dots, z$. In this case the retardation times are given by

$$\tau_p = \frac{\rho_s a^2 z^2}{3\pi^2 k T p^2} \quad p = 1, 3, 5, \dots, z$$

Show that

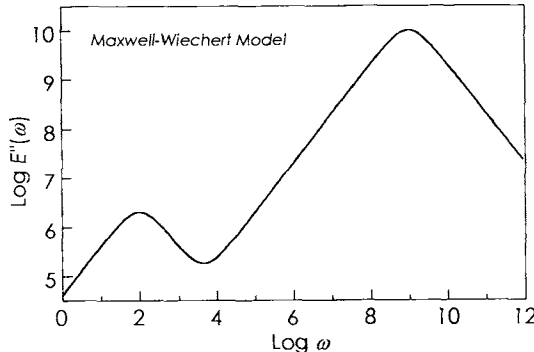
- (a) The retardation times can be rewritten as

$$\tau_p = \frac{12\eta}{N\pi^2 k T p^2}$$

- (b) The partial compliances of the equivalent Voigt-Kelvin model are

$$D_p = \frac{8}{3NkT\pi^2 p^2}$$

7. Determine the parameters for a two-element generalized Maxwell model (E_1, E_2, τ_1, τ_2) which would give a $\log E''(\omega)$ versus $\log \omega$ response similar to that shown below:



8. Show that equation (3-90) yields the viscosity for a generalized Maxwell model.
 9. Calculate the slope of a stress relaxation master curve at some time t when $\tau_{\min} < t < \tau_{\max}$ where

$$\tau_p = \frac{\tau_{\max}}{p} \quad E_p = k$$

10. It is frequently necessary to obtain the function $H(\tau)$ from experimental data, and various approximations are useful in carrying out this transformation. Show that the so-called first approximation:

$$H_1(\tau) \equiv - \left. \frac{dE(t)}{d \ln t} \right|_{t=\tau}$$

results from approximating the expression in equation (3-42) by a unit step at $t = \tau$.

11. (a) Derive an expression for $H_1(\tau)$ for a Maxwell body. Plot this function as $\log H_1(\tau)/E_0$ versus $\tau / \tau_{\text{Maxwell}}$. Be sure to remember that the relaxation time for the Maxwell body is a constant.

(b) Compare the above result with $H_2(\tau)$, a second approximation of $H(\tau)$ which is given as

$$H_2(\tau) \equiv \left(-\frac{dE(t)}{d \ln t} + \frac{d^2 E(t)}{d(\ln t)^2} \right)_{t=2\tau}$$

12. (Computer) Consider the Rouse model depicted in Figures 3-16 and 3-18, and as described by equations (3-88) and (3-89).

(a) Verify numerically the behavior of $G(t/\tau_1)$, $G'(\tau_1 \omega)$, $G''(\tau_1 \omega)$, and $|\eta^*(\tau_1 \omega)|$ as the number of modes becomes large.

(b) Compare your numerical results for $G(t/\tau_1)$ using a stretched exponential (Kohlraush-Williams-Watts) relaxation function $G(t) = G(0)\exp[(-t/a\tau_1)^b]$, where a and b are adjustable parameters.

(c) Using your numerical results, invent a continuous empirical expression for the frequency response of $G'(\tau_1 \omega)$, where τ_1 is the longest relaxation time ($p = 1$ mode). Assume limiting slopes of 2 and $\frac{1}{2}$ at low and high frequencies, respectively. Use equation 3-78 for guidance.

13. (Computer) Starting the double reptation relationship equation (3-116) for a bimodal mixture, use an iterative process to estimate the molecular-weight ratio of the two components of the blend with the relaxation data listed in file MW-Blend.TXT in the CD. This data is for a 50:50 blend. Assume exponential forms for the $F(t, M_i)$.

14. If $G(t) = G_0/(1 + t/\tau)^n$, what is the lowest value of n that will give a finite shear viscosity. (Refer to Figure 3-19 and accompanying discussion.)

15. Explore the nature of $dG(t)/dt$ and $d \log G(t)/d \log t$ for the Maxwell, KWW and Rouse relaxation functions as $t \rightarrow 0$ and ∞ .

16. An *isochronal* stress-strain curve is established by applying deformation to a sample at various strain rates and cross-plotting the results at a fixed time. In this fashion the effects of strain can be separated from the effects of time.

(a) Show that the isochronal stress-strain curve is linear for a generalized Maxwell material. Calculate the time-dependent modulus from this result.

(b) Calculate and plot vs. t/τ the isochronal modulus for a single Maxwell model [$G(t) = Ge^{-\mu t}$] where the data are gathered using stress growth, creep and stress relaxation experiments. Compare the results.

17. Using the Rouse model for bulk materials, estimate the molecular weight of the PMMA described by the data in PMMA45.TXT in the CD. Compare with the reported molecular weight of 45 kDa.

18. (Computer) Repeat the calculation of viscosity of PIB shown in Figure 3-19 using the data PIB-Rel-1.TXT or PIB-Rel-2.TXT (either one) in the CD. Use both a KWW and an exponential function to extrapolate data to long times. Comment on differences, if any between these two methods.

REFERENCES

1. J. D. Ferry, *Viscoelastic Properties of Polymers*, 3rd ed., Wiley, New York, 1980, p. 213.
2. B. Gross, *Mathematical Structure of the Theories of Viscoelasticity*, Herman, Paris, 1953.
3. S. W. Provencher, *Comput. Phys. Commun.* **27**, 229 (1982).
4. P. E. Rouse, *J. Chem. Phys.*, **21**, 1272 (1953).
5. W. L. Peticolas, *Rubber Chem. Technol.* **36**, 1422 (1963).
6. F. Bueche, *J. Chem. Phys.*, **22**, 603 (1954).
7. B. H. Zimm, *J. Chem. Phys.*, **24**, 269 (1956).
8. P. E. Rouse and K. Sittel, *J. Appl. Phys.*, **24**, 690 (1954).
9. R. B. DeMallie Jr., M. H. Bimboim, J. E. Frederick, N. W. Tschoegl, and J. D. Ferry, *J. Phys. Chem.*, **66**, 586 (1962).
10. J. D. Ferry, R. F. Landel, and M. L. Williams, *J. Appl. Phys.*, **26**, 359 (1955).
11. M. L. Williams, *J. Polym. Sci.*, **62**, 57 (1962).
12. A. V. Tobolsky and D. B. DuPré, *Adv. Polym. Sci.*, **6**, 103 (1969).
13. J. J. Aklonis and V. B. Rele, *J. Polym. Sci., Polym. Symp.*, **46**, 127 (1974).
14. M. Abramowitz and I. A. Stegun, Eds., *Handbook of Mathematical Functions with Formulas, Graphs and Mathematical Tables*, Dover, New York, 1972.
15. W. H. Press, B. P. Flannery, S. A. Teukolsky and W. T. Vetterling, *Numerical Recipes*, 2nd ed., Cambridge University Press, Cambridge, UK 1992.
16. A. V. Tobolsky, *J. Chem. Phys.*, **37**, 1575 (1962).
17. M. Shen, W. F. Hall, and R. E. DeWames, *J. Macromol. Sci.*, **C2**, 183 (1968).
18. L. Duffrène, R. Gy, H. Burlet, R. Pignes, *J. Rheol.*, **41**, 1021-1038 (1997).
19. F. Kohlrausch, *Pogg. Ann. Phys.* **8**, 337 (1876).
20. K. Okun, M. Wolfgardt, J. Baschnagel, and K. Binder, *Macromolecules*, **30**, 3075 (1997).
21. J. G. Curro and P. Pincus, *Macromolecules*, **16**, 559 (1983)
22. R. Chasset and P. Thirion, *Chim. Ind. Gén. Chim.* **97**, 617 (1967).
23. P. G. De Gennes, *Scaling Concepts in Polymer Physics*, Cornell University Press, Ithaca, N.Y., 1979.
24. R. G. Larson, T. Sridhar, L. G. Leal, G. H. McKinley, A. E. Likhtman and T. C. B. McLeish, *J. Rheol.*, **47**, 809 (2003)

106 VISCOELASTIC MODELS

25. R. B Bird, W. E. Stewart, E. N. Lightfoot, *Transport Phenomena*, Wiley, New York, 1960.
26. A. W. Adamson, *A Textbook of Physical Chemistry*, 2nd edition, Academic Press, New York, 1979, p. 60.
27. J. des Cloizeaux, *Macromolecules*, **23**, 4679 (1990)

4

Time–Temperature Correspondence

Having examined some of the basic manifestations of the phenomenological aspects of viscoelasticity in Chapter 2, along with the efforts to model this behavior in Chapter 3, we now shift our emphasis to the results of experiments on polymers, and the interpretation of these results in terms of the accepted molecular mechanisms. We then explore the important idea of time–temperature correspondence and demonstrate the close relationship between these two variables in determining the viscoelastic responses of polymers.

A. FOUR REGIONS OF VISCOELASTIC BEHAVIOR

Once again, let us begin by considering an experiment. A polymer sample of unit cross-sectional area is subjected to an instantaneous tensile strain that is thereafter maintained constant. The tensile stress $\sigma_E(t)$ is monitored as a function of time, and the tensile stress relaxation modulus is obtained using equation (2-32). Let t in equation (2-32) be any arbitrary time, perhaps 10 seconds. Next the stress is removed, allowing the sample to relax, and the temperature is changed. The same experiment is carried out, yielding E (10 seconds) at this new temperature. The experiment is repeated at many temperatures to yield the "ten-second tensile relaxation modulus" as a function of temperature.¹ For short, this is referred to as a "modulus-temperature curve." Alternatively, we might run the experiment in shear using a dynamic

test and record the shear storage modulus G' at, say, 0.1 rad/s as a function of temperature.*

The types of behavior most often observed are shown in Figures 4-1 to 4-3. (We have selected tensile relaxation as an example; other types of deformation would have been equally suitable.) Figure 4-1 shows idealized modulus-temperature curves for typical linear and crosslinked amorphous polymers. In this plot, four regions of viscoelastic behavior are identified. At low temperatures where the modulus is higher than 10^9 Pa, the polymer is hard and brittle; this is the glassy region. The glassy modulus, E_1 , a slowly decreasing function of temperature, is a useful parameter to use in characterizing polymeric behavior. In this glassy region, thermal energy is insufficient to surmount the potential barriers for rotational and translational motions of segments of the polymer molecules. The chain segments are essentially "frozen" in fixed positions on the sites of a disordered quasi-lattice with their segments vibrating around these fixed positions much like low-molecular-weight molecules in a molecular crystal. With increasing temperature, the amplitude of vibrational motion becomes greater, and eventually the thermal energy becomes roughly comparable to the potential energy barriers to segment rotation and translation. In this temperature region, the polymer is at the glass transition temperature where short-range diffusional motions begin. Segments are free to "jump" from one lattice site to another; the brittle glass becomes a resilient leather.

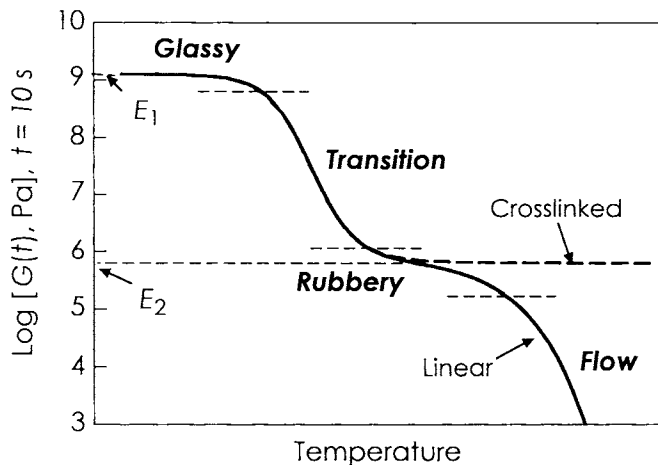


Figure 4-1. Schematic modulus-temperature curve showing various regions of viscoelastic behavior.

* The data for the "modulus-temperature curve" are most often gathered in the dynamic mode at a fixed frequency of around 1 rad/s, either in shear or flex, depending on the stiffness range of the test material over the desired temperature range. See Appendix 3 of Chapter 2.

The glass transition is accompanied by a precipitous decrease in the modulus of several decades, as indicated in Figure 4-1. The breadth of this transition region ranges from 5 °C to more than 20 °C, depending on the nature of the polymer in question.

As the temperature is further increased, the modulus again reaches a plateau region. This rubbery plateau is characterized by the modulus E_2 , as shown in Figure 4-1. In this temperature interval, the short-range diffusional motions of the polymer segments that initially gave rise to the glass transition occur very much faster than our measurement time of 10 seconds. On the other hand, the long-range cooperative motions of chains that would result in diffusion of complete molecules are still greatly restricted by the presence of strong local interactions between neighboring chains. In the case of the crosslinked material, these interactions consist of primary chemical bonds. In the linear polymer, they are known as entanglements, and their precise nature is not clear. In any case, in the rubbery plateau region, segments of chains reorient relative to each other but large-scale translational motion does not occur in the allotted 10 seconds.

The viscoelastic responses of linear and crosslinked polymers through the rubbery plateau region are essentially identical. As the temperature is further increased, however, differences between these two categories of polymers become evident, as shown in Figure 4-1. First consider a crosslinked network. As temperature is increased, the crosslinks consisting of primary chemical bonds remain intact, preventing the chains from translating relative to one another. Thus, although the modulus changes slightly with temperature in the rubbery plateau region of a crosslinked polymer (Chapter 6, Section A), the changes are small compared to those exhibited during the glass transition. Thus, to a first approximation, the modulus will remain constant for a crosslinked rubber up to temperatures where chemical degradation begins to occur.

The situation is quite different for a linear polymer. In this case, increasing temperature causes larger scale molecular motions until eventually whole polymer molecules begin to translate. When the temperature is high enough, local chain interactions are no longer of sufficiently high energy to prevent molecular flow. During the 10-second test, the molecules will slip by one another, and the polymer sample will exhibit a correspondingly low modulus. Because the molecules are translating relative to one another in this region, it should be expected that a considerable amount of permanent flow will result from experiments carried out under these conditions. When the strain is released in our stress relaxation experiment, the sample will not recover to its former length but will relax to a new equilibrium state having a greater length.

Thus, during the experiment the sample has undergone flow, and this area of the 10-second modulus temperature curve is therefore called the flow region.

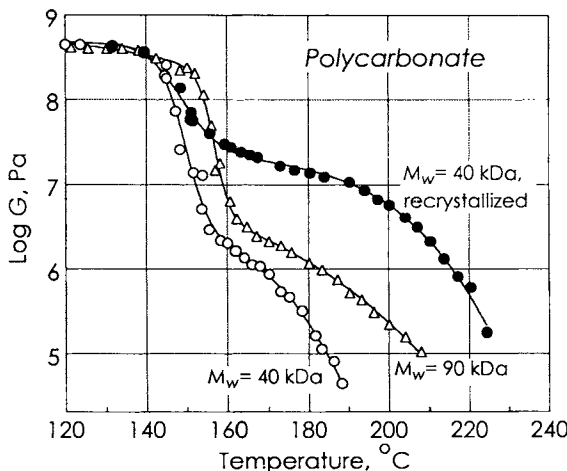


Figure 4-2. Shear modulus[†] vs. temperature behavior for two polycarbonate samples of different molecular weights, along with the response of a partially crystallized sample. (See Chapter 5 for additional discussion.) [Adapted from J. P. Mercier, J. J. Aklonis, M. Litt and A. V. Tobolsky, *J. Appl. Polym. Sci.* **9**, 447-459 (1965). Copyright 1965 © Wiley Periodicals, Inc., a Wiley Company.]

If temperature is increased still further, barring chemical reaction the sample will become a viscous liquid. Our simple experimental setup is no longer applicable at high temperatures where the sample will not support its own weight. The modulus will, however, continue to decrease.

With this background, it will be easy to proceed with the analysis of the modulus-temperature behavior of more complicated systems.

First consider the effect of different molecular weights in linear amorphous systems. Figure 4-2 shows the modulus-temperature behavior of two polycarbonate samples. The 40-kDa sample was available in two forms: amorphous (open circles) and partially crystalline (filled circles). A higher molecular weight sample, 90 kDa, was available only in the amorphous form. At temperatures below 140 °C, the materials are identical. There is no differentiation between the samples since short-range segmental motions are determining the behavior. Such motions are essentially independent of molecular weight at high molecular weights. At higher temperatures, however, where translational motions of the complete molecules determine the relaxation

[†] These historical data⁴ were gathered using the Clash-Berg creep apparatus, which yields $J(t)$ at $t = 10$ s. The inversion of these data is the value plotted in Figure 4-2, and clearly will be different than $G(t)$ at $t = 10$ s, especially in the transition regions. This will result in a slight temperature shift (see Problem 4-10).

behavior of the sample, it is most reasonable to expect longer molecules to maintain a pseudo-network to higher temperatures. This is indeed observed as shown in Figure 4-2. We notice that the initial decay of the glassy modulus for the 40-kDa sample occurs at lower temperatures than is the case with the high-molecular-weight polymer and the rubbery plateau is less pronounced. The behavior of the 40-kDa sample in the glass transition region may be qualitatively accounted for on the basis of "free volume" considerations as follows (more detail is given in Chapter 5). Because a linear polymer chain has two ends, decreasing the length of the chains leads to an increase in the concentration of ends in the sample. However, because a chain middle is attached to other segments on both sides, it is less mobile than a chain end attached on only one side. Thus a polymer sample that has a greater concentration of chain ends than another comparable sample will exhibit greater chain mobility at a given temperature. In other words, a decrease in molecular weight leads to a decrease in glass transition temperature. The abbreviated rubbery plateau is due to the fact that the short molecules present in this low molecular weight sample form relatively few entanglements, and these are able to disentangle at a relatively low temperature compared to the 90-kDa sample. The semicrystalline sample, on the other hand, has a pronounced and high rubbery plateau because the crystallites are acting like crosslinks until they start melting at around 200 °C.

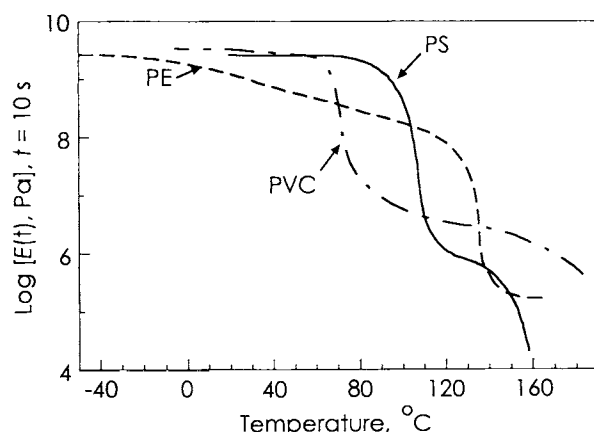


Figure 4-3. Comparison of ten-second modulus vs. temperature curves for three common thermoplastics: polyvinyl chloride (PVC), polystyrene (PS) and polyethylene (PE).

For a polymer where crystallinity dominates its relaxation behavior, the situation is quite different. Figure 4-3 shows the 10-second modulus vs. temperature curve for such a crystalline polymer, polyethylene (PE). Included also in this figure is the modulus-temperature curve for polyvinyl chloride

(PVC), a polymer with extremely low crystallinity. These two are contrasted with atactic polystyrene (PS), a typical noncrystalline polymer.

It should be emphasized that all of the crystalline polymers discussed here are not totally crystalline but partly crystalline and partly amorphous. Thus one expects to see behavior characteristic of the crystalline regions superposed upon behavior characteristic of the amorphous regions. This superposition is not necessarily a linear one but may rather be a complex coupling of the response of each region. Furthermore, the degree of crystallinity as well as the crystallite size is not a unique feature of any polymer system. Both of these properties are determined by prior thermal history.

The general characteristics attributed to the amorphous portion are not greatly modified in crystalline polymers with low crystallinity, such as PVC and to some extent the polycarbonate sample shown in Figure 4-2. There is still a glass-to-rubber transition, a rubbery plateau, and finally, in uncrosslinked systems, a flow region. The amorphous material, however, couples with the crystalline portion of the polymer. The main transition exhibited by the crystalline part of the polymer is a melting from an ordered crystal to a liquid, disordered state. The temperature of this melting is usually given the symbol T_m ; however, it should be recognized that the melting process does not occur at a single temperature but over a range of temperatures corresponding to the range of sizes and morphologies of the crystallites.

With these thoughts in mind, one may now analyze the curves in Figure 4-3. Consider polyethylene; T_m is about 125 °C. While the temperature of the glass transition is not yet known with certainty, it seems clear that it is low, probably lower than -70 °C. At temperatures between the glass transition temperature and T_m , the polymer exhibits a very high modulus. Molecularly, this is to be expected because, in polyethylene, a large portion of the polymer is crystalline. Therefore, in this region one is observing the relaxation of a small amount of material held together by numerous hard crystallites, leading to a high modulus. As T_m is approached, changes in the crystalline superstructure and in the degree of crystallinity result in a rapid decrease of the modulus. At the melting point, the modulus drops sharply to the rubbery plateau characteristic of amorphous polyethylene. With the crystallites gone, we are left with essentially a normal amorphous polymer that will exhibit behavior characteristic of amorphous polymers. This, indeed, is so for polyethylene where a rubbery plateau and eventually a flow region are observed at temperatures above T_m .

The situation is somewhat similar in the case of polyvinyl chloride (PVC). PVC has a far lower degree of crystallinity than polyethylene so that the viscoelastic response of PVC might be expected to approximate more closely that of an amorphous polymer than does polyethylene. Figure 4-3 indicates that

this is indeed the case. Specifically, the modulus drop in PVC at T_g is considerably greater than that in polyethylene, although the rubbery plateau modulus is higher than that of amorphous polymers and the rubbery plateau extends to the melting point of the PVC crystallites, about 180 °C. In polymers of low crystallinity like PVC and the recrystallized polycarbonate sample in Figure 4-2, the rubbery plateau can be well explained by the postulate that the crystallites act as both filler particles and as crosslinks. ("Filler" is used here in the sense of a the particulate solids often added to polymers to increase stiffness and improve other properties.) The PVC has a minor amount; the polycarbonate, considerably more.

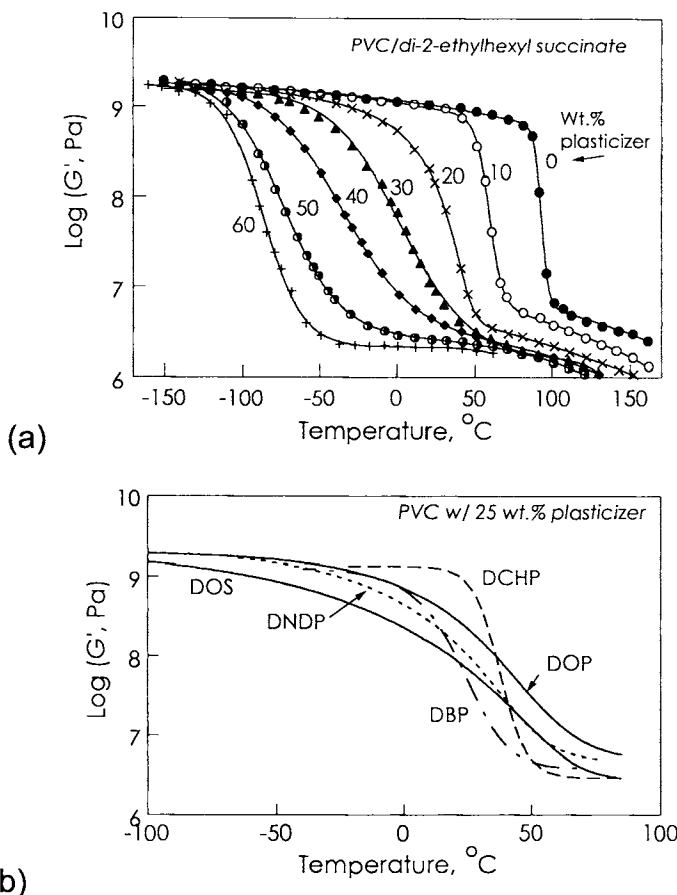


Figure 4-4. Panel (a) shows the influence of plasticizer content on the modulus-temperature response of PVC through the glass transition region. Note that increasing plasticizer content tends to broaden the transition markedly at first and then the effect decreases at even higher concentrations.² [From Figure 7 in K. Schmieder and K. Wolf, *Kolloid Z.* 127 65 (1952), © Springer-Verlag, 1952. With kind permission of Springer Science and Business Media.] The data in panel (b) suggests that the broadening effect is highly dependent on the chemical nature of the plasticizer as well. [After K. Boo, Ph.D, Thesis, University of Connecticut, Storrs, CT, (1990), with permission.]. See also Problem 5-8.

Once again, it should be pointed out that the exact shape of the modulus-temperature curve of a crystalline polymer depends on the thermal history of the sample, particularly on the rate of cooling from the melt and annealing treatment. Two crystalline polymers are mechanically "equivalent," for practical purposes, if they have the same values of T_g , T_m chain length, percentage of crystallinity, and crystalline structure. Because this is rarely the case, semicrystalline polymers exhibit a wide spectrum of properties.

The incorporation of soluble diluents (solvents, plasticizers) into polymers alters the viscoelastic properties to a greater or lesser extend depending on the exact polymer diluent system and the amount of diluent present. One of the most important polymers used in the plasticized state is polyvinyl chloride. Figure 4-4a shows that PVC plasticized with di-2-ethyloctyl succinate differs significantly from pure PVC in viscoelastic behavior. Although E_1 and E_2 appear to be essentially independent of the presence of diluents, other characteristic parameters show important effects. For example, T_i , the inflection temperature of the modulus-temperature curve, is depressed systematically with plasticizer content. In addition, the transition region is broadened at low plasticizer concentrations, and then narrows. It was pointed out previously that rubbery flow commences in PVC when T_m is exceeded. Since T_m is depressed due to the presence of diluent, the flow region begins at a lower temperature than for unplasticized PVC. If we regard diluent as part of the polymer system, then the occurrence of the flow region at lower temperatures might be interpreted as being due to the lowering of the number average molecular weight. An alternative interpretation is to regard the diluent as simply lowering the thermodynamic activity of polymer segments in the amorphous region relative to those in the crystalline region, thus shifting the equilibrium in favor of a "solution" of segments in the plasticizer-rich "phase." The markedly different behavior of the different plasticizers shown in Figure 4-4b tend to support the latter hypothesis.

As the plasticizer molecules are small, the explanation for the low glass transition temperature of the plasticized systems is likely to be associated with the easier motions of the smaller molecules due to fewer constraints than macromolecules of equivalent chemical structure. More detailed and quantitative arguments concerning the role of plasticizers can be found in Chapter 5.

B. TIME-TEMPERATURE SUPERPOSITION

Remembering that the modulus is a function of time as well as temperature leads us to wonder about the parallels between modulus measured as a function

of time at constant temperature and modulus measured as a function of temperature at constant time, as discussed in the first part of this chapter. In principle, the complete modulus-time behavior of any polymer can be measured at any temperature using the techniques outlined in Chapter 2. In practice, the experiment is difficult to do over a time "window" of more than about 4 decades. The results of such an experiment with a limited time window are shown on the left side of Figure 4-5, where tensile stress relaxation has been chosen as the experiment. Clearly, only a small range of viscoelastic response manifests itself during the accessible time window, but the adjacent curves at different temperatures curiously appear to suggest something about what might happen if the time window were larger. Indeed, experimentalists have found a shifting procedure that enables one to construct a "master curve"—a complete modulus-time behavior at a constant temperature. This empirical procedure, referred to as time-temperature superposition, leads to a more general hypothesis called time-temperature correspondence that can be rationalized by consideration of fundamental molecular motions in polymers (Chapter 7).

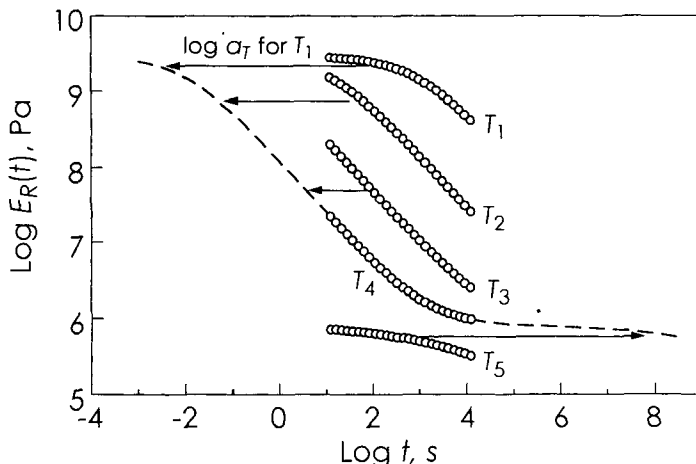


Figure 4-5. Construction of a master curve using tensile stress relaxation data gathered at five temperatures.

The time-temperature correspondence principle states that there are two methods to use to determine the polymer's behavior at longer (or shorter) times than those covered by a stress-relaxation experiment run at T_1 . First, one may improve the experiment to measure directly the response at longer (shorter) times. For the longer times, however, this procedure rapidly becomes prohibitively time-consuming because the change is so slow (note that Figure 4-5 is plotted on a log scale). (For the shorter times, the limitations are equipment related, e.g., transducer response time, problems with instrument and sample inertia, etc.) An alternative, according to the time-temperature

correspondence principle, is to increase the temperature to T_2 , for example, and again carry out the relaxation experiment using the experimentally accessible time range. Then, shifting curve T_2 horizontally to the right will result in an exact superposition of the curves measured at T_1 and T_2 in the areas where the modulus values overlap and an extension of the curve measured at T_1 to modulus values lower than those measured at temperature T_1 . The time-temperature correspondence principle asserts that this extension is identical to the response that would be found at long times at the temperature T_1 , if one were able to do the experiment. Thus, one effectively has a measure of the complete modulus-time behavior by applying the time-temperature correspondence principle to experimental measurements of polymer relaxations carried out on experimentally accessible time scales.

Again it should be emphasized that there are two aspects to time-temperature superposition: (1) empirical superposition of data gathered at different temperatures to form a single master curve, and (2) representation of the actual relaxation of the polymer at a single temperature by this composite curve. The second does not automatically follow from the first; indeed, Plazek has shown that equivalence is not quantitatively correct except in limited time-temperature ranges.³ However, there have been positive demonstrations of time-temperature equivalence for a few polymers and many successful applications to amorphous polymers. It should be clear from the previous discussion that the principle cannot be expected to apply to multiphase or semicrystalline polymers.

Mathematically, time-temperature equivalence may be expressed as

$$G(t, T_1) = G(t/a_T, T_2) \quad (4-1)$$

where the notation indicates that the stress relaxation modulus G is a function of both time and temperature. It can be seen from this expression that the effect of changing temperature is the same as applying a multiplicative factor to the time scale, which corresponds to an additive shift to the log time scale. Note that the development here uses the shear modulus, but could as well be done with the tensile modulus, E , or the corresponding compliance or dynamic functions.⁴

When shifting experimental data, one additional correction is necessary. We have, by shifting horizontally, compensated for a change in the time scale brought about by changing temperature. There is also, however, an inherent, but small, change in the modulus brought about by a change in temperature. (Remember, we are trying to describe the behavior at T_1 using data taken at T_2 but as if the data had been taken at T_1 .) In Chapter 6 it is shown that the modulus of a rubbery network is directly proportional to T , the absolute

temperature. Thus, in applying a reducing procedure to make a master curve for individual relaxation experiments, not only must one take into account the time-scale shift, one must also consider that there will be a slight vertical shift due to the temperature variation. Similarly, since the volume of a polymer is a function of temperature, and the modulus, being defined per unit cross-sectional area, will obviously vary with the amount of matter contained in unit volume, a corresponding correction must be made to account for the change of mass per unit volume with temperature. The density is obviously the parameter that must be used. These considerations lead one to write:³

$$\frac{G(t, T_1)}{\rho(T_1)T_1} = \frac{G(t/a_T, T_2)}{\rho(T_2)T_2} \quad (4-2)$$

Division by the temperature corrects for the changes in modulus due to the inherent dependence of modulus on temperature, while division by the density corrects for the changing number of chains per unit volume with temperature variation.

When constructing a master curve, one arbitrarily picks a reference temperature, T_0 . (Instead of T_0 , many authors choose to use T_R to signify the reference temperature.) The modulus at any time t , which one would observe at the temperature T_0 in terms of the experimentally observed modulus values at different temperatures T , is therefore given as

$$G(t, T_0) = \frac{\rho(T_0)T_0}{\rho(T)T} G(t/a_T, T) \quad (4-3)$$

where a_T is to be discussed more fully. If one is considering compliance functions, e.g., $J(t)$, equation (4-2) takes the form

$$\rho(T_1)T_1 J(t, T_1) = \rho(T_2)T_2 J(t/a_T, T_2) \quad (4-4)$$

and

$$J(t, T_0) = \frac{\rho(T)T}{\rho(T_0)T_0} J(t/a_T, T) \quad (4-5)$$

C. MASTER CURVES

We may now consider the preparation of a master curve from the data in Figure 4-5; these are depicted by circles and cover the experimental time range from about 10 to 10^4 s. First, let us arbitrarily pick T_4 as the reference temperature.

With a knowledge of the density at all the temperatures T_i , one applies the vertical correction factor stated in equation (4-3) to all the curves. For T_4 the factor $\rho(T_0)T_0/\rho(T)T$ is unity, resulting in no shift. This must be so since T_4 has been chosen as the reference. At the other temperatures, however, the correction factor will not in general be unity. Let us now consider that these corrections have been made to the experimental data to give the reduced modulus E_R as depicted. Next, the curve at T_3 is shifted to the left, giving rise to the dotted extension of the $E(t, T_4)$ curve. At temperature T_5 , which is higher than T_4 , the curve needs to be shifted to the right. This shifting process is repeated until a smooth master curve is formed.[†] Again this procedure is mathematically described by equation (4-3), but with E instead of G . The a_T 's are functions of temperature and are known as the shift factors. The subscript T indicates that the shift factors are taken relative to some reference temperature, but remember that the value of a_T depends on both temperatures.

It should be clear that any temperature might have been chosen as the reference temperature. If T_3 had been chosen, for example, only two of the shifts (T_1 and T_2), would have been to the left with shift factors larger than 1.0, while two of the shift factors (T_4 and T_5) would have been to the right with shift factors less than 1.0. In fact, one does not need to use one of the experimental temperatures as the reference temperature; any value within the temperature range can be used simply by interpolation.⁵

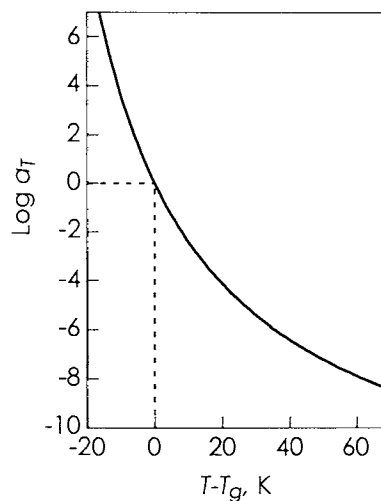


Figure 4-6. The WLF equation using the constants for polystyrene listed in Table 4-1

[†] The algorithm for accurately establishing the amount of shift is not completely trivial, as the data segments are often not perfectly superposable. See, e.g., Gordon and Shaw.⁵

D. THE WLF EQUATION

A common practice is to reduce relaxation or creep data to the temperature T_g ; thus, the reference temperature is picked as the glass transition temperature measured by some slow technique such as dilatometry. The reason for choosing T_g as the reference temperature is founded on the idea that all amorphous polymers at their glass transition temperature will have similar viscoelastic behavior. This type of corresponding states principal is often expressed in terms of a hopefully universal mathematical relationship between the shift factor a_T at a particular temperature and the difference between T_g and this temperature. Perhaps the most well known of these relationships is the WLF equation

$$\log a_T = \frac{-C_1(T - T_g)}{C_2 + T - T_g} \quad (4-6)$$

after its discoverers Williams, Landel, and Ferry.⁶ The constants, C_1 and C_2 , originally thought to be universal constants, have been shown to vary from polymer to polymer. A list of C_1 and C_2 for several of the most common polymers is presented in Table 4-1, while Figure 4-6 shows the dependence of a_T on the temperature offset $T - T_g$. Note that the shift factor a_T at the reference temperature T_g (i.e., $T - T_g = 0$) is 1.0, and thus $\log a_T$ is zero.

Table 4-1. WLF Parameters⁴

Polymer	C_1	C_2 , K	T_g , K
Polyisobutylene	16.6	104	202
Natural rubber (Hevea)	16.7	53.6	200
Polyurethane elastomer	15.6	32.6	238
Polystyrene	14.5	50.4	373
Poly(ethyl methacrylate)	17.6	65.5	335
"Universal constants"	17.4	51.6	

The form of equation (4-6) is predicted in a straightforward way from rather simple theoretical considerations. First, however, we must realize that the shift factor a_T is not only meaningful in terms of moduli, but material properties such as diffusivity and viscosity. Taking the latter as an example, we start with the equation (Chapter 3, Problem 3-8)

$$\eta(T) = \int_0^\infty G(t, T) dt \quad (4-7)$$

where $\eta(T)$ is the shear viscosity of a polymer at the temperature T . Now consider two master curves at two different temperatures. The two temperatures that we choose are T_g , our reference temperature, and T , any other temperature. We can write

$$G(t/a_T, T_g) = G(t, T) \quad (4-8)$$

where we have assumed time-temperature correspondence; that is, every modulus value $G(t/a_T, T_g)$ has a corresponding modulus value of equal magnitude $G(t, T)$ on the master curve at temperature T . (We are neglecting the vertical shifts for simplicity; their inclusion would substantially add to the complexity of this discussion but would not substantially affect the outcome.)

Equation (4-7) can be written as well for the shear viscosity at T_g , becoming

$$\eta(T_g) = \int_0^\infty G(t', T_g) dt' \quad (4-9)$$

where t' is a dummy variable for this integration and could be given any symbol without influencing the outcome. Because of the limits of integration, 0 and ∞ , we can make the following substitution:

$$t'' = a_T t' \quad \text{and} \quad dt'' = a_T dt' \quad (4-10)$$

in equation (4-9) to give

$$\eta(T_g) = \int_0^\infty G(t', T_g) dt' = \int_0^\infty G(t''/a_T, T_g) dt''/a_T \quad (4-11)$$

Note that the limits of the integral are unchanged as can be seen from equation (4-10). Because a_T is dependent only on temperature, it can be treated as a constant that can be factored out of the integral, giving

$$\eta(T_g) = \left[\int_0^\infty G(t''/a_T, T_g) dt'' \right] / a_T = \left[\int_0^\infty G(t'', T) dt'' \right] / a_T = \eta(T) / a_T \quad (4-12)$$

where once again use has been made of equations (4-7) and (4-8). The general result of equation (4-12) is that the time shift factor for any temperature relative to any reference temperature, T_0 , including $T_0 = T_g$, is simply the ratio of the viscosities at the two temperatures, that is,

$$a_T = \frac{\eta(T)}{\eta(T_g)} = \frac{\eta(T)}{\eta(T_0)} \quad (4-13)$$

With this result in hand, we may now return to the theoretical rationalization of the form of the WLF equation. The starting point is the semiempirical Doolittle equation for the viscosity of a liquid

$$\ln \eta = \ln A + B \left(\frac{V - V_f}{V_f} \right) \quad (4-14)$$

which gives an expression for the viscosity of a system in terms of two constants A and B .⁷ As was stated earlier, this viscosity could be the tensile viscosity or the shear viscosity. V is the total volume of the system while V_f is the free volume available to the system (a qualitative rather than quantitative view of free volume is sufficient for this discussion). The interpretation of equation (4-14) is that viscosity is intimately connected with mobility, which is closely related to free volume. As the free volume increases, the viscosity rapidly decreases. This equation has been found to express the viscosity dependence of simple liquids to a high degree of accuracy. Rearrangement of equation (4-14) gives

$$\ln \eta = A + B \left(\frac{1}{f} - 1 \right) \quad (4-15)$$

where f is the fractional free volume V_f/V . It is now assumed that above the glass transition temperature, the fractional free volume increases linearly with temperature, that is,

$$f = f_g + \alpha_f (T - T_g) \quad (4-16)$$

where f is the fractional free volume at T , any temperature above, f_g is the fractional free volume at T_g , and α_f is the coefficient of thermal expansion of the fractional free volume above T_g . In terms of equation (4-16), the Doolittle equation becomes

$$\begin{aligned} \ln \eta(T) &= \ln A + B \left(\frac{1}{f_g + \alpha_f (T - T_g)} - 1 \right) \quad \text{at } T > T_g \\ \ln \eta(T_g) &= \ln A + B \left(\frac{1}{f_g} - 1 \right) \quad \text{at } T_g \end{aligned} \quad (4-17)$$

Subtraction yields

$$\ln \frac{\eta(T)}{\eta(T_g)} = B \left(\frac{1}{f_g + \alpha_f (T - T_g)} - \frac{1}{f_g} \right) \quad (4-18)$$

which simplifies to

$$\log \frac{\eta(T)}{\eta(T_g)} = \log \alpha_T = -\frac{B}{2.303 f_g} \left(\frac{T - T_g}{f_g / \alpha_f + T - T_g} \right) \quad (4-19)$$

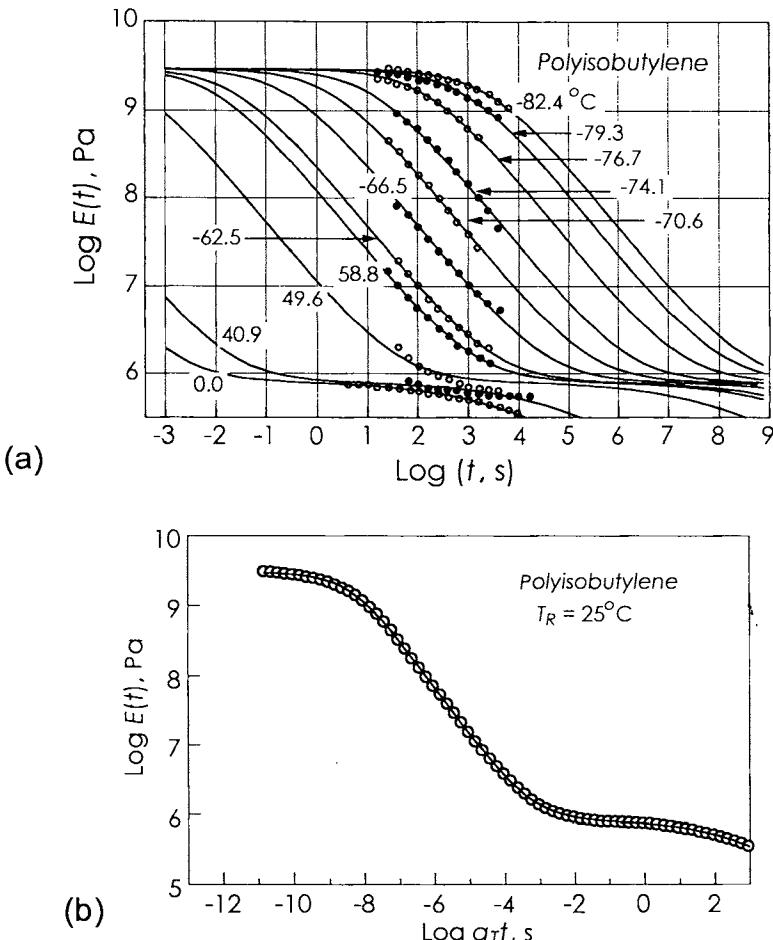


Figure 4-7. (a) Plot of the relaxation master curve for each of the temperatures indicated. The line through each of the data sets indicates the relaxation behavior over the entire time range expected for that temperature. The curves are moved only in the horizontal direction to fit the data. The empirical description for the curves follows an equation suggested by Smith,⁸ i.e., $E = (E_g - E_r) / [1 + (\tau / \tau_g)^a] + E_r / [1 + (\tau / \tau_g)^b]$, where the constants were obtained by a fit as shown in (b), to the original superposed data (open circles) listed in Ferry⁴ while the line is from the equation of Smith. [Data originally published by E. Castiff and A. V. Tobolsky, *J. Colloid Sci.*, **10**, 375 (1955)]

a form identical to the WLF equation where C_1 is identified with $B/2.303f_g$ and C_2 with f_g/α_f . Thus the form of the WLF equation is consistent with the empirical Doolittle equation and the assumption of a linear expansion of free volume above T_g .

Assuming that the WLF equation does indeed describe the time-temperature shifts, the complete viscoelastic response of any polymer under any experimental conditions may be obtained from knowledge of any two of the following three functions: the master curve at any temperature, the modulus-temperature curve at any time, and the shift factors relative to some reference temperature. For example, suppose we are given the constants C_1 , and C_2 for a polymer whose master curve is known. (The values given for C_1 and C_2 are those that result from fitting equation (4-6) to the α_T vs. T data.⁵) For simplicity, we can assume that the master curve is at the same reference temperature as that in the WLF equation, perhaps T_g . Suppose it is desired to calculate the 10-second modulus-versus-temperature curve for this polymer.

The 10-second modulus at T_g is read directly from the master curve. Now, however, the master curve can be shifted to exhibit the behavior of the polymer at some other temperature. Applying this horizontal shift, with the slight additional vertical correction, if significant, allows one to "predict" the 10-second modulus, at this new temperature from the shifted curve. This procedure is repeated until the entire modulus-time curve is generated (Figure 4-7).

Having thus generated the manifold of curves shown in Figure 4-7, it is possible to view the dependence of the modulus-temperature plots on the arbitrary choice of time. This is done merely by picking points off intersections of the master curves with vertical lines drawn from the point of interest on the time scale. The result of such treatment is shown by the simulations in Figure 4-8. (Problem 4-3 shows that the effects are less pronounced with real data because of experimental difficulties combined with the failure of the WLF equation below T_g .) It is apparent that the longer the constant time of measurement, the sharper the resulting curves. In fact, if it is assumed that the ideas embodied in the WLF equation are applicable at temperatures considerably below T_g , it can be shown that an experiment of the type depicted in Figure 4-8 carried out infinitely slowly would result in a type of second-order thermodynamic transition, that is, a discontinuity in the modulus, at a temperature about 50 °C below T_g .

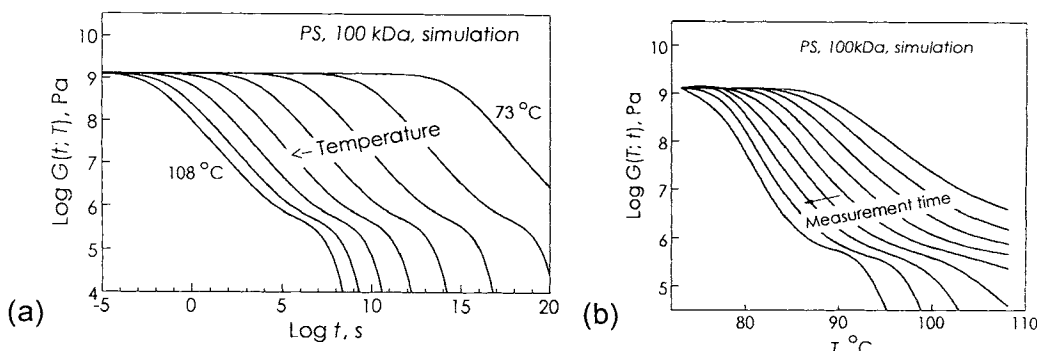


Figure 4-8. Simulations of master curves and modulus vs. temperature curves for a glassy polymer. (a) The master curves, shown at increments of 5 °C tend to be spaced more widely as the temperature is lowered because of the nature of the WLF relationship used for the temperature dependence [see Figure (4-6)]. (b) Demonstration of the influence of measurement time on the shape of the modulus-temperature curve. As the measurement time increases (by 1-decade increments), the apparent T_g decreases but the sharpness of the transition increases. (Simulation uses Smith empiricism⁸ for glass transition and the KWW function for the rubbery flow region.)

In reviewing equation (4-6), it is evident that temperatures other than T_g can be used as the reference temperature with corresponding linear changes in the values of C_1 and C_2 (see Problem 4-2). One choice of particular interest is that suggested by the discussion above—the second-order transition temperature, T_2 where $\log a_T$ becomes unbounded. In this case

$$\log a_T = \frac{1}{\alpha(T - T_2)} - \beta \quad (4-20)$$

This result is known as the Vogel equation. (See also Problem 4-6.) For polystyrene, the Vogel temperature T_2 is expected to be around 50 °C

E. MOLECULAR INTERPRETATION OF VISCOELASTIC RESPONSE

We now briefly discuss the molecular interpretation of the behavior exhibited by polymers that are held at constant temperature and studied as a function of time in a stress relaxation experiment covering the entire time scale (possibly 14 decades, or more).

In the very short time ranges, the molecules, not having sufficient time to reorient substantially, probably react to a deformation by distorting intermolecular distances. These distortions, being of a relatively high energy, result in a high modulus. At longer times, however, reorientation and translation of chain segments is possible and occurs more extensively. The

chain motion, while mainly chaotic, is biased in a fashion to relieve the stress. Such motion allows the most severely distorted parts of the chains to relax to lower energy conformations, resulting in a modulus decrease. This is the glass transition process, which can be looked at as a balancing of stress along the contour length of the chain. At still longer times, the stress is very low, but the elongation and orientation of the chains is nearly maintained due to entanglement interactions that hinder long-range motions. Such a network of interacting flexible chains is a rubber. In the longest time range of interest, the chains can move past one another, resulting in extensive relaxation and a modulus characteristic of a polymer melt. Now the end-to-end distance returns its equilibrium value, and the end-to-end vectors become randomized. The stress drops toward zero.

In this discussion, it is impossible to describe quantitatively the time ranges that give rise to each type of behavior, since the temperature variable causes all of these ranges to be relative. According to these ideas, a plastic would have the modulus of a rubber on a time scale of perhaps thousands of years while a rubber might behave as a plastic on a nanosecond time scale.[§]

PROBLEMS

1. An apparent activation energy E^* for viscoelastic relaxation may be obtained as the slope (multiplied by the gas constant R) of a plot of $\ln a_T$ as a function of $1/T$, according to the Arrhenius equation

$$\ln a_T = -\frac{E^*}{R} \left(\frac{1}{T_0} - \frac{1}{T} \right)$$

For materials showing WLF-like behavior, such a plot yields a curved line and thus a temperature-dependent activation energy.

- (a) Obtain an analytical expression for the activation energy from the WLF equation in terms of the WLF constants C_1 and C_2 and $T_0 = T_g$. Using the "universal" values for the constants C_1 and C_2 , find the activation energies at T_g if (1) $T_g = 200$ K (2) $T_g = 400$ K?

[§] It was once considered that direct evidence of the long-term flow of a glass was provided by the variation in thickness of the glass found in ancient cathedral windows. However, modern studies of this hypothesis have instead found that the thickness variations are most likely the result of manufacturing processes for the panes combined with the craftsman's propensity for placing the thicker edge of the pane down. For more details, see: R. C. Plumb, Antique windowpanes and the flow of supercooled liquids, *J. Chem. Educ.*, **66**, 994-996 (1989). See also problem 7, this chapter.

(b) Show that the activation energy becomes independent of temperature for $T \gg T_g$ and approaches a value of about 33 kJ/mol for all materials. Would you expect the activation energy for real polymers to obey this prediction? Why or why not?

2. The WLF equation may be written using any convenient temperature as the reference temperature. The form of the equation remains the same but the values of the constants C_1 and C_2 change. Using the "universal" values for C_1 and C_2 at T_g , calculate C_1 and C_2 for a reference temperature of $T_g + 50$.

3. Tabulated below, and listed in BPA-PC-Rel.TXT in the accompanying CD, are the results of stress relaxation measurements made on bis-phenol A polycarbonate. Construct the master curve and calculate C_1 and C_2 , the WLF equation parameters, for a reference temperature of 150.8 °C.

Stress Relaxation-Polycarbonate $M_n = 40,000$ [after Mercier, J. P. et al., *J. Appl. Polym. Sci.*, 9, 447-459 (1965)].⁹

130.	10	3.50	9.63	2.75	7.72	3.50	6.78
2.00	10.25	3.75	9.47	3.00	7.69	3.75	6.63
2.25	10.25	4.00	9.22	3.25	7.64	4.00	6.41
2.50	10.25	144.9	6	3.50	7.59	4.25	6.13
2.75	10.25	2.25	9.66	3.75	7.55	4.50	5.85
3.00	10.22	2.50	9.50	4.00	7.50	4.75	5.53
3.25	10.19	2.75	9.28	4.25	7.44	161.5	9
3.50	10.16	3.00	9.03	4.50	7.34	2.25	7.06
3.75	10.13	3.25	8.88	4.75	7.25	2.50	6.97
4.00	10.06	3.50	8.66	156.	13	2.75	6.85
4.25	10.03	145.6	6	2.00	7.59	3.00	6.64
141.	10	2.75	9.03	2.25	7.55	3.25	6.50
2.00	10.19	3.00	8.72	2.50	7.50	3.50	6.31
2.25	10.19	3.25	8.50	2.75	7.41	3.75	6.06
2.50	10.16	3.50	8.25	3.00	7.34	4.00	5.78
2.75	10.13	3.75	8.09	3.25	7.25	4.25	5.47
3.00	10.09	4.00	7.94	3.50	7.19	167.	6
3.25	10.03	146.	7	3.75	7.06	2.25	6.72
3.50	9.94	2.50	8.72	4.00	6.94	2.50	6.50
3.75	9.82	2.75	8.47	4.25	6.78	2.75	6.25
4.00	9.66	3.00	8.25	4.50	6.59	3.00	5.97
4.25	9.50	3.25	8.06	4.75	6.38	3.25	5.63
142.	9	3.50	7.94	5.00	6.13	3.50	5.22
2.00	10.13	3.75	7.82	159.	11	171.	5
2.25	10.09	4.00	7.67	2.25	7.34	2.25	6.00
2.50	10.03	150.8	12	2.50	7.25	2.50	5.72
2.75	9.97	2.00	7.97	2.75	7.16	2.75	5.41
3.00	9.88	2.25	7.85	3.00	7.03	3.00	5.03
3.25	9.67	2.50	7.78	3.25	6.94	3.25	4.63

Data are arranged by groups headed by the temperature in °C and the number of points in the group. Data are $\log(t, s)$, and $\log(E, \text{dyn/cm}^2)$.
 $1 \text{ dyn/cm}^2 = 0.1 \text{ Pa}$.

4. (Computer) Determine the 10-s modulus-versus-temperature curve for a material whose tensile stress relaxation modulus is given as

$$E(t, T_g) = E_1 e^{-t/\tau_1} + E_2 e^{-t/\tau_2}$$

where $E_1 = 3.0 \times 10^9$ Pa, $E_2 = 5.0 \times 10^5$ Pa, $\tau_1 = 1$ s and $\tau_2 = 10^4$ s. Use the "universal" values for the constants in the WLF equation.

5. Derive an expression for $\log a_T$ for a polymer whose shear stress relaxation modulus is given as

$$G(t, T) = \sum_{i=1}^N G_i e^{-t/\tau_i(T)}$$

where each G_i is independent of temperature and each τ_i is of the Arrhenius form:

$$\tau_i = A_i e^{E^*/RT}$$

Assume that A_i is independent of T , and that E^* is constant for all relaxation times.

6. The Vogel equation,

$$\log a_T = \frac{1}{\alpha(T - T_2)} - \beta$$

is often used to treat the temperature dependence of viscoelastic properties. Show that the Vogel equation is identical to the WLF equation by expressing α , β and T_2 , in terms of C_1 and C_2 and T_g .

7. (Open-ended) If the ancient craftsmen had used polycarbonate in cathedral windows instead of glass, calculate the expected thickness variation after 1500 years in a pane 25 cm high that was initially uniform. Assume that the pane is rectangular and is not constrained by its frame except vertically at the bottom edge to keep the pane from falling. See Chapter 2 for hints on converting $E(t)$ to $D(t)$. Carefully list all assumptions and approximations as part of your answer.

8. (Open-ended) Investigate the applicability of the Doolittle equation to a simple fluid with the objective of showing that temperature per se has no influence on viscosity. To approach this problem, find high-accuracy viscosity and specific-volume data in, for example, the *Handbook of Chemistry and Physics*. Compare these data with the predictions of the Doolittle equation, carefully noting any systematic discrepancies.

9. (Open-ended, Computer) Using the WLF constants of Table 4-1, generate log shift factors at 5 temperatures above T_g , e.g., $T_g + 2, 7, 12, 17$, and 22 °C. To these add a small amount of error, using random deviates with 0.03-decade standard deviation (many spread sheets will generate these for you). Using the two linearized forms of the WLF equation:

$$-\frac{1}{\log a_T} = \frac{1}{C_1} + \frac{C_2}{C_1} \frac{1}{T - T_g}$$

$$-\frac{T - T_g}{\log \alpha_T} = \frac{C_2}{C_1} + \frac{1}{C_1}(T - T_g)$$

recalculate C_1 and C_2 from your error-containing data and compare these results with the original values. Include in your comparisons the results from the direct fitting of equation (4-6). A thorough report will include sample graphs showing the plots of the data according to above equations. (If this procedure is repeated many times, one can establish the confidence limits of the calculated values of C_1 and C_2 . This method is known as the Monte Carlo method of error analysis.)

- 10. (Computer)** The Figure 4-2 data for amorphous polycarbonate is listed in file PC40kDa.TXT in the CD. As explained in the footnote of Figure 4-2, these data are actually $1/J(10 \text{ s})$. Using the WLF constants for polycarbonate of $C_1 = 16.4$ and $C_2 = 54.3$, with $T_g = 150.8 \text{ }^\circ\text{C}$, correct these data using the approximation of Problem 2-5. Plot on the same graph the modulus-temperature curves based on your $G(10 \text{ s})$ and the original $1/J(10 \text{ s})$, and comment on the differences.

REFERENCES

1. A. V. Tobolsky, *Properties and Structure of Polymers*, Wiley, New York, 1960.
2. K. Schmieder and K. Wolf, *Kolloid Z.*, **127** 65 (1952).
3. D. J. Plazek, *J. Phys. Chem.*, **69**, 3480 (1965).
4. J. D. Ferry, *Viscoelastic Properties of Polymers*, 3rd ed., Wiley, New York, 1980.
5. G. V. Gordon and M. T. Shaw, *Computer Programs for Rheologists*, Hanser, 1994.
6. M. L. Williams, R. F. Landel, and J. D. Ferry, *J. Amer. Chem. Soc.*, **77**, 3701 (1955).
7. A. K. Doolittle and D. B. Doolittle, *J. Appl. Phys.*, **31**, 1164 (1959).
8. T. L. Smith, *Trans. Soc. Rheol.* **2**, 131 (1958).
9. J. P. Mercier, J. J. Aklonis, M. Litt, and A. V. Tobolsky, *J. Appl. Polym. Sci.*, **9**, 447 (1965).
10. E. Catsiff and A. V. Tobolsky, *J. Colloid Sci.*, **10**, 375 (1955).

5

Transitions and Relaxation in Amorphous Polymers

Amorphous polymers, as we have seen in Chapter 4, undergo a transition from glassy behavior to rubbery behavior. This transition is quite sharp, usually occurring over a temperature range of a few degrees. The decrease in modulus of about three orders of magnitude that accompanies this transition makes it clear that it is the single most important parameter characterizing the mechanical behavior of amorphous polymers.

In this chapter, the glass transition phenomenon is treated in moderate detail, including phenomenological aspects, molecular theories, and the effect of molecular structure. In addition, relaxation occurring in the glassy state below the glass transition temperature (T_g) is discussed.

A. PHENOMENOLOGY OF THE GLASS TRANSITION

The classic method for the experimental determination of the glass transition temperature is dilatometry. Thus, as briefly mentioned in Chapter 1, the temperature dependence of the specific volume is determined by a suitable technique, and the temperature at the change in slope upon cooling is taken as T_g . Such a plot is indicated in Figure 5-1, where it is shown that the T_g is

determined as the intersection of the straight-line portions* of the curve above and below T_g . The slope is, of course, related to the cubical coefficient of thermal expansion, α , which exhibits a discontinuity at T_g . As is apparent from Figures 5-1 and 5-2, the glass transition is a rate-dependent phenomenon. Dilatometric methods are simple in principle but complex in practice. The

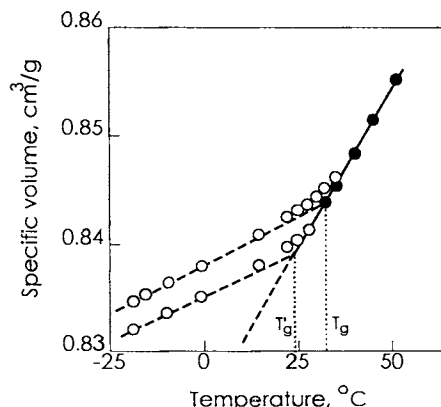


Figure 5-1. Specific volume versus temperature for a polyvinylacetate sample quick-quenched from well above T_g to the experimental temperatures. Volumes measured 0.02 hours and 100 hours after quenching as indicated. Filled points represent equilibrium behavior. [After A. J. Kovacs, *J. Polym. Sci.*, **30**, 131 (1958).]

displacement method is perhaps the most commonly used. The thermal expansion coefficient is determined by measuring the amount of confining fluid displaced by the polymer. The success of the method depends on the selection of a confining fluid that is not absorbed by the polymer and undergoes no phase transitions in the temperature range of interest. Mercury is often used, although it possesses obvious temperature limitations. In addition to dilatometry, calorimetry has been extensively employed, a discontinuity or peak in heat capacity being observed at T_g , depending on thermal history and heating rate (Figure 5-2). The continuing development of instrumentation and techniques for differential scanning calorimetry¹ have enhanced the importance of thermodynamic measurements associated with the determination of T_g . For information on instrumentation, the reader is referred to the manufacturers' websites, which are normally listed at www.njacs.org/thermal.html.

It has been repeatedly emphasized throughout this book that the glass transition in amorphous polymers is accompanied by profound changes in their viscoelastic response. Thus the stress relaxation modulus commonly decreases

* In fact, the data, as well as the theoretical equation of state for polymer fluids, exhibit gradual curvature, but this does not have a substantial effect on the determination of T_g .

by about three orders of magnitude in the vicinity of the T_g determined by calorimetry or dilatometry, and the creep compliance increases by about three orders of magnitude. In addition, under dynamic experimental conditions, the storage moduli and compliances behave in a similar manner to the corresponding static quantities. The loss moduli and compliances, on the other hand, exhibit maxima in the glass transition region, as does $\tan \delta$. Figure 5-3 summarizes these results for a styrene-butadiene copolymer. The data in Figure 5-3 were collected at a constant frequency of 1 Hz over the temperature range indicated. (The $\tan \delta$ plotted in Figure 5-3 was calculated from the original $\log \Delta$ using the relationship $\Delta \approx \pi \tan \delta$. The decrement, Δ , is commonly found directly from the response of a resonant torsional pendulum, which was used to gather the data shown.) It can be seen from Figure 5-3 that

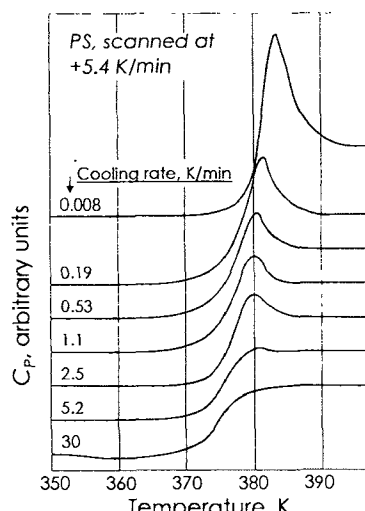


Figure 5-2. Thermal scans of polystyrene at 5.4 K/min (0.09 K/s) after cooling from well above T_g at the rates indicated. Curves have been shifted vertically for clarity. After B. Wunderlich, D. M. Bodily and M. H. Kaplan, *J. Appl. Phys.*, **35**, 95 (1964).

the maxima in $\tan \delta$ and G'' occur at different temperatures, the G'' maximum being lower. Frequently, the $\tan \delta$ or G'' peak temperatures are taken as the T_g , but it is clear that they will not be identical and that, in general, they will both yield higher values than those obtained by dilatometric or thermodynamic methods, owing to differences in the time scale.

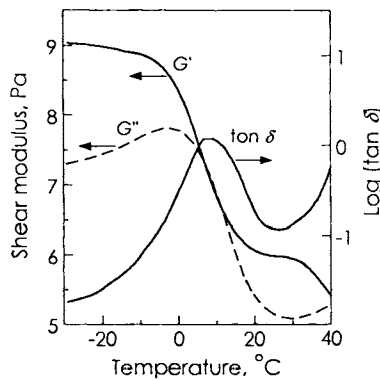


Figure 5-3. Temperature dependencies of G' , G'' and $\tan \delta$ for styrene butadiene copolymer. [After L. E. Nielsen, *Mechanical Properties of Polymers*, Reinhold, New York, 1962.]

Figure 5-4 gives the temperature dependence of E' and $\tan \delta$ for polyvinyl chloride at various frequencies. The shift of the $\tan \delta$ peak maximum to higher temperatures with increasing frequency occurs in accordance with the WLF equation and is again an illustration of the rate dependence of the glass transition phenomenon.

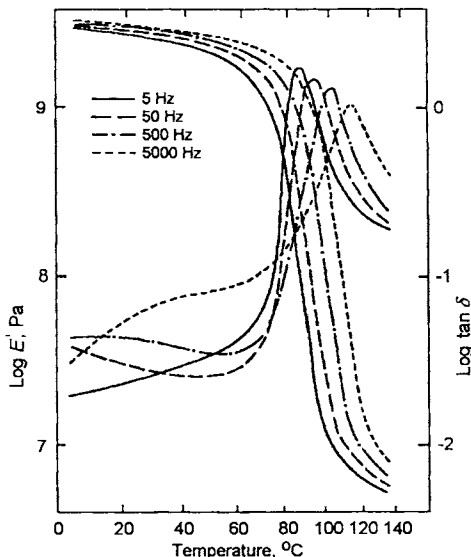


Figure 5-4. Temperature dependencies of E' and $\tan \delta$ for polyvinyl chloride at various frequencies. After G. W. Becker, *Kolloid-Z.* 140 1 (1955). [Reprinted by permission of Dr. Dietrich Steinkopff Verlag.]

One of the oldest methods for the determination of T_g involves the temperature dependence of viscosity. Figure 5-5 is a plot of the variation of viscosity with temperature for polystyrene. Various authors have argued that

the glass transition temperature represents an isoviscous state with viscosity 10^{12} Pa s. Such a high viscosity is not easily measurable by normal flow techniques and, in fact, its determination is usually accomplished from creep or stress relaxation measurements by the techniques of Chapter 2.

Many profound physical changes occur at T_g in addition to those already mentioned. The refractive index undergoes an abrupt change at T_g . In the case of polar polymers, the dielectric loss tangent passes through a maximum in the vicinity of T_g , as does the imaginary part of the complex dielectric constant (Chapter 7, Section A). Because of the increased mobility at T_g , the line width in a nuclear magnetic resonance experiment² undergoes an abrupt narrowing at this temperature (see Chapter 7, Section B). All of these effects, and many others, have been used as measures of T_g , and they all arise from the fundamental changes in molecular dynamics which occur in the vicinity of T_g . It should be apparent from the discussion that each experimental method will yield a different value for T_g and that even the same method will yield different results depending on the time scale. Thus, in order to compare T_g values, both the method of measurement and the rate of measurement should be specified.

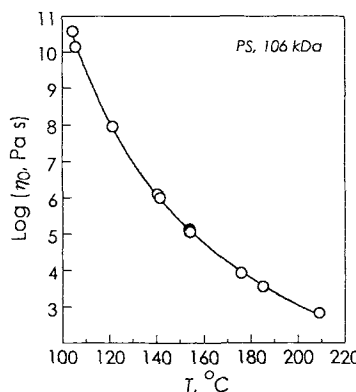


Figure 5-5. Temperature dependence of viscosity for a cyclic polystyrene sample of molecular weight 106,000. The line is a fit with the WLF relationship, equation (4-6). [Adapted with permission from G. B. McKenna et al., *Macromolecules*, **20**, 498-512 (1987). Copyright 1987 American Chemical Society]¹⁶

B. THEORIES OF THE GLASS TRANSITION

1. Free-Volume Theory

In Section D of Chapter 4 the WLF equation was derived on the basis of free-volume concepts. In particular, we may write

$$\log a_T = \frac{B}{2.303} \left(\frac{1}{f_T} - \frac{1}{f_{T_0}} \right) \quad (5-1)$$

where f_T and f_{T_0} are the fractional free volumes at temperatures T and T_0 , respectively, and B , a parameter in the Doolittle equation, is experimentally found to be close to unity. Unfortunately, the concept of free volume is difficult to define in a precise manner. In an approximate way we can represent the segments of a polymer chain by rigid bodies and the free volume as the holes present between these segments as a result of packing requirements. Presumably the free volume reaches a constant value at T_g that is too small to allow the large-scale conformational rearrangements of the chain backbones associated with T_g to occur on the time scale of the experiment. Above T_g , on the other hand, free volume increases and becomes sufficiently large to allow such motions to occur. These ideas are embodied in equation (4-16), which we quote here.

$$\begin{aligned} f &= f_g + \alpha_f(T - T_g) & T > T_g \\ f &= f_g & T < T_g \end{aligned} \quad (4-16)$$

The fractional free volume f reaches a constant value, f_g , at T_g and increases linearly above T_g with the coefficient of expansion α_f . Following Chapter 4, substitution of equation (4-16) into equation (5-1) with T_g as the reference temperature yields the WLF equation where the constants C_1 and C_2 are given by

$$C_1 = \frac{B}{2.303 f_g} \quad C_2 = \frac{f_g}{\alpha_f} \quad (5-2)$$

Knowledge of the numerical values of C_1 and C_2 thus leads to the parameters f_g and α_f through equation (5-2), if B is taken as unity. The constants C_1 and C_2 were originally taken to be universal for all amorphous polymers with $C_1 = 17.44$ and $C_2 = 51.6$. It was later found that C_1 values were indeed approximately constant for all systems but that C_2 varied quite widely. This is illustrated by Table 4-1. Equation (5-2) indicates that this result means that f_g is approximately constant at a value of 0.025, but that α_f varies from one amorphous polymer to another. It is clear that the WLF equation predicts that T_g represents an iso-free-volume state. While this concept is not strictly true it is nevertheless of wide utility, as we shall see in the following discussion.

It is possible to identify α_f with $\Delta\alpha = \alpha_r - \alpha_g$, that is, the difference between the expansion coefficients above and below T_g . If this is done, good agreement

is obtained for many polymers between experimentally determined values of $\Delta\alpha$ and α_f obtained from C_2 values through equation (5-2). Inasmuch as there is no *a priori* method of defining α_f , the above agreement is perhaps the best justification for the identification of α_f with $\Delta\alpha$.

The free-volume approach embodied in equation (4-16) may be easily generalized to include the effect of pressure. Intuitively, pressure may be thought of as having the effect of "squeezing out" free volume and thus raising the glass transition temperature; such has actually been found to be the case. The magnitude of the effect is predictable as follows. Assume the polymer is taken from state 1 characterized by P_1 , and T_{g1} to state 2 characterized by P_2 and T_{g2} . In general, any change from state 1 to state 2 may be characterized by

$$f_2 = f_1 + \alpha_f(T_2 - T_1) - \beta_f(P_2 - P_1) \quad (5-3)$$

where β_f refers to the isothermal compressibility of free volume, assumed independent of pressure over the range of interest. If the polymer remains at T_g in going from state 1 to state 2, f_2 must also remain equal to f_1 , since T_g is an iso-free-volume state. Thus, under these conditions,

$$\alpha_f(T_{g2} - T_{g1}) = \beta_f(P_2 - P_1) \quad (5-4)$$

For small changes, equation (5-4) becomes

$$\frac{dT_g}{dP} = \frac{\beta_f}{\alpha_f} \quad (5-5)$$

Let $\beta_f = \Delta\beta$, the compressibility above and below T_g , and $\alpha_f = \Delta\alpha$. Then

$$\frac{dT_g}{dP} = \frac{\Delta\beta}{\Delta\alpha} \quad (5-6)$$

Although precise pressure measurements are difficult and not very much data have been reported, amorphous polymers at least approximately obey equation (5-6). (See Table 5-1.)

The free-volume theory finds ready application in predicting the effect on T_g of diluents and molecular weight, among others. As an example, we shall derive an expression for the dependence of T_g on plasticizer concentration. The total fractional free volume of a polymer-diluent system may be written as

$$f = 0.025 + \alpha_p(T - T_{g,p})\phi_p + \alpha_d(T - T_{g,d})\phi_d \quad (5-7)$$

Table 5-1. Pressure Dependence of T_g

Polymer	$TV\Delta\alpha/\Delta C_p$, K/atm	dT_g/dP , K/atm	$\Delta\beta/\Delta\alpha$, °K/atm
Polyvinyl acetate	0.025 ^a	0.02 ^a	0.05 ^a
Polystyrene	—	0.036 ^b	0.10 ^b
Natural Rubber	0.020 ^a	0.024 ^c	0.024 ^c
Polymethyl methacrylate	—	0.023 ^d	0.065 ^e

^aJ. M. O'Reilly, *J. Polym. Sci.*, **57**, 429 (1962).^bS. Matsuoka and B. Maxwell, *J. Polym. Sci.*, **32**, 131 (1958).^cJ. E. McKinney, H. V. Belcher, and R. S. Marvin, *Trans. Soc. Rheol.*, **4**, 347 (1960).^dN. Shishkin, *Sov. Phys.-Solid State*, **2**, 322 (1960).^eG. Allen, D. Sims, and G. J. Wilson, *Polymer*, **2**, 375 (1961).

In equation (5-7) the subscripts *p* and *d* refer to polymer and diluent, respectively, and ϕ is the volume fraction. At the T_g of the polymer-diluent mixture, *f* becomes 0.025. Using this fact and substituting $1-\phi_p$ for ϕ_d , we have

$$T_g = \frac{\alpha_p \phi_p T_{g,p} + \alpha_d (1 - \phi_p) T_{g,d}}{\alpha_p \phi_p + \alpha_d (1 - \phi_p)} \quad (5-8)$$

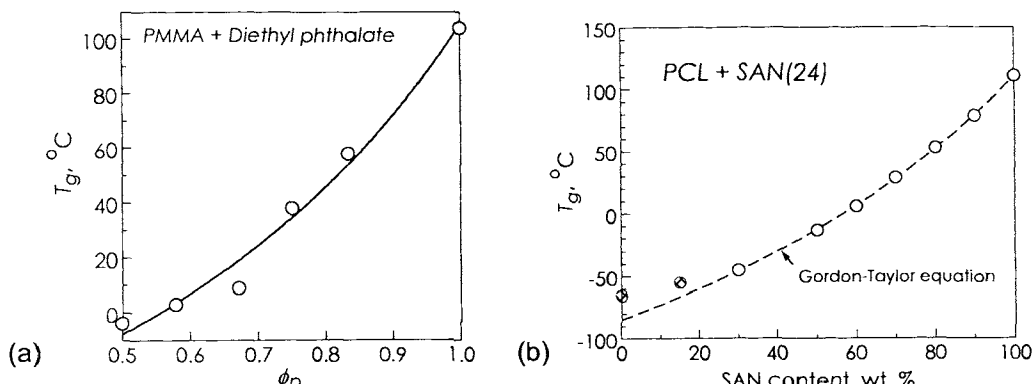


Figure 5-6. (a) Dependence of T_g on ϕ_p for mixtures of polymethyl methacrylate with diethyl phthalate. Comparison of experimental results with equation (5-8). Parameters found were: $\alpha_d/\alpha_p = 2.32$, $T_{g,d} = -57$ °C, $T_{g,p} = 104$ °C.^t [After F. N. Kelley and F. Bueche, *J. Polym. Sci.*, **50** 549 (1961)]; (b) Variation of T_g for a miscible polymer blend of polycaprolactone (PCL) and poly(styrene-co-acrylonitrile) (SAN), with a description of the data using the Gordon-Taylor relationship, equation (5-27). The two points at low SAN content have a higher-than-expected T_g because of crystallization of the PCL. [After S-C. Chiu and T. G. Smith, *J. Appl. Polym. Sci.*, **29**, 1797 (1984). Copyright © 1984, Wiley Periodicals, Inc., a Wiley Company.]

^t The form of equation (5-8) does not allow α_p and α_d to be determined separately.

This is a form of the Gordon-Taylor relationship, equation (5-27), although the original equation was expressed in terms in mass rather than volume fraction.

The dependence of T_g on ϕ_P as predicted from equation (5-8) is plotted in Figure 5-6a for the system poly(methyl methacrylate)-diethyl phthalate, together with some experimental results. T_g can also be modified by blending with a miscible polymer component, which is widely practiced, particularly for PVC. A classical polymer blend comprising polycaprolactone (PCL) and poly(styrene-*co*-acrylonitrile) (SAN) is illustrated in Figure 5-6b.

2. Thermodynamic Theory

Equilibrium phase transitions are well treated using the classical thermodynamic approach. In particular, the phenomena of melting and vaporization are characterized by the equality of the molar Gibbs free energy of the two phases at the transition temperature.

$$F_1 = F_2 \quad (5-9)$$

Also

$$dF_1 = dF_2 \quad (5-10)$$

However, the volumes and entropies of the two phases are not equal.

$$\begin{aligned} S_1 &\neq S_2 \\ V_1 &\neq V_2 \end{aligned} \quad (5-11)$$

Ehrenfest³ refers to the type of phase transition described above as a first-order transition because there are discontinuities in the first partial derivatives of the Gibbs free energy at the transition point. For example,

$$dF = -SdT + VdP \quad (5-12)$$

and we have

$$\begin{aligned} S &= -\left(\frac{\partial F}{\partial T}\right)_P \\ V &= \left(\frac{\partial F}{\partial P}\right)_T \end{aligned} \quad (5-13)$$

This notion is easily generalized to higher-order transitions. Thus a second-order transition is described as one in which the second partial derivatives of

the Gibbs free energy show discontinuities at the transition point, a third-order transition involves discontinuities in the third partial derivatives, and so on.

In particular, for a second-order transition,

$$\begin{aligned} -\left(\frac{\partial^2 F}{\partial T^2}\right)_P &= \left(\frac{\partial S}{\partial T}\right)_P = \frac{C_p}{T} \\ \left(\frac{\partial^2 F}{\partial P^2}\right)_T &= \left(\frac{\partial V}{\partial P}\right)_T = -\beta V \\ \left(\frac{\partial}{\partial T}\left(\frac{\partial F}{\partial P}\right)_T\right)_P &= \left(\frac{\partial V}{\partial T}\right)_P = \alpha V \end{aligned} \quad (5-14)$$

So, at the second-order transition temperature, the following discontinuities are observed:

$$\begin{aligned} \Delta C_p &= C_{P_2} - C_{P_1} \\ \Delta \beta &= \beta_2 - \beta_1 \\ \Delta \alpha &= \alpha_2 - \alpha_1 \end{aligned} \quad (5-15)$$

It is just these discontinuities that often occur in experiments involving the glass transition, and, because of this, T_g is often referred to as the second-order transition point. It is clear, however, that the observed T_g is a rate-dependent phenomenon. The thermodynamic analysis given above refers only to an equilibrium process and thus cannot be directly applied to the experimental T_g . The kinetic nature of the observed T_g does not, however, preclude the existence of a true second-order transition temperature. Thus, in a dilatometric experiment, when the polymer is cooled from the rubbery or liquid states, volume contractions take place involving conformational rearrangements. At temperatures far above T_g thermal equilibrium is maintained during the cooling process, but as the temperature is lowered a point is eventually reached at which the rate of volume contraction becomes comparable with the rate of cooling. Below this temperature, volume relaxation and hence conformational rearrangements are not possible during the time scale of the experiment, and the discontinuities C_p , $\Delta\beta$, and $\Delta\alpha$ are observed. Such an analysis indicates that an infinitely slow cooling rate would be required to observe the true thermodynamic second-order transition temperature, if it exists at all.

Kauzmann⁴ noted that if the entropies of simple glass-forming liquids were extrapolated to low temperatures, they would go to zero long before the

absolute zero of temperature was reached. Such a result, requiring negative entropies, is clearly meaningless in a physical sense. Kauzmann resolved this paradox by suggesting that the glassy state is not an equilibrium state and that the glasses would pass over into crystalline solids at equilibrium before the temperature of zero-extrapolated entropy could be achieved. Such an explanation denies the existence of a second-order thermodynamic transition. However, many polymeric substances have never been obtained in a crystalline state and it is difficult to imagine the possibility of crystallizing a material such as atactic polystyrene, for example. It was subsequently suggested by Gibbs and DiMarzio⁵ that the conformational entropy at equilibrium would indeed attain a value of zero at a finite temperature, defined as T_2 , undergoing no further change between T_2 and absolute zero.⁵ This idea is schematically illustrated in Figure 5-7 in which the dotted line represents Kauzmann's extrapolation. The T_2 of Gibbs and DiMarzio is a true second-order transition temperature. In this view the observed T_g is the kinetic reflection of the underlying thermodynamic phenomenon that would occur at T_2 .

Gibbs and DiMarzio suggest that at high temperatures a very great number of conformations are accessible to each chain. They assume that for each chain segment there is one definite lowest energy conformation, so that at equilibrium at low temperatures there is just one conformation available to the entire chain. Thus, as the chain is cooled from high to low temperatures, fewer and fewer high-energy conformations become accessible until at T_2 only the one lowest energy state is allowed.

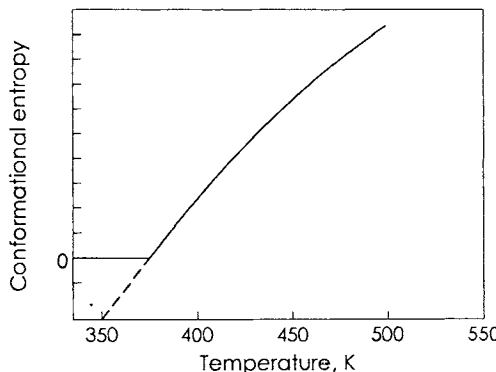


Figure 5-7. Schematic representation of conformational entropy vs. temperature for a glass-forming substance. The temperature at which the entropy attains a value of 0 is the T_2 of Gibbs and DiMarzio. The dotted line is the extrapolation of Kauzmann designed to illustrate the infeasibility of a glassy equilibrium state, and the proposal of Gibbs and DiMarzio. [After J. H. Gibbs in *Modern Aspects of the Vitreous State*, Vol. 1, J. D. Mackenzie, Ed., Butterworths, Washington, 1960.]

In reality, however, there are so many states accessible at high temperatures that the reorientation from one state to any other particular state may take quite some time. In fact, as we cool the sample and intrinsically slow down molecular movement, it should take longer and longer to get to any particular conformation. To insure getting all the chains into the lowest energy conformation, the experiment would have to be carried out infinitely slowly.

The temperature at which the second-order transition would occur, according to these ideas, may be calculated using the WLF equation (4-6). To shift an experiment from a finite time-scale to an infinite time-scale would take a value of $\log a_T$ approaching infinity. Clearly this will be the case if the denominator of the right side of equation (4-6) goes to zero while the numerator remains finite.

$$C_2 + T_2 - T_g = 0 \quad (5-16)$$

Since C_2 is relatively constant for most polymers, one derives the relation that

$$T_2 = T_g - C_2 \approx T_g - 52 \quad (5-17)$$

Thus the second-order phase change would be observed about 50 K below T_g for an experiment carried out infinitely slowly.

The Gibbs-DiMarzio model is characterized by two parameters. These are the hole-formation energy, u_0 , and the flex energy, ε . The parameter u_0 is a reflection of intermolecular energy contributions and ε is a reflection of intramolecular energy contributions. Specifically, for hydrocarbon chains such as polymethylene, u_0 is the energy of interaction, or the "van der Waals bond" energy between a pair of chemically nonbonded but nearest neighboring segments in the lattice. In order to define ε , we note that if Z is the number of primary valences of each backbone chain atom, there are $(Z - 1)$ possible orientations of a bond i with respect to the coordinate system formed by the bonds $(i - 1)$ and $(i - 2)$ of the same molecule. In the case of a hydrocarbon chain, $Z = 4$. It is assumed that an energy ε_1 is associated with one of the three possible orientations and an energy ε_2 is associated with the other two, with $\varepsilon_2 > \varepsilon_1$. Then ε is defined as the difference between ε_2 and ε_1 . It should be emphasized that ε , a thermodynamic quantity, has nothing to say about the magnitude of potential energy barriers to rotation about chain backbone bonds. Rather, ε refers only to the energy difference between low-lying rotational isomeric states. According to the theory, it is found that u_0 is directly proportional to T_2 and that ε/kT_2 is a constant for all polymers. Recasting this ratio in terms of T_g rather than T_2 , it can be shown that ε/kT_g possesses the "universal" value of 2.26 for all amorphous polymers.⁶

We can demonstrate the utility of the Gibbs-DiMarzio theory by applying it to the calculation of the T_g of a random copolymer. Let us assume that the flex energy of a random copolymer composed of A and B monomer units is given by

$$\varepsilon = x_A \varepsilon_A + x_B \varepsilon_B \quad (5-18)$$

where x_A and x_B are the mole fractions of monomer units A and B, respectively.

Substituting the "universal" value of $\varepsilon = 2.26 \text{ } kT_g$ in equation (5-18) immediately leads to

$$T_g = x_A T_{gA} + x_B T_{gB} \quad (5-19)$$

which is identical in form to an empirical equation of Wood⁷ found to have wide applicability to random copolymers.

The Gibbs-DiMarzio approach, as has been stated, rests on the existence of a true second-order thermodynamic transition at a temperature T_2 below the observed T_g . The pressure dependence of T_2 can thus be obtained by the methods of equilibrium thermodynamics. For a first-order phase transition, the pressure dependence of the transition temperature is given by the Clapeyron equation

$$\frac{dT}{dP} = \frac{\Delta V}{\Delta S} \quad (5-20)$$

Straightforward application of the Clapeyron equation to a second-order transition is not possible because both ΔV and ΔS are 0, and thus dT/dP is indeterminate. However, we may invoke L'Hopital's rule and differentiate both numerator and denominator of the right side of equation (5-20) independently to obtain the limiting behavior. This may be done with respect to either temperature or pressure. Thus, recalling equation (5-14) and differentiating equation (5-20) with respect to temperature:

$$\frac{dT_2}{dP} = \frac{\partial \Delta V / \partial T}{\partial \Delta S / \partial T} = \frac{V \Delta \alpha T_g}{\Delta C_p} \quad (5-21)$$

Differentiating with respect to pressure, there results

$$\frac{dT_2}{dP} = \frac{\partial \Delta V / \partial P}{\partial \Delta S / \partial P} = \frac{\Delta \beta}{\Delta \alpha} \quad (5-22)$$

Thus the pressure dependence of T_2 and hence T_g is given by either equation (5-21) or equation (5-22). Equation (5-22) is, of course, identical to the free-volume result, equation (5-6). A comparison of these quantities has been given in Table 5-1.

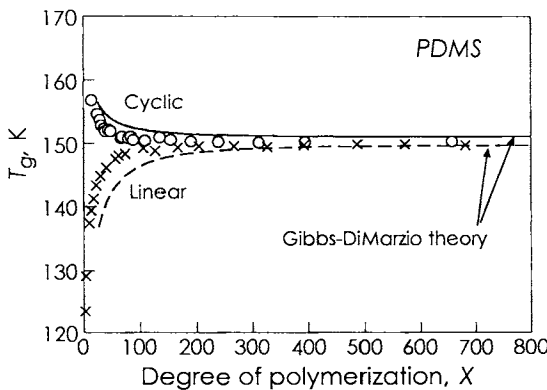


Figure 5-8. Molecular weight trends in the glass transition temperature trends in cyclic and linear oligomers of poly(dimethyl siloxane), and the comparison of these data with the prediction of the Gibbs-DiMarzio theory. [Reprinted with permission from E. A. DiMarzio and C. M. Guttmann, *Macromolecules*, 20, 1403 (1987). Copyright 1987, American Chemical Society]

The Gibbs DiMarzio theory has been applied to the understanding of other behavior, e.g., the molecular weight dependence of the glass transition temperature of cyclic vs. linear oligomers. The prediction of the Gibbs DiMarzio theory is that for the cyclic oligomers, the glass transition temperature should fall with molecular weight because of the entropy decrease brought about by forming the chain into a ring. This behavior is illustrated using poly(dimethyl siloxane) oligomers in Figure 5-8. The linear oligomers, on the other hand, behave in the normal fashion as can be seen from the results for these included in Figure 5-8.

3. Kinetic Theories

Several kinetic theories have been particularly successful in explaining various features of the glass transition phenomenon. Here the emphasis is on separating fundamental molecular aspects of the transition from factors introduced by the particular way in which an experiment is carried out. Such theories have become moderately complicated in the past several years. However, by concentrating on models with a single ordering parameter, we will attempt to convey the general framework of these theories without tackling the conceptual and mathematical complications that are necessary to realize quantitative agreement between theory and experiment.

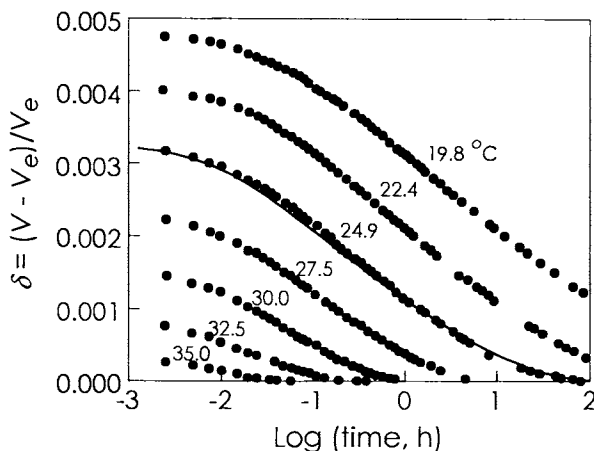


Figure 5-9. Contraction isotherms for glucose, a low-molecular-weight glass-forming substance. Samples were quenched from equilibrium at 40 °C to the temperatures indicated. Solid line through the points at 24.9 °C were calculated using equations (5-23) and (5-25) with $T_g = 35$ °C, $f_g = 0.025$, $a_f = 3.6 \times 10^{-4}$ K⁻¹, and $\tau(T_g, \delta = 0) = 0.015$. Fits to the other temperatures are possible using the same equations, but require small changes in the parameters. [After A. J. Kovacs, *Fortschr. Hochpolym.*, **3**, 394 (1964), © by Springer-Verlag, 1964. With kind permission of Springer Science and Business Media.]

For the purpose of this discussion, the data to be analyzed are of a slightly different sort from those considered previously. In Figure 5-9, we have plotted several volume-contraction isotherms for glucose. First of all, it should be noted that glucose is not a high-molecular-weight polymer, but rather a low-molecular-weight material that is easily vitrified. In fact, many aspects of the glass transition phenomenon are virtually independent of molecular weight. Thus, the behavior exhibited by glucose in its glass transition region is essentially the same as that of any high-molecular-weight amorphous polymer. The experiments represented in this figure involve annealing the sample at 40 °C (a temperature above the usually quoted glass transition temperature, $T_g = 35$ °C) until equilibrium is established. Then, the sample is quickly cooled to the experimental temperature. In addition to an "instantaneous" volume adjustment, one finds a substantial and often prolonged volume adjustment that takes place after the temperature jump. In Figure 5-9 this time-dependent volume change is shown for several experimental temperatures ranging from 35.0 to 19.8 °C. Here, the normalized volume departure from equilibrium, $(V - V_e) / V_e$ which we shall call δ , is plotted as a function of log time. One can clearly see that volume equilibrium is established rapidly at the higher experimental temperatures but has not been attained even after several days at 19.8 °C.

The kinetic theories under discussion have as a goal the explanation for such time-dependent approaches to equilibrium. For most simple substances such as gases or single-phase liquids, the specific volume is a unique function of temperature and pressure. In the case of vitrifiable materials in the glass transition region, this is no longer so. As is clear from Figure 5-8, at 19.8 °C, for example, it is possible to prepare a material with a volume almost 0.5% greater than its equilibrium volume and the sample will retain much of this volume excess for very long periods of time. Under such circumstances, rather than indicating that volume is a unique function of temperature and pressure, kinetic theories suggest writing $V(T, P, \xi)$ where ξ is called an ordering parameter and is a general measure of how far the sample is away from volume equilibrium. With the establishment of equilibrium, the volume again becomes a unique function of temperature and pressure as ξ itself depends only on T and P at equilibrium.

At this point in the development, a differential equation is usually written. Since we are interested in the establishment of equilibrium under isothermal conditions after a single temperature jump applied to the sample initially at equilibrium, the equation is particularly simple:

$$\frac{d\delta}{dt} = -\frac{\delta}{\tau(\delta)} \quad (5-23)$$

Once again, δ is the normalized departure from equilibrium and the equation postulates that the rate of approach toward equilibrium ($d\delta/dt$) is proportional to δ itself. The retardation time τ may be thought of as the proportionality constant; if τ is small, equilibrium is achieved rapidly and if large, slowly.

A very important aspect of kinetic theories now surfaces. Equation (5-23) is concerned with the time dependence of volume recovery after a temperature jump. For the volume to change, the molecules must move. However, as discussed in Chapters 3 and 4, the rate at which the molecules can move is a sensitive function of the free volume, and the free volume is varying with time in Figure 5-9. Thus, it is clear that the retardation time in equation (5-23) must itself depend upon δ and vary with time. This situation can be treated in quite a straightforward way by modifying equation (4-16) as

$$f = f_g + \alpha_f(T - T_g) + \delta \quad (5-24)$$

where f , the fractional free volume, adopts equilibrium values whenever $\delta = 0$. (The usual restriction of applying equation (4-16) only to temperatures above T_g is normally relaxed at this point.) The fractional free-volume dependence of

the viscosity should be the same as that of the retardation time under discussion, so that equation (4-18) may be generalized to:

$$\tau(T, \delta) = \tau(T_g, \delta = 0) \exp\left(\frac{1}{f_g + \alpha_f (T - T_g) + \delta} - \frac{1}{f_g}\right) \quad (5-25)$$

This equation explicitly relates a reference retardation time $\tau(T_g, \delta=0)$ measured under conditions of volume equilibrium at T to a retardation time applicable under any other conditions of temperature and volume via the usual free-volume parameters.

Equations (5-23) and (5-25) have been used to calculate the solid line through the data points in Figure 5-9 at 24.9 C. Reasonable values for the free-volume parameters and the reference retardation time were used and are listed in the figure legend.

While the agreement between the experimental data and the theoretical calculation is very satisfying, other types of volume and enthalpy recovery experiments show that the single-ordering parameter model is not sufficiently flexible to rationalize many of the important aspects of the glass transition phenomenon. As a result, more complex models based on multiple ordering parameters are now under development.⁸

C. STRUCTURAL PARAMETERS AFFECTING THE GLASS TRANSITION

We have seen that the free-volume, thermodynamic, and kinetic theories serve to rationalize the glass transition phenomenon in a wide variety of polymeric systems. There are, of course, additional effects that cannot be well explained

Table 5-2. Glass Transition Temperatures for Selected Polymers

Organic Polymers	$T_g, ^\circ\text{C}$
Polyacenaphthalene	264
Polyvinyl pyrrolidone	175
Poly-o-vinyl benzyl alcohol	140
Poly-p-vinyl benzyl alcohol	160
Polymethacrylonitrile	120
Polyacrylic acid	106
Polymethyl methacrylate	105
Polyvinyl formal	105
Polystyrene	100
Polyacrylonitrile	96

Table 5-2. (*Continued*)

Organic Polymers	T_g , °C
Polyvinyl chloride	87
Polyvinyl alcohol	85
Polyvinyl acetal	82
Polyvinyl propional	72
Polyethylene terephthalate	69
Polyvinyl isobutyral	56
Polycaprolactam (nylon 6)	50
Polyhexamethylene adipamide (nylon 6,6)	50
Polyvinyl butyral	49
Polychlorotrifluorethylene	45
Polyhexamethylene sebacamide (nylon 6, 10)	40
Polyvinyl acetate	29
Polyperfluoropropylene	11
Polymethyl acrylate	9
Polyvinylidene chloride	-17
Polyvinyl fluoride	-20
Poly-1-butene	-25
Polyvinylidene fluoride	-39
Poly-1-hexene	-50
Polychloroprene	-50
Polyvinyl-n-butyl ether	-52
Polytetramethylene sebacate	-57
Polybutylene oxide	-60
Polypropylene oxide	-60
Poly-1-octene	-65
Polyethylene adipate	-70
Polyisobutylene	-70
Natural rubber	-72
Polyisoprene	-73
Polybutadiene	-85
Polydimethyl siloxane	-123
Inorganic Polymers	T_g , °C
Silicon dioxide	1200–1700
Polycalcium phosphate	525
Polysodium phosphate	285
Boron trioxide	200–260
Arsenic trisulfide	195
Arsenic trioxide	160
Sulfur	75
Selenium	30
Polyphosphoric acid	-10

on the basis of either of these approaches. In this section we examine some structural parameters affecting T_g in a qualitative manner, pointing out exceptions to the theories quoted above.

The details of the molecular structure of polymers profoundly influence the observed T_g 's, as illustrated by Table 5-2, where we may contrast the T_g of polydimethyl siloxane, -123°C , with that of poly(calcium phosphate), $+525^\circ\text{C}$. At least approximately, we may separate the observed effects into intermolecular and intramolecular parts. The latter refer to structural parameters affecting the stiffness of the chain backbone; we shall examine these first.

The internal mobility of a chain reflects the ease of rotation of backbone bonds about one another. This is determined by the barrier to internal rotation and by steric hindrance introduced by the presence of substituents on the backbone chain atoms. Thus, the low T_g of polydimethyl siloxane may be rationalized on the basis of a low rotational energy barrier. A similar explanation may be advanced for the low T_g of linear polyethylene, -78°C . (Some controversy still exists concerning the T_g of linear polyethylene. For example, values as low as -128°C have been proposed by Beatty and Karasz,⁹ while others report higher values. Check the latest issue of *Polymer Handbook*¹⁰ for an extensive listing of T_g 's.) The steric hindrance factor may be illustrated by considering the effect of the substitution of various groups for hydrogen atoms on a linear polyethylene chain. The placement of a methyl group on alternate carbon atoms results in polypropylene, which has a T_g of -20°C . Polystyrene, which has a phenyl group on alternate carbon atoms, has a T_g of $+100^\circ\text{C}$, over 200° higher than that of unsubstituted polymethylene. This type of correlation must be applied with caution, however. Consider polyisobutylene, containing two methyl groups on alternate carbon atoms. In this case the T_g is -80°C , some 60° lower than the monosubstituted case, polypropylene, while poly(α -methylstyrene) has a T_g of about 180°C .[‡]

An increase in side group bulkiness generally serves to raise T_g . Ring-substituted polystyrenes show this effect and, in the case of polyacenaphthalene, the motions of the chain are so severely restricted that the T_g occurs at 264°C . Chain microstructure is clearly important in determining chain mobility. We have already discussed the case of random copolymers on the basis of the Gibbs-DiMarzio theory and have developed equation (5-19), which shows that the T_g of a random copolymer is intermediate between the T_g 's of the corresponding homopolymers. Equation (5-19) is similar in form to the empirical expression of Wood⁷

[‡] N. G. McCrum, B. E. Read and G. Williams, *Anelastic and Dielectric Effects in Polymeric Solids*, Wiley, New York, 1967, p. 416. Other values have been reported.¹⁰

$$K_A W_A (T_g - T_{g_A}) + K_B W_B (T_g - T_{g_B}) = 0 \quad (5-26)$$

where W_A and W_B are the weight fractions of the comonomers A and B, and K_A and K_B are constants characteristic of A and B, respectively. Equation (5-26) may be rearranged to

$$T_g = \frac{T_{g_A} + (kT_{g_B} - T_{g_A})W_B}{1 - (1-k)W_B} = \frac{W_A T_{g_A} + kW_B T_{g_B}}{W_A + kW_B} \quad (5-27)$$

where $k = K_B/K_A$. Thus equation (5-27) has one more parameter (k) than equation (5-19).

Equation (5-27), also known as the Gordon-Taylor¹¹ equation, has found wide application to random amorphous copolymers. Figure 5-10 shows the experimental results for a series of styrene-butadiene copolymers along with the corresponding T_g 's calculated from equation (5-27) with $k = 0.34$. (See problems at the end of this chapter for additional equations.)

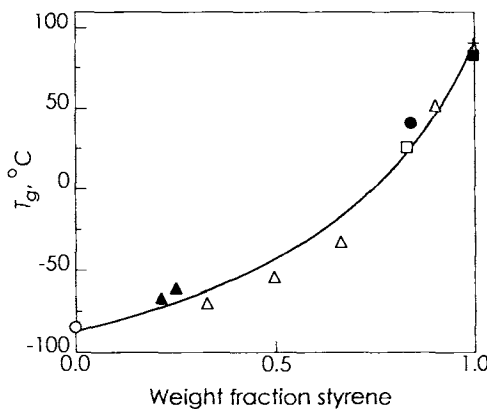


Figure 5-10. Composition dependence of T_g for a series of random styrene-butadiene copolymers compared to the predicted curve calculated on the basis of equation (5-27) with $k = 0.34$. [After M. Gordon and J. S. Taylor, *J. Appl. Chem.* **2**, 493 (1952).]

Equation (5-27) is applicable only to random copolymers; very different phenomena are observed in the case of block and graft copolymers. Frequently in these situations, two T_g 's are observed as a consequence of the occurrence of microphase separation. This subject is beyond the scope of this book, however.

In addition to copolymer composition, geometrical and steric isomerism play important roles in the determination of chain stiffness and thus of T_g . Polydienes, for example, can exist as cis and trans geometrical isomers. In the case of poly(1, 5-butadiene), the cis isomer has a T_g of -102°C while the stiffer trans isomer shows a T_g of -48°C . The effect is not nearly so marked in the

case of polyisoprene where the cis isomer exhibits a T_g of -73°C and the trans isomer a T_g of -53°C .

Vinyl polymers of the type CH_2CHX and vinylidene polymers of the type CH_2CXY are capable of existing in different stereoregular forms. These are generally referred to as isotactic, syndiotactic, and atactic forms; it is here assumed that the reader is familiar with this nomenclature and the specific structures associated with it. It has been shown that steric isomerism has little effect on the T_g of vinyl polymers but profoundly affects the T_g of vinylidene polymers.¹² In the latter case, the isotactic form invariably is associated with the lowest T_g values. This result has also been rationalized on the basis of the Gibbs-DiMarzio theory, but again the details are beyond the scope of this book.

Turning to intermolecular effects, we first note that the free-volume approach is of great utility here, although by no means universally applicable. One example is the effect of low-molecular-weight diluents or plasticizers, which have already been accounted for by the free-volume theory through equation (5-8). The general idea is that plasticizers lower T_g by introducing free volume into the system, the final T_g being intermediate between that of the plasticizer and that of the polymer. The free-volume theory cannot account, however, for the plasticizing effect of water on polar polymers. Water exerts a dramatic plasticizing effect on nylons, greater than 30°C for the first weight per cent. However, the addition of water in low concentrations actually increases the density of the polymer-water mixture and would thus be expected to raise the T_g on the basis of the free-volume theory rather than lowering it as actually observed. The explanation is that water acts to break intermolecular hydrogen bonds present in the nylon, thus allowing greater chain mobility and also more efficient packing, the net result leading to a decrease in T_g .

The effect of molecular weight has been approached in Chapters 3 and 4. Specifically, free volume around chain ends is taken to be greater than that around chain middles because of imperfect packing at the chain ends. It is expected that T_g will become independent of molecular weight at high molecular weights due to the negligible concentration of chain ends in high-molecular-weight polymers. It follows directly from the free-volume theory (see Problem 5-1) that

$$T_g = T_g^\infty - \frac{c}{M_n} \quad (5-28)$$

where M_n is the number-average molecular weight of the polymer. This relationship is known as the Fox-Flory equation.

Figure 5-11 illustrates equation (5-28) for the case of polystyrene; it is seen that the data are well fitted for $c = 1.7 \times 10^5$. The c values vary from polymer

to polymer but are generally of the same order of magnitude as the polystyrene case.

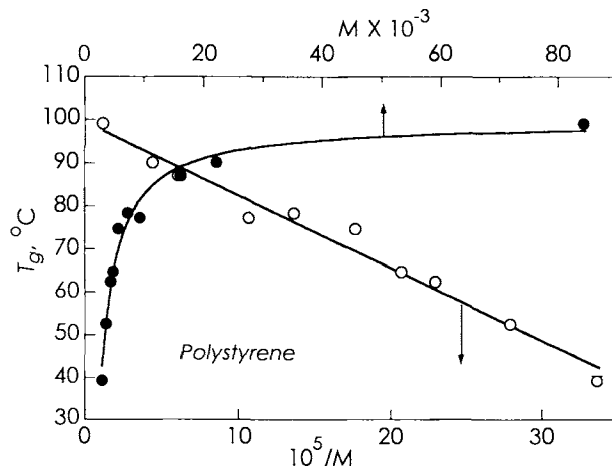


Figure 5-11. T_g versus reciprocal molecular weight for polystyrene fractions. The solid line is a plot of equation (5-28) with $c = 1.7 \times 10^5$. [After T. G. Fox and P. J. Flory, *J. Appl. Phys.* **21**, 581 (1950), by permission of the American Institute of Physics.]

A second important intermolecular structural feature is crosslinking, which often has a strong influence on T_g . Both the free-volume and the Gibbs-DiMarzio theories give a result of the form:

$$T_g = T_{g0} / (1 - kN_0) \quad (5-29)$$

where T_{g0} is the glass transition temperature for the uncrosslinked polymer and N_0 is the number density of crosslinks. The two theories differ in that the constant k has different dependencies on structure and bulk material properties. For the Gibbs-DiMarzio theory, k will depend explicitly on the molecular structure of the network chains, whereas the free-volume theory predicts a dependence of k on the ratio of the differences in expansion coefficients, that is,

$$k \propto \frac{\alpha_m - \alpha_r}{\alpha_r - \alpha_g} \quad (5-30)$$

where α_m is the expansion coefficient of the monomer, while α_r and α_g are the expansion coefficients for the uncrosslinked polymer above and below T_g , respectively.

These ideas are difficult to test experimentally. One system that has been investigated, however, is poly(styrene-*co*-divinylbenzene), which has the desirable feature of a strong structural similarity between the main-chain

monomer, styrene, and the crosslinker, divinylbenzene. The results for this system are shown in Figure 5-12.

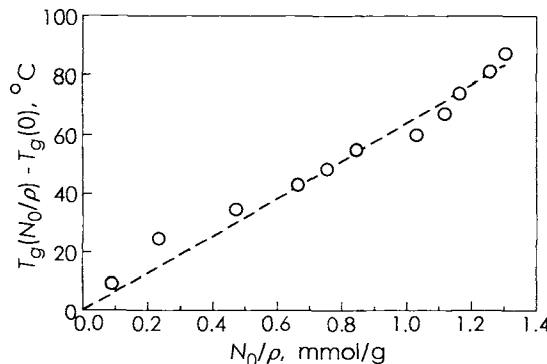


Figure 5-12. Glass transition change in the system poly(styrene-*co*-divinylbenzene) as a function of the crosslink density. N_0 is the number density (e.g., mmol/cm³) crosslinks, whereas ρ is the bulk mass density (e.g., g/cm³). The dotted line is the fit of equation (5-29) with the result that $k\rho$ is 130 ± 10 g/mol. [Adapted from T. G. Fox and S. Loshaek, *J. Polym. Sci.*, **15**, 371 (1955). Copyright © 1955, Wiley Periodicals, Inc., a Wiley Company.]

D. RELAXATIONS IN THE GLASSY STATE

In addition to the glass transition, amorphous polymers usually exhibit at least one so-called secondary relaxation region. Secondary relaxations are manifestations of motions within the polymer in the glassy state. Since large-scale motions such as those accompanying the glass transition are impossible in the glassy state, the secondary relaxations must arise from localized motions. These are conveniently classified into two types: main-chain motions and side-group motions. In this section we describe methods of detecting secondary relaxations and give examples of secondary relaxations belonging to both side-group and main-chain motions.

In contrast to other T_g methods, dynamic measurements easily detect glassy state relaxations and have been extensively applied to their study. These include dynamic mechanical methods, dielectric relaxation, and nuclear magnetic resonance (NMR). Since we are primarily concerned with viscoelastic response at this point, we shall confine the discussion to the dynamic mechanical technique and delay our consideration of dielectric and NMR methods until Chapter 7.

As should be apparent, it is possible to detect secondary relaxations by performing measurements over a frequency range at constant temperature or over a temperature range at constant frequency. The latter technique is usually employed, largely because extended mechanical frequency ranges are difficult

to achieve experimentally and many secondary relaxations of interest occur at very high frequencies at room temperature.

As an example the case of polymethyl methacrylate may be cited. Figure 5-13 shows a plot of the logarithmic decrement versus temperature for this polymer at a constant frequency of 1 Hz in the temperature range -50 to +160 °C. Two relaxation peaks are discernible: the higher temperature relaxation corresponding to the glass transition ($T_g = -105$ °C) and a secondary relaxation at 50 °C. It becomes necessary to adopt a labeling scheme for the various relaxations observed. Several schemes are currently in use and we shall choose one of the most popular, that of labeling the peaks α , β , γ , and so on, in order of decreasing temperature. Thus, in a linear amorphous polymer, the α relaxation corresponds to the glass transition, the β relaxation to the highest temperature glassy-state relaxation, and so forth. Polymethyl methacrylate exhibits only one secondary relaxation in the temperature range of Figure 5-13 and this is the β relaxation at 50 °C.

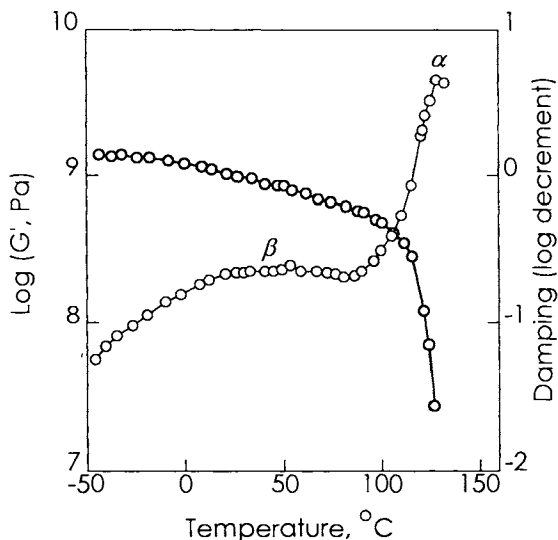


Figure 5-13. Temperature dependence of $\tan \delta$ for polymethyl methacrylate showing the α and β relaxations. [After L. E. Nielsen, Mechanical Properties of Polymers, Reinhold, New York, 1962, p. 178.]

Much of the discussion of the motions underlying the glass transition has been presented without reference to the details of molecular structure. Because of the relatively long-range motions characterizing the glass transition, it is possible to construct general theories applicable to all amorphous polymers without regard to fine structural details. Such is not the case with the localized secondary relaxations. We must in general consider structural features involving only a few main-chain or side-group atoms. Many different

mechanisms have been proposed for the large variety of secondary relaxations observed, and a detailed consideration is beyond the scope of this treatment. More detailed accounts exist in the work of McCrum, Read, and Williams,¹³ Ferry¹⁴ and Murayama,¹⁵ which should be consulted for more details. We shall present only two mechanisms here.

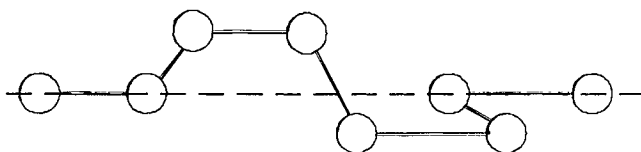


Figure 5-14. The crankshaft mechanism according to Schatzki.

First is the crankshaft mechanism of Schatzki.¹⁶ It has been observed for many polymers containing linear (CH_2) sequences with $n = 4$ or greater, that a secondary relaxation occurs at about -120°C at 1 Hz. This seems to be true regardless of whether the CH_2 sequences occur in the main chain or in the side groups. Thus both polyethylene and poly-n-butyl methacrylate exhibit this relaxation. The mechanism proposed by Schatzki is shown in Figure 5-14.

The motion responsible for the relaxation is a rotation about the two co-linear bonds 1 and 7 such that the carbon atoms between bonds 1 and 7 move in the manner of a crankshaft. The co-linearity of the two terminal bonds is achievable if there are four intervening carbon atoms on the assumption of tetrahedral valence angles and a rotational isomeric state model. Support is to be found for the crankshaft mechanism in the fact that the activation energy estimated for the model, 54 kJ/mol, is close to the experimental results, 50–63 kJ/mol, and in the fact that the predicted free volume of activation, about four times the molar volume of a CH_2 unit, is also in good agreement with experimental estimates based on pressure studies.

An outstanding example of the identification of a secondary relaxation with a specific molecular structure lies in the work of Heijboer.¹⁷ Heijboer studied a large number of methacrylate polymers containing the cyclohexyl group in the ester side chain. His results for a series of methyl methacrylate-cyclohexyl methacrylate copolymers are shown in Figure 5-15. It can be seen that the magnitude but not the temperature of the low temperature relaxation is affected by the concentration of cyclohexyl groups. The observed activation energy for this relaxation is 48 kJ/mol, identical with that observed for a mechanical relaxation in many low-molecular-weight cyclohexyl derivatives. This led to the identification of the polymeric relaxation with a flipping of the substituted cyclohexyl ring from one conformation to another.

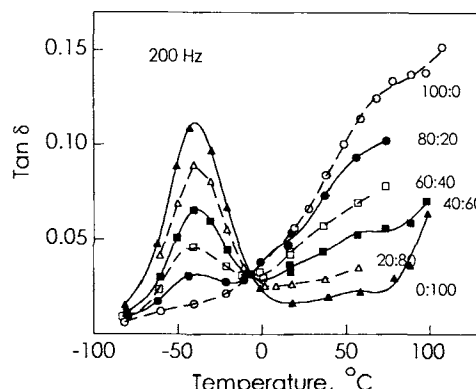


Figure 5-15. Temperature dependence of $\tan \delta$ for copolymers of methyl methacrylate and cyclohexyl methacrylate. Open circles are pure polymethyl methacrylate. [After J. Heijboer, *Kolloid-Z.* 171 7 (1960), by permission of Dr. Dietrich Steinkopff Verlag.]

The time-temperature or frequency-temperature superposition scheme discussed in Chapter 4, Section B, is applicable to secondary relaxations as well as to the glass transition, assuming that the observed secondary relaxation peaks are well resolved. When the shift factors are obtained for these secondary relaxations, it is found that their temperature dependencies do not obey the WLF equation but follow an equation of the Arrhenius form, that is:,

$$\log a_T \propto -\frac{H_a}{2.303RT} \quad (5-31)$$

Thus plots of $\log a_T$ versus $1/T$ for a secondary relaxation will yield straight lines, not curves as in the WLF case. This fact has been used to distinguish the main glass transition from other relaxations occurring in semicrystalline polymers.[§]

E. RELAXATION PROCESSES IN NETWORKS

1. Physical Relaxation

The equilibrium mechanical properties of soft polymeric networks (gels, elastomers) are described in some detail in Chapter 6. Ideally elastomers and covalently crosslinked gels are perfect solids that have no time dependence. The reality is quite different, in that there may be significant dissipation in the network due to a number of mechanisms, the most of important of which are retraction of loose network ends and the chemical scission of the network

[§] It should be emphasized that data of good precision covering a broad temperature range are needed to distinguish between the Arrhenius and WLF relationships.

chains or crosslinks. (The viscoelastic properties of networks below T_g are similar in most cases to the uncrosslinked polymer.)

Early experiments with elastomers showed that the relaxation toward equilibrium was sharply dependent on crosslink density. It was found that tightly crosslinked networks relaxed very quickly, whereas networks with low crosslink density exhibited relaxation that covered an extremely broad time scale. These early experiments were correlated in terms of the expression for the tensile relaxation modulus $E(t)$:

$$E(t) = E_\infty [1 + (t/\tau)^{-m}] \quad (5-32)$$

where E_∞ is the equilibrium modulus, τ is the relaxation time and m is the shape coefficient. This form is often referred to as the Chasset-Thirion equation after the experimentalists Chasset and Thirion.¹⁸ Values of m generally fall around 0.1, meaning that the relaxation is very broad. Figure 5-16 shows an example of this relaxation and its description with the Chasset-Thirion relationship.

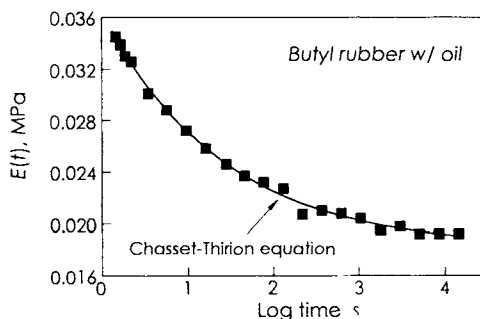


Figure 5-16. Physical stress relaxation at 25 °C in a crosslinked network made by a zinc oxide cure of a halobutyl rubber. The elastomer has been soaked in oil to speed the relaxation. The line is the fit to the data using the Chasset-Thirion equation with $E_\infty = 0.018$ MPa, $\tau = 1.04$ s and $m = 0.31$. The nature of the polymer and the cure makes for a chemically stable structure; otherwise, the plot would begin to curve downward at long time.

Theoretical justification of the Chasset-Thirion expression has been provided in terms of reptation of the free ends of the network.¹⁹ (See Chapter 3, Section G for a general description of reptation.) The elastomeric network provides each dangling end with constraints that do not release; thus the chain must relax by reptation along its own contour. According to the ideas of the tube models, the chain must push a loop through the tube wall, which will then allow the chain end to move along the tube. On release of the loop, the dangling chain end can penetrate into the network in a relaxed configuration. Other possible mechanisms are path retracement, i.e., the end of the chain retraces the path of the rest of the chain to achieve a relaxed configuration. All

of these processes take many steps, and the time required climbs markedly as the structure of the chain end becomes more complex.

2. Chemical Processes

Many elastomers exhibit relaxation processes due to chemical changes in the network, a process that can become dominant at high temperatures. Chemical changes in elastomers are expected in part because of their flexible chain structure, which precludes the use of electronically stabilized conjugated ring structures commonly found in high-performance engineering thermoplastics such as polyimides. Fundamentally chemically stable main chains such as found in perfluoroelastomers may feature curing mechanisms that give less stable crosslinks (see Chapter 6 for a full discussion of these terms). Regardless of the particular moiety responsible for the chemical change, the net result is an observed decay of stress in a stress relaxation experiment. This is referred to as chemical stress relaxation, and classically was done in extension to allow ample exposure of the sample to the surrounding environment. In some polymers, such as natural rubber shown in Figure 5-17, the relaxation is nearly exponential, suggesting a first-order chemical degradation of the network chains of concentration N_0 , that is,

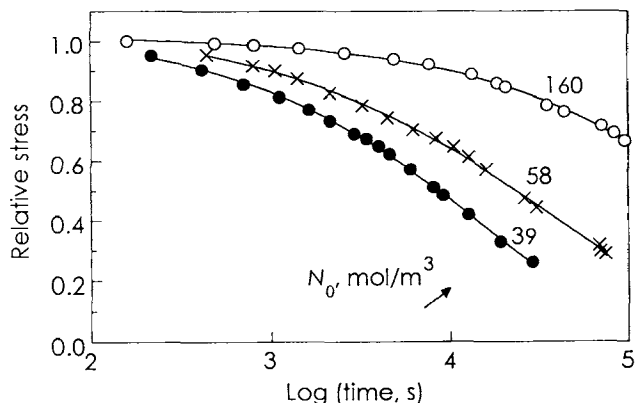


Figure 5-17. Chemical stress relaxation of Natural Rubber cured with dicumyl peroxide. [Data from Y. Takahashi and A. V. Tobolsky, Technical report No. 125, Office of Naval Research, N00014-67-A-0151-0011 (1970).]

$$dN_0 / dt = -kN_0 \quad (5-33)$$

or

$$N_0(t) = N_0(0)e^{-kt} \quad (5-34)$$

where k is the first-order rate constant. The connection of this behavior to the shear stress relaxation modulus G is through equation (6-59) developed in Section B of Chapter 6

$$G = fN_0RT \quad (6-59)$$

where f is a constant factor near 1. As introduced in Chapter 6, Section A, the observed tensile stress σ_E for an elastomer is related linearly to the shear modulus through the relationship

$$\sigma_E = G(\lambda^2 - 1/\lambda) \quad (6-60c)$$

where λ is the stretch ratio. (Review Chapter 2 to recall the relationship between tensile and shear properties.) The net result on combining equations (6-60c), (6-59) and (5-34) is the relationship

$$\frac{\sigma_E(t)}{\sigma_E(0)} = e^{-kt} \quad (5-35)$$

where $\sigma_E(t)$ and $\sigma_E(0)$ are the stress at time t and zero, respectively. Invariably, however, if this hypothesis is checked by measuring the time dependence of G using dynamic methods (see Chapter 2), there is a large discrepancy—the latter does not fall as fast, or may even increase! This discrepancy has been explained in terms of the chemistry of the network, which can include reversible reactions that slow the loss of network chains or side reactions that lead to the formation of new network chains. These ideas are embodied in the two-network hypothesis of Andrews, Tobolsky and Hanson,²⁰ which describes the chemical processes as a superposition of an original strained network and a new network formed in a relaxed state. This mechanism also explains the widely used standard test referred to as compression set, wherein the recovery of strain following chemical stress relaxation is measured.²¹ This simple test involves compression of the sample between two plates for a fixed period of time while exposed to elevated temperatures. At the end of the exposure the plates of the removed and the thickness of the sample is measured and compared with the original thickness. According to the two-network hypothesis, the network formed in the relaxed state resists the recovery of the sample to its original thickness; a balance of the original and new networks determines the recovered thickness.

In a few special cases, remarkable quantitative agreement between independently measured chemical degradation reactions and chemical stress relaxation has been achieved. However, in most cases quantitative interpretation is confounded by other effects such as many parallel reactions,

simultaneous physical relaxation, crystallization processes, the influence of stress on some chemical reactions, and the contributions of physical entanglements in the networks. Thus the main attributes of chemical stress relaxation of elastomer networks are:

- High sensitivity to small amounts of chemical degradation. The high sensitivity results from the amplification due to the large number of degradable links in each network chain combined with the fact that a chain becomes ineffective in supporting stress after but a single scission step.
- Direct relationship to important technological properties such as the sealing pressure exerted by a compressed o-ring.
- Facile detection of interchange reactions in elastomers. Interchange reactions cause breakage of network chains but the chains quickly reform in another configuration. Networks that undergo interchange reactions will exhibit no time dependence of the dynamic modulus, whereas they will exhibit exponential decay of stress in a stress-relaxation experiment. An example of an elastomer that shows interchange is polysulfide, which has main-chain structures involving sequences of labile sulfur-sulfur bonds.
- Ability to distinguish degradation reactions confined to bonds in the crosslink vs. general degradation of the main-chain bonds. These two can be distinguished by comparing the behavior of networks that are crosslinked to a different extent. See Problem 5-12.

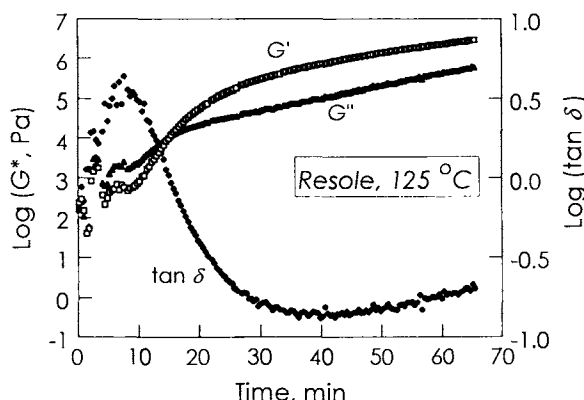


Figure 5-18. Dynamic mechanical behavior during the chemical cure of a phenolic resole resin at 125 °C. The noise at the beginning of the experiment results from the rapid evolution of moisture, which causes some bubbles to form. [From J. Rose, MS Thesis, University of Connecticut, Storrs, CT (2001).]

Relaxation processes during the curing (crosslinking) of networks have also been studied extensively, particularly with respect to the curing of thermosets

for composites. Typical behavior during the cure of a resin starting from low molecular weight to a relatively high state of cure is shown in Figure 5-18. The results show that the cure kinetics slow markedly at times beyond 30 min.

PROBLEMS

1. Assuming that the molecular-weight dependence of the fractional free volume is given by

$$f_M = f_\infty + \frac{A}{M_n}$$

where f_M is the fractional free volume at number-average molecular weight M_n , f_∞ is the fractional free volume at infinite molecular weight, and A is a constant, derive equation (5-28).

2. It has been observed that methacrylate polymers containing linear $(\text{CH}_2)_n$ sequences in the ester side chain exhibit a regular decrease in T_g with increasing n . Some data are provided in file Tg-Alkyl-MA.TXT on the CD.

- (a) Plot this data as T_g vs. n .
 - (b) Devise an explanation for this on the basis of the free-volume theory.
 - (c) (Computer) Use the data provided, along with your explanation in part (b) to predict the T_g of polyethylene. (*Hint:* Consider the equation in part b of Problem 5-4.)
3. Qualitatively predict the dependence of T_g on tensile stress on the basis of
- (a) The free-volume theory
 - (b) The Gibbs-DiMarzio theory.

Might your results suggest an experimental test to distinguish between the two theories?

4. (a) If we consider a polymer to be made of only chain ends and chain middles, show that the following equation may be obtained from equation (5-28):

$$T_g = T_g^\infty - \frac{Cw_e}{M_e}$$

where w_e is the weight fraction of the chain ends and M_e is the weight of chain ends per mole of chains.

- (b) One of the equations used to predict glass transition temperature depression due to the incorporation of solvent is

$$T_g = T_{g,p}w_p + T_{g,s}w_s + Kw_p w_s$$

where subscripts p and s refer to the polymer and the solvent, respectively, and K is a constant. Rearrange this equation into a form similar to the one in part (a) by considering chain ends as solvent.

5. (a) For a miscible blend (mixture) of polymer 1 with polymer 2, derive the following formula for T_g , the glass transition temperature of the blend:

$$\ln T_g = \frac{m_1(\Delta C_{p,1})\ln T_1 + m_2(\Delta C_{p,2})\ln T_2}{m_1(\Delta C_{p,1}) + m_2(\Delta C_{p,2})}$$

m_1 and m_2 are mass fractions, T_1 and T_2 are glass transition temperatures and $\Delta C_{p,1}$ and $\Delta C_{p,2}$ are heat capacity differences (per unit mass) between the liquid and glassy states for polymers 1 and 2 respectively. You may assume that the entropy of the blend is given as

$$S = x_1 S_1 + x_2 S_2$$

where x_i denotes mole fraction and that at all glass transition temperatures,

$$S_{\text{glass}} = S_{\text{liquid}}$$

- (b) Also show that if T_1 and T_2 are close and $\Delta C_{p,1} = \Delta C_{p,2}$, the above relationship reduces to: $T = W_1 T_1 + W_2 T_2$ where W_i are the weight fractions. [See P. B. Couchman, *Phys. Lett.*, **70A**, 155 (1979).]

6. (Open-ended) To estimate the importance of the variation of retardation time with recovery in the single-ordering-parameter kinetic view of the glass transition, contrast the experimentally observed behavior given in Figure 5-9 with that predicted by a single-ordering parameter model with a structurally independent retardation time:

$$\frac{d\delta}{dt} = -\frac{\delta}{\tau}$$

For the consideration of the 24.9 °C curve in the figure, values of $\delta_0 = 3.0 \times 10^{-3}$ and $\tau = 1.0$ h are appropriate. Data for this curve are listed in Glucose-.txt in the CD.

7. (Open-ended; Computer) The influence of film thickness on the glass transition temperature is an important problem in thin-film technology. In dealing with very thin films, thickness is not the only factor—preparation method, the nature of the substrates (if any) and even the method of measurement may influence the result. Considering the data below (also in file Film-Tg.TXT in the accompanying CD) for films cast on a single surface, and assuming that the film's surface is a layer δ in thickness and featuring twice the free volume of the bulk polymer, derive an expression for the film's T_g in terms of surface layer thickness δ , film thickness h , and the T_g of the bulk. Choose any reasonable method of averaging the T_g 's of the two layers. Use your equation to fit the data provided, and plot the result. If this approach is valid, suggest what would happen if two surfaces of the film were exposed to the air.

Log (thickness, m)	T_g , K
-7.746	320.6
-7.577	322.1
-7.465	324.2
-7.451	325.0
-7.437	325.7
-7.338	327.0
-7.282	327.0
-7.099	327.9
-7.042	329.1
-5.352	330.4
-4.296	330.9

Data from Fig. 4 of F. Kremer and L. Hartmann, *Dielectrics Newsletter*, September 2001, pp. 4-6.

8. (Open end; Computer) The curves in Figure 4-4a are drawn according to the empirical function

$$\log G(T) = \log G_g - \frac{\log G_g - \log G_r}{1 + e^{-(T-T_i)/\Delta T_i}} - \frac{\log G_r}{1 + e^{-(T-T_f)/\Delta T_f}}$$

where T_i and ΔT_i the inflection temperature and breadth of the glass transition, respectively, can be determined quite accurately from the available data. The symbols G_g , and G_r , represent the moduli of the glass and rubbery plateau, respectively; and T_f and ΔT_f , the inflection temperature and breadth of the rubbery flow transition, respectively. Some of the parameters associated with the fits are:

Plasticizer amount, wt%	T_i , °C	ΔT_i , °C
0	93.2	2.3
10	59.4	4.3
20	31.1	12.9
30	2.3	22.5
40	-35	23.6
50	-73.7	18.6
60	-86.7	12.7

(a) Using the Fox equation,²²

$$\frac{1}{T_g} = \frac{W_A}{T_{g,A}} + \frac{W_B}{T_{g,B}}$$

estimate the inflection temperature for the glass transition of the plasticizer, assuming the plasticized mixture is a single phase. Compare prediction of the Fox equation to

that of the Fox-Flory equation (5-28), assuming the polymer molecular weight is 150 kDa.

(b) If the highly plasticized polymer instead separates into two liquid phases, sketch the phase diagram of the mixture assuming a melting point of the semicrystalline polymer of 180 °C and that the ΔT_i represents the breadth of the two-phase liquid-liquid region. Name the phases present in each composition-temperature region.

(c) Assuming the log modulus response is proportional to the amount of each phase, calculate the modulus-temperature response for equilibrium phases of 0.2 and 1. weight fraction plasticizer with an overall amount of 0.3, and using the T_i 's from part (a) and ΔT_i for pure PVC. Comment on the result.

9. Data for the T_g 's of PDMS oligomers are listed in file Tg-PDMS . TXT on the CD, whereas the T_g 's of low-molecular-weight PVC resins are listed in Tg-PVC . TXT.

(a) After converting the degree of polymerization (d_p) to molecular weight for the PDMS (assume all methyl substitution and that $d_p = 2$ is $(\text{CH}_3)_3\text{Si-O-Si}(\text{CH}_3)_2\text{-O-Si}(\text{CH}_3)_3$, compare the deviations of these two polymers from the Fox-Flory equation.

(b) (Computer, Challenging) Compare the fits from (a) with those of the two-parameter Gibbs-DiMarizio equation²⁴

$$\frac{2\beta e^\beta}{1+2e^\beta} - \ln(1+2e^\beta) = \frac{x}{x-3} \left\{ \frac{1+v_0}{1-v_0} \ln \left[\frac{(x+1)(1-v_0)}{2xv_0} + 1 \right] + \frac{\ln 3(x+1)}{x} + \frac{\ln v_0}{1-v_0} \right\}$$

where $x = d_p$, and $\beta = -\varepsilon/kT_g$. The two parameters are v_0 and ε , the fraction of holes and flex energy, respectively. The independent variable is implicit in the left-hand side of the equation, which makes this problem challenging.

10. (Open-ended) Problem 5-3 addresses in a qualitative fashion the predicted effects of tensile stress on T_g . This problem calls for a quantification of these predictions using a polymer of your choice. The following steps are suggested:

(a) Pick an elastomer with readily available tabulations of physical properties. Find T_g , the expansion coefficient α , the isothermal compressibility β and the change of C_p through the glass transition.

(b) Using equation (5-6) for the influence of pressure on T_g , calculate the change of tensile stress σ_E . (Hint: Refer to Chapter 2 to find the relationship between tensile stress and pressure.)

(c) The simplified Gibbs-DiMarizio formula for T_g change is:

$$T_g(\lambda) = T_g(1) \exp \left[\frac{G}{2\Delta C_p T_0} (\lambda^2 + 2/\lambda - 3) \right]$$

where λ is the stretch ratio, G is the modulus at T_0 and ΔC_p is the change of C_p through the glass transition. After learning in Chapter 6 that $\sigma_E = G(\lambda^2 - 1/\lambda)$ and finding the magnitude of G for crosslinked elastomers, calculate $T_g(\lambda) - T_g(1)$.

(d) Plot both results of a stress range that could conceivably be achieved with the elastomer you choose.

(e) Comment of the magnitude of the T_g changes and design an experiment using the tensile mode of a dynamic mechanical thermal analyzer (DMTA) to carry out your experiment.

11. (Computer) (a) Compare the Chasset-Thirion equation with an exponential relaxation to equilibrium such as

$$E(t) = E_\infty [1 + a \exp(-t/\tau)]$$

at times considerably longer than τ and such that the modulus is only 10% greater than E_∞ at $t = \tau$. One approach is to generate “data” with the exponential expression, and then fit these results with the Chasset-Thirion equation to find m . Is there any limit to the value of m as the t/τ grows?

(b) The data used for Figure 5-16 are listed in Butyl-Rel.TXT in the CD. Using this data, compare the quality of fit of the exponential equation with that of the Chasset-Thirion equation. Is there any evidence in favor of either?

12. Examine the influence of crosslink density N_c on the chemical stress relaxation of a network assuming that each main chain have an equal number of equally susceptible bonds that undergo first-order chemical scission with a rate constant k_1 , whereas all N_c crosslinks (per unit volume) have only one susceptible bond that undergoes first-order scission with a rate constant k_2 . Start with a perfect network with modulus given by $G = N_0 RT$ where $N_0 = 2 N_c = \rho/M_c$ where N_c is the number density of crosslinks, ρ is the mass density and M_c is the molecular weight of each network chain. Assume that each mainchain linkage has a molecular weight of M_0 .

REFERENCES

1. R. S. Porter and J. F. Johnson, Eds., *Analytical Calorimetry*, Plenum, New York, 1969.
2. See, for example, J. C. Randall, ed., *NMR and Macromolecules*, ACS Symp. Ser. 247 (1984).
3. P. Ehrenfest, *Proc. Acad. Sci. Amsterdam*, **36**, 153 (1933).
4. W. Kauzmann, *Chem. Rev.*, **43**, 219 (1948).
5. J. H. Gibbs and E. A. DiMarzio, *J. Chem. Phys.*, **28**, 373 (1958).
6. R. Simha and R. F. Boyer, *J. Chem. Phys.*, **37**, 1003 (1962).
7. L. A. Wood, *J. Polym. Sci.*, **28**, 319 (1958).

164 TRANSITIONS AND RELAXATIONS IN AMORPHOUS POLYMERS

8. A. J. Kovacs, J. J. Aklonis, J. M. Hutchinson and A. R. Ramos, *J. Polym. Sci., Polym. Phys. Ed.*, **17**, 1097 (1979).
9. C. L. Beatty and F. E. Karasz, *J. Macromol. Sci., Rev. Macromol. Chem.*, **C17**, 37 (1979).
10. P. Peyser "Glass Transition Temperatures of Polymers," in *Polymer Handbook*, 3rd ed., J. Brandrup and E. Immergut, eds., Wiley Interscience, New York, pp. VI 209-VI 277.
11. M. Gordon and J. S. Taylor, *J. Appl. Chem.*, **2**, 493 (1977).
12. F. E. Karasz and W. J. MacKnight, *Macromolecules*, **1**, 537 (1968).
13. N. G. McCrum, B. E. Read, and G. Williams, *Anelastic and Dielectric Effects in Polymeric Solids*, Wiley, New York, 1967.
14. J. D. Ferry, *Viscoelastic Properties of Polymers*, 3rd ed., Wiley, New York, 1980.
15. T. Murayama, *Dynamic Mechanical Analysis of Polymer Materials*, Elsevier Science, New York, 1978.
16. T. F. Schatzki, *J. Polym. Sci.*, **57**, 496 (1962).
17. J. Heijboer, *Kolloid-Z.*, **171**, 7 (1960).
18. R. Chasset and P. Thirion, "Viscoelastic Relaxation of Rubber Vulcanizates between the Glass Transition and Equilibrium," *Proceedings of the International Conference on the Physics of Non-Crystalline Solids*, J. A. Prins, ed., American Elsevier, New York, 1965, pp. 345-359.
19. J. G. Curro and P. Pincus, *Macromolecules*, **16**, 559 (1983).
20. R. Andrews, A. V. Tobolsky and E. E. Hanson, *J. Appl. Phys.* **17**, 352 (1946).
21. American Society for Testing Materials (ASTM) "Standard Test Methods for Rubber Property—Compression Set," D395-03. See www.ASTM.org for more details.
22. T. G Fox, *Bull. Am. Phys. Soc.*, **1**, 123 (1956).
23. G. B. McKenna, G. Hadzioannou, P. Lutz, G. Hild, C. Strazielle, C. Straupe, P. Rempp and A. J. Kovacs, *Macromolecules*, **20**, 498-512 (1987).
24. G. Pezzin, F. Zilio-Grandi and P. Sanmartin, *Eur. Polym. J.*, **6**, 1053 (1970).

6

Elasticity of Rubbery Networks

The high elasticity of rubberlike materials is certainly their most striking characteristic. A crosslinked elastomer strip, extended to several times its original length when released, will return to that original length exhibiting little or no permanent deformation as a result of the extension. This is, of course, in marked contrast to the behavior of crystalline solids and glasses, which cannot normally be extended to more than a very small fraction of their original length without undergoing fracture. It is also in contrast to the behavior of ductile materials such as some metals, which can undergo large deformations without fracture but which do not return to their original length upon removal of the deforming stress.

The elastic response of elastomers has been the subject of a great deal of study by many investigators because of its very great technological importance as well as its intrinsic scientific interest. Starting from one material, namely natural rubber, the development of polymerization techniques has resulted in a host of substances that may properly be called rubbers, and a giant synthetic-rubber industry has developed to exploit them commercially. The term "elastomer" has become the generic scientific name for a rubbery material.

In this chapter, we first discuss the thermodynamics of rubber elasticity. The classical thermodynamic approach, as is well known, is only concerned with the macroscopic behavior of the material under investigation and has nothing to do with its molecular structure. The latter belongs to the realm of statistical mechanics, which is the subject of the second section, and has as its

basis the statistical description of the flexible polymer chain, a subject that is introduced in Appendix 1. We next examine the relative significance of energy and entropy in rubber elasticity. A phenomenological treatment then follows, which provides an extension of the description of elasticity to three dimensions and large deformations. Finally, we discuss various effects on rubber elasticity, such as degree of crosslinking, swelling, fillers, and crystallinity.

A. THERMODYNAMIC TREATMENT

The experimental techniques for investigating the thermodynamic behavior of elastomers are quite numerous and varied. It is possible to investigate the elastomer's response to various kinds of deformations, such as shear, tension, and compression, and it is also possible to vary temperature, pressure, and volume. Conceptually, one of the easiest experiments to perform is to extend an elastomer strip to some fixed length and then measure the restoring stress exerted by the strip as a function of temperature at constant (atmospheric) pressure. It turns out that such a simple experiment embodies the fundamental thermodynamic principles of rubber elasticity and thus serves to provide a point of departure for the ensuing development. As we shall treat rubber elasticity by *equilibrium* thermodynamics, our measurements must be done in accordance with this condition. Experimentally, equilibrium is attained after stretching by allowing stress relaxation (see Chapter 5, Section E) to proceed for a long time until constant modulus is obtained.* Achievement of equilibrium can be evidenced by the reversible changes in elastic force upon changing the temperature.

Figure 6-1 illustrates the equilibrium stress-temperature behavior of natural rubber at various extension ratios.¹ The curves are linear over considerable temperature ranges with negative slopes at low degrees of elongation and positive slopes at higher degrees of elongation. This behavior is not confined to natural rubber but is general for all elastomers.

The analysis of the experimental results begins with the combined first and second laws of thermodynamics, applicable to reversible processes. As shown in the Appendix 2, it reads

$$dU = TdS - dW \quad (6-1)$$

* Recent theory described in Section E of Chapter 5 suggests that true equilibrium will be difficult to achieve by stress relaxation of an elastomer, but provides a relationship for extrapolation to equilibrium.

In equation (6-1) the increment of work, dW , refers to all of the work (i.e., electrical, mechanical, pressure-volume, chemical, etc.) performed by the system (the sample) on its surroundings. The development of thermodynamics given in most physical chemistry texts is confined to gases where dW becomes simply pressure-volume work, PdV , where P is the external environment. In the case of an elastomer deformed by an amount dL in tension and exerting a restoring force f , the mechanical work performed on the system to accomplish the deformation, namely fdL , must also be included in dW . Thus, for an elastomer strained uniaxially in tension,

$$dW = PdV - fdL \quad (6-2)$$

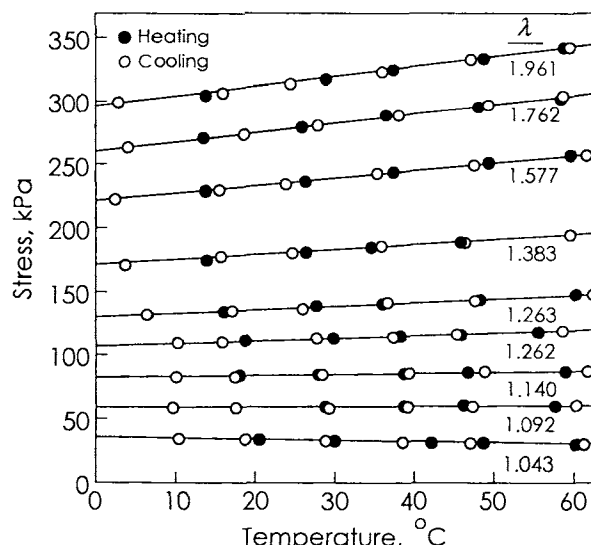


Figure 6-1. Stress-temperature curves of natural rubber. Extension ratios λ are indicated on the right of the figure. [After M. Shen, D. A. McQuarrie, and J. L. Jackson, *J. Appl. Phys.*, **38**, 791 (1967), by permission of the American Institute of Physics.]

In the measurements discussed above, P is the atmospheric pressure and dV is the volume dilation accompanying the elongation of the elastomer. Generally, PdV is much smaller than fdL and may sometimes be neglected in comparison to fdL . However, for completeness the treatment following will include pressure-volume work. The sign of fdL is the opposite of the PdV term because the symbol f is conventionally assigned to the force exerted by the environment on the sample, which is the opposite of the convention used for the PdV term,

which represents work done by the sample on the environment. The sign of the differential dL is positive when the sample becomes longer.[†]

Equation (6-1) now becomes

$$dU = TdS - (PdV - fdL) \quad (6-3)$$

Because the experiments discussed were performed under constant pressure conditions, it is appropriate to use the thermodynamic entity H , the enthalpy. H is defined as

$$H \equiv U + PV \quad (6-4)$$

Differentiating equation (6-4) at constant pressure results in

$$dH = dU + PdV \quad (6-5)$$

Substituting for dU from equation (6-3) we obtain

$$dH = TdS + fdL \quad (6-6)$$

Thus, the restoring force exerted by the elastomer when it has undergone a deformation by the amount dL at constant temperature and pressure is:

$$f = \left(\frac{\partial H}{\partial L} \right)_{T,P} - T \left(\frac{\partial S}{\partial L} \right)_{T,P} \quad (6-7)$$

Equation (6-7) shows that the restoring force originates in the enthalpy and entropy changes that occur in the elastomer as a result of the deformation that it undergoes.

The change in slope of the stress–temperature curve from negative values at low degrees of elongation to positive values at high degrees of elongation is known as the thermoelastic inversion phenomenon (Figure 6-1). To understand why this should occur, it is necessary to derive a thermodynamic expression for the slope of this curve, that is, an expression for $(\partial f / \partial T)_{P,L}$. This can be done as follows. Changes in the Gibbs free energy of a closed system are given by the expression

$$dF = -SdT + VdP + fdL \quad (6-8)$$

One of Maxwell's relations states that

[†] The sign convention for the thermodynamic work varies; many thermodynamic textbooks now use the convention that positive work is that applied to the sample by the environment. We will use the classical sign convention here.

$$\left(\frac{\partial S}{\partial L}\right)_{T,P} = -\left(\frac{\partial f}{\partial T}\right)_{P,L} \quad (6-9)$$

Substitution for $(\partial S / \partial L)_{T,P}$ in equation (6-7) yields

$$f = \left(\frac{\partial H}{\partial L}\right)_{T,P} + T\left(\frac{\partial f}{\partial T}\right)_{P,L} \quad (6-10)$$

which, upon rearrangement, leads to the desired result:

$$\left(\frac{\partial f}{\partial T}\right)_{P,L} = \frac{f - (\partial H / \partial L)_{T,P}}{T} \quad (6-11)$$

This expression shows that for the slope of the f versus T curves to be negative, it must be that $(\partial H / \partial L)_{T,P} > f$; likewise, for the slope to be positive, it must be that $(\partial H / \partial L)_{T,P} < f$. The experimental results show that the former inequality holds at low elongations and the latter inequality holds at high elongations. At sufficiently high elongations it is possible to neglect $(\partial H / \partial L)_{T,P}$ in comparison with f ; and, as a result,

$$f = T\left(\frac{\partial f}{\partial T}\right)_{P,L} = -T\left(\frac{\partial S}{\partial L}\right)_{T,P} \quad (6-12)$$

Thus f becomes directly proportional to the absolute temperature, meaning that the elastic response of the elastomer is entirely governed by the decrease in entropy resulting from chain extension upon deformation of the sample.

Although equation (6-12) adequately describes the behavior of an elastomer at high extensions ($> 10\%$ for natural rubber), it is nevertheless true that the coefficient $(\partial H / \partial L)_{T,P}$ has a finite value and cannot be neglected in a complete treatment of rubber elasticity. [It should be stated that equation (6-12) is inadequate to describe the behavior of most elastomers at very high extensions because of increasing limitations on chain extension and motion, as well as the onset of crystallization in many elastomers. When this occurs, the term $(\partial H / \partial L)_{T,P}$ once again becomes important and may actually outweigh the term $T(\partial S / \partial L)_{T,P}$.]

To explore the origins of the coefficient $(\partial H / \partial L)_{T,P}$ we return to equation (6-5). Differentiation of equation (6-5) at constant temperature yields:

$$\left(\frac{\partial H}{\partial L}\right)_{T,P} = \left(\frac{\partial U}{\partial L}\right)_{T,P} + P\left(\frac{\partial V}{\partial L}\right)_{T,P} \quad (6-13)$$

We wish to separate effects arising from volume changes and effects arising from deformations of the material. To do this, we proceed as follows: Expressing changes in U as functions of length and volume changes yields

$$dU = \left(\frac{dU}{dV} \right)_{L,T} dV + \left(\frac{\partial U}{\partial L} \right)_{V,T} dL \quad (6-14)$$

From equation (6-14):

$$\left(\frac{\partial U}{\partial L} \right)_{T,P} = \left(\frac{\partial U}{\partial V} \right)_{L,T} \left(\frac{\partial V}{\partial L} \right)_{T,P} + \left(\frac{\partial U}{\partial L} \right)_{V,T} \quad (6-15)$$

which, upon substitution into equation (6-13) and rearrangement, gives

$$\left(\frac{\partial H}{\partial L} \right)_{T,P} = \left(\frac{\partial U}{\partial L} \right)_{T,V} + \left[\left(\frac{\partial U}{\partial V} \right)_{T,L} + P \right] \left(\frac{\partial V}{\partial L} \right)_{T,P} \quad (6-16)$$

Equation (6-16) shows that the coefficient $(\partial H/\partial L)_{T,P}$ consists of a part arising from internal energy changes occurring during a change of length at constant volume and a volume-dependent part. Although the thermodynamic development is not concerned with the molecular nature of the elastomer, the coefficient $(\partial U/\partial L)_{T,V}$ can be related to intramolecular energy effects. This is so because of the constant-volume condition. Real elastomers usually have nonzero values for this coefficient.

The coefficient $(\partial U/\partial L)_{T,L}$ may be transformed into experimentally accessible quantities as follows. The Helmholtz free energy, dA , is given by

$$dA = -SdT - PdV + fdL \quad (6-17)$$

From this it follows that

$$\left(\frac{\partial S}{\partial V} \right)_{T,L} = \left(\frac{\partial P}{\partial T} \right)_{V,L} \quad (6-18)$$

Returning to equation (6-3) and differentiating with respect to V at constant T and L :

$$\left(\frac{\partial U}{\partial V} \right)_{T,L} = T \left(\frac{\partial S}{\partial V} \right)_{T,L} - P \quad (6-19)$$

or, making use of equation (6-18):

$$\left(\frac{\partial U}{\partial V}\right)_{T,L} = T \left(\frac{\partial P}{\partial T}\right)_{V,L} - P \quad (6-20)$$

Using the chain rule of partial differentiation,

$$\left(\frac{\partial P}{\partial T}\right)_{V,L} = - \left(\frac{\partial P}{\partial V}\right)_{T,L} \left(\frac{\partial V}{\partial T}\right)_{P,L} \quad (6-21)$$

The cubical coefficient of thermal expansion is defined by

$$\alpha = \frac{1}{V} \left(\frac{\partial V}{\partial T}\right)_{P,L} \quad (6-22)$$

and the coefficient of isothermal compressibility by

$$\beta = - \frac{1}{V} \left(\frac{\partial V}{\partial P}\right)_{T,L} \quad (6-23)$$

(Note that both α and β may be weak functions of length inasmuch as the volume of the elastomer undergoes changes on extension.) Using these definitions, we have

$$\left(\frac{\partial P}{\partial T}\right)_{V,L} = \frac{\alpha}{\beta} \quad (6-24)$$

and

$$\left(\frac{\partial U}{\partial V}\right)_{T,L} = T \frac{\alpha}{\beta} - P \quad (6-25)$$

Inserting equation (6-25) into equation (6-16) yields:

$$\left(\frac{\partial H}{\partial L}\right)_{T,P} = \left(\frac{\partial U}{\partial L}\right)_{T,V} + T \frac{\alpha}{\beta} \left(\frac{\partial V}{\partial L}\right)_{T,P} \quad (6-26)$$

The quantity $(\partial H / \partial L)_{T,P}$ is directly accessible from experimental f versus T curves (at constant L) as the intercept at $T = 0$ of the tangent to the experimental curve at any desired temperature [see equation (6-10)]. Its evaluation thus involves no difficulty for any elastomer provided equilibrium constant-pressure stress-temperature data are available. In principle, the second term on the right side of equation (6-26) is also directly measurable, but precise values turn out

to be very difficult to obtain in practice. Measurements of α and β can be carried out with relative ease, but the coefficient $(\partial V/\partial L)_{T,P}$ is very small for most elastomers and usually depends on extension; thus great experimental skill is required to obtain a measurement of any accuracy.^{2,3}

By combining equation (6-26) with equation (6-10), the energetic component of the elastic force f_e becomes

$$\begin{aligned} f_e &= \left(\frac{\partial U}{\partial L} \right)_{T,V} \\ &= f - T \left(\frac{\partial f}{\partial T} \right)_{P,L} - \frac{T\alpha}{\beta} \left(\frac{\partial V}{\partial L} \right)_{T,P} \end{aligned} \quad (6-27)$$

Thus, from equation (6-27) one should be able to compute the relative importance of contributions from energy and entropy to rubber elasticity. Once again, the difficulty of measuring accurate values of the partial $(\partial V/\partial L)_{T,P}$ renders this separation difficult at best.

In general, direct measurements have not been fruitful and various approximate methods have been devised.⁴ The latter are discussed in more detail in Section B2 of this chapter.

B. STATISTICAL TREATMENT

A rubber-like solid is unique in that its physical properties resemble those of solids, liquids, and gases in various respects. It is solidlike in that it maintains dimensional stability, and its elastic response at small strains (<5%) is essentially Hookean. It behaves like a liquid because its coefficient of thermal expansion and isothermal compressibility are of the same order of magnitude as those of liquids. The implication of this is that the intermolecular forces in an elastomer are similar to those in liquids. It resembles gases in the sense that the stress in a deformed elastomer increases with increasing temperature, much as the pressure in a compressed gas increases with increasing temperature. This gas-like behavior was, in fact, what first provided the hint that rubbery stresses are entropic in origin.

1. Derivation

The molecular model for the ideal gas is a collection of point masses in ceaseless, random, thermal motion, the motion of any two of the point masses being completely uncorrelated with one another. The counterpart to this in the case of the ideal elastomer is a collection of volumeless, long, flexible chains

that are continually undergoing conformational rearrangements due to thermal motion but with all conformations equally accessible. The latter implies that all conformations are isoenergetic, that is, there are no energy differences among conformations. It is assumed that fewer chain conformations are accessible upon stretching, leading to a decrease in entropy, and hence to the restoring stress exerted by the elastomer.

To exhibit an equilibrium elastic stress, it is necessary for the collection of linear polymer chains in an elastomer to be tied together into an infinite network. Otherwise the Brownian motions of the macromolecules will cause them to move past each other, thus exhibiting flow. Chemical crosslinking reactions to form covalent bonds are many and varied. In addition, microphase separation of parts of the chain (e.g., a chemically different sequence in a block copolymer) can provide a strong tie. It suffices for our purposes to consider a crosslink to be a permanent tie-point between two chains (Figure 6-2).

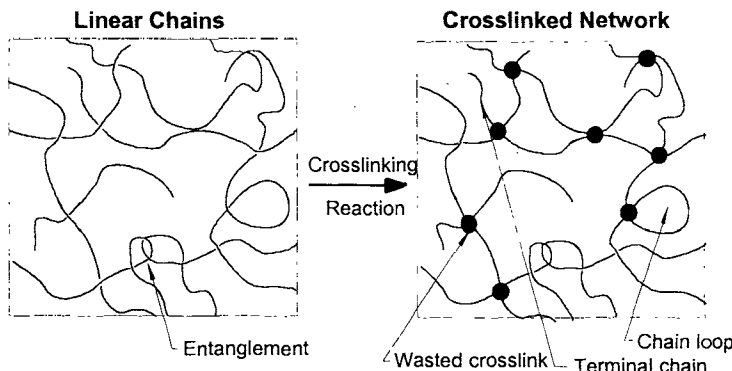


Figure 6-2. Schematic diagram of an ensemble of linear polymer chains being crosslinked into an infinite network.

To compare the ideal elastomer with the ideal gas on a more quantitative basis, we note from equation (6-3) that

$$f = \left(\frac{\partial U}{\partial L} \right)_{T,V} - T \left(\frac{\partial S}{\partial L} \right)_{T,V} \quad (6-28)$$

Equation (6-28) resembles the relation

$$-P = \left(\frac{\partial U}{\partial V} \right)_T - T \left(\frac{\partial S}{\partial V} \right)_T \quad (6-29)$$

applicable to gases. For ideal gases the internal energy is independent of volume, $(\partial U / \partial V)_T = 0$, and the entropy has two components: one is associated with the heat capacity of the gas, but independent of volume; the other is

related to the configurational entropy of the system, and thus a function of the volume. By analogy, the ideal elastomer may be looked at in the same way. Its internal energy is independent of elongation as required by the model, and thus $(\partial U / \partial L)_{T,V} = 0$ and the stress can be attributed to the configurational entropy alone.

The term configurational entropy has been applied historically to the volume-dependent portion of the entropy in an ideal gas; by analogy, the elongation-dependent entropy in the ideal elastomer was also referred to as configurational entropy. A difficulty arises with this terminology in elastomers. Elastomer molecules are capable of geometrical isomerization, such as cis and trans isomers as well as stereoisomerism, which results in, for example, isotactic and syndiotactic forms. These various isomers are known as configurations and cannot be transformed from one into another without breaking chemical bonds. Thus, upon stretching, no configurational changes are possible and there is no configurational contribution to the entropy. What does take place are rotations about single bonds in the chain backbone. It is these conformational changes that give rise to the entropy decrease upon stretching. The conformational statistics of a single chain were the subject of the last chapter. Thus conformational entropy changes upon stretching are the major sources of rubber elasticity, and we shall refer to the entropy involved as conformational entropy in the discussion that follows.

In the formulation of the statistical theory of rubber elasticity,⁵⁻¹¹ the following simplifying assumptions are made:

1. The internal energy of the system is independent of the conformations of the individual chains.
2. An individual network chain is freely joined and volumeless; consequently, it obeys Gaussian statistics (Appendix 1).
3. The total number of conformations of an isotropic network of such Gaussian chains is the product of the number of conformations of the individual network chains.
4. Crosslink junctions in the network are fixed at their mean positions. Upon deformation, these junctions transform affinely, that is, in the same ratio as the macroscopic deformation ratio of the elastomer sample.

Now, from equation (6-17):

$$f = \left(\frac{\partial A}{\partial L} \right)_{T,V} \quad (6-30)$$

But by definition,

$$A \equiv U - TS \quad (6-31)$$

Because of assumption 1, however, we need not find an explicit expression for U but can concentrate on the entropy expression. For this we shall again invoke the Boltzmann relation [Appendix 2, equation (g)], as we did for the isolated chain:

$$S = k \ln \Omega \quad (6-32)$$

where Ω is the total number of conformations available to the rubber network. According to assumption 2, the number of conformations available to the i th individual chain is given by the Gaussian distribution function [Appendix 1, equation (k)]:

$$\omega(x_i, y_i, z_i) = \left(\frac{b}{\pi^{1/2}} \right)^3 \exp \left[-b^2 (x_i^2 + y_i^2 + z_i^2) \right] \quad (6-33)$$

Equation (6-33) describes the probability density for one end of the chain at the coordinates (x_i, y_i, z_i) in the unstrained state, the other end being at the origin of the Cartesian coordinate system. The chain's end-to-end vector \mathbf{r}_i has a magnitude of $(x_i^2 + y_i^2 + z_i^2)^{1/2}$. (Figures 6-14 and 6-15, Appendix 1). Following assumption 3, the total number of conformations available to a network of N such chains is

$$\Omega = \prod_{i=1}^N \omega(r_i) \quad (6-34)$$

and the conformational entropy of the undeformed network is just

$$S_u = 3k \ln \frac{b}{\pi^{1/2}} - k \sum_{i=1}^N b^2 (x_i^2 + y_i^2 + z_i^2) \quad (6-35)$$

or

$$A_u = A_0 + kT \sum_{i=1}^N b^2 (x_i^2 + y_i^2 + z_i^2) \quad (6-36)$$

where A_0 is that portion of the Helmholtz free energy that is not related to conformational entropy changes.

In the strained state, the chain is deformed to \mathbf{r}'_i with the chain end now at coordinates (x'_i, y'_i, z'_i) . To relate the microscopic strain of the chains to the macroscopic strain of the elastomer sample, we assume the deformation to be affine (assumption 4). Consider a unit cube of an isotropic rubber sample

(Figure 6-3a). In the general case of a pure homogeneous strain, the cube is transformed into a rectangular parallelepiped (Figure 6-3b). The dimensions of the parallelepiped are λ_1 , λ_2 and λ_3 in the three principal axes, where the λ_i 's are called the principal extension ratios. Choosing the coordinate axes for the chain to coincide with the principal axes of strain for the sample, then

$$x'_i = \lambda_1 x_i \quad y'_i = \lambda_2 y_i \quad z'_i = \lambda_3 z_i \quad (6-37)$$

The Helmholtz free energy of the deformed network can thus be written as

$$A_d = A_0 + kT \sum_{i=1}^N b^2 (\lambda_1^2 x_i^2 + \lambda_2^2 y_i^2 + \lambda_3^2 z_i^2) \quad (6-38)$$

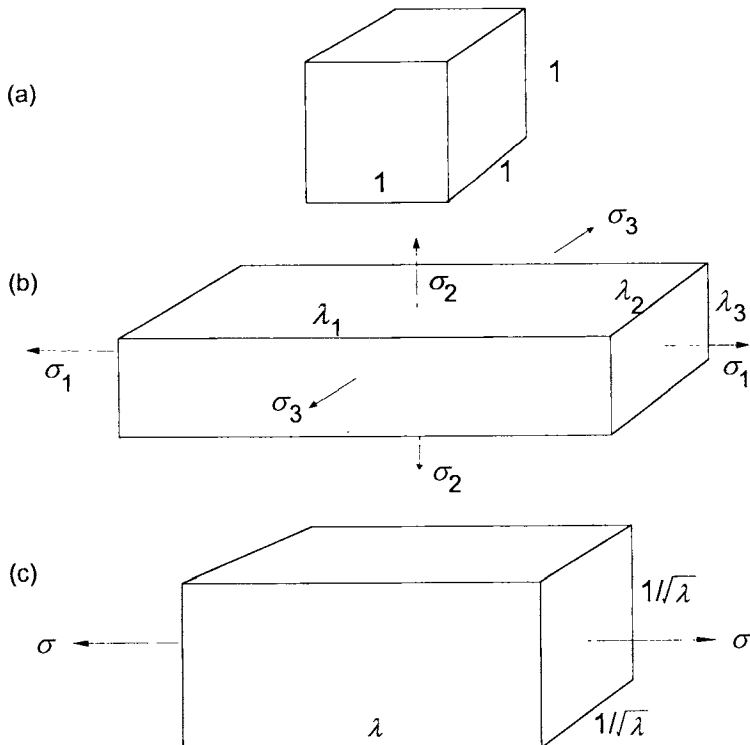


Figure 6-3. A unit cube of elastomer: (a) in the unstrained state; (b) in the homogeneous strained state; (c) under uniaxial extension.

The total change in free energy of the elastomer network due to the deformation is simply the difference between equations (6-36) and (6-38):

$$\Delta A = kT \left[(\lambda_1^2 - 1) \sum_{i=1}^N b^2 x_i^2 + (\lambda_2^2 - 1) \sum_{i=1}^N b^2 y_i^2 + (\lambda_3^2 - 1) \sum_{i=1}^N b^2 z_i^2 \right] \quad (6-39)$$

We recall that by definition:

$$r_i^2 = x_i^2 + y_i^2 + z_i^2 \quad (6-40)$$

For a random, isotropic network all directions are equally probable; then

$$x_i^2 = y_i^2 = z_i^2 = \frac{1}{3} r_i^2 \quad (6-41)$$

Equation (6-39) now becomes

$$\begin{aligned} \Delta A &= \frac{1}{3} kT \sum_{i=1}^N b^2 r_i^2 (\lambda_1^2 + \lambda_2^2 + \lambda_3^2 - 3) \\ &= \frac{1}{3} kNT \overline{b^2 r^2} (\lambda_1^2 + \lambda_2^2 + \lambda_3^2 - 3) \end{aligned} \quad (6-42)$$

where we have written $\overline{b^2 r^2} = \sum_{i=1}^N b^2 r_i^2 / N$. In Appendix 1 we defined b^2 for an unstrained freely orienting random chain as

$$b^2 = \frac{3}{2r_f^2} \quad (6-43)$$

If the network chains in the unstrained state have the same distribution of conformations as an ensemble of free chains, then $b^2 r^2 = 3/2$. However, in real networks this condition may not be met. For instance, some of the chains may already be partially strained during the crosslinking process. The details of the crosslinking process; that is, whether it is carried out in solution or in bulk, may also affect the state of the network. It is therefore more general to write the following:

$$\overline{b^2 r^2} = \overline{b^2} \sum_{i=1}^N \frac{r_i^2}{N} = \frac{3}{2} \frac{\overline{r_0^2}}{\overline{r_f^2}} \quad (6-44)$$

where $\overline{b^2}$ is averaged over all the free chains, that is $\overline{b^2} = 3/2\overline{r_f^2}$. Here $\overline{r_0^2} = \sum r_i^2 / N$ refers to the mean square end-to-end distance of the chain in the network, and $\overline{r_f^2}$ to the mean square end-to-end distance of the isolated chain. Substitution of equation (6-44) into equation (6-42) yields

$$\Delta A = \frac{T}{2} Nk \frac{\overline{r_0^2}}{\overline{r_f^2}} (\lambda_1^2 + \lambda_2^2 + \lambda_3^2 - 3) \quad (6-45)$$

The parameter $\overline{r_0^2}/\overline{r_f^2}$, sometimes referred to as the front factor, can be regarded as the average deviation of the network chains from the dimensions they would assume if they were isolated and free from all constraints. For an ideal elastomer network, the front factor is unity.

The treatment of rubber elasticity presented above represents one possible extreme of behavior. The assumption that the crosslink points in the network are fixed at their mean positions and that the crosslink points deform affinely gives rise to this extreme. In real polymer networks, each crosslink point finds itself in the neighborhood of many other crosslink points. This can be verified by estimating the order of magnitude of the concentration of crosslinks and then calculating the number of crosslink points that would be found within some reasonable distance (perhaps 2 nm) of any given crosslink point. Upon deformation, the affine assumption insists that all of these crosslinks remain in the neighborhood of the particular crosslink point under consideration and, moreover, that their relative positions are fixed.

In the consideration of real networks, it is clear that this assumption is overly restrictive. For example, consider a particular chain that happens to be reasonably extended in the unstrained network state. In the neighborhood of a crosslink point for this chain, we will find many other crosslink points for other chains. At least some of these other chains are expected to be in less extended configurations than the chain under consideration. Upon deformation, the tendency for the already extended chain to further elongate would be expected to be less than the tendency for the more relaxed chains to elongate. This being the case, the positions of crosslink points would be expected to move past one another in a manner not strictly defined by the affine deformation.

The other extreme of behavior involves the "phantom chain" approximation. Here, it is assumed that the individual chains and crosslink points may pass through one another as if they had no material existence; that is, they may act like phantom chains. In this approximation, the mean position of crosslink points in the deformed network is consistent with the affine transformation, but *fluctuations* of the crosslink points are allowed about their mean positions and these fluctuations are not affected by the state of strain in the network. Under these conditions, the distribution function characterizing the position of crosslink points in the deformed network cannot be simply related to the corresponding distribution function in the undeformed network via an affine transformation. In this approximation, the crosslink points are able to readjust, moving through one another, to attain the state of lowest free energy subject to the deformed dimensions of the network.

For an ideal network with tetrafunctional crosslink points, it can be shown for the phantom chain approximation that¹²

$$\Delta A = \frac{T}{4} Nk (\lambda_1^2 + \lambda_2^2 + \lambda_3^2 - 3) \quad (6-46)$$

It is clear that the Helmholtz free-energy change upon deformation predicted by equation (6-46) is just one-half as large as that given in equation (6-45) based on the affine deformation of crosslink points.¹² Real networks probably exhibit behavior that is between these two extremes. Not all crosslink points move affinely; however, steric interactions are strong enough to prevent the phantom approximation from being completely realistic.

From this point forward, we continue with our development of rubber elasticity theory using equation (6-45) as a starting point. We must remember however, that this equation is based on a limiting approximation and that the behavior of real networks may not be quantitatively consistent with this expression.

Suppose our unit cube has volume V_0 and length L_0 . After a uniaxial extension ($\lambda_1 = L/L_0$) is applied, the length in the direction of stretch is L and the volume dilates to V . We have mentioned previously that the strain-induced volume dilation for unfilled elastomers is very small, of the order of magnitude of 10^{-4} . Nevertheless, the deformation process is not a volume-preserving one as required by equation (6-30). The device that is generally employed to circumvent this difficulty is to redefine the reference state. A hypothetical hydrostatic pressure is imagined to have been applied to the sample so that its volume in the unstretched state is also V . The initial length is no longer L_0 , but is

$$L' = L_0 \left(\frac{V}{V_0} \right)^{1/3} \quad (6-47)$$

and the extension ratio in the direction of the uniaxial stretch based on L' becomes

$$\lambda^* = \frac{L}{L'} \quad (6-48a)$$

or

$$\lambda_1^* = \lambda_1 \left(\frac{V_0}{V} \right)^{1/3} \quad (6-48b)$$

The average chain dimensions become $\overline{r^2} = \overline{r_0^2} (V/V_0)^{2/3}$. Because of the redefined reference state

$$\lambda_1^* \lambda_2^* \lambda_3^* = 1 \quad (6-49a)$$

while previously

$$\lambda_1 \lambda_2 \lambda_3 = \frac{V}{V_0} \quad (6-49b)$$

Since the network is isotropic, the contractions along the two lateral axes are equal and

$$\lambda_2 = \lambda_3 = \frac{1}{\sqrt{\lambda_1^*}} \left(\frac{V}{V_0} \right)^{1/3} \quad (6-50)$$

The uniaxial extension of the unit cube is illustrated in Figure 6-3c. Inserting equation (6-50) into equation (6-45), the change in Helmholtz free energy upon deformation becomes

$$\Delta A = \frac{T}{2} Nk \frac{\overline{r_0^2}}{\overline{r_f^2}} \frac{(\lambda^*)^2 + 2}{\lambda^* - 3} \quad (6-51)$$

for simple uniaxial extension. Since

$$\left(\frac{\partial A}{\partial L} \right)_{T,V} = \left(\frac{\partial A}{\partial \lambda^*} \right)_{T,V} \left(\frac{\partial \lambda^*}{\partial L} \right)_{T,V} \quad (6-52a)$$

$$f = \frac{1}{L'} \left(\frac{\partial A}{\partial \lambda^*} \right)_{T,V} \quad (6-52b)$$

Performing the indicated differentiation on equation (6-51), we obtain the equation of state for rubber elasticity:

$$f = \frac{NkT}{L'} \frac{\overline{r_0^2}}{\overline{r_f^2}} \left[\lambda^* - \frac{1}{(\lambda^*)^2} \right] \left(\frac{V}{V_0} \right)^{2/3} \quad (6-53)$$

In equation (6-53) f is the *total* elastic restoring force exerted by the sample. For many purposes it is more convenient to deal with expressions relating the stress to the deformation rather than the total force as in equation (6-53). For this purpose we define a stress $\sigma_{E0} = f/A_0$, where A_0 is the cross-sectional area of the undeformed sample. We further define $N_0 = N/V_0$ as the number of network chains per unit volume of the undeformed sample, where $V_0 = L_0 A_0$.

We shall also use the term N_0 to represent the number of *moles* of network chains per unit volume (mol/m^3) when used with R , the gas constant ($8.315 \text{ Pa m}^3/\text{mol K}$), instead of k , the Boltzmann constant ($1.381 \times 10^{-23} \text{ Pa m}^3/\text{K}$). With the aid of equation (6-48), we can rewrite equation (6-53) in terms of the nominal stress σ_{E0} as

$$\sigma_{E0} = N_0 RT \frac{\overline{r_0^2}}{\overline{r_f^2}} \left(\lambda - \frac{V}{V_0 \lambda^2} \right) \quad (6-54)$$

where $R = N_A k$, N_A being Avogadro's number ($6.022 \times 10^{23} \text{ mol}^{-1}$). The ratio V/V_0 is very nearly unity, which means also that $A = A_0/\lambda$; thus, it is often adequate to write equation (6-54) as

$$\sigma_E = N_0 RT \frac{\overline{r_0^2}}{\overline{r_f^2}} \left(\lambda^2 - \frac{1}{\lambda} \right) \quad (6-55)$$

where σ_E is the true stress. The difference between equations (6-54) and (6-55) is numerically trivial, although conceptually important.

The extension ratio may be written as

$$\lambda = 1 + \varepsilon \quad (6-56)$$

where ε is the tensile strain, $\Delta L/L_0$. By the binomial expansion

$$\lambda^2 = (1 + \varepsilon)^2 = 1 + 2\varepsilon + \dots \text{ and } 1/\lambda = 1/(1 + \varepsilon) = 1 - \varepsilon + \dots \quad (6-57)$$

For very small strains, higher-order terms can be neglected and equation (6-55) may be recast as

$$E \equiv \lim_{\varepsilon \rightarrow 0} \frac{\sigma_E}{\varepsilon} = 3N_0 RT \frac{\overline{r_0^2}}{\overline{r_f^2}} \quad (6-58)$$

where E is the equilibrium tensile modulus. If the volume of the material does not change, then the tensile modulus is three times the shear modulus G (Chapter 2, Section A), then

$$G = N_0 RT \frac{\overline{r_0^2}}{\overline{r_f^2}} \quad (6-59)$$

Thus the equation of state can be recast as

$$f = GA_0 \left(\lambda - \frac{1}{\lambda^2} \right) \quad (6-60a)$$

expressed as nominal tensile stress $f/A_0 = \sigma_{E0}$

$$\sigma_{E0} = G \left(\lambda - \frac{1}{\lambda^2} \right) \quad (6-60b)$$

or the true tensile stress $\sigma_E = F/A$

$$\sigma_E = G \left(\lambda^2 - \frac{1}{\lambda} \right) \quad (6-60c)$$

where G is the shear modulus defined by equation (6-59). Note that if we were somehow able to calculate G via equation (6-59) for a real elastomer, the value would not, in general, agree with the experimental value as determined by direct measurements in simple shear. In the absence of experimental problems, the discrepancy would be due to shortcomings in the molecular theory.[†]

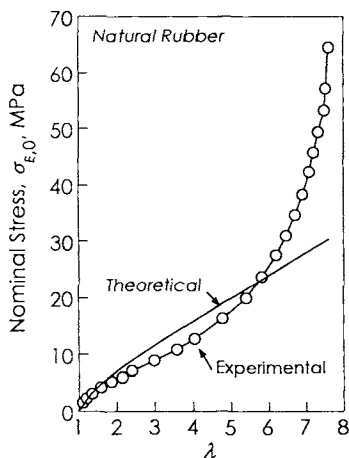


Figure 6-4. Stress-strain curve for natural rubber. The theoretical curve was calculated from equation (6-60) with $G = 4$ MPa. [After L. R. G. Treloar, *Trans. Faraday Soc.*, **40**, 59 (1944), by permission of the Faraday Society.]

The equation of state for rubber elasticity, embodied by any of equations (6-53) through (6-60), is important not only because it is historically the first quantitative treatment of molecular theories for elastomers but also because it laid a conceptual foundation for theories for the physical properties of polymers in general. Some of these have been discussed in detail in previous chapters. Perhaps the single most significant contribution is its recognition of the role of

[†] Somewhat beyond the scope of this book is to demonstrate that the theory, when simplified to this point, predicts that $\sigma = G\gamma$, even at high strains (see problem 22). Note that the solid defined by the high-strain theory in equation (6-60) reduces to the Hookean solid at low strains, and is referred to occasionally as a neo-Hookean solid (see Section C).

entropy in polymers, in contradistinction to the predominant role of energy in "ordinary" solids. The equation predicts that the elastic force is directly proportional to temperature and to the total number of chains in the network. Both of these are experimentally observed. The strain dependence of the elastic force is clearly not Hookean, as it is for a single polymer chain [Appendix 2, equation (j)]. Figure 6-4 compares the theory with the experimental stress-strain curve.¹³ The agreement is good for strains below 50% or $\lambda < 1.5$, but is poor at high extensions. At these high strains the network chains approach their limiting extensions, and the Gaussian assumption is no longer valid. Another complicating factor is the onset of strain-induced crystallization. Even though the Gaussian theory is only valid at relatively low strains, it is extremely valuable in providing a molecular interpretation for rubber elasticity.

2. Energy Contribution

In our statistical treatment of an ideal elastomer, we have assumed that the elastic force is entirely attributable to the conformational entropy of deformation, energy effects being neglected. That the theory reproduces the essential features of the elasticity of real elastomers attests to the basic soundness of this assumption. On the other hand, we know that in real elastomers such energy effects cannot be entirely absent, and deviations from the ideal elastomer model may be expected to occur. Let us now examine in greater detail the extent to which the neglect of energy effects is justified. We can rewrite equation (6-28):

$$f = f_e + f_s \quad (6-61)$$

with

$$f_e = \left(\frac{\partial U}{\partial L} \right)_{T,V} \quad (6-62)$$

$$f_s = -T \left(\frac{\partial S}{\partial L} \right)_{T,V} \quad (6-63)$$

Since we can experimentally determine f and obtain f_s from the thermodynamic identity [Maxwell relationship resulting from equation (6-17)],

$$\left(\frac{\partial S}{\partial L} \right)_{T,V} = - \left(\frac{\partial f}{\partial T} \right)_{V,L} \quad (6-64)$$

We can find f_e by

$$f_e = f - T \left(\frac{\partial f}{\partial T} \right)_{V,L} \quad (6-65)$$

As discussed in the previous section, the condition of constant volume is difficult to achieve experimentally. Similarly, the alternative expression, equation (6-28), also contains terms that are not accurately measurable. We can, however, take advantage of the exact expression of the statistical theory:

$$f = GA_0 \left(\lambda - \frac{V}{V_0 \lambda^2} \right) \quad (6-66)$$

where G is defined by equation (6-59). Assuming that G is constant, we can differentiate equation (6-66) with respect to T , keeping V and L constant. (Note, however, that V_0 and L_0 are not constant.) The result is

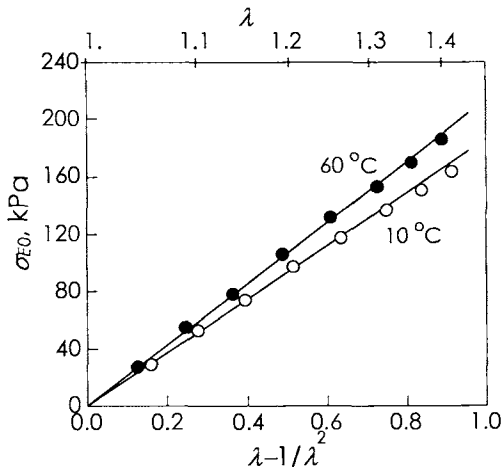


Figure 6-5. Determination of shear moduli for natural rubber at 10°C and 60°C by plotting nominal stress σ_{E0} against $\lambda - 1/\lambda^2$. [After M. Shen and P. J. Blatz *J. Appl. Phys.*, **39**, 4937 (1968), by the permission of the American Institute of Physics.]

$$\left(\frac{\partial f}{\partial T} \right)_{V,L} = \frac{f}{G} \frac{dG}{dT} + \frac{\alpha f}{3} \quad (6-67)$$

Combining equations (6-67) and (6-65), we obtain:

$$f_e = f - f \frac{d \ln G}{d \ln T} - \frac{\alpha T f}{3} \quad (6-68)$$

The advantage of equation (6-68) is that experimental errors in stress-strain data at various temperatures are averaged out in plotting f/A_0 (i.e., σ_{E0}) against

$(\lambda - \lambda^{-2})$, the slope of which is the shear modulus (Figure 6-5). Knowing shear moduli as a function of temperature, values of f_e can be readily calculated.¹⁴

For the sake of comparison, it is more meaningful to use the relative energy contribution f_e/f . Thus equation (6-68) can be rewritten as:

$$\frac{f_e}{f} = 1 - \frac{d \ln G}{d \ln T} - \frac{\alpha T}{3} \quad (6-69)$$

Table 6-1. Thermoelastic Data of Selected Elastomers at 30 °C

Polymer	$(\frac{\alpha}{3}, \text{K}^{-1}) \times 10^4$	$(\frac{d \ln G}{dT}, \text{K}^{-1}) \times 10^3$	f_e/f	Ref.
Poly(ethylene-co-propylene) (EPR)	2.5	2.9	0.04	^b
Poly(tetrafluoroethylene-co-perfluoropropylene) (Viton A)	3.0	2.8	0.05	^b
Poly(butadiene-co-styrene) (SBR)	2.9	3.4	-0.12	^b
Poly(butadiene-co-acrylonitrile) (Hycar)	2.6	2.9	0.03	^b
Poly(cis-1,4-butadiene)	2.1	2.8	0.10	^b
Poly(cis-isoprene) (natural rubber)	2.2	2.5	0.18	^c
Poly(2-hydroxypropyl acrylate)	2.8	3.6	-0.53 ^a	^d
Poly(isobutylacrylate)	2.4	3.4	-0.42 ^a	^d
Poly(isobutylmethacrylate)	2.2	2.3	0.02 ^a	^d

^a Reference temperature: 120°C.

^b E. H. Cirlin, H. M. Gebhard, and M. Shen, *J. Macromol Sci.*, Part A, **5**, 981 (1971).

^c M. Shen, *Macromolecules*, **2**, 358 (1969).

^d M. Shen, E. H. Cirlin, and H. M. Gebhard, *Macromolecules*, **2**, 682 (1969).

Values of f_e/f calculated from equation (6-69) are independent of λ , as long as they are obtained within the region of strain for which the Gaussian theory is valid.

Table 6-1 shows the values of f_e/f for several elastomers. We see that in general we cannot expect the contribution of energy to rubber elasticity to be zero. Rather, a fraction of the stress is attributable to energy, the rest to entropy. However, since this fraction is a constant as a function of strain, the general shape of the stress-strain curve is still unaffected. Thus the neglect of

energy effects in the statistical theory essentially causes the predicted curve to differ from the experimental one by a constant factor. The shear modulus in the statistical theory expression [equation (6-60)] is normally obtained by fitting the experimental stress-strain curve rather than calculating *a priori* from equation (6-59) (neither N_0 nor \bar{r}_0^2/r_f^2 can at present be determined with certainty by independent measurements). For this reason the energy component of the elastic force is often "absorbed" in the equation of state, rather than separated according to equation (6-61).

We recall that one of the assumptions used in the derivation of the statistical theory is the free-energy additivity principle (assumption 3). According to this principle, the number of conformations available to a network of chains is just the product of all the conformations of the individual chains, or the entropy of the network is the sum of the entropies of individual chains in the network. In order for this assumption to be valid, it is required that chains in the network behave as if they were in free space and unaffected by the presence of other chains. This stipulation can only be satisfied if interchain interactions are absent. Thus the energy effects present in rubber elasticity must only come from intrachain interactions, such as the energy barriers hindering rotations along the polymer chain. It is reasonable to expect that real polymer chains are not isoenergetic, that is, energies of the individual chains are not constant as a function of their conformations. It follows that changes in the supply of thermal energy (changes in temperature) would produce changes in the chain dimensions as well. We can derive an expression for the temperature coefficient of the unperturbed dimension of the polymer chain by differentiating equation (6-59) and remembering that $N_0 = N/V_0$ and \bar{r}_0^2 is proportional to $V_0^{2/3}$:

$$\frac{d \ln \bar{r}_f^2}{d \ln T} = 1 - \frac{d \ln G}{d \ln T} - \frac{\alpha T}{3} \quad (6-70)$$

Inserting equation (6-70) into equation (6-69), we see that

$$\frac{f_e}{f} = \frac{d \ln \bar{r}_f^2}{d \ln T} \quad (6-71)$$

The temperature dependence of the end-to-end distance of the isolated chain is related to the energy barriers between the rotational configurations of the chain (see Appendix 1). Thus the energy effects in rubber elasticity can, in principle, be related directly to structural features of the molecular chains.

C. PHENOMENOLOGICAL TREATMENT

The statistical theory of rubber elasticity discussed in the preceding section was arrived at through considerations of the underlying molecular structure. The equation of state was obtained directly from the Helmholtz free energy of deformation (or simply conformational entropy of deformation, since the energy effects were assumed to be absent), which we can recast with the aid of equations (6-45) and (6-59) as

$$A = -TS = \frac{1}{2}G(\lambda_1^2 + \lambda_2^2 + \lambda_3^2 - 3) \quad (6-72)$$

As we have already seen in Figure 6-4, the theory does not give a complete description of the stress-strain behavior of rubberlike materials. This is perhaps to be expected in view of the many rather drastic simplifying assumptions that have been made in its derivation. That the theory predicts many of the essential features of rubber elasticity is a tribute to the depth of its insight. However, it is desirable to be able to describe mathematically the stress-strain relations of elastomers over a larger region of strain. For this purpose we must resort to continuum mechanics for a phenomenological treatment of elasticity at large strains.

The phenomenological theory, as its name implies, concerns itself only with the observed behavior of elastomers. It is not based on considerations of the molecular structure of the polymer. The central problem here is to find an expression for the elastic energy stored in the system, analogous to the free energy expression in the statistical theory [equation (6-72)]. Consider again the deformation of our unit cube in Figure 6-3. In order to arrive at the state of strain, a certain amount of work must be done which is stored in the body as strain energy:

$$\bar{W}(\lambda_i) = \int_1^{\lambda_1} \sigma_{1,0} d\lambda'_1 + \int_1^{\lambda_2} \sigma_{2,0} d\lambda'_2 + \int_1^{\lambda_3} \sigma_{3,0} d\lambda'_3 \quad (6-73)$$

where \bar{W} is the strain energy density (J/m^3 or Pa), the $\sigma_{i,0}$ are the principal “engineering” stresses (f_i/A_0) and the λ_i 's are again the principal extension ratios. This energy is a unique function of the state of strain but, unlike the values of the stresses, is independent of the type or orientation of the coordinate system. If the value of \bar{W} is known as a function of strain, the elastic properties of the material can then be completely defined by differentiation of equation (6-73) (see Problem 6-11). Note that \bar{W} has been created without any regard for the nature of the material or the molecular mechanism of elasticity; it is purely a mechanical construct. As such, it must satisfy certain logical constraints, in the case of isotropic solids. For example, to avoid dependence

on the type or orientation of the coordinate system, it logically must be expressible of in terms of the so-called strain invariants:^{15,16}

$$\overline{W} = \overline{W}(I_i) \quad i=1, 2, 3 \quad (6-74)$$

where

$$I_1 = \lambda_1^2 + \lambda_2^2 + \lambda_3^2$$

$$I_2 = \lambda_1^2 \lambda_2^2 + \lambda_2^2 \lambda_3^2 + \lambda_3^2 \lambda_1^2 \quad (6-75)$$

$$I_3 = \lambda_1^2 \lambda_2^2 \lambda_3^2$$

[Note that there are alternative, but equivalent, definitions of these in the literature, comprising sums or products of the ones shown here; for example, $I_2 = \lambda_1^{-2} + \lambda_2^{-2} + \lambda_3^{-2}$, which is quotient of the I_1 and I_2 in equation (6-75).] The third strain invariant is obviously

$$I_3 = \left(\frac{V_0}{V} \right)^2 \quad (6-76)$$

which is equal to unity for an incompressible material. In the undeformed state, $I_1 = 3$, $I_2 = 3$ and $I_3 = 1$.

As with all functions, a general form of the strain energy function for an isotropic material can be formed by a Taylor expansion. The result is:

$$\overline{W} = \sum_{i,j,k=0}^{\infty} C_{ijk} (I_1 - 3)^i (I_2 - 3)^j (I_3 - 1)^k \quad (6-77)$$

Note that the quantities in the parentheses are chosen such that the strain energy vanishes at zero strain. As we cannot determine *a priori* the set of terms in equation (6-77), let us examine the lowest members of the series. For $i = 1, j = 0, k = 0$:

$$\overline{W} = C_{100} (I_1 - 3) \quad (6-78)$$

which is functionally identical to the Gaussian free energy of deformation [equation (6-72)]. We recall from the thermodynamic treatment that the stress-strain relation can then be obtained from \overline{W} ($\sim \Delta A$) by differentiation. Again for the special case of uniaxial extension, using equation (6-50) and setting $C_{100} = C_1$, and observing the incompressibility condition, it follows that

$$\sigma_E = \lambda^* \frac{\partial \bar{W}}{\partial \lambda^*} = 2C_1 \left(\lambda^{*2} - \frac{1}{\lambda^*} \right) \quad (6-79)$$

where σ_E is the tensile stress and λ^* is the extension ratio under constant volume conditions. Equation (6-79) is a form of the general expression for a so-called neo-Hookean solid, and represents a highly significant extension of the basic Hookean model to higher strains. If $C_1 = G/2$, equation (6-79) is just the statistical expression [equation (6-60)].

In principle, even better descriptions of behavior at high strains can be found by retaining more terms in the Taylor expansion. Suppose, for example, we retain an additional term with $i = 0, j = 1, k = 0$; then

$$\bar{W} = C_{100}(I_1 - 3) + C_{010}(I_2 - 3) \quad (6-80)$$

For uniaxial extension, we obtain

$$\sigma_E = 2C_1 \left(\lambda^{*2} - \frac{1}{\lambda^*} \right) + 2C_2 \left(\lambda^* - \frac{1}{\lambda^{*2}} \right) \quad (6-81)$$

where again for simplicity we have set $C_1 = C_{100}$ and $C_2 = C_{010}$. Equation (6-81) is known as the Mooney–Rivlin equation, which can alternatively be expressed as

$$\sigma_E = 2 \left(C_1 + \frac{C_2}{\lambda} \right) \left(\lambda^2 - \frac{1}{\lambda} \right) \quad (6-82)$$

since $\lambda = \lambda^*$ in the incompressible case.

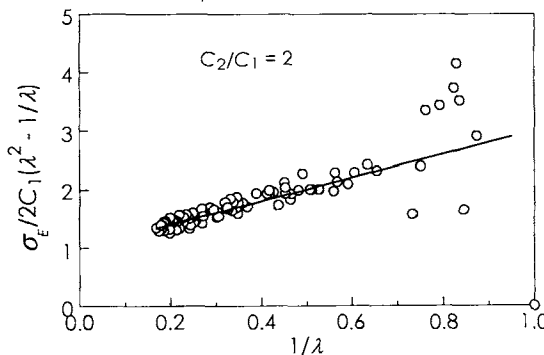


Figure 6-6. Simulated Mooney–Rivlin plot, equation (6-82), for $C_2/C_1=2$. Solid line is the undistorted response of the material; "data" are the results with a 1% (standard deviation) random error incorporated into both the force and length "measurements."

The conventional test of equation (6-82) is to plot experimental stress-strain data as $\sigma_E / (\lambda^2 - 1/\lambda)$ or $\sigma_{E_0} / (\lambda - 1/\lambda^2)$ against $1/\lambda$. The plot, often referred to as Mooney-Rivlin plot, should yield a straight line with an intercept at $1/\lambda = 0$ of $2C_1$, and a slope of $2C_2$. Figure 6-6 shows a schematic Mooney-Rivlin plot for $C_2/C_1 = 2$. At low strains both $(\lambda^2 - 1/\lambda)$ and $1/\lambda$ are extremely sensitive to experimental errors in extension ratio measurements. Thus if the measured λ varies around the true λ by only 1%, significant deviations can be expected in this region of strain, as shown by the points in the figure. To a large extent, this problem can be avoided by a direct nonlinear treatment of equation (6-82), that is, fitting force and length data directly to equation (6-82) to derive C_1 and C_2 , and possibly the initial sample length as well (recall that $\lambda = L/L_0$).¹⁷

Example 1. As can be seen from Figure 6-6, the Mooney elastic material is "softer" than an ideal elastomer with the same modulus G , and thus can describe the observed negative deviations from ideal behavior such as shown in Figure 6-4. If C_1 and C_2 are equal, what is the ratio (Mooney/Ideal) of the tensile stresses at an elongation of 100%?

The expressions required are equation (6-60) for the ideal elastomer and equation (6-82) for the Mooney solid. As we are seeking a ratio, either nominal or actual stresses can be calculated. An elongation of 100% means that the sample length is increased by 100% of the original length; thus, the value of λ is simply:

$$\lambda = L/L_0 = (L_0 + L_0)/L_0 = 2$$

As the moduli of the two materials are the same and $C_1 = C_2$

$$2(C_1 + C_2) = G \text{ and } C_1 = C_2 = G/4$$

The ratio of the two stresses is then

$$\frac{2(C_1 + C_2/2)}{G} = \frac{2(G/4 + G/8)}{G} = 3/4$$

D. FACTORS AFFECTING RUBBER ELASTICITY

1. Effect of Degree of Crosslinking

According to the statistical theory of rubber elasticity, the elastic stress of an elastomer under uniaxial extension is directly proportional to the concentration

of network chains N_0 . For an elastomer sample whose density is ρ (g/cm³), if the molecular weight of each chain in the network is on the average M_c (g/mol), then $N_0 = \rho/M_c$ (mol/cm³). Thus the shear modulus of the elastomer [equation (6-59)] can be written as

$$G = \frac{\rho R T}{M_c} \frac{\overline{r_0^2}}{\overline{r_f^2}} \quad (6-83)$$

Equation (6-83) assumes that the network is a perfect one in that all chains in the network are effective in giving rise to the elastic stress. Ideally each crosslink connects four network chains, while each such chain is terminated by two crosslinks. However, as illustrated in Figure 6-2, a number of network imperfections are possible. Each linear polymer chain with molecular weight M , even if all crosslinks are "normal," must give rise to two terminal chains that are incapable of supporting stress. Thus the number of effective chains must not include the imperfections due to chain ends. On incorporating this correction, the shear modulus can be written as:¹⁸

$$G = RT \frac{\overline{r_0^2}}{\overline{r_f^2}} \left(\frac{\rho}{M_c} - \frac{2\rho}{M} \right) = \frac{\rho R T}{M_c} \frac{\overline{r_0^2}}{\overline{r_f^2}} \left(1 - \frac{2M_c}{M} \right) \quad (6-84)$$

Note, however, that if the initial molecular weight of the linear polymer is infinite, equation (6-84) reduces to equation (6-83). Figure 6-7 shows a plot of G against $1/M$ for a series of natural rubber samples; the trend predicted by equation (6-84) is clearly supported by the data.¹⁹

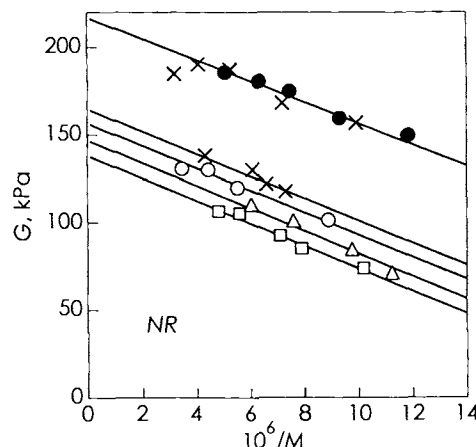


Figure 6-7. Variation of shear moduli of natural rubber with reciprocal initial molecular weight for various degrees of crosslinking. [After L. Mullins, *J. Appl. Polym. Sci.*, **2**, 257 (1959), by the permission of John Wiley & Sons, Inc.]

Another type of deviation from the "normal" crosslink structure of the elastomer is the effect of chain entanglements (Figure 6-2). Such entanglements would impose additional conformational restrictions on the network chains and thus would have the effect of a "quasi-crosslink" in increasing the elastic stress. Because the chains in actual elastomers are rather closely packed together, one might expect several such entanglements to occur between the crosslinks. Thus their contribution to stress may be quite significant, especially for chains that are sufficiently long to permit a number of such entanglements. In the absence of an effective way to calculate this quantity, we simply add its contribution to the shear modulus as:

$$G = \left(\frac{\rho RT}{M_c} + a \right) \frac{r_0^2}{r_f^2} \left(1 - \frac{2M_c}{M} \right) \quad (6-85)$$

where a represents the entanglement contribution.

In addition to terminal chains and entanglements, there are other types of network imperfections. Figure 6-2 shows that if a short chain were crosslinked only once, the crosslink is a wasted one because the chain cannot support elastic stress. Also, if a crosslink forms an intrachain loop, it is again an ineffective crosslink. Unfortunately, owing to its very complexity, it is at present impossible to completely characterize the network structure of an elastomer.

2. Effect of Swelling

Linear polymers are capable of dissolving in appropriate solvents to form homogeneous polymer solutions. However, if crosslinks are introduced to tie the chains into an infinite network, the polymer can no longer dissolve. Instead the solvent is absorbed into the polymer network, giving rise to the phenomenon of swelling. A swollen elastomer is in fact a solution, except that its mechanical response is now elastic rather than viscous. As solvents fill the network, chains are extended. The resulting refractive force operates in opposition to the swelling force. There is a maximum degree of swelling, at which point these two forces are at equilibrium.

If the elastomer is swollen to below the equilibrium swelling so that no deswelling will occur upon deformation, the statistical expression for the shear modulus [equation (6-59)] can be readily modified. We define V_r as the ratio of the unswollen volume to the swollen one, which is identical to the volume fraction of polymer in the mixture. The number of network chains per unit volume then becomes $N_0 V_r$, and the mean square end-to-end distance of the network chain is now $r_0^2 / V_r^{2/3}$. Equation (6-59) then reads

$$G_s = N_0 RT V_r^{1/3} \frac{\overline{r_0^2}}{\overline{r_f^2}} \quad (6-86)$$

for swollen elastomers. The equation of state is now

$$\sigma_{E,s} = N_0 RT V_r^{1/3} \left[\frac{\overline{r_0^2}}{\overline{r_f^2}} \right] \left(\lambda_s^2 - \frac{1}{\lambda_s} \right) \quad (6-87)$$

where subscripts *s* refer to the swollen sample and the stress is based on the swollen, stretched cross-sectional area. The stretch ratio λ_s is defined with respect to the *unstrained, swollen* state. If stress is expressed in terms of per-unit cross-sectional area of *unstrained, unswollen* sample, then

$$\sigma_{E0,d} = N_0 RT V_r^{-1/3} \frac{\overline{r_0^2}}{\overline{r_f^2}} \left(\lambda_s - \frac{1}{\lambda_s^2} \right) \quad (6-88)$$

since $A_{0d} = A_{0s} V_r^{2/3}$, where subscript *d* refer to the dry (unswollen) sample. The λ_s is still as before.

We can also derive an expression on the basis of the Mooney-Rivlin strain energy function for swollen elastomers. A dry elastomer sample will undergo two types of deformation: one due to swelling and the other due to extension. The strain energy function per unit volume of swollen elastomer is related to that of the dry sample by

$$\overline{W}_s = V_r \overline{W}_d = V_r [C_1(I_1 - 3) + C_2(I_2 - 3)] \quad (6-89)$$

where subscripts *s* and *d* refer to swollen and dry samples respectively. In equation (6-89) the strain invariants I_1 and I_2 are defined by $\lambda_{i,d}$'s, that is, strains suffered by the dry elastomer (both swelling and extension). The deformation due to isotropic swelling is just $V_r^{-1/3}$ for all three principal axes; thus, the $\lambda_{i,d}$'s are related to the $\lambda_{i,s}$'s (deformation of swollen elastomer by extension) by

$$\lambda_{1d} = \lambda_{1s} V_r^{-1/3} \quad \lambda_{2d} = \lambda_{2s} V_r^{-1/3} \quad \lambda_{3d} = \lambda_{3s} V_r^{-1/3} \quad (6-90)$$

For the case of simple uniaxial extension, assuming incompressibility for the sake of convenience, we obtain with the aid of equations (6-49), (6-50) and (6-80)

$$\bar{W}_s = C_1 V_r^{1/3} \left(\lambda_s^2 + \frac{2}{\lambda_s} - 3 \right) + C_2 V_r^{5/3} \left(2\lambda_s + \frac{1}{\lambda_s^2} - 3 \right) \quad (6-91)$$

The stress-strain relation can thus be obtained directly by differentiating with respect to λ_s [equation (6-79)]:

$$\sigma_{E,s} = 2C_1 V_r^{1/3} \left(\lambda_s^2 - \frac{1}{\lambda_s} \right) + 2C_2 V_r^{5/3} \left(\lambda_s - \frac{1}{\lambda_s^2} \right) \quad (6-92)$$

In terms of per-unit cross-sectional area of unswollen sample, unstretched sample, the nominal stress σ_{E0} is:²⁰

$$\sigma_{E0,d} = 2V_r^{-1/3} \left(C_1 + \frac{C_2 V_r^{4/3}}{\lambda_s} \right) \left(\lambda_s - \frac{1}{\lambda_s} \right) \quad (6-93)$$

The C_1 term of the Mooney–Rivlin equation is often identified with the shear modulus of the statistical equation; we see that both C_1 's depend on V_r in the same manner [compare equation (6-92) with (6-87) or (6-93) with (6-88)].

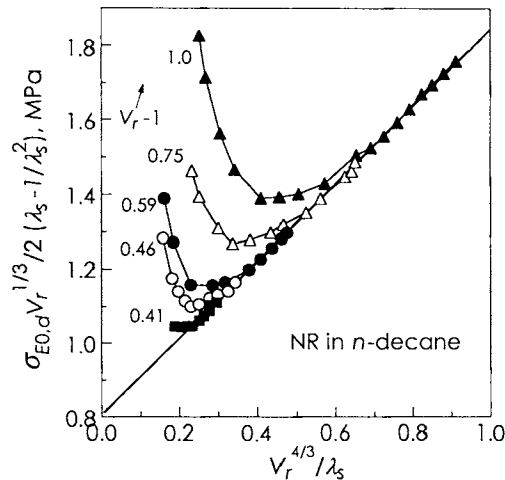


Figure 6-8. Effect of swelling on the Mooney–Rivlin plot of natural rubber where V_r is the volume fraction of elastomer in the swollen sample, (swelling liquid, *n*-decane). [After Mullins, *J. Appl. Polym. Sci.*, **2**, 257 (1959), by the permission of John Wiley & Sons, Inc.]

For comparison with experimental data, we follow equation (6-93) and plot $\sigma_{E0,d} V_r^{1/3} / 2(\lambda_s - 1/\lambda_s^2)$ as a function of $V_r^{4/3} / \lambda_s$. In Figure 6-8 we see that for natural rubber swollen to various degrees, the data all fall on a straight line with the same slope (C_2) and intercept (C_1) in excellent agreement with theory. The

upturns in the region of large strains are due to strain-induced crystallization and finite extensibility of the polymer chains, which are not taken into account by either statistical or phenomenological theories.²¹

3. Effect of Fillers

The use of fillers in elastomers is of paramount technological significance. Such items as automotive tires depend on the addition of fillers to confer on them enhanced wear resistance, strength, and elastic modulus. A wide variety of fillers are commonly employed, such as carbon black, zinc oxide, carbonates and silicates of calcium and magnesium. Generally there are two types of filler: reinforcing and nonreinforcing. The filler is reinforcing if it is capable of increasing the stiffness of the elastomer without impairing its strength and losing its rubbery character.

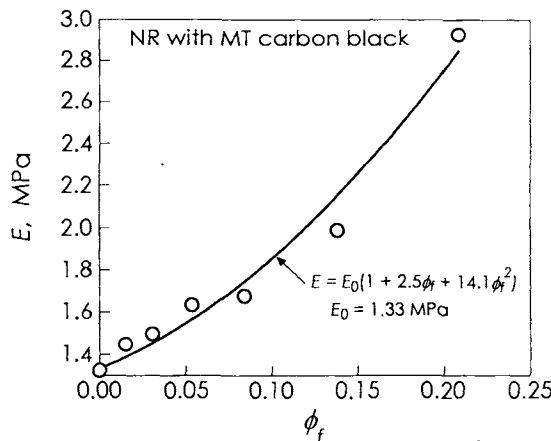


Figure 6-9. Effect of filler concentration on the moduli of natural rubber samples (filler: MT carbon black). The curve was calculated from equation (6-94). [After L. Mullins and N. R. Tobin, *J. Appl. Polym. Sci.*, **9**, 2993 (1965), by permission of John Wiley & Sons, Inc.]

Commonly used expressions for describing the effect of hard fillers on the elastic modulus of elastomers are the Guth-Smallwood equation^{22,23}

$$\frac{E_f}{E_0} = 1 + 2.5\phi_f + 14.1\phi_f^2 \quad (6-94)$$

the Krieger-Douherty equation²⁴

$$\frac{E_f}{E_0} = \left[\frac{1}{1 - \phi_f / \phi_m} \right]^{2.5\phi_m} \quad (6-95)$$

and the Mooney equation²⁵

$$\frac{E_f}{E_0} = \left[\frac{2.5\phi_f}{1 - \phi_f/\phi_m} \right] \quad (6-96)$$

In these equations, ϕ_f is the volume fraction of filler, and subscripts f and 0 refer to the filled and unfilled elastomers respectively. Note that equations (6-95) and (6-96) introduce a parameter ϕ_m that accounts for the maximum packing fraction of the filler. For randomly placed spherical filler particles, $\phi_m = 0.637$.

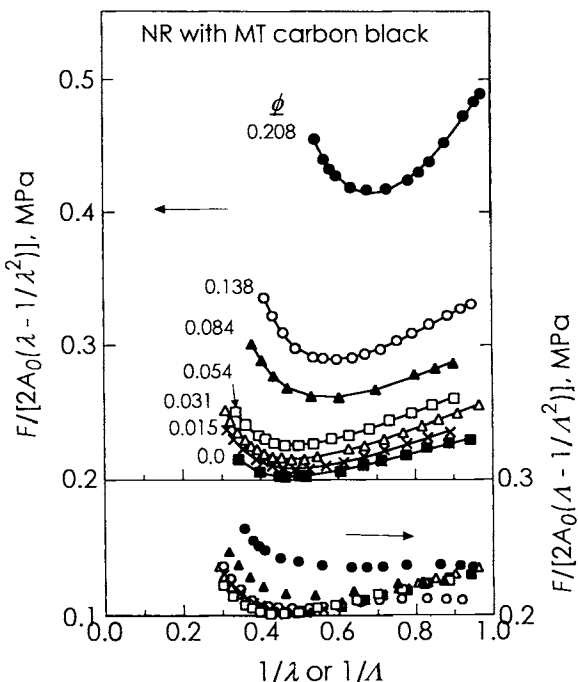


Figure 6-10. Mooney-Rivlin plots of natural rubber filled with MT carbon black: Top set: actual data without using the strain amplification factor. Bottom curves: after reduction using the strain amplification factor, equation (6-95). [After L. Mullins and N. R. Tobin, *J. Appl. Polym. Sci.*, 9, 2993 (1965), by permission of John Wiley & Sons, Inc.]

Equation (6-94) has been found to be valid for a number of filled systems up to a value of ϕ_f of about 0.3, whereas (6-95) and (6-96c) can be used at somewhat higher concentrations. These equations were first used to describe the viscosity of liquids with suspended solid particles. In fact equation (6-94) was derived using basic hydrodynamic principles. Equations of this type have been "borrowed" to be used for the elasticity of filled elastomers, based on the analogy between steady viscous flow and elastic deformation as described in equations (3-4) and (2-14), respectively. Certainly an additional justification

for adoption is to be found in the good agreement with experimental data,²⁶ as illustrated, for example, in Figure 6-9.

The right side of equation (6-94) is sometimes referred to as the strain amplification factor. Suppose we have a sample of elastomer in which is dispersed fillers of concentration ϕ_f . The fillers are rigid solid particles with very high modulus. When the filled elastomer is deformed, since the fillers are so much more rigid than the elastomer, they essentially remain undeformed. Thus all the strain must be suffered by the rubbery phase of the sample. The actual strain sustained by the elastomer is greater than the applied strain by the factor given by the right side of equation (6-94). Thus we can write the extension ratio appropriate to the elastomer matrix as²⁶

$$\Lambda = 1 + \varepsilon(1 + 2.5\phi_f + 14.1\phi_f^2) \quad (6-97)$$

where ε is the applied strain on the filled sample.

Figure 6-10 shows the Mooney–Rivlin plot of a series of natural rubbers filled with carbon black using the applied strain on the filled sample. As expected, the stress increases as a function of increasing filler concentration. The rise at high strains (low $1/\lambda$) can again be attributed to crystallization or finite extensibility of the chains in the filled sample. Now if we plot the same data on the basis of the strain sustained by the elastomer matrix (Λ), using the strain amplification factor according to equation (6-97), the curves in Figure 6-10 are seen to be brought much closer together. Note especially that the minima in the curves fall roughly at the same value of $1/\Lambda$. From the slopes and intercepts of these curves, C_1 , and C_2 can be readily obtained. The values of these Mooney–Rivlin parameters for the filled samples are quite close to those of the unfilled sample. The agreement is excellent for elastomers filled up to 5%; it is poorer for higher filled contents. These results strongly suggest that the role of fillers is to amplify the applied strain according to equation (6-97). The elastic properties of the elastomer itself are unaffected by the presence of these fillers.

Another important effect of fillers is stress softening, or the Mullins effect. If a filled sample is stretched for the first time to 100%, the stress–strain curve²⁷ will follow that illustrated in Figure 6-11. Now the strain is removed, and the sample is restretched to 200%. The stress in the second cycle is lower than that in the first up to 100%, after which it continues in a manner following the first cycle. If we repeat the stress–strain in a third cycle, we again see a softening up to 200% due to the previous strain history. This stress-softening effect was first discovered by Mullins, after whom it is named.

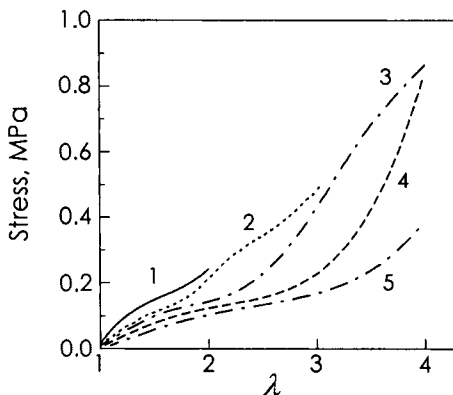


Figure 6-11. Stress softening of natural rubber filled with MPC carbon black (Mullins effect). Numerals indicate the stress-strain cycles. [After F. Bueche, *J. Appl. Polym. Sci.*, **4**, 107 (1960) by permission of John Wiley & Sons.]

A molecular interpretation was first given by F. Bueche²⁸ for the Mullins effect. Figure 6-12 shows that for a reinforced elastomer, the polymer chains are attached to the filler particles. Some of the chains may be relaxed, but others are already relatively extended. Upon stretching, the "prestrained" chains will reach maximum extension first and either will become detached from the fillers or will be broken. In the second cycle, these broken chains no longer support the stress, thus giving rise to the observed softening in stress. If the stress-strain cycle is repeated for the third time, the same process will be repeated. The softened elastomer can be "healed" by annealing at higher temperatures.

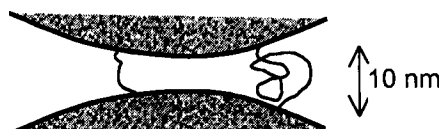


Figure 6-12. Schematic diagram of polymer chains attached to filler particles. [After F. Bueche, *Physical Properties of Polymers*, Interscience, New York 1962, p. 49.]

4. Effect of Strain-Induced Crystallization

When a sample of elastomer is stretched, it becomes anisotropic in that the network chains tend to orient themselves more in the direction of stretch than in the lateral directions. The more ordered chains favor the formation of crystallites. These crystallites will tie together a number of neighboring network chains, thereby exerting an additional crosslinking effect. This increase in the degree of crosslinking will in turn cause a rise in the elastic stress. The reason that these crystallites in fact act as crosslinks is attributable

to their high modulus, which is estimated to be of the order of 10^{11} Pa. This value is some five orders of magnitude greater than that of most elastomers, which is in the range of 10^6 Pa. If crystallization is allowed to proceed further, more and more of the amorphous material is replaced. At high degrees of crystallinity it is not adequate to regard crystallites just as crosslinks. They will also now act as fillers in further increasing the elastic stress.

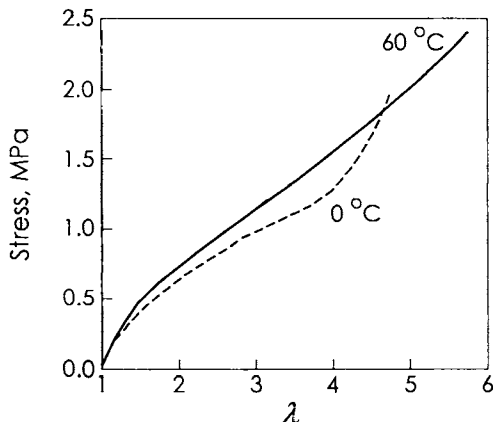


Figure 6-13. Stress-strain curves of natural rubber at 0 °C and 60 °C. The rise in stress at 0 °C at $\lambda > 3$ is attributed to strain-induced crystallization. [After K. J. Smith, A. Greene, and A. Ciferri, *Kolloid-Z.*, **194**, 49 (1964), by permission of Dr. Dietrich Steinkopff Verlag.]

That crystallization increases the elastic stress has already been demonstrated in Figure 6-8, in which the Mooney-Rivlin plot shows a rise at high extension ratios. However, it should be remembered that part of this increase is due to finite extensibility of network chains. In Figure 6-13 we show the stress-strain curves of natural rubber at two temperatures.²⁹ At 0 °C there is considerable strain-induced crystallization, and we observe a dramatic rise in the elastic stress above $\lambda = 3.0$. Wide-angle X-ray measurements show the appearance of crystallinity above this strain. At 60 °C there is little or no crystallization, and the stress-strain curve shows a much smaller upturn at high strains. The latter is presumably due only to the finite extensibility of the polymer chains in the network.

APPENDIX 1: STATISTICS OF A POLYMER CHAIN

The special structure of polymer molecules that distinguishes them from other species is their long, flexible chain structure. To describe this situation, let us first consider an isolated polymer chain and then extend the results to ensembles of chains, that is, to the bulk polymer. An isolated linear polymer chain is capable of assuming many different conformations. Because of

thermal agitation, such a chain is also constantly changing from one conformation to another; namely, it is undergoing Brownian motion. Because of the presence in real chains of short- and long-range interactions between segments, bond-angle restrictions, potential energy barriers, and other characteristics, an exact statistical calculation becomes a very complex mathematical problem. However, because these chains have such a large number of conformations, idealized models can be used to derive the average properties. In most cases, these quantities provide a good asymptotic approximation to the true values for any sufficiently long linear polymer chain.

We shall first derive the average properties of an ideal polymer chain that is infinitely long, possesses negligibly small volume, and has freely jointed links. Next we shall examine the influence of fixed bond angles between adjacent links. The concept of the statistically equivalent random chain will then be introduced to rationalize the validity of using these model chains to represent the behavior of real polymer chains. Finally, the equation of state for a single polymer chain will be discussed. This equation is the starting point for equations (6-32) and (6-33).

Suppose our ideal polymer chain has n links, each of length l ; then the fully extended length of the chain would be:

$$R = nl \quad (a)$$

However, the fully extended conformation is only one of a great many; it would be more meaningful to consider an average size of the macromolecule such as the mean square end-to-end distance, \bar{r}^2 . As the name implies, the end-to-end distance is just the length of the vector connecting the two ends of the ideal chain. This average can be that for a given molecule at a number of times or that of an ensemble of identical molecules at the same time.[§] Thus, for p chains that do not interact with one another,

$$\bar{r}^2 = \frac{1}{p} \sum_{i=1}^p \mathbf{r}_i^2 \quad (b)$$

where \mathbf{r}_i refers to the end-to-end distance of the i th chain. Considering now a single chain of n links, let \mathbf{l}_j designate the vectorial length of link j ; then

$$\mathbf{r}_i = \sum_{j=1}^n \mathbf{l}_j = \mathbf{l}_1 + \mathbf{l}_2 + \mathbf{l}_3 + \dots + \mathbf{l}_n \quad (c)$$

[§] For a justification of this assertion, the reader is referred to standard statistics texts such as R. C. Tolman, *Principles of Statistical Mechanics*, Oxford, 1938.

The square of the end-to-end distance of a particular chain is obtained from equation (c).

$$\begin{aligned} \overline{r_i^2} &= \mathbf{r}_i \cdot \mathbf{r}_i \\ &= \sum_{j=1}^n \mathbf{l}_j \cdot \mathbf{l}_j + 2 \sum_{k < j} \mathbf{l}_k \cdot \mathbf{l}_j \end{aligned} \quad (d)$$

The dot product of two vectors, however, is just the product of their absolute values times the cosine of the angle, θ , between one vector and the other vector; thus, for identical links

$$\begin{aligned} \mathbf{l}_k \cdot \mathbf{l}_j &= |\mathbf{l}_k| |\mathbf{l}_j| \cos \theta_{kj} \\ &= l^2 \cos \theta_{kj} \end{aligned} \quad (e)$$

The angle between the same vectors \mathbf{l}_j in the first sum of equation (d) is zero, and the cosine of zero is unity. Thus the first sum in equation (d) is simply

$$\sum_{j=1}^n \mathbf{l}_j \cdot \mathbf{l}_j = nl^2 \quad (f)$$

Now in the second sum of equation (d) we deal with the product of two different vectors \mathbf{l}_k and \mathbf{l}_j . As any two links can assume any orientation whatsoever with respect to each other, any angle θ between two vectors \mathbf{l}_k and \mathbf{l}_j is just as probable as any other angle. Thus for every $\cos \theta$ in the second term of equation (d) there is a $\cos(\pi + \theta) = -\cos \theta$ that exactly cancels it. The result is that the second term in equation (e) is 0. This gives us the mean square end-to-end distance of a freely orienting chain³⁰⁻³⁴

$$\begin{aligned} \overline{r^2} &= \frac{1}{p} \sum_{i=1}^p nl^2 \\ &= nl^2 \end{aligned} \quad (g)$$

via equation (b).

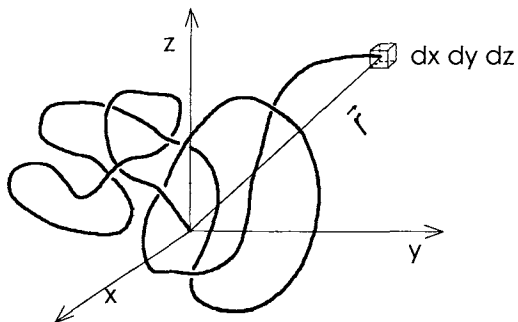


Figure 6-14. Conformation of a polymer chain with one end fixed at the origin of a Cartesian coordinate system.

In addition, it is possible to calculate the property \bar{x}^2 , which is the average of the square of the projection of \mathbf{r}_i on to any fixed axis, in this case the x axis. This average distance is clearly less than the average end-to-end distance; a geometrical exercise gives:

$$\bar{x}^2 = \frac{nl^2}{3} = \frac{\bar{r}^2}{3} \quad (\text{h})$$

The next important step is to find, for a chain of n links each of length l , the probability of achieving a particular end-to-end length. To be more precise, if one end of this chain is at the origin of a Cartesian coordinate system, what are the chances of finding the other end in a small volume element $dx dy dz$ which is at a distance r from the origin (Figure 6-14)? This problem is known as the random flight problem³⁴⁻³⁵ and will be solved for the one-dimensional case first. We thus constrain \mathbf{r} to lie on the x -axis, then calculate the probability $\omega(x)$ that x has a value between x and $x + dx$. For a chain consisting of a large number of links, we can assume that every link contributes a length $l/\sqrt{3}$ [equation (h)] to the component on the x -axis. Some of them will be in the positive x direction (n_+ of them in number) and some in the negative (n_-). Since the chain is freely jointed, the probability of taking either direction will be equal, namely 1/2. The total length of the x -axis component is then trivially:

$$x = \frac{(n_+ - n_-)l}{\sqrt{3}} \quad (\text{i})$$

The derivation continues by writing the probability ω of a random flight with n_+ positive steps and n_- negative steps³⁶

$$\omega(n_+, n_-) = \frac{(1/2)^2 n!}{n_+! n_-!} \quad (j)$$

where $n = n_+ + n_-$. After expanding the factorials and normalizing the total probability to unity, we get the very important equation:

$$\omega(x)dx = \left(\frac{3}{2\pi nl^2} \right)^{1/2} \exp\left(-\frac{3x^2}{2nl^2} \right) dx \quad (k)$$

Equation (k) is known as the Gaussian distribution function. It can be generalized to the three-dimensional case, as follows:

$$\begin{aligned} \omega(x, y, z) dxdydz &= \omega(x)dx \omega(y)dy \omega(z)dz \\ &= \left(\frac{b}{\pi^{1/2}} \right)^3 \exp(-b^2 r^2) dx dy dz \end{aligned} \quad (l)$$

where

$$b^2 = \frac{3}{2nl^2} = \frac{3}{2r^2} \quad (m)$$

$$r^2 = x^2 + y^2 + z^2 \quad (n)$$

Equation (l) gives the probability that if one end of a freely orienting chain is fixed at the origin, the other end will be found in a volume element $dx dy dz$ located at \mathbf{r} away from the origin. The probability of finding the free chain end in a spherical shell of radius r centered at the origin, referred to as the radial distribution function $\omega(r)dr$, is simply obtained by multiplying $\omega(x, y, z)$ by the volume of a spherical shell of thickness dr located at a distance r from the origin, that is, $4\pi r^2 dr$. The result is:

$$\omega(r)dr = \left(\frac{b}{\pi^{1/2}} \right)^3 \exp(-b^2 r^2) 4\pi r^2 dr \quad (o)$$

Equation (o) is illustrated in Figure 6-15. (Note that $\omega(r)$ has dimensions of reciprocal length.) The maximum in the curve corresponds to the most probable end-to-end distance, and it can be found easily by differentiating equation (o). The result, or the most probable value of r , is $1/b$ or $(2nl^2/3)^{1/2}$. The mean square end-to-end distance is given by the second moment of the radial distribution function:

$$\overline{r^2} = \frac{\int_0^\infty r^2 \omega(r) dr}{\int_0^\infty \omega(r) dr} \quad (p)$$

However, the denominator of the right side of equation (p) is unity, since the radial distribution function is normalized. Integration yields:

$$\overline{r^2} = \frac{3}{2} b^{-2} = nl^2 \quad (q)$$

which is just the expression derived previously using geometrical arguments [equation (g)].

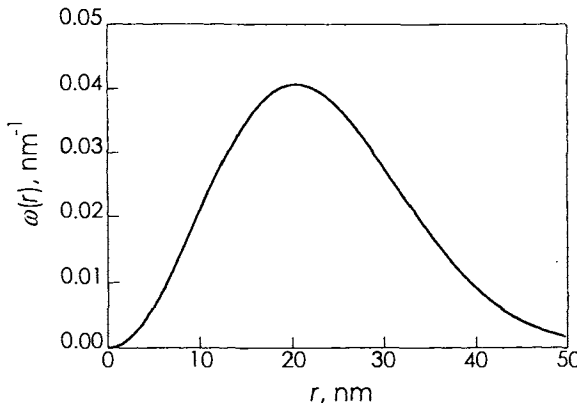


Figure 6-15. Radial distribution function of a chain of 10^4 freely orienting segments each of length 0.25 nm.

If instead of allowing the links in the chain to rotate freely, we fix the angle between successive links at an angle θ , the chain becomes considerably longer. An approximate expression for this effect is:

$$\overline{r^2} \approx nl^2 \frac{1 + \cos\theta}{1 - \cos\theta} \quad (r)$$

For example, for a polymethylene chain having nearly tetrahedral bond angles, the angle between a given segment and its projection on the next segment is about 70° . Thus, $\cos\theta = 0.34$, and

$$\overline{r^2} \approx 2.03nl^2 \quad (s)$$

which is *twice* the value of a freely orienting chain. However, on considering the structure of more complicated polymers with stiff rings in the chain, there is really little guidance on what can be designated as a link. It certainly would be

very incorrect to use a structural repeat unit, for example. To avoid these ambiguities, the concept of a statistically equivalent random chain has been devised.³⁷ For any sufficiently long real chain, we can find a random chain with the same mean square end-to-end distance, that is:

$$\overline{r^2} = \overline{r_e^2} = n_e l_e^2 \quad (\text{t})$$

where the subscript e refers to the equivalent random chain. However, if both the number and the lengths of segments of the equivalent random chain can be chosen at will, there would be an infinite selection. Thus, we must impose another condition: the fully extended length of the equivalent random chain must be equal to that of the real chain without the distortion of bond angles and lengths. If this is the case, then

$$R = R_e = n_e l_e \quad (\text{u})$$

Thus there is only one model chain that is statistically equivalent to the real chain with

$$n_e = \frac{R^2}{\overline{r^2}}; \quad l_e = \frac{\overline{r^2}}{R} \quad (\text{v})$$

By implication, the real chain then obeys the same Gaussian distribution function as model chain.

As an example, we consider a polymethylene chain (Figure 6-16). Its fully extended length and mean square end-to-end distance are, respectively, (considering only bond angle restrictions)

$$R = nl \cos \frac{\theta}{2} = nl \cos 35^\circ = 0.82nl \quad (\text{w})$$

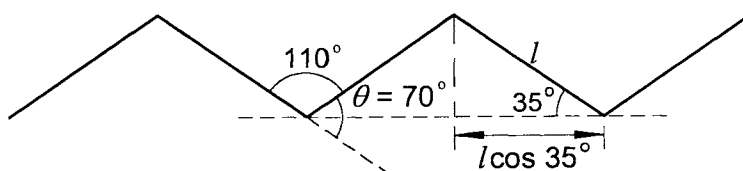


Figure 6-16. Polymethylene backbone in the fully extended conformation.

Remembering that

$$\overline{r^2} \approx 2.03nl^2 \quad (\text{s})$$

we get via equations (v) we get

$$n_e = 0.331 n \quad \text{and} \quad l_e = 2.48 l \quad (\text{x})$$

Thus each statistically equivalent random segment is equal to about three carbon-carbon bonds in the real polymethylene chain.

The effect of tetrahedral bond angles on the radial distribution function enters through the parameter b , the value of which decreased from $3/2nl^2$ in the freely orienting chain to $3/4nl^2$ in the chain with tetrahedral bond angles.

APPENDIX 2: EQUATION OF STATE FOR A POLYMER CHAIN

Appendix 1 describes the statistical properties of a single chain that has no external constraints imposed on it. If one end of this polymer chain is fixed at the origin of a coordinate system, then due to Brownian motion the position of the other end of the chain will fluctuate according to the Gaussian distribution function [equation (o), Appendix 1]. In general, there are a large number of conformations that the chain can assume consistent with its ends being separated by a distance r . The number of conformations for each r is proportional to the radial distribution function. If we constrain the chain ends to remain a fixed distance r apart, conformations consistent with all other end-to-end distances become unavailable. As a consequence, the "degree of randomness" is now lessened – in other words, the entropy is decreased. A tension must therefore be set up owing to this perturbation.

The development for a single chain follows the same line of attack as for the ensemble, starting with the first law of thermodynamics

$$dU = TdS - dW \quad (6-1)$$

where U is the internal energy, T is temperature, S is entropy, and W is work done by the system on the surroundings. By definition, the Helmholtz free energy is

$$dA = dU - TdS \quad (\text{a})$$

at constant temperature. Equations (a) and (b) thus tell us that

$$dA = dW \quad (\text{b})$$

for an isothermal process where the stress-strain work is just

$$dW = -fdr \quad (\text{c})$$

where the force and the end-to-end vector \mathbf{r} are always aligned. The tensile force on a polymer chain at constant temperature and length is just

$$\begin{aligned} f &= -\left(\frac{\partial W}{\partial r}\right)_T = +\left(\frac{\partial A}{\partial r}\right)_T \\ &= \left(\frac{\partial U}{\partial r}\right)_T - T\left(\frac{\partial S}{\partial r}\right)_T \end{aligned} \quad (\text{d})$$

In the case of our model chain, which has no energy barrier hindering the rotation of the segments, the internal energy of the chain is the same for all conformations. Thus the first term on the right side of equation (d) is zero, and

$$f = -T\left(\frac{\partial S}{\partial r}\right)_r \quad (\text{e})$$

To calculate the entropy for our Gaussian chain, we use the Boltzmann's relation from statistical mechanics

$$S = k \ln \Omega \quad (\text{f})$$

where k is Boltzmann's constant and Ω is the total number of conformations available to the system. In our case, we want Ω to be a function of \mathbf{r} the vector separation of the chain ends. Let there be some large fixed number of conformations, N_T , available to a chain. Then the number of conformations consistent with a certain \mathbf{r} is just

$$\Omega(r) = N_T \omega(r) \quad (\text{g})$$

where $\omega(r)$ is just $\omega(r)$ of equation (o) in Appendix 1. Thus

$$\Omega(r) = N \left(\frac{b}{\pi^{1/2}} \right)^3 e^{-b^2 r^2} \quad (\text{h})$$

Inserting equation (h) into equation (f) and differentiating according to equation (e), we obtain the equation of state for a single polymer chain:^{36,38,39}

$$\mathbf{f} = 2kTb^2 \mathbf{r} \quad (\text{i})$$

In equation (i), \mathbf{f} is a vector aligned with the vector \mathbf{r} . Thus if the ends of a chain are held a fixed distance $r = |\mathbf{r}|$ apart by a tensile force, then this force is directly proportional to r , and to absolute temperature. It is also inversely proportional to the mean square length of the chain, since $b^2 = 3/2r^2$ [equation

(m)]. In fact, equation (i) is just Hooke's law for a spring with spring constant $2kTb^2$. The elasticity of this spring originates in the decrease in conformational entropy with chain end separation and thus it is often referred to as an "entropy spring." This entropy spring concept is basic to the formulation of the molecular theory of polymer viscoelasticity. If, instead of a single chain, we have a network of chains, an analogous derivation will give us the equation of state for rubber elasticity, as has been shown in this chapter.

PROBLEMS

1. Starting with the equation of state of rubber elasticity [equation (6-60)], show that for an ideal elastomer

$$(a) \quad \left(\frac{\partial H}{\partial L} \right)_{T,P} = \frac{\alpha T}{3} \left(\frac{\lambda^3 + 2}{\lambda^3 - 1} \right)$$

$$(b) \quad \left(\frac{\partial U}{\partial L} \right)_{T,V} = 0$$

$$(c) \quad \left(\frac{\partial V}{\partial L} \right)_{T,P} = \frac{\beta}{3} \left(\frac{\lambda^3 + 2}{\lambda^3 - 1} \right)$$

2. From the above equations and equation (6-11), find an expression for the stress-temperature coefficient of an ideal elastomer at constant pressure and length, that is $(\partial f / \partial T)_{P,L}$.
3. If an elastomer sample in the form of a unit cube is deformed by pure shear, then the three principal extension ratios are $\lambda_1 = \lambda$, $\lambda_2 = 1$, $\lambda_3 = 1/\lambda$. [Compare with the case of simple extension where $\lambda_2 = \lambda_3 = 1/\sqrt{\lambda}$.] Following the arguments of Section B, derive an expression relating σ_E and λ , where σ_E is the true tensile stress.
4. Repeat Problem 3 using the Mooney-Rivlin strain energy function [equation (6-80)].
5. In analogy to the kinetic theory of ideal gases, the statistical theory of rubber elasticity is often called the kinetic theory of rubber elasticity. Reflect upon the similarities and differences between the basic philosophies of these two theories.
6. For a piece of ideal elastomer whose density is 0.95 g/cm³, calculate its shear modulus at room temperature if its initial molecular weight is 100,000 g/mol and the molecular weight of the network chain after crosslinking is 5000 g/mol (assuming absence of other network defects).
7. What is the maximum degree of swelling for an elastomer that would fail at 100% extension in the unswollen state?

8. If the tensile modulus for an unfilled elastomer is 5×10^6 Pa, what value would it have if it were filled to $\phi_f = 0.3$? Suppose after several strain cycles, half of the filler is ineffective due to Mullins effect. What is its tensile modulus now?

9. Starting with equation (6-66), derive equation (6-67).

10. An alternative expression for the energy contribution to the extension force is

$$\frac{f_e}{f} = 1 - \left(\frac{\partial \ln f}{\partial \ln T} \right)_{P,L} - \frac{\alpha T}{\lambda^*{}^3 - 1}$$

where λ^* is the extension ratio under constant-volume conditions [see equations (6-48b) and (6-50)]. Making any necessary assumptions (list), derive this expression.

11. The "Leibniz formula" for differentiation of an integral is

$$\frac{d}{du} \int_{a_1(u)}^{a_2(u)} f(x, u) dx = \int_{a_1(u)}^{a_2(u)} \frac{\partial f(x, u)}{\partial u} dx + f(a_2, u) \frac{da_2(u)}{du} - f(a_1, u) \frac{da_1(u)}{du}$$

Using this formula, show that differentiation of the strain-energy function equation (6-73) does indeed give the stress, as suggested by equation (6-79). Assume uniaxial stretching by application of external force only in the stretching direction, and an incompressible material. (*Hint:* Note that the upper limits λ_i on the integrals in equation (6-73) are not the same as the integrals' dummy variable λ'_i , and can be treated as constants.)

12. (Computer) Examine Figure 6-5 carefully and note that the data at higher strains tend to fall below the line representing the statistical theory for an ideal elastomer. However, the data might be accurately represented by the Mooney-Rivlin equation.

10 °C		60 °C	
$\lambda - 1/\lambda^2$	σ_{E0} , MPa	$\lambda - 1/\lambda^2$	σ_{E0} , MPa
0.160	0.288	0.125	0.271
0.276	0.526	0.245	0.549
0.394	0.737	0.362	0.779
0.515	0.971	0.488	1.058
0.636	1.173	0.609	1.316
0.748	1.367	0.725	1.530
0.836	1.504	0.811	1.699
0.914	1.636	0.889	1.859

210 RUBBER ELASTICITY

The data for this figure are provided above and in the CD in file NR-Mod.TXT. Using a spreadsheet, generate a Mooney-Rivlin plot and calculate C_1 and C_2 . In addition, fit the data to the equivalent multivariate linear form

$$\sigma_{E0} = 2C_1(\lambda - 1/\lambda^2) + 2C_2(1 - 1/\lambda^3)$$

and compare the resulting constants with those from the Mooney-Rivlin plot. Plot the resulting curves using the same scales as the original drawing. In addition, plot the residuals, that is, the experimental values of nominal stress minus the predicted values, for the two Mooney-Rivlin fits, as well as the statistical theory fit based on the first 5 points. (*Hint:* Note that it will be necessary to solve for λ , given the group $\lambda - 1/\lambda^2$.)

13. (Computer) The Mooney-Rivlin plots often show poor linearity at low strains. Considering that a likely systematic error is an inaccurate value of L_0 , the unstretched length of the sample, the observed λ should be corrected by a multiplicative constant close to 1.0 to get the true stretch ratio $a\lambda$. Using the form of the Mooney-Rivlin equation

$$\sigma_{E0} = 2(C_1 + C_2/a\lambda)[a\lambda - (1/a\lambda)^2]$$

and nonlinear regression analysis, vary the parameter a , along with C_1 and C_2 , to give the best fit to the data of problem 12. Calculate and plot the residuals (see problem 12) and compare with those for a fixed at 1.0.

14. Write out in detail equation (b), Appendix 1, with the aid of equations (c) and (d) if $n = 4, p = 1$.

15. The radial distribution function [equation (6-33) and equation (l), Appendix 1] was derived for a chain possessing negligible volume. Suppose we now have a chain whose segments have excluded volume (no two segments can occupy the same space). How would the most probable distance (the maximum in Figure 6-15) be affected?

16. Carry out the integrations indicated in equation (p), Appendix 1. *Hint:*

$$\int_b^\infty x^{2a} e^{-bx^2} dx = \frac{1 \cdot 3 \cdot 5 \cdots (2a-1)}{2^{a+1} b^a} \sqrt{\frac{\pi}{b}}$$

17. It is known that for a poly-*cis*-isoprene chain, each monomer unit is 0.46 nm long and $\overline{r^2} = 0.162n$ nm². What is the statistically equivalent random chain for this macromolecule?

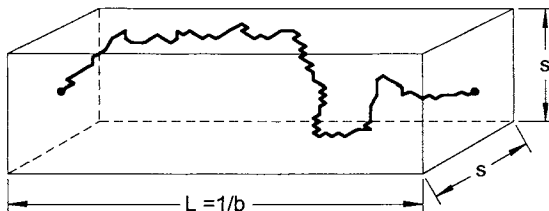
18. Using the following more exact statement of Stirling's approximation,

$$\ln n! = (n + \frac{1}{2}) \ln(n) - n + \frac{1}{2} \ln 2\pi$$

derive equation (k) from equation (j), Appendix 1.

19. Calculate $\overline{r^2}$ for a Gaussian chain considering only chain conformations for which $r > 1/2b$.

20. Calculate \bar{r} , the average end-to-end distance for a Gaussian chain.
21. Suppose that a Gaussian chain is attached to the ends of a rectangular box as shown.



Further, suppose that the length of the box L is equal to the most probable end-to-end separation of the chain ($1/b$) and that the ends of the box are square, having cross-sectional area s^2 .

- (a) Derive an expression relating P , the pressure on the ends of the box, to the temperature.
- (b) What temperature is necessary to generate a pressure of 100 atm if $L = 10$ nm and the area s^2 of the end of the box is 0.1 nm^2 .
22. Starting with the expression for the strain energy, derive the stress-strain expressions for an ideal elastomer when deformed in simple shear ($\lambda_1 = \gamma/2 + [(\gamma/2)^2 + 1]^{1/2}$, $\lambda_2 = 1/\lambda_1$, $\lambda_3 = 1$), where γ is the shear strain).
23. Starting with equation (6-59), derive the important result given in equation (6-70).

REFERENCES

1. M. Shen, D. A. McQuarrie, and J. L. Jackson, *J. Appl. Phys.*, **38**, 791 (1967).
2. G. Gee, J. Stern, and L. R. G. Treloar, *Trans. Faraday Soc.*, **46**, 1101 (1950).
3. F. G. Hewitt and R. L. Anthony, *J. Appl. Phys.*, **29**, 1411 (1958).
4. G. Allen, U. Bianchi, and C. Price, *Trans. Faraday Soc.*, **59**, Part 11, 2493 (1963).
5. E. Guth and H. F. Mark, *Monatsh.*, **65**, 93 (1934).
6. W. Kuhn, *Kolloid-Z.*, **68**, 2 (1934); *Kolloid-Z.*, **76**, 258 (1936).
7. F. T. Wall, *J. Chem. Phys.*, **10**, 132, 485 (1942); *J. Chem. Phys.*, **11**, 527 (1943).
8. H. M. James and E. Guth, *J. Chem. Phys.*, **11**, 455 (1943); *J. Polym. Sci.*, **4**, 153 (1949).
9. P. J. Flory and J. Rehner, Jr., *J. Chem. Phys.*, **11**, 512, 521 (1943); P. J. Flory, *J. Am. Chem. Soc.*, **78**, 5232 (1956); *Trans. Faraday Soc.*, **56**, 722 (1960).
10. M. S. Green and A. V. Tobolsky, *J. Chem. Phys.*, **14**, 80 (1946); A. V. Tobolsky, D. W. Carlson, and N. Indictor, *J. Polym. Sci.*, **54**, 175 (1961).
11. J. J. Hermans, *Trans. Faraday Soc.*, **43**, 591 (1947); *J. Polym. Sci.*, **59**, 191 (1962).
12. P. J. Flory, *Proc. R. Soc. Lond.*, **A351**, 351 (1976).
13. L. R. G. Treloar, *Trans. Faraday Soc.*, **40**, 59 (1944).

212 RUBBER ELASTICITY

14. M. Shen and P. J. Blatz *J. Appl. Phys.*, **39**, 4937 (1968); M. Shen, *Macromolecules*, **2**, 358 (1969).
15. M. Mooney, *J. Appl. Phys.*, **11**, 582 (1940).
16. R. S. Rivlin, *Philos. Trans.*, **A241**, 379 (1948).
17. G. V. Gordon and M. T. Shaw, *Computer Programs for Rheologists*, Hanser, Munich, 1994, Chapters 2 and 3.
18. P. J. Flory, *Chem. Revs.*, **35**, 51 (1944).
19. L. Mullins, *J. Appl. Polym. Sci.*, **2**, 1 (1959).
20. B. M. E. Van der Hoff, *Polym. Sci.*, **6**, 397 (1965).
21. L. Mullins, *J. Appl. Polym. Sci.*, **2**, 257 (1959).
22. E. Guth, R. Simha, and O. Gold, *Kolloid-Z.*, **74**, 266 (1936); E. Guth, *J. Appl. Phys.*, **16**, 20 (1945).
23. H. M. Smallwood, *J. Appl. Phys.*, **15**, 758 (1944).
24. I. M. Krieger and T. J. Dougherty, *Trans. Soc. Rheol.*, **3**, 137-152 (1959).
25. M. Mooney, *J. Colloid Sci.*, **6**, 162-170 (1951).
26. L. Mullins and N. R. Tobin, *J. Appl. Polym. Sci.*, **9**, 2993 (1965).
27. L. Mullins and N. R. Tobin, *Trans. IRI*, **33**, 2 (1956).
28. F. Bueche, *J. Appl. Polym. Sci.*, **4**, 107 (1960); *J. Appl. Polym. Sci.*, **5**, 27 (1961).
29. K. J. Smith, A. Greene, and A. Ciferri, *Kolloid-Z.*, **194**, 49 (1964).
30. H. Eyring, *Phys. Rev.*, **39**, 746 (1932).
31. F. T. Wall, *J. Chem. Phys.*, **11**, 67 (1943).
32. P. Debye, *J. Chem. Phys.*, **14**, 636 (1946).
33. B. H. Zimm and W. H. Stockmayer, *J. Chem. Phys.*, **17**, 1301 (1949).
34. Lord Raleigh, *Philos. Mag.*, **37**, 321 (1919).
35. W. Kuhn, *Kolloid-Z.*, **68**, 2 (1934).
36. M. V. Volkenstein (Vol'kenshtein), *Configurational Statistics of Polymer Chains*, Interscience, New York, 1963.
37. W. Kuhn, *Kolloid-Z.*, **76**, 256 (1936); *Kolloid-Z.*, **87**, 3 (1939).
38. P. J. Flory, *Principles of Polymer Chemistry*, Cornell University Press, Ithaca, NY, 1950, Chapter 10.
39. L. R. G. Treloar, *Physics of Rubber Elasticity*, 3rd ed., Oxford University Press, London, 1975, Chapter 3.

7

Dielectric and NMR Methods

While viscoelastic phenomena are commonly studied by perturbing the material with a mechanical stress, it is possible and sometimes convenient to perturb the sample by application of a field. The field interacts with the material to move it slightly away from equilibrium. The response of the material to the field, or its relaxation to equilibrium on removal of the field then provides a direct picture of molecular motion. In the case of dielectric methods, an electric field is applied, which causes charges (e.g., ions) in the material to move and structural dipoles to align. In the case of nuclear magnetic resonance (NMR), the situation is more complex in that the equilibrium state of electronic spins of selected atoms is disturbed by a radio-frequency field. The relaxation of these spins to equilibrium is assisted by interaction with the surrounding material, and mobility in this material is thus indirectly measured. The advantages of these methods over the mechanical methods include their sensitivity to specific structural details of the molecules in the material and, for the dielectric method, the ability to cover a wide frequency range.

A. DIELECTRIC METHODS

When an insulating material is subjected to an applied electric field, charge separation and molecular rearrangement occur within the material, causing the phenomenon of polarization. The magnitude of the polarization is measured by a property of the material called the dielectric constant. This macroscopic

property is in turn related to the molecular structure of the dielectric through the molecular polarizability and the molecular dipole moment. The exact form of this connection is far from obvious, and several theories have been proposed to explain it.

Dielectric relaxation, as the name implies, is concerned with the time, frequency, and/or temperature dependence of the dielectric constant. Since the magnitude of the dielectric constant is related to the molecular structure, its dependence on time, frequency, and/or temperature generally reflects molecular motion. In the case of homogeneous polymers, the dielectric relaxation technique may therefore be used as a probe for the study of transitions and relaxations in a manner analogous to that already discussed for mechanical relaxation. In this chapter we are concerned with the application of dielectric relaxation to amorphous polymers, and we attempt to point out differences between the dielectric and mechanical relaxation techniques.

In a manner now familiar, we start by treating dielectric relaxation phenomenologically, that is, in macroscopic terms, where the existence of molecules is ignored. In Section 2, we extend our development by incorporating molecular considerations. Applications of these ideas to polymers are treated in Sections 3 through 4.

1. Phenomenology

For the purposes of this discussion, we need only be concerned with electrical circuits that contain capacitances, C , and resistances, R . The resistance is the dissipative element, formally analogous to the dashpot in the mechanical model case. It is defined by Ohm's law:

$$R = \frac{V}{I} \quad (7-1)$$

where V is the voltage in volts, I is the current in amps, and R has units of ohms. A capacitor consists of two ideal electrodes separated by vacuum and is a conservative element, playing the same role as the spring in the mechanical model case. If a voltage V is applied to the capacitor plates in vacuum, the capacitor will hold a charge Q , which is measured in coulombs and which is related to the voltage as:

$$Q = C_0 V \quad (7-2)$$

C_0 is the capacitance and is measured in farads. If the plates are separated by a dielectric, that is, by an insulating material (rather than a vacuum), the capacitor will accept more charge at the same potential due to polarization of the dielectric. Under these conditions, the capacitance becomes

$$C = \epsilon C_0 \quad (7-3)$$

where ϵ is the dielectric constant. (The “dielectric constant” is more properly referred to as the relative permittivity because it is the ratio of the permittivity of the dielectric to that of vacuum, ϵ_0) As is clear from the definition, ϵ is a dimensionless quantity. For vacuum, $\epsilon = 1$ by definition; $\epsilon = 81$ for water, $\epsilon \sim 6$ for various types of inorganic glasses, and $\epsilon = 1.0006$ for air. Since ϵ is a function of time or frequency, as well as temperature, these values change with experimental conditions. The quoted numbers are for low-frequency experiments (equilibrium values) at room temperature. The dielectric constant of water decreases to about 1.8 for frequencies involved in optical experiments ($\sim 10^{15}$ Hz). At these frequencies an approximation for the dielectric constant is given by the Maxwell equation $\epsilon \approx n^2$, where n is the refractive index of the material.

We shall now show that a series combination of a capacitor and a resistance in an electrical circuit leads to the same linear differential equation describing the time dependence of the charge as that for the Voigt model describing the time dependence of the stress in the mechanical case.¹

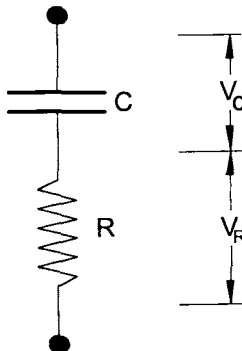


Figure 7-1. Schematic representation of an RC circuit.

Figure 7-1 is a schematic representation of the circuit in question. For series electrical circuits, the voltage across the terminals is the sum of the voltages across the elements:

$$V = V_C + V_R \quad (7-4)$$

Now V_C is given by equation (7-2) and V_R by equation (7-1). The current is defined by

$$I = \frac{dQ}{dt} \quad (7-5)$$

Substituting equation (7-5) into equation (7-4):

$$V = \frac{Q}{C} + R \frac{dQ}{dt} \quad (7-6)$$

Now if we define

$$\tau = RC \quad (7-7)$$

equation (7-6) may be rearranged to give

$$\tau \frac{dQ}{dt} + Q = CV \quad (7-8)$$

This equation is entirely analogous to the equation of motion for the Voigt element in the mechanical case [equation (3-26)].

By comparing these two equations, it can be seen that charge is the electrical analogue of the strain, voltage is the electrical analogue of the stress, and capacitance corresponds to the mechanical compliance. It should be noted that a series electrical model gives rise to an equation of motion of the same form as a parallel mechanical model. This is because voltages add when in series while stresses add when in parallel.

Not surprisingly, equation (7-8) may be integrated for various boundary conditions in the same manner as the mechanical Voigt element described in Chapter 3. For example, for a constant voltage V_0 , applied at time $t = 0$, the result is

$$Q(t) = CV_0(1 - e^{-t/\tau}) \quad (7-9)$$

The integration of equation (7-8) is carried out using the integrating factor technique, which was fully explained in Chapter 3, equation (3-28). It should be clear that equation (7-9) represents the electrical analogue of the mechanical-creep experiment on a single Voigt element.

In the development so far, we have assumed that capacitance is independent of time, which is only strictly true for a vacuum. All real materials exhibit time-dependent capacitances, which arise from the time dependence of the dielectric constant. We are interested in this time dependence since it contains information about molecular motion. We can utilize the approach used to obtain equation (7-8), since a capacitor containing a dielectric itself behaves like an RC circuit. This means that the same differential equations apply to the real capacitor as to a fictitious RC circuit that may be treated as its analogue. One of the simplest of such circuits is that represented in Figure 7-1 and described by equation (7-8).

To proceed, it is necessary to introduce several relationships from elementary electrostatic theory.

For an infinite-plate capacitor with parallel plates:

$$E = \frac{V}{d} \quad (7-10)$$

where E is the applied electric field and d is the distance between the plates. The charge density σ may be defined as

$$\sigma = \frac{Q}{A} \quad (7-11)$$

where A is the cross-sectional area of the plates. With a vacuum between the plates, the charge density is σ_0 and the electric field becomes*

$$E = 4\pi\sigma_0 \quad (7-12)$$

Now suppose that while the capacitor is connected to a constant voltage source, a dielectric (such as the sample under study) is inserted in the space between the capacitor plates. Additional current will flow into the capacitor owing to polarization of the dielectric material. The polarization itself is time dependent but, at equilibrium, the original charge density σ_0 will increase to σ , where

$$\sigma = \epsilon_R \quad (7-13)$$

and where ϵ_R is the limiting value of the dielectric constant of the sample at long times.

The polarization at infinite time, P_R , is defined by

$$\sigma_0 + P_R = \sigma \quad (7-14)$$

and represents an increase in the charge density due to the presence of the dielectric. The physical origin of the polarization, although not of immediate interest in this discussion of phenomenology, is the displacement of positive and negative charges within the dielectric as well as the reorienting of permanent molecular dipoles under the influence of the electric field.

* The relationship between the electric field strength and the charge density in our capacitor derives from the application of Gauss's flux theorem, which is beyond the scope of this book. Standard texts on electricity and magnetism, such as that by A. D. Kip (McGraw-Hill, New York, 1969), treat this subject in depth. The student should be forewarned, however, that numerous subtle differences in notation and definition abound in this area. The same symbol is often used for different, although related, quantities in various texts.

By combining equations (7-12, 7-13, and 7-14), we obtain an expression for the limiting value of the electric polarization at long times in terms of ϵ_R :

$$\epsilon_R - 1 = \frac{4\pi}{E} P_R \quad (7-15)$$

Although the polarization is generally time dependent, experimentally one finds that it can be partitioned into an instantaneous component, which we will designate P_U , and a time-dependent term $P_D(t)$. Thus

$$P(t) = P_D(t) + P_U \quad (7-16)$$

at infinite time (equilibrium)

$$P_D(t) = P_D \quad (7-17)$$

and

$$P_R = P_D + P_U \quad (7-18)$$

Thus, equation (7-15) becomes

$$\epsilon_R - 1 = \frac{4\pi}{E} (P_D + P_U) \quad (7-19)$$

Without loss of generality, the limiting value of the dielectric constant may also be partitioned in the same way, that is, $\epsilon_R = \epsilon_D + \epsilon_U$. By analogy with equation (7-15), we define ϵ_U as

$$\epsilon_R - 1 = \frac{4\pi}{E} P_U \quad (7-20)$$

We may now specifically consider the kinetics of polarization. We may assume that the polarization, $P(t)$, approaches its equilibrium value, P_R , at a rate proportional to its distance from equilibrium [see equation (5-23), which is closely related]:

$$\frac{dP(t)}{dt} = -\frac{P(t) - P_R}{\tau} \quad (7-21)$$

The time constant τ is not the same as that in equation (7-7). Via equations (7-16 and 7-18), the time-dependent part becomes

$$\frac{dP_D(t)}{dt} = -\frac{P_D(t) - P_D}{\tau} \quad (7-22)$$

Eliminating P_D through equations 7-18, 7-15, and 7-20 gives

$$\tau \frac{dP_D(t)}{dt} + P_D(t) = (\varepsilon_R - \varepsilon_u) \frac{E(t)}{4\pi} \quad (7-23)$$

where the electric field is time dependent [$E = E(t)$]. Now if the real capacitor, which we are viewing as a fictitious RC circuit, is subjected to an electric field periodic in time,

$$E^*(\omega, t) = E_0 e^{i\omega t} \quad (7-24)$$

we may solve equation (7-23) to yield

$$P_D^*(\omega) = \frac{\varepsilon_R - \varepsilon_u}{1 + i\omega\tau} \frac{E^*(\omega)}{4\pi} \quad (7-25)$$

The integration of equation (7-23) is carried out in the same fashion as equation (7-8). In addition, it has been assumed that the oscillatory field has been applied to the sample long enough ($t \gg \tau$) so that a steady condition has developed. This being the case, terms involving $e^{-t/\tau}$ are dropped since this factor approaches zero. These exponentials are, in fact, associated with initial transients, arising at the start of the experiment, which quickly become unimportant under most experimental conditions. The complex dielectric constant as a function of frequency can now be defined as

$$\varepsilon^*(\omega) = \frac{4\pi P_D^*(\omega, t)}{E^*(\omega, t)} + \varepsilon_U \quad (7-26)$$

where the ε_U term on the right must be included since $P_D^*(\omega, t)$ contains no information about time-independent (instantaneous) properties of the dielectric. Combining equations 7-25 and 7-26 gives

$$\varepsilon^*(\omega) - \varepsilon_U = \frac{\varepsilon_R - \varepsilon_U}{1 + i\omega\tau} \quad (7-27)$$

Separating $\varepsilon^*(\omega)$ into its real and imaginary parts by multiplying the numerator and denominator by the complex conjugate ($1 - i\omega\tau$) of the denominator yields

$$\varepsilon^*(\omega) = \varepsilon' - i\varepsilon''$$

$$\varepsilon' = \varepsilon_U + \frac{\varepsilon_R - \varepsilon_U}{1 + \omega^2\tau^2}$$

(7-28)

$$\epsilon'' = \frac{(\epsilon_R - \epsilon_U)\omega\tau}{1 + \omega^2\tau^2}$$

$$\tan \delta = \frac{\epsilon''}{\epsilon'}$$

These equations are plotted in Figure 7-2. They are formally identical to the compliance response of a Voigt element in series with a spring when the entire model is subjected to a sinusoidal stress. The complex dielectric constant is thus the analogue of the complex compliance, with the electric field playing the role of stress and the electric displacement $4\pi\sigma$ playing the role of strain.

The dielectric behavior described by equation (7-28) is known as the Debye dispersion.² Note the key assumption of first-order relaxation in equation (7-21).

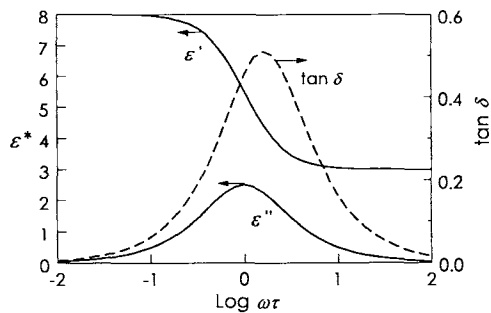


Figure 7-2. Debye plots for dielectric relaxation.

2. Molecular Interpretation of the Dielectric Constant

In Section 1 we developed the concept of polarization under the influence of an electric field from a phenomenological point of view. Now we direct our attention to the underlying molecular properties and supermolecular structure that give rise to the observed phenomena.

First, consider a molecule that has an asymmetrical distribution of positive and negative charges. HCl is an example; the large disparity in the electronegativities of chlorine and hydrogen causes the bonding electron distribution in the molecule to be denser on the halogen than on the hydrogen. This asymmetrical charge distribution in the molecule gives rise to a permanent dipole moment with a magnitude of 1.08 D (D = Debye). For two charges of opposite sign having magnitudes of the charge of the electron, separated by a distance of 1 Å,

$$\mu \equiv er = (4.8 \times 10^{-10} \text{ esu})(1 \times 10^{-8} \text{ cm})$$

$$= 4.8 \times 10^{-18} \text{ esu cm} = 4.8 \text{ D} \quad (7-29)$$

When such a permanent dipole is placed in an electric field, orientation takes place as the molecule attempts to align with the field in order to adopt a low-energy configuration. This orientation is clearly time dependent and gives rise to $P_D(t)$, the time-dependent macroscopic polarization discussed previously.

In addition to orienting dipoles, electric fields *induce* dipole moments in molecules, since electrons and nuclei experience forces in opposite directions in the same electric field and since electrons, being less massive, move much more easily than nuclei in a field. The quantity that measures the ease with which the electron cloud in a certain molecule can be distorted is the molecular polarizability α_0 . The magnitude of an induced dipole is given as

$$\mu = \alpha_0 E \quad (7-30)$$

Electrons move very rapidly because of their small mass; consequently the electronic distortion produced by an electric field is essentially instantaneous. Thus the formation of induced dipoles gives rise to the time-independent P_U term described above.

It remains now to relate the molecular quantities α_0 and μ to the macroscopic polarizability or dielectric constant, which can be measured experimentally. This is a very difficult task and will not be carried out in a rigorous fashion here. Rather, we start our discussion with an approximate equation, given by Debye, which describes the complex dielectric constant in terms of molecular properties. We rationalize the form of the equation through the Clausius-Mosotti equation and then show how $\epsilon'(\omega)$ and $\epsilon''(\omega)$ can be derived from this expression. Additional factors that were not included in Debye's original work, such as the effect of the reaction field and orientation correlation—which are important in condensed phases—will also be discussed before extending the treatment to dielectric relaxation in polymers.

Debye² showed that

$$\frac{\epsilon^* - 1}{\epsilon^* + 2} \frac{M}{\rho} = \frac{4\pi N_A}{3} \alpha_0 + \frac{4\pi N_A \mu^2}{9kT} \frac{1}{1 + i\omega\tau} \quad (7-31)$$

This equation is derived for a pure substance with molecular weight M and density ρ . Each molecule of the substance has a permanent dipole moment μ and polarizability α_0 . N_A stands for Avogadro's number.

Our explanation of equation (7-31) makes use of the Clausius-Mosotti equation, which is derived as follows:

The electric field E_s , produced inside a sphere of uniform dielectric, when placed into an electric field E , is given as

$$E_s = \frac{3}{\epsilon + 2} E \quad (7-32)$$

This internal field is less than the external field because of polarization of the dielectric in the external field. Clearly, when $\epsilon = 1$, that is, for a vacuum, $E_s = E$.

The total electric moment, M_s , induced in the sphere is just

$$M_s = \alpha_s E \quad (7-33)$$

where α_s is the polarizability of the material in the sphere.

According to equation (7-20), however, the instantaneous polarization P_U , is related to the corresponding dielectric constant; for the sphere in question

$$P_{U,s} = \frac{\epsilon_U - 1}{4\pi} E_s \quad (7-34)$$

Since the polarization is the electric moment per unit volume,[†]

$$M_s = P_{U,s} V_s = P_{U,s} \left(\frac{4}{3} \pi a_s^3 \right) \quad (7-35)$$

where a_s is the radius of the dielectric sphere. Combining equations (7-32) through (7-35) leads to

$$\frac{\epsilon_U - 1}{\epsilon_U + 2} = \frac{\alpha_s}{a_s^3} \quad (7-36)$$

a macroscopic form of the Clausius–Mosotti equation.

To extend this relationship to the molecular domain, suppose that the dielectric sphere contains N_s molecules, each of which has polarizability α_0 . Then,

$$\alpha_s = N_s \alpha_0 \quad (7-37)$$

Furthermore, assuming that the molecules are themselves spheres with radii a gives

[†] As defined in equation (7-14), polarization has the same units as σ , charge density, equation (7-11). However, in developing the definition, we employed a parallel plate capacitor with plate area A and spacing d . Multiplication of P_U by d/d shows that polarization may be regarded as electric moment (Qd) per unit volume (Ad).

$$\frac{4}{3}\pi a^3 = \frac{V}{N_s} = \frac{4\pi a_s^3}{3N_s} \quad (7-38)$$

so that equation (7-36) becomes

$$\frac{\varepsilon_U - 1}{\varepsilon_U + 2} = \frac{N_s \alpha_0}{N_s a^3} = \frac{\alpha_0}{a^3} \quad (7-39)$$

Furthermore, since the molecular volume can be written as $\frac{4}{3}\pi a^3$ or $M/(\rho N_A)$,

$$\frac{M}{\rho} \frac{\varepsilon_U - 1}{\varepsilon_U + 2} = \alpha_0 \frac{4\pi}{3} N_A \quad (7-40)$$

which is the usual form of the Clausius–Mosotti equation for a pure material. It relates the instantaneous value of the dielectric constant ε_U , a macroscopic quantity (the instantaneous dielectric constant), to α_0 , the molecular polarizability.

We will now shift our attention from ε_U to ε_R , the long-time limiting value of the dielectric constant. Here the tendency of the permanent dipoles to orient in the electric field becomes important.

The energy, U , of a permanent dipole aligned with an electric field of strength E is

$$U = -E\mu \quad (7-41)$$

If the dipole is not perfectly aligned with the field, but rather is directed at some angle θ to the field direction, this energy becomes

$$U = -E\mu \cos \theta \quad (7-42)$$

In a real material, the tendency of dipoles to align under the influence of the field is counteracted by molecular collisions (Brownian motion), which disrupt order. The Boltzmann equation of statistical mechanics provides a simple method by which the average dipole moment $\bar{\mu}$ in the direction of the electric field can be evaluated in this situation:

$$\bar{\mu} = \frac{\int_0^\pi A e^{(E\mu \cos \theta)/kT} \mu \cos \theta 2\pi \sin \theta d\theta}{\int_0^\pi A e^{(E\mu \cos \theta)/kT} 2\pi \sin \theta d\theta} \quad (7-43)$$

where A is a normalization constant and the term $2\pi \sin \theta d\theta$ measures the geometric probability that a dipole has an orientation angle θ in the limit that E

$\rightarrow 0$. (See Figure 7-3). Since it turns out that experimentally we are interested in conditions where kT is large compared with orienting energies, the exponential in equation (7-44) may be expanded and terms higher than

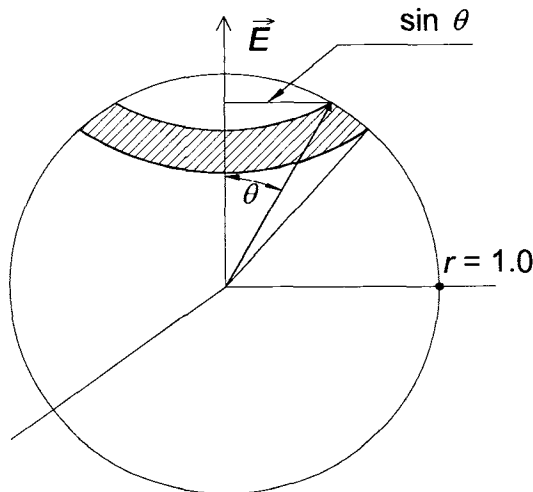


Figure 7-3. Alignment of dipoles in a field.

second order ignored.

$$\bar{\mu} = \frac{\int_0^\pi (1 + E\mu \cos \theta / kT) \mu \cos \theta \sin \theta d\theta}{\int_0^\pi (1 + E\mu \cos \theta / kT) \sin \theta d\theta} \quad (7-44)$$

This expression can be integrated by standard techniques to yield

$$\bar{\mu} = \frac{\mu^2 E}{3kT} \quad (7-45)$$

Debye added this contribution to the induced dipole moment [equation (7-30)] to get

$$\alpha_0 E + \frac{\mu^2 E}{3kT} = \left(\alpha_0 + \frac{\mu^2}{3kT} \right) E$$

or

$$\alpha = \alpha_0 + \frac{\mu^2}{3kT} \quad (7-46)$$

where α is an effective polarizability, which measures the tendency for induced dipoles to be formed as well as the tendency for the field to orient the permanent dipoles in the long-time limit.

With this value of α , the Clausius–Mosotti expression may be written for ε_R as

$$\frac{\varepsilon_R - 1}{\varepsilon_R + 2} \frac{M}{\rho} = \frac{4\pi N_A}{3} \left(\alpha_0 + \frac{\mu^2}{3kT} \right) \quad (7-47)$$

It is now easy to understand the origin of equation (7-31). One sees that it is of the form of the Clausius–Mosotti equation where the complex dielectric constant rather than ε_U or ε_R values is used. The complex formulation introduces a frequency dependence, which appears in the last term of equation (7-31). One would expect the time-dependent contribution to be related to the difference between instantaneous and long-time behavior and, indeed, this is correct, because the factor multiplying the frequency dependence in equation (7-31) is merely the difference between equations (7-47) and (7-40). In fact, these two expressions may be combined with equation (7-47) to yield

$$\frac{\varepsilon^* - 1}{\varepsilon^* + 2} = \frac{\varepsilon_U - 1}{\varepsilon_U + 2} + \left(\frac{\varepsilon_R - 1}{\varepsilon_R + 2} - \frac{\varepsilon_U - 1}{\varepsilon_U + 2} \right) \frac{1}{1 + i\omega\tau} \quad (7-48)$$

Solving for ε^* gives

$$\varepsilon^* = \frac{3\varepsilon_U + 2[(\varepsilon_R - 1)Y - \varepsilon_U + 1][1/(1 + i\omega\tau)]}{3 - [(\varepsilon_R - 1)Y - \varepsilon_U + 1][1/(1 + i\omega\tau)]} \quad (7-49)$$

where

$$Y = \frac{\varepsilon_U + 2}{\varepsilon_R + 2}$$

Clearing fractions, one has

$$\varepsilon^* = \frac{\varepsilon_R + i\varepsilon_U X}{1 + iX} \quad (7-50)$$

where

$$X = \frac{\varepsilon_R + 2}{\varepsilon_U + 2} \omega\tau$$

Multiplication by the complex conjugate of the denominator, collecting real and imaginary terms, and remembering the definition of ϵ^* in terms of ϵ' and ϵ'' in equation (7-28) leads to

$$\epsilon' = \epsilon_U + \frac{\epsilon_R - \epsilon_U}{1 + X^2} \quad (7-51)$$

$$\epsilon'' = X \frac{\epsilon_R - \epsilon_U}{1 + X^2}$$

It is clear that these equations are closely related to the phenomenological expression equation (7-28) except that the "molecular rotational relaxation time" τ is now replaced by an effective relaxation time τ^* where

$$\tau^* = \frac{X}{\omega} = \frac{\epsilon_R + 2}{\epsilon_U + 2} \tau \quad (7-52)$$

Equations (7-51) and (7-52) are called the Debye equations; taken in conjunction with equation (7-40) and equation (7-47), they relate experimentally measurable macroscopic quantities to molecular properties within the framework and limitations of the model developed by Debye.²

Onsager was the first to obtain an expression for the dielectric constant for a more realistic picture of a condensed phase of dipolar molecules.³ In condensed phases, where molecules are close together, account must be taken of the so-called reaction field. This effect stems from the fact that a dipolar molecule itself polarizes the surrounding medium and this additional polarization reacts back on the molecule. Although Onsager took the reaction field effect into account, he nevertheless neglected orientation correlations between molecules. Derivation of the Onsager equation is beyond the scope of this treatment. The reader is referred to the standard references.³⁻⁵ We merely quote the final result for the dipole moment as a function of the limiting dielectric constants:

$$\mu^2 = \frac{3kT}{4\pi N} \frac{2\epsilon_R + \epsilon_U}{3\epsilon_R} \left(\frac{3}{\epsilon_U + 2} \right)^2 (\epsilon_R - \epsilon_U) \quad (7-53)$$

where N is the number of molecules per unit volume. It is possible to solve equations similar to equation (7-23) for the Onsager model in an alternating electric field, but the result is quite complex. It can be shown, however, that

this treatment gives numerical values close to those obtained from the Debye model.⁶

The orientation correlation between dipoles in condensed phases was considered by Kirkwood and finally evaluated by Frölich⁷ in terms of the limiting values of the dielectric constant. We shall content ourselves with quoting the Kirkwood–Frölich equation as follows,

$$\varepsilon_R - \varepsilon_U = \frac{3\varepsilon_R}{2\varepsilon_R + \varepsilon_U} \frac{4\pi N}{3kT} \left(\frac{\varepsilon_U + 2}{3} \right)^2 g\mu^2 \quad (7-54)$$

where g is the Kirkwood correlation factor (see Section 4) and μ is the dipole moment of the isolated molecule.

The reader can see from the above developments that the value of the static and instantaneous dielectric constants can be related to molecular structure for simple dipolar fluids. The main results that translate quite well to polymers is the dielectric constant will be highly dependent on the concentration of dipoles and the difference $\varepsilon_U - \varepsilon_R$ will generally decrease with temperature if the polymer is sufficiently fluid.

3. Interfacial Polarization

Polymers are quite special dielectrics in that they can be highly insulating and have extremely low dielectric constants. For example, polyethylene can exhibit a dielectric constant as low as 2.2 and conductivity as low as 10^{-19} S/cm. These two characteristics make polymers very susceptible to another source of polarization—accumulation of virtual charge at the interface between the polymer matrix and any more polar or conducting phase, for example, water droplets. This interfacial polarization can dominate the dielectric characteristics of the polymer at low to intermediate frequencies. As a result, the detection of this polarization becomes an effective means of demonstrating the presence of two phases in the polymer. Even phases in the nanometer range will show this effect. A schematic of such polarization is shown in Figure 7-4.

Interfacial polarization in biphasic dielectrics was first described by Maxwell (same Maxwell as the Maxwell model) in his monograph *Electricity and Magnetism* of 1892.¹² Somewhat later the effect was described by Wagner in terms of the polarization of a two-layer dielectric in a capacitor and showed that the polarization of isolated spheres was similar. Other more complex geometries (ellipsoids, rods) were considered by Sillars; as a result, interfacial polarization is often called the Maxwell-Wagner-Sillars (MWS) effect.

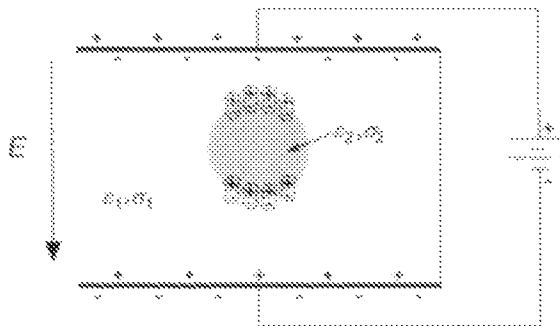


Figure 7-4. Polarization at the interface between a polymer and a polar inclusion. The interfacial charges are illustrated as effective dipoles, showing that distinguishing interfacial from dipolar polarization will depend critically on the characteristic time of the former.

In the case of isolated spheres, the equations are quite straightforward, and bring out clearly the effects of field frequency ω and filler volume fraction ϕ . The expression for the components of the complex dielectric constant ϵ^* are:

$$\epsilon' = \epsilon'_U \left(1 + \frac{k}{1 + \omega^2 \tau^2} \right) \quad \text{and} \quad \epsilon'' = \epsilon''_U \frac{k \omega \tau}{1 + \omega^2 \tau^2} \quad (7-55)$$

where

$$\epsilon'_U = \epsilon'_1 \left(1 + \frac{3\phi_2(\epsilon'_2 - \epsilon'_1)}{2\epsilon'_2 + \epsilon'_1} \right) \quad (7-56)$$

$$k = \frac{9\phi_2\epsilon'_1}{2\epsilon'_1 + \epsilon'_2} \quad (7-57)$$

$$\tau = \frac{\epsilon_0(2\epsilon'_1 + \epsilon'_2)}{\sigma_2} \quad (7-58)$$

In these equations the subscript 1 is used to identify the properties of the matrix, while 2 is used for the particles. These equations are for the special case of a highly insulating matrix of constant dielectric properties containing a small amount of well-dispersed spherical particles that are somewhat conductive. The important aspect of this result is that the particles produce a Debye-like dispersion centered at a frequency of roughly σ_2/ϵ_0 . With a conductivity of, say, 10^{-7} S/m (Siemens/meter) and $\epsilon_0 = 8.84 \times 10^{-12}$ F/m (Farads/meter) the frequency of the MWS dispersion will be around 10 kHz, where it can be easily confused with a dipolar relaxation process. As shown by equation (7-57), the magnitude of the MWS dispersion should increase linearly

with the amount ϕ_2 of the dispersed phase, which is one way of distinguishing MWS and dipolar dispersions.

4. Application to Polymers

The original forms of the Debye and Onsager treatments are not directly applicable to macromolecules, since they are concerned with assemblies of rigid dipoles in which the magnitudes of the dipole moments do not change as a result of thermal motions. In the case of flexible chain macromolecules whose shapes are constantly changing due to random thermal motions, this is obviously not a realistic approximation.¹¹ In addition, both the Debye and Onsager treatments give rise to relaxation behavior characterized by a single relaxation time and it is quite clear from the discussion in previous chapters of this book that the single relaxation time model is inadequate to describe the viscoelastic response of polymers.

The Kirkwood–Frölich expression [equation (7-54)] is, however, applicable to flexible chain polymers if we write for the correlation factor

$$g = 1 + \frac{1}{N} \sum_{j=2}^N \langle \cos \gamma_{1j} \rangle \quad (7-59)$$

where γ_{1j} is the angle between the first unit (1) of the chain and the j th unit, and N is the number of repeat units in the chain. The symbol μ in equation (7-54) is now understood to refer to the dipole moment of the isolated repeat unit. In the case of the freely jointed chain, when the dipoles of the repeat units lie along the chain contour, it is clear that $g = 1$, since all of the cosine averages are zero (see Chapter 6, Appendix 1). It should also be apparent that g will depend on the chain geometry, and more sophisticated calculations such as those taking into account the interdependence of bond rotational potentials are necessary to obtain values of g for real chains. If the structure of the polymer chain is known exactly, so that the dipole moment of the isolated repeat unit is available together with its angular relationship to the chain backbone, information about the conformational properties of the chain in solution can be obtained by experimental determinations of g through the use of the Kirkwood–Frölich equation. Comparisons may also be made between the experimental value of g and those obtained by theoretical calculations.

Molecular theories describing the dielectric relaxation behavior of polymers have been developed and are summarized in references 5, 12 and 13. Again, if the dipoles are rigidly attached along the chain contour, normal mode theories such as those of Rouse and Bueche described in Chapter 3 for the mechanical case might be expected to be applicable. In addition, the time–temperature superposition principle also generally applies.

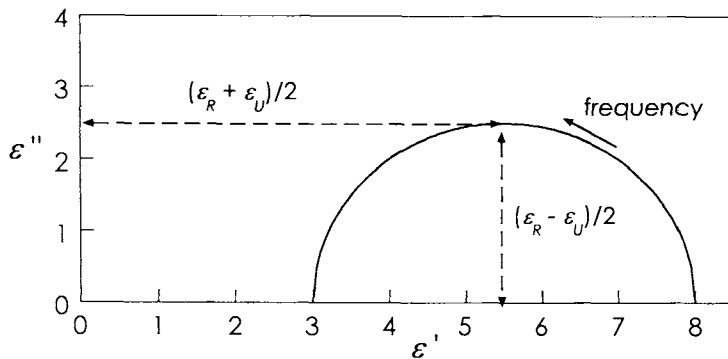


Figure 7-5. Cole-Cole plot for a single relaxation time, $\epsilon_R = 8$, $\epsilon_U = 3$.

A particular treatment of dielectric relaxation data is quite common. This is the so-called Cole-Cole plot¹⁴ obtained by plotting ϵ'' against ϵ' , each point corresponding to one frequency. From equation (7-28), we have

$$\left(\epsilon' - \frac{\epsilon_R + \epsilon_U}{2} \right)^2 + (\epsilon'')^2 = \left(\frac{\epsilon_R - \epsilon_U}{2} \right)^2 \quad (7-60)$$

which may be verified by direct substitution. Thus, for the single-relaxation-time model, the Cole-Cole plot is a semicircle of radius $(\epsilon_R - \epsilon_U)/2$ with its center on the ϵ' axis at a distance $(\epsilon_R + \epsilon_U)/2$ from the origin. Note that the relaxation time does not appear in equation (7-60) so the Cole-Cole plot is independent of this parameter. An example of a Cole-Cole plot for a single-relaxation-time model with $\epsilon_R/\epsilon_U = 2.67$ is shown in Figure 7-5. This is the same example as that depicted in Figure 7-2.

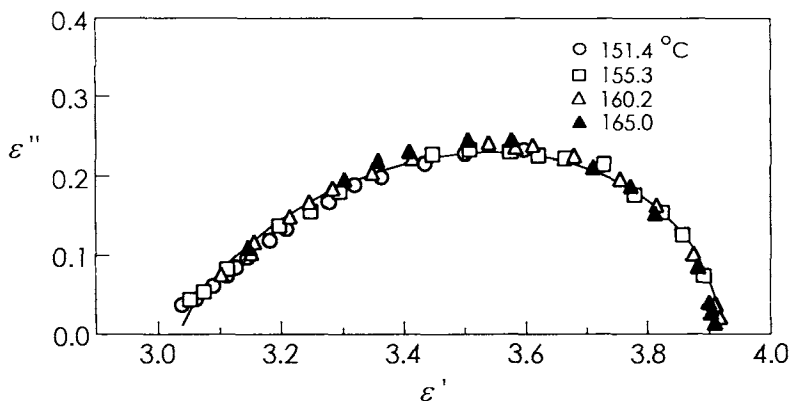


Figure 7-6. Cole-Cole plot for the α relaxation in poly (2 chlorostyrene).

As with mechanical relaxation, the single-relaxation-time model is inadequate for polymers and the Cole-Cole plots are not semicircles. Figure 7-

6 is an experimental ColeCole plot for the dielectric relaxation of poly (2-chlorostyrene) in the glass transition region. It can be seen that the semicircle of the single-relaxation-time model has become flattened and shows pronounced asymmetry at the high-frequency end (low values of ϵ' and ϵ''). This behavior is typical of that for most amorphous polymers in their primary relaxation regions. A number of empirical distribution functions have been proposed to fit such data. Some of these are described in references 5 and 12. As can also be seen from Figure 7-6, the Cole-Cole plot is also rather insensitive to temperature.

It should be noted that the Cole-Cole method can also be applied to dynamic mechanical data, but this is not often done because most such data are collected over very restricted frequency ranges.

5. Experimental Methods

Among the attractive features of the dielectric relaxation method are its relative ease of application and the availability of a very large frequency range in a more or less continuous manner. In fact, measurements can be made over the frequency range from 10^{-4} Hz to 3×10^{10} Hz, using a variety of techniques. These are summarized in Table 7-1.

Table 7-1. Methods for Dielectric Measurements

Method	Frequency Range (Hz)
DC transient	10^{-4} to 10^{-1}
Ultra-low-frequency bridge (Harris bridge)	10^{-2} to 10^2
Schering bridge; transformer bridge; transformer ratio arm bridge	10 to 10^7
Resonance circuits; Q meters	10^5 to 10^8
Coaxial (slotted) line; reentrant cavity	10^8 to 10^9
Coaxial line and waveguide	10^9 to 3×10^{10}

DC Transient-Current Method. In this method a step voltage is applied to the sample and the current response is measured by a fast-response electrometer. For the single- relaxation-time model, the current response would be given by equation (7-9). In recent years this method has been of renewed interest because with the advent of modern computing methods, it is possible to Fourier-transform the response in the time domain to obtain the frequency response. Several Fourier-transform dielectric spectrometers have been designed. We may note the one of historical significance due to Johnson et al.¹⁵, as well as modern commercial instruments.¹⁶ The method has the great

advantage that a complete dielectric relaxation spectrum can be recorded in a reasonably short time. Practical considerations limit the frequency range available from about 10^{-4} Hz to 10^4 Hz. However, this is a very convenient range for the study of molecular motion in polymers, as well as interfacial polarization.

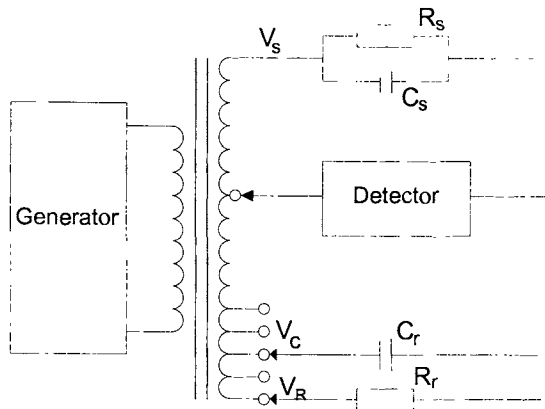


Figure 7-7. Schematic of transformer ratio arm bridge.

Bridge Methods. A commonly employed technique for measuring dielectric relaxation in polymers makes use of the transformer ratio arm bridge. A schematic of such a bridge appears in Figure 7-7. Referring to this figure, the resistance and capacitance of the sample R_s and C_s are balanced by the reference elements R_r and C_r , which have voltages V_R and V_C across them. The conditions for the capacitive and resistive balances are then

$$\begin{aligned} V_s C_s &= V_C C_r \\ V_s R_s &= V_R R_r \end{aligned} \tag{7-61}$$

It is thus possible to balance the bridge by varying the reference resistor R_r and capacitor C_r or by varying the voltages V_R and V_C . Transformer ratio arm bridges may be conveniently employed over a frequency range from about 10 Hz to 10^6 Hz. Other bridge designs have been described so that the frequency range available by these methods can be said to extend from 10^{-2} Hz to 10^7 Hz.

Impedance Spectroscopy. The term “Impedance Spectroscopy” has been applied to a bridge method wherein the sample is analyzed in terms of several circuit elements all of which are frequency independent. An example circuit is shown in Figure 7-8b. The analysis then uses the frequency information to derive all the circuit elements. This approach is particularly useful for samples that are somewhat more conductive than the usual polymeric solutions and solids. Examples include hydrogels and ionomers.

The complex impedance of a sample is merely the ratio of the complex current and the complex voltage. It is a sample property rather than a material property, but material properties (e.g., conductivity) can be derived from the result. Figure 7-8a shows an impedance plot, termed a Nyquist plot, for a reasonably conductive sample (a composite of an ionomer in a crosslinked epoxy matrix). The circular part of the response can be analyzed in terms of a simple circuit comprising a resistor in series with a capacitor and another resistor shown in Figure 7-8b.

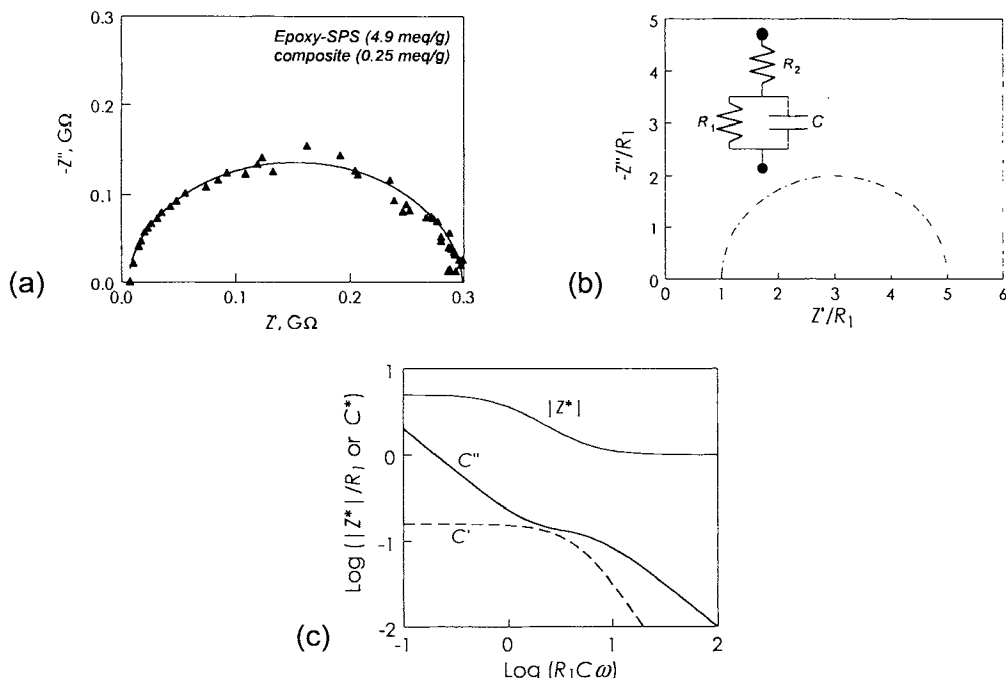


Figure 7-8. (a) Impedance spectroscopy result for an ionically conductive epoxy composite [adapted with permission of S. Boob, © 2003]; (b) the equivalent circuit (inset) for the circular part of the response; and (c) same as (b), but plotted on a frequency scale.

The connection between the impedance and dielectric measurements can be seen easily for only relatively simple examples. In Figure 7-8c the complex capacitance plot for the same equivalent circuit is similar to typical dielectric response dielectric only in the low-frequency region. The plot of the magnitude of the complex impedance, also shown in this panel, is known as the Bode plot.

Thermally Stimulated Current (TSC). This relatively straightforward method has been used for years as a method of thermal analysis comparable in some aspects to Thermal Mechanical Analysis (TMA). For example, TSC is able to detect many of the same transitions as seen by the mechanical methods. The advantages of TSC include its extremely high sensitivity and its low

frequency. A recent review with numerous references has been written by Lavergne and Lacabanne.¹⁷

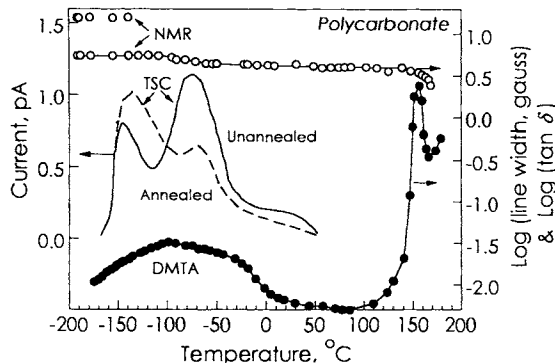


Figure 7-9. TSC results for polycarbonate compared with NMR line width and dynamic mechanical (DMTA) measurements. [TSC data from Y. Aoki and J. O. Brittain, *J. Appl. Polym. Sci., Polym. Phys. Ed.* **15**, 199 (1977) Copyright © 1977 by Wiley Periodicals, Inc., a Wiley Company; NMR data from S. Matsuoka and Y. Ishida, in *Transitions and Relaxations in Polymers*, Polym. Symp. No. 14, 247 (1966). Copyright © 1966 by Wiley Periodicals, Inc., a Wiley Company; DMTA data from K. Illers and H. Breuer, *Kolloid Z.* **176**, 110 (1961), © by Springer-Verlag, 1961. With kind permission of Springer Science and Business Media.]

The TSC method, also known as thermally stimulated discharge (TSD), involves polarization of the polymer at a temperature well above all transitions. Polarization is carried out using a high DC voltage, which creates a high enough field to align dipoles in spite of the high temperature. While maintaining the field, the sample is cooled down to a temperature well below all transitions. On removing the field, a residual polarization remains. The contacts on the sample are now attached to a high-impedance resistor and a sensitive current-measuring circuit, for example, an extremely high-impedance digital voltmeter connected across the resistor. At this point, the temperature T of the sample is increased according to the program:

$$T = a + bt \quad (7-62)$$

where t is time and a and b are constants. As the sample passes through a transition, some dipoles are able to relax, and a current $J(t)$ is recorded. A maximum in this current is observed which corresponds to the maximum rate of relaxation of the dipoles and the amount of charge connected with the transitions. An expression connecting the maximum to the characteristic time τ_0 for the relaxation is

$$\tau_0 = \frac{kT_M^2}{b\Delta E} \exp(-\Delta E / kT_M) \quad (7-63)$$

where T_m is the temperature of maximum current flow, and ΔE derives from a plot of $\ln J(T)$ vs. $1/T$ at temperatures below the transition. An example of a TSC result is provided in Figure 7-9. Included for comparison are the mechanical results and the NMR line width for the same temperature range.

Other Methods. Bridge methods cannot be used above about 10^7 Hz because the effects of stray inductance become increasingly important at high frequencies. According to Table 7-1, resonance circuits may be used at frequencies up to 10^8 Hz. Above this range, microwave technology must be employed. As measurements in this frequency range are somewhat more difficult to make and are rarely done on polymers, we shall content ourselves with merely mentioning the existence of appropriate techniques without explaining them further. All the techniques listed in Table 7-1, up through resonance techniques, are referred to as lumped circuit methods. They all have in common that the capacitance of the sample to be measured can be represented by a series model consisting of a capacitance and a resistor, as in Figure 7-1.

The lumped circuit methods also have in common that the polymer sample to be examined can be conveniently arranged in the form of a circular disc that is mounted between metal electrodes. The best method of assuring good electrical contact between the polymer and the electrodes is to evaporate a thin film of a conducting metal such as silver onto the polymer surface. This is rarely done in practice, however. It is more common to attach aluminum foil to the sample surface, using silicone grease. Care must be taken to ensure that the sample disc is truly flat and has a smooth surface. Sample cells used to investigate the dielectric relaxation behavior of polymers are usually homemade, although several have been described in the literature.^{5,12,13} It is a relatively easy matter to adapt such cells for the measurement of polymeric liquids as well as solids.

The methods listed in Table 7-1 for the frequency range above 10^8 Hz are referred to as distributed circuit methods. The analysis of the circuits in such methods is not so straightforward as in the case of the lumped circuit methods and the sample cell and geometry are considerably more complex also.

6. Application of Dielectric Relaxation to Polymethyl Methacrylate

In Chapter 5 we cited dynamic mechanical relaxation data for polymethyl methacrylate (PMMA). There it was shown that PMMA possesses two mechanical relaxation regions over the temperature range – 50° to 160°C at low frequencies. These were labeled α for the relaxation accompanying the glass transition and β for a secondary relaxation that has generally been associated with motions of the ester side group. PMMA has a predominantly nonpolar

backbone with flexible polar side groups. It would therefore be expected that motions involving the side groups are very prominent dielectrically. Figure 7-10 shows a comparison between the dielectric loss tangent and the mechanical loss tangent in PMMA as a function of temperature. It can be seen that the dielectric β relaxation is of much greater magnitude than the mechanical β relaxation, while just the reverse holds true for the dielectric and mechanical α processes. It is generally accepted that the β relaxation in PMMA is due to the hindered rotation of the $-COOCH_3$ group about the carbon–carbon bond linking it to the main chain. The steric hindrance to this rotation comes mainly from the α methyl substituents of the two adjacent repeat units.

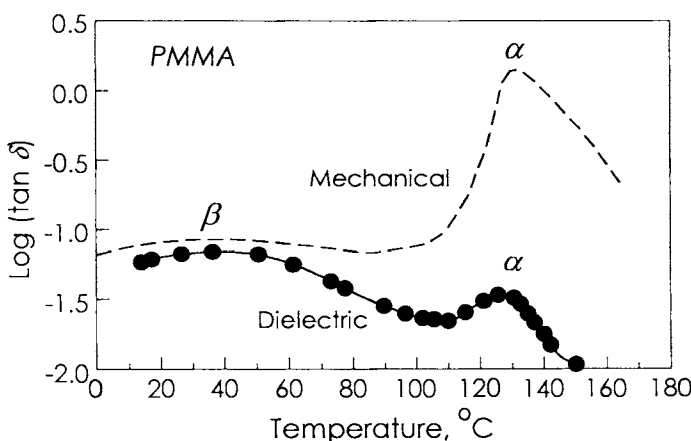


Figure 7-10. Comparison between $\tan \delta_e$ and $\tan \delta$ for PMMA. Dielectric and mechanical data from Figures 8.9 and 8.12, respectively, in McCrum et al.⁵ Original data were, respectively, from G. P. Mikhailov and T. I. Borisova, *Polym. Sci. USSR*, **2**, 387 (1961) and J. Heijboer, *Physics of Noncrystalline Solids*, North Holland, Amsterdam, 1965, p. 231.

The data cited in Figure 7-10 are for "conventional" (or somewhat syndiotactic) PMMA. In the case of isotactic PMMA, the glass transition temperature is reduced so that the α and β relaxations merge even at low frequencies and the dielectric β relaxation appears as a shoulder on the much larger α relaxation. It must be assumed in this case that the onset of side-chain ester group rotation corresponds to the onset of main-chain micro-Brownian motion so that the magnitude of the dielectric relaxation is enhanced.

7. Comparisons Between Mechanical and Dielectric Relaxation for Polymers

It would appear from the foregoing discussion that a correspondence between dielectric and mechanical relaxation can be expected when the molecular motions responsible for a mechanical relaxation involve reorientation of a polar group. Since there is a formal analogy between the complex mechanical

compliance J^* and the complex dielectric constant ε^* , it would seem that comparisons between dielectric and mechanical relaxation data is best made by comparing these two quantities or their in-phase and out-of-phase components. This is rarely done in practice, however. It is much more common to construct so-called correlation diagrams in which the frequency of maximum loss is plotted against reciprocal temperature. If the positions of a relaxation region on such a diagram correspond for various relaxation techniques, it can be assumed that the relaxation arises from the same underlying motions. Such a correlation map is shown for the α and β relaxations in PMMA in Figure 7-11. It can be seen that the mechanical and dielectric data correspond well for the α relaxation region, but the positions of the mechanical and dielectric β relaxations do not coincide although the lines are parallel. Despite this discrepancy, the two β relaxations are both understood to arise from motions of the ester side-chain, partly because of their similar temperature dependencies. It can also be seen from Figure 7-10 that the α and β relaxations merge at frequencies in excess of about 5×10^5 Hz. This figure also includes limited NMR results, a subject to be discussed in the next section.

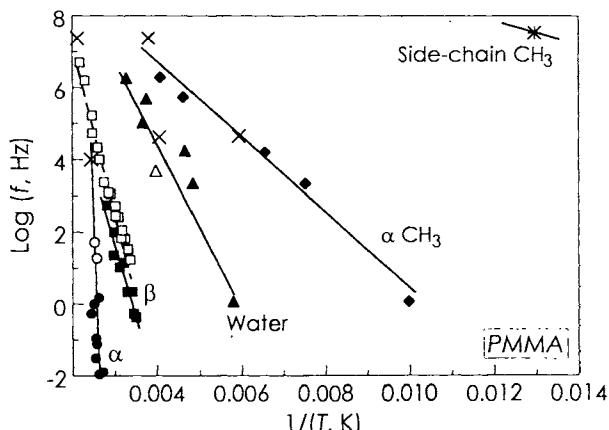


Figure 7-11. Correlation map for PMMA. Solid symbols, mechanical; open symbols, dielectric; and crosses, NMR. [Adapted from N. McCrum, B. E. Read and G. Williams, *Anelastic and Dielectric Effects in Polymeric Solids*, Wiley, London, 1967.]

B. NUCLEAR MAGNETIC RESONANCE METHODS

Because of its breadth and complexity, the discussion of nuclear magnetic resonance (NMR) must necessarily be extremely focused on the methods used to examine the motions of polymer molecules. The reader is referred to several classical monographs and collections for more information.¹⁸⁻²¹

NMR relaxation techniques are a useful complement to mechanical and dielectric methods in that they examine the polymer in a different fashion and thus may be able to reveal structure-motion correlations that cannot be seen with the other methods. To put this in perspective, we remind ourselves that mechanical methods for investigating molecular motion can cover with some facility the time span from 1 ms to 10^5 s. Times as low as 0.01 ms can be reached by sonic wave methods, but these are generally limited to rigid polymers that have negligible mechanical dissipation. With NMR, the fundamental (Larmor) frequency is the low end of the time scale, and depends on the magnetic field strength. For example, a 300-MHz instrument could in principle probe motions on the time scale of $\sim 10^{-9}$ s, whereas NMR relaxation experiments can probe time scales as long as 1 s. Thus the NMR can be regarded as complementing the mechanical measurements with extension to a far shorter time scale. However, and most importantly, NMR methods hold the potential for associating directly the relaxation processes with specific structural groups, whereas this information must be inferred from mechanical measurements done on various structures.

In this section, we will concern ourselves mainly with relaxation processes in solid polymer samples, as distinct from high-resolution NMR used for diagnosing the chemical structure of molecules. The latter can be done on solid samples using cross-polarization, magic-angle spinning (CP-MAS), but these techniques can eliminate valuable information on the very relaxation processes of interest to us. An interesting exception, however, is the WISE experiment, which is discussed below.

Many atoms found commonly in polymers (^1H , ^{13}C , ^{14}N , ^{19}F , etc.) possess magnetic moments, or “nuclear spins” that precess at convenient frequencies in achievable magnetic fields due to the interaction of their angular momentum with the torque exerted by the field on the dipole. This phenomenon, somewhat analogous to a spinning top, is by itself not very useful. However, the existence of two (or more) quantized energy states in a magnetic field means that a spin state can be changed by irradiation with externally applied electromagnetic energy. For example, with ^1H , an applied field of only 2.1 Tesla gives a precessional frequency of about 90 MHz, which is at the low end of the FM radio broadcast band. The important aspect of this is that the nuclear spin becomes a probe of local time-dependent magnetic fields because this frequency is sensitive to the total (local + external) field. Additionally, changes in energy state, and thus the relative population of upper and lower energy states, can be brought about not only by the applied RF field, but also by motions of other spins.

To understand the interrelationship of these spins with their host polymer molecules it is useful to regard the spins as a separate system that is able, on the average, to behave substantially independently of the surrounding matrix or "lattice." In contrast, electric dipoles are attached rigidly to the polymer chains and thus follow the directional motions of the molecule. While the nuclei are attached also to the molecules, and thus change *position* with the molecules, they are not forced along a particular *direction* with respect to the bond directions in the chain. With such a "loose" connection, how does one use the magnetic dipoles, which give rise to the NMR signal, to examine the lattice? While the influence of the lattice on the nuclear spins is small, it is not negligible, because the spins couple to each other through the magnetic polarization of the lattice. The rigidity of the lattice has a direct influence on this coupling.

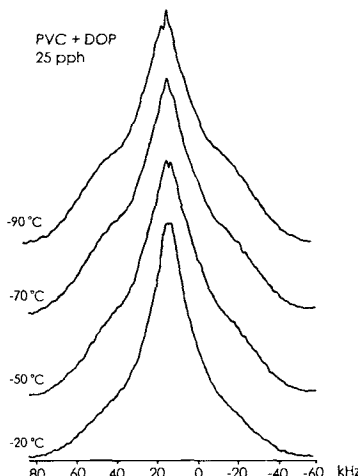


Figure 7-12. Broadline investigation of plasticized PVC. [K. Boo and M. Shaw, *Proc. Xth Int. Congr. Rheol.*, 1, 195 (1988).]

For those familiar with high-resolution NMR, the simplest experiment to visualize is a very classic one—*line broadening*. High-resolution NMR depends on high mobility of the nuclear spins to gain narrow line widths. Thus line width itself is an indicator of the lack of mobility, or rigidity.

Considering only protons for the moment, there are two principal sources of line broadening in the spectrum of a solid sample: chemical-shift anisotropy and dipole-dipole interactions. The former results from the fact that the chemical groups in a solid polymer are fixed in different orientations with respect to the applied magnetic field. For example, the influence of motion of electrons around the ring of the phenyl group in polystyrene will depend highly on the orientation of the ring with respect to the field. Thus the deshielding

effect on the protons attached to the ring will vary and result in varying fields (or, equivalently, frequencies) for the resonance of these protons. The second source of broadening is dipole-dipole interaction. (Here again we are referring, of course, to magnetic dipoles, not the familiar electric dipoles). For protons with a spin of $\frac{1}{2}$, the two possible states are with the spin aligned with the field or against the field. All dipoles in the sample interact with each other and the strength of the interaction depends on the distance between them and the angle between the applied field and the line connecting the two dipoles. If the lattice is completely rigid, the resonance frequencies of the nuclei vary greatly because of different dipole-dipole (spin-spin) interactions between the active nuclei in various locations in the structure. This *dipolar coupling* is similar to the *scalar coupling* important to high-resolution analytical NMR, but the nuclei of the lattice are not necessarily chemically bonded to the resonating nucleus. The coupling is through space.

For the reasons outlined above, the line width with solid samples is exceedingly broad, often covering 30–40 kHz and as much as 100 kHz. The associated relaxation time is inversely proportional to this line breadth (multiplied by π), and thus is on the order of 10 μ s for a very rigid solid. This relationship between breadth and relaxation time is:

$$\text{Breadth, Hz} \propto 1/(\pi \times \text{relaxation time, s}) \quad (7-64)$$

Figure 7-12 shows the results of a broadline investigation of plasticized PVC. As the system is cooled, the proton resonance broadens and appears to split into two distinct contributions, one narrow and the other broad. It is not possible, without additional information, to assign the sources of these resonances; however, one would guess that the narrow resonance is associated with motions of the plasticizer. The additional molecular motion in the soft regions means that the spin-spin coupling is not as efficient.

As one might suppose, the transition between broad and narrow is an indicator of the viscosity of the matrix, and thus is a method of gaining viscoelastic information. This so-called broadline NMR technique fell out of favor a number of years ago because of its nonselective nature, but selective techniques and better instrumentation have reversed this trend. In particular, there are techniques available that use both ^{13}C (carbon 13) and ^1H (normal hydrogen) resonance to pinpoint the source of broad and narrow resonances. For example, Figure 7-13 shows this “two-dimensional” wide-line separation (WISE) technique applied to a modified polypropylene. A highly convoluted broadline spectrum for this mixture has been resolved by the WISE technique into peaks that can be easily assigned to the motions of proton-containing groups on the polypropylene and the additive.

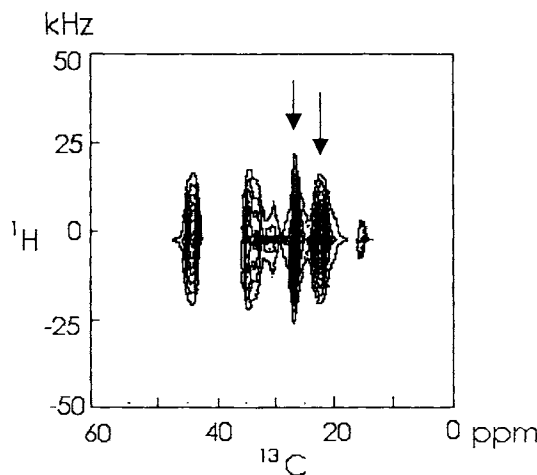


Figure 7-13. Crossplot of broadline ^1H and CP-MAS (narrow line) ^{13}C spectra for a 43% mixture of erucamide with i-PP. Erucamide is a fatty acid amide used with PP film to reduce adhesion of adjacent layers of film. The contours indicated by arrows are due to polypropylene -CH₃, >CH- and -CH₂- groups, respectively. This shows that the >CH- group at ~ 26 ppm on the ^{13}C resonance axis has the lowest mobility, as its proton resonance is the broadest. [Adapted from I. Quijada-Garrido, M. Wilhelm, H. W. Spiess, J. M. Barrales-Rienda, *Macromol. Chem. Phys.* **199**, 985 (1998). Copyright © 1998, Wiley Periodicals, Inc., A Wiley Company.]

With time-domain (pulsed) instruments, more direct observations of relaxation processes can be realized. The most common experiment is to polarize the system of spins and then remove or change the field, watching the spin system relax. The polarization is accomplished by exposing the material to a radio-frequency field at the resonance frequency of the spins, which populates the excited state. The very slight increase in the population of the high-energy state is reduced principally by two processes: coupling with neighboring spins precessing at the same frequency, and by random magnetic radiation produced by the lattice. If the material is rigid, the first process occurs rapidly because there are usually many properly aligned spins in the ground state that can couple with those in the excited state. The second process is much slower because of limited motions in the lattice.

The spin-spin relaxation time is given the symbol T_2 , whereas T_1 is used for the spin-lattice relaxation time. In the absence of field inhomogeneities, the theoretical expression for the line shape is Lorentzian and is given by the expression

$$g(f) \propto \frac{2T_2}{1 + [2\pi T_2(f - f_0)]^2} \quad (7-65)$$

where $g(f)$ is the intensity, f is the frequency, and f_0 is the frequency at maximum intensity. Our expectation is that the value of T_2 will be low in the glassy state and increase through the glass transition. Typical values range from about a second in low-viscosity melts to less than a millisecond in the glassy state. The process of spin-spin relaxation takes place on a time scale that reflects motions that are most efficient at removing the coupling between the spins. Typically for glassy polymers, there is an abrupt increase in T_2 through the glass transition, as shown in Figure 7-14.

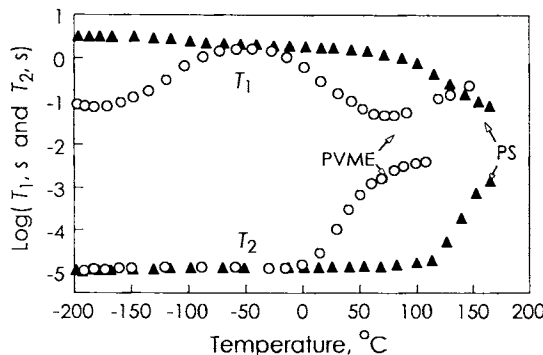


Figure 7-14. Changes in NMR spin-spin and spin-lattice relaxation times with temperature for a low- T_g polymer PVME and a high- T_g polymer PS. [Adapted with permission from T. K. Kwei, T. Nishi and R. F. Roberts, *Macromolecules*, 7, 667 (1974). Copyright 1974 American Chemical Society]

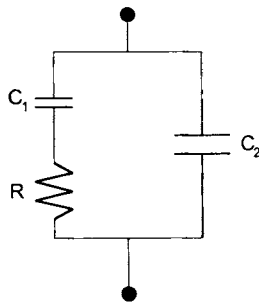
T_1 on the other hand, reflects the efficiency of the coupling of the spin with the lattice, which, it should be recalled, is the surrounding ensemble of material that can couple with the subject spin through any motions that produce electromagnetic waves of the resonant (Larmor) frequency. T_1 usually shows a minimum near the glass transition, or at the onset of any motion that produces additional interaction with the subject spin. This interaction promotes a return of the spin to its ground state, with a consequent loss of polarization signal. In Figure 7-14, T_1 for PVME also shows a shallow minimum at -180°C corresponding to the onset of motion of the methyl groups on the side chain of the PVME. At high temperatures, the two times approach each other.

The classical technique to find these two times is to subject the spin system to a magnetic pulse with the direction of the pulse at 180° to the primary field, that is, in the opposite direction. Such a pulse inverts the populations of the ground and excited states (parallel and antiparallel to the field, respectively). For this reason, the technique is referred to as inversion recovery. Measurement of the magnetization associated with the return to equilibrium gives T_1 . A 180° pulse can be followed by a pulse at 90° to induce a transverse magnetization. (This does not orient the dipoles at 90° , but merely biases the

phase of the precessing dipoles in the two allowed states.) The relaxation of the transverse magnetization, or more properly the dephasing of the dipoles, gives T_2 . These two experiments give their respective times by definition; the reason that they reflect spin-lattice and spin-spin processes in a distinct fashion is a more advanced subject, and the interested reader is referred to the appropriate literature including the references provided at the end of this chapter.¹⁸⁻²¹ In addition, one can also look at third time, called $T_{1\rho}$, which involves a more complex pulse and measurement scheme. $T_{1\rho}$ is useful for examining motions in the 10-100 kHz range. It should be noted that both T_1 and $T_{1\rho}$ can be found using cross-polarization, magic-angle spinning (CP-MAS) experiments on solid polymers. Again the reader should examine the references and similar literature for more details.

PROBLEMS

1. Consider an electrical circuit consisting of a capacitor and resistor in series and a second capacitor in parallel with the whole array.



Show that, for a step function in voltage, the capacitance of the circuit is

$$C(t) = (C_R - C_u)(1 - e^{-t/\tau}) + C_u$$

where

$$C_R = C_1 + C_2, \quad \tau = C_1 R, \quad \text{and} \quad C_u = C_2$$

2. Consider a freely jointed chain of N links, each having a dipole moment of magnitude μ_0 along the chain contour.

(a) In the absence of fixed valence angles and bond rotational potentials, calculate the mean square dipole moment of the chain, $\langle \mu^2 \rangle$.

(b) Repeat the calculation in (a) for a chain with tetrahedral (fixed) valence angles. What is the value of g for such a chain?

(c) If the chain in (b) possesses barriers to rotations about backbone bonds, what would be the qualitative effect on the value of g ?

244 DIELECTRIC AND NMR METHODS

- (d) If the barriers to rotation about the backbone bonds are such that a given bond can only assume rotation angles of $\pi/2$, π , and $3\pi/2$ with respect to the first bond in the chain, and the bond rotation potentials are independent of one another, what is the value of g and $\langle \mu^2 \rangle$?
3. Derive equation (7-56) from equation (7-28).
 4. It was shown that a "real" capacitor containing a dielectric behaves by itself like an RC circuit. Note the similarity between equations (7-8) and (7-23). If the real capacitor is regarded as a "black box," relate ε' and ε'' to the equivalent series capacitance, C_s , and resistance, R_s .
 5. Calculate the power dissipated as a function of ω for a Debye dielectric subjected to a sinusoidal voltage. $\omega = 2\pi f$
 6. Show that ε^* defined by equation (7-28) is formally identical to the compliance, D^* , of a Voigt element in series with a spring.
 7. Using the relationships developed in Problem 7-4, create Nyquist and Bode plots for the complex impedance Z^* of the circuit shown in Figure 7-1. You will need to use the relationship $Y^* = 1/Z^*$, where Y^* is the admittance. Finally develop the relationships between Z^* and ε^* for this circuit.
 8. (Computer) Using a scanner and the program TRACER.EXE in the CD, or an equivalent, digitize the data in Figure 7-6 and attempt to describe it the Cole-Cole relationship. Plot your results.

REFERENCES

1. V. V. Daniel, *Dielectric Relaxation*, Academic Press, New York, 1967.
2. P. Debye, *Polar Molecules*, Dover Publications, New York, 1945. (Originally published by Chemistry Catalog, New York, 1929)
3. L. Onsager, *J. Am. Chem. Soc.*, **58**, 1486 (1936).
4. C. P. Smyth, *Dielectric Behavior and Structure*, McGraw-Hill, New York, 1955.
5. N. G. McCrum, B. E. Read, and G. Williams, *Anelastic and Dielectric Effects in Polymeric Solids*, Wiley, London, 1967.
6. N. E. Hill, *Proc. Phys. Soc.*, **78**, 311 (1961).
7. H. Frölich, *Theory of Dielectrics*, 2nd ed., Oxford University Press, Oxford, 1958.
8. J. C. Maxwell, *Electricity and Magnetism*, Oxford University Press, Oxford, 1892.
9. K. W. Wagner, *Arch. Elektrotechn.* **2**, 371 (1914).
10. R. W. Sillars, *J. Inst. Electr. Engr.*, **80**, 378 (1937)
11. P. J. Flory, *Statistical Mechanics of Chain Molecules*, Interscience, New York, 1969.

12. P. Hedvig, *Dielectric Spectroscopy of Polymer*, Wiley (Halsted), New York, 1971.
13. A. R. Blythe, *Electrical Properties of Polymers*, Cambridge University Press, 1979.
14. R. H. Cole and K. S. Cole, *J. Chem. Phys.*, **9**, 341 (1941).
15. G. E. Johnson, E. W. Anderson, G. Z. Link, and D. W. McCall, *Bull. Chem. Phys. Soc.*, **19**(3), 266 (1974).
16. F. I. Mopsik, *Rev. Sci. Instr.* **55** 79 (1984).
17. C. Lavergne and C. Lacabanne, *IEEE Electr. Engr. Mag.* **9**(2), 5-21 (1993).
18. F. Bovey and P. Marau, *NMR of Polymers*, Academic, 1996.
19. V. J. McBrierty and K. J. Packer in *Nuclear Magnetic Resonance in Solid Polymers* (D. R. Clarke, S. Suresh and I. M. Ward, Eds.) Cambridge University Press; (1993).
20. K. Schmidt-Rohr and H. Spiess, *Multidimensional Solid-State NMR and Polymers*, Academic Press (1994).
21. M. H. Levitt, *Basics of Nuclear Magnetic Spin Resonance*, Wiley, New York, 2001.

Answers to Problems

CHAPTER 2

2-1. The shear strain wanted is given, according to equation (2-5), as

$$\gamma = \frac{\Delta X}{Y} = \frac{0.40 \text{ cm}}{2.0 \text{ cm}} = 0.20$$

At $t = 10^{-4}$, the compliance is numerically equal to 10^{-9} Pa^{-1} . Thus, making use of equation (2-30),

$$\sigma_0 = \frac{\gamma(t)}{J(t)} = \frac{0.20}{\left(10^{-9} + \frac{10^{-4}}{10^9}\right)} = 0.20 \times 10^9 \text{ Pa}$$

However, since the sample cross-sectional area, $X \times Y$, is $4 \text{ cm}^2 (4 \times 10^{-4} \text{ m}^2)$ the constant force necessary to observe this strain is

$$F_0 = \sigma_0(X \times Y) = 0.8 \times 10^5 \text{ N}$$

and division by g , the acceleration due to gravity (9.81 m/s^2), yields

$$m = F_0/g = 8.2 \times 10^3 \text{ kg}$$

Thus 8.2×10^3 kg (roughly 9 tons) placed on the sample pan in Figure 2-9 would cause the pointer to move down 0.40 cm in 10^{-4} s. Clearly all the apparatus is assumed to have an infinite modulus and inertial effects are ignored. Clearly, this is not the preferred way to run a shear creep experiment on such a polymer. Torsional deformation of a rod would be a much better choice.

2-2. Since G' and G'' are given, our problem is to express $\tan \delta$, $|G^*|$, $|J^*|$, J' and J'' in terms of these given parameters. Equation (2-39) gives

$$\tan \delta = \frac{G''}{G'}$$

The key to the other quantities is Equation (2-40)

$$G^* = G' + iG''$$

$$J^* = 1/G^* = J' - iJ''$$

which together give the relationship

$$J^* = 1/G^* = \frac{1}{G' + iG''}$$

Multiplying numerator and denominator by the complex conjugate $G' - iG''$ and separating the real and imaginary parts gives:

$$J^* = \frac{G'}{G'^2 + G''^2} - \frac{iG''}{G'^2 + G''^2}$$

Thus we have the answers for J' and J'' , and it remains to find the magnitudes. By definition of the magnitude of a complex variable, $|G^*| = [(G')^2 + (G'')^2]^{1/2}$, which in many math books would be referred to as simply $|G|$ where G is understood to be complex without the aid of the asterisk. As $J^* = 1/G^* = \gamma^*/\sigma^*$, we expect that the magnitudes will be reciprocally related, i.e., $|G^*| = 1/|J^*|$. To show this unquestionably, simply multiply out

$$|J^*|^2 = \left(\frac{G'}{G'^2 + G''^2} - \frac{iG''}{G'^2 + G''^2} \right) \left(\frac{G'}{G'^2 + G''^2} + \frac{iG''}{G'^2 + G''^2} \right)$$

The other parts of the question follow a similar pattern.

2-3. Equation (2-46) maybe restated as

$$\sigma_E(t) = \int_{-\infty}^t \frac{d\varepsilon(u)}{du} E(t-u) du \quad (a)$$

for a tensile experiment. The strain history, in terms of the variable u , is

$$-\infty < u \leq 0 \quad \frac{d\varepsilon(u)}{du} = 0$$

$$0 < u \leq t_1 \quad \frac{d\varepsilon(u)}{du} = k$$

$$t_1 < u \leq 2t_2 \quad \frac{d\varepsilon(u)}{du} = -k$$

$$2t_2 < u \leq t \quad \frac{d\varepsilon(u)}{du} = 0$$

where k is magnitude of the slope of the lines in the sketch. This strain history can be built into equation (a) to yield

$$\begin{aligned} \sigma_E(t) = & \int_0^{t_1} k [E_1 e^{-[(t-u)/\tau_1]} + E_2 e^{-[(t-u)/\tau_2]}] du \\ & + \int_{t_1}^{2t_2} (-k) [E_1 e^{-[(t-u)/\tau_1]} + E_2 e^{-[(t-u)/\tau_2]}] du \end{aligned}$$

which can be integrated to give

$$\sigma(t) = k \{ E_1 e^{-t/\tau_1} \tau_1 [2e^{t_1/\tau_1} - e^{2t_1/\tau_1} - 1] + E_2 e^{-t/\tau_2} \tau_2 [2e^{t_1/\tau_2} - e^{2t_1/\tau_2} - 1] \}$$

2-4. Mechanical work due to application of a force is defined as the integral of $f dl$ (technically $\vec{f} \cdot d\vec{l}$). Here we will consider work per unit volume. Thus

$$W = \int \frac{f dl}{V} = \int \frac{f}{A} \frac{dl}{l} = \int \sigma d\gamma$$

for a shear experiment. Now let

$$\sigma = \sigma_0 \cos \omega t$$

so that in-phase strain is

$$\gamma = \gamma_0 \cos \omega t$$

Substitution of these functions into equation (a) yields

$$W = \sigma_0 \gamma_0 \int_0^{2\pi} \cos \omega t \sin \omega t d(\omega t) = \sigma_0 \gamma_0 \left[\frac{1}{2} \sin^2 \omega t \right]_0^{2\pi}$$

which is zero. Thus the work done in going through one cycle of deformation (ωt goes from 0 to 2π) is zero if the stress and strain are in phase. All the work done on the sample in the first quarter of the cycle is recovered on the next quarter, etc.

For out-of-phase strain:

$$\gamma = \gamma_0 \sin \omega t$$

which yields for the integral work

$$W = \sigma_0 \gamma_0 \int_0^{2\pi} \cos \omega t \cos \omega t d(\omega t) = \sigma_0 \gamma_0 \left[\frac{1}{2} \omega t + \frac{1}{4} \sin 2\omega t \right]_0^{2\pi}$$

The second term is zero, but the first gives

$$W = \gamma_0 \sigma_0 \pi$$

Clearly work is done when the stress and strain are out of phase.

2-5. Equation (q) of Appendix 1 in Chapter 2 gives

$$\frac{1}{p^2} = L[G(t)]L[J(t)]$$

which is a statement of the relationship between $G(t)$ and $J(t)$ in transform space. The Laplace transform of the $J(t)$ given is

$$L[J(t)] = \frac{A\Gamma(1+m)}{p^{m+1}}$$

which yields, upon substitution into equation (q), the result for the transform of $G(t)$

$$L[G(t)] = \frac{1}{A\Gamma(m+1)p^{1-m}} \frac{\Gamma(1-m)}{\Gamma(1-m)}$$

the last multiplication term being added to facilitate return from transform space. Thus

$$G(t) = \frac{t^{-m}}{A\Gamma(m+1)\Gamma(1-m)}$$

Rearrangement and use of the expressions given in the problem yield the desired result.

2-6. Equation (q) of Appendix 1, Chapter 2, relates $G(t)$ and $J(t)$ in transform space.

$$\frac{1}{p^2} = L[G(t)]L[J(t)]$$

It is simple to solve in this space and then transform back

$$\begin{aligned} L[G(t)] &= \int_0^\infty e^{-pt} G(t) dt \\ &= \int_0^\infty e^{-pt} G_0 e^{-t/\tau} dt = G_0 \int_0^\infty e^{-(p+1/\tau)t} dt \\ &= G_0 \left(p + \frac{1}{\tau} \right)^{-1} \int_0^\infty e^{-x} dx = G_0 \left(p + \frac{1}{\tau} \right)^{-1} (-e^{-x}) \Big|_0^\infty \\ &= G_0 \left(p + \frac{1}{\tau} \right)^{-1} \end{aligned}$$

Thus

$$L[J(t)] = \frac{1}{p^2} \frac{1}{L[G(\tau)]} = \frac{(p+1/\tau)}{p^2 G_0} = \frac{1}{p G_0} + \frac{1}{p^2 G_0 \tau}$$

Transforming back into real space,

$$\begin{aligned} J(t) &= L^{-1} \frac{1}{p G_0} + L^{-1} \frac{1}{p^2 G_0 \tau} \\ &= \frac{1}{G_0} L^{-1} \left(\frac{1}{p} \right) + \frac{1}{\tau G_0} L^{-1} \frac{1}{p^2} \\ &= \frac{1}{G_0} + \frac{1}{G_0 \tau} t \\ \therefore J(t) &= \frac{1}{G_0} \left(1 + \frac{t}{\tau} \right) \end{aligned}$$

2-7. From equations (2-56) and (2-57) we know that

$$G'(\omega) = \omega \int_0^\infty \sin \omega s G(s) ds$$

$$G''(\omega) = \omega \int_0^\infty \cos \omega s G(s) ds$$

For this problem

$$\begin{aligned} G'(\omega) &= \omega \int_0^\infty \sin \omega s G_0 e^{-s/\tau} ds \\ &= G_0 \omega \int_0^\infty (\sin \omega s) e^{-s/\tau} ds \end{aligned}$$

$$\boxed{\int_0^\infty e^{-ax} \sin mx dx = \frac{m}{a^2 + m^2}}$$

$$G(\omega) = \frac{G_0 \omega^2}{(1/\tau)^2 + \omega^2} = G_0 \frac{\omega^2 \tau^2}{1 + \omega^2 \tau^2}$$

also

$$\begin{aligned} G''(\omega) &= \omega \int_0^\infty \cos \omega s G_0 e^{-s/\tau} ds \\ &= \omega G_0 \int_0^\infty (\cos \omega s) e^{-s/\tau} ds \end{aligned}$$

$$\boxed{\int_0^\infty e^{-ax} \cos mx dx = \frac{a}{a^2 + m^2}}$$

$$G''(\omega) = \frac{\omega G_0 1/\tau}{(1/\tau)^2 + \omega^2} = \frac{G_0 \omega \tau}{1 + \omega^2 \tau^2}$$

2-8.

$$G^* \equiv \frac{\sigma^*}{\gamma^*} = \frac{\sigma_0 e^{i(\omega t + \delta)}}{\gamma_0 e^{i\omega t}} = \frac{\sigma_0 e^{i\delta}}{\gamma_0}$$

but $e^{ix} = \cos x + i \sin x$ so that

$$G^* = \frac{\sigma_0}{\gamma_0} (\cos \delta + i \sin \delta)$$

However, $G^* = G + iG''$, and we have:

$$G = \frac{\sigma_0}{\gamma_0} \cos \delta \quad \text{and} \quad G'' = \frac{\sigma_0}{\gamma_0} \sin \delta$$

2-9.

$$\eta^* = \frac{\sigma^*}{d\varepsilon^*/dt}$$

For a dynamic experiment, $\varepsilon^* = \varepsilon_0 e^{i\omega t}$

$$\therefore \frac{d\varepsilon^*}{dt} = \varepsilon_0 i\omega e^{i\omega t} = i\omega \varepsilon^*$$

$$\eta^* = \frac{\sigma^*}{i\omega \varepsilon^*}$$

But

$$G^* = \frac{\sigma^*}{\varepsilon^*}$$

and

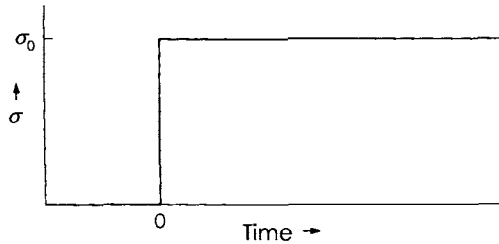
$$\begin{aligned}\eta^* &= \frac{G^*}{i\omega} = \frac{-iG^*}{\omega} \\ \eta^* &= \eta' - i\eta'' = \frac{-iG^*}{\omega} = \frac{-i}{\omega}(G - iG'') = \frac{-iG}{\omega} + \frac{G'}{\omega}\end{aligned}$$

Thus

$$\eta' = \frac{G'}{\omega} \quad \text{and} \quad \eta'' = \frac{G}{\omega}$$

2-10.

$$\gamma(t) = \int_{-\infty}^t \frac{d\sigma(u)}{du} J(t-u) du \quad (2-45)$$



At time zero, the stress is instantaneously increased from 0 to σ_0 .

To observe how the delta function works, consider

$$\sigma(t) = \int_{-\infty}^t \frac{d\sigma(u)}{du} du$$

as the normal relationship between the stress and stress rate. For an instantaneously applied stress with an infinite stress rate we may write

$$\sigma(t) = \int_{-\infty}^t \delta(u) \sigma_0 du$$

where $\delta(u)$ is the Dirac delta function. According to the definition of this function given in the equation

$$\sigma(t) = 0 \quad t < 0$$

$$\sigma(t) = \sigma_0 \quad t \geq 0$$

Similarly for equation (2-27):

$$\gamma(t) = \int_{-\infty}^t \delta(u) \sigma_0 J(t-u) du$$

For all $t > 0$ this becomes

$$\gamma(t) = \sigma_0 J(t)$$

or

$$J(t) = \frac{\gamma(t)}{\sigma_0} \quad (2-30)$$

2-11. Leibnitz's rule for differentiation of an integral is:

$$\boxed{\frac{d}{da} \int_p^q f(x, a) dx = \int_p^q \frac{\partial}{\partial a} [f(x, a)] dx + f(q, a) \frac{dq}{da} - f(p, a) \frac{dp}{da}}$$

$$\begin{aligned}\sigma_E(t) &= \int_{-\infty}^t \frac{d\varepsilon(u)}{du} E(t-u) du \\ \frac{d}{dt} \sigma_E(t) &= \frac{d}{dt} \int_{-\infty}^t \frac{d\varepsilon(u)}{du} E(t-u) du \\ \dot{\sigma}_E(t) &= \int_{-\infty}^t \frac{\partial}{\partial t} \left[\frac{d\varepsilon(u)}{du} E(t-u) \right] du + \frac{d\varepsilon(t)}{dt} E(0) \\ \text{if } \frac{d\varepsilon(t)}{dt} &= \begin{cases} k \text{ for } t \geq 0 \\ 0 \text{ for } t < 0 \end{cases} \\ \dot{\sigma}_E(t) &= \int_0^t k \frac{\partial}{\partial t} [E(t-u)] du + kE(0)\end{aligned}$$

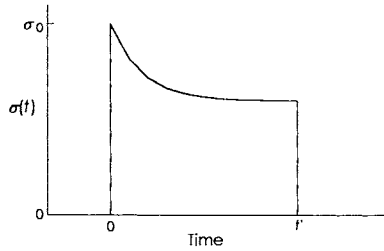
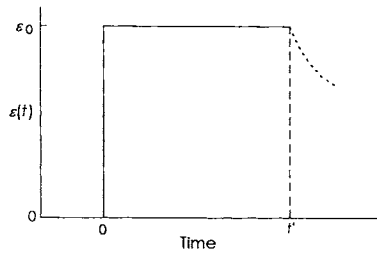
But

$$\begin{aligned}\frac{\partial}{\partial t} E(t-u) &= \frac{dE(t-u)}{d(t-u)} \frac{\partial(t-u)}{\partial t} = \frac{dE(t-u)}{d(t-u)} \\ \therefore \sigma_E(t) &= \int_0^t k \frac{dE(t-u)}{d(t-u)} du + kE(0)\end{aligned}$$

or

$$\begin{aligned}\dot{\sigma}_E(t) &= \int_0^t -kd(E(t-u)) + kE(t-u) \Big|_0^t + kE(0) \\ &= -kE(0) + kE(t) + kE(0) \\ \frac{\dot{\sigma}_E}{\dot{\varepsilon}} &= \frac{dE(t)}{d\varepsilon} = E(t)\end{aligned}$$

2-12. This will be done in two steps utilizing different forms of the Boltzmann principle.



(a)

$$u < 0 \quad \sigma(u) = 0$$

$$0 \leq u \leq t' \quad \sigma(u) = \varepsilon_0 E(u)$$

$$t' < u \quad \sigma(u) = 0$$

Starting off with equation (p), Appendix 1 of Chapter 2, an expression for the Boltzmann principle in Laplace space,

$$L[\sigma(t)] = p L[\varepsilon(t)] L[E(t)]$$

$$L[\varepsilon(t)] = \frac{1}{p} \frac{L\sigma(t)}{L[E(t)]}$$

But $L[F(t)] = \int_0^\infty e^{-pt} F(t) dt$, so

$$L[\sigma(t)] = \int_0^\infty e^{-pt} \sigma(t) dt = \int_0^{t'} \varepsilon_0 E(t) e^{-pt} dt = \int_0^{t'} \varepsilon_0 E_0 e^{-t/\tau} e^{-pt} dt$$

$$= \varepsilon_0 E_0 \int_0^\infty e^{-(p+1/\tau)t} dt = \frac{\varepsilon_0 E_0}{p+1/\tau} (-e^{-x})_0^{t'(p+1/\tau)}$$

$$= \frac{E_0 \varepsilon_0}{p+1/\tau} [1 - e^{-t'(p+1/\tau)}]$$

$$L[E(t)] = \int_0^\infty e^{-pt} E_0 e^{-t/\tau} dt = E_0 \int_0^\infty e^{-(p+1/\tau)t} dt = \frac{E_0}{p+1/\tau}$$

$$\begin{aligned}\therefore L[\varepsilon(t)] &= \frac{1}{p} \frac{L\sigma(t)}{L[E(t)]} = \frac{[E_0\varepsilon_0/(p+1/\tau)][1-e^{-t'(p+1/\tau)}]}{pE_0/(p+1/\tau)} \\ &= \frac{\varepsilon_0}{p}[1-e^{-t'(p+1/\tau)}] \\ &= \frac{\varepsilon_0}{p} - \frac{\varepsilon_0}{p}e^{-t'(p+1/\tau)} = \frac{\varepsilon_0}{p} - \frac{\varepsilon_0}{p}e^{-t'p}e^{-t'/\tau}\end{aligned}$$

Taking inverse transforms,

$$\varepsilon(t) = \varepsilon_0 - \varepsilon_0 e^{-t'/\tau} L^{-1}\left(\frac{e^{-pt'}}{p}\right)$$

From tables,

$$L^{-1}\left[\frac{e^{-ks}}{s^u}\right] = \begin{cases} 0 & \text{when } 0 < t < k \\ \frac{(t-k)^{u-1}}{\Gamma(u)} & \text{when } t > k \end{cases} \quad \text{for } u > 0$$

In our case $u = 1$, which is greater than zero. Also $k = t'$ and $t > t'$ always, since we are interested in strains after the stress relaxation experiment. Thus, the general situation holds and

$$\varepsilon(t) = \varepsilon_0 - \varepsilon_0 e^{-t'/\tau} \left[\frac{(t-t')^0}{\Gamma(1)} \right]$$

$$(t-t')^0 = 1 \quad \text{and} \quad \Gamma(1) = 0! \equiv 1$$

Thus,

$$\varepsilon(t) = \varepsilon_0(1 - e^{-t'/\tau})$$

(b) The other technique involves transforming $\varepsilon(t)$ and to $D(t)$ via the techniques used in Problem 2-6, and then using a more familiar form of the Boltzmann principle such as that given in equation (2-45). (To simplify the nomenclature, the symbol σ will signify the tensile stress σ_E .)

A modulus of the form $E(t) = E_0 e^{-ut}$ corresponds to a compliance $D(t) = 1/E_0 + t/E_0\tau$. Thus, using equation (2-45), adopted for tension, we get:

$$\varepsilon(t) = \int_{-\infty}^t \frac{d\sigma(u)}{du} D(t-u) du$$

$$\varepsilon(t) = \sigma_0 D(t) + \int_0^t \frac{d\sigma(u)}{du} D(t-u) du - \sigma(t') D(t-t')$$

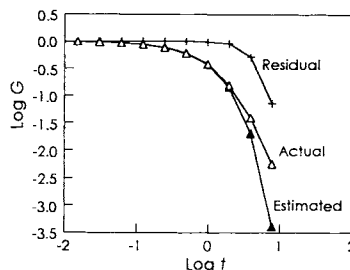
The first and last terms arise from the fact that step stresses of σ_0 at 0 and $-\sigma(t')$ at t' are applied to the sample. When $0 < u < t'$, $\sigma(u) = \varepsilon_0 E_0 e^{-u/\tau}$ so that $d\sigma(u)/du = -(\varepsilon_0 E_0 / \tau) e^{-u/\tau}$ and

$$\begin{aligned} \varepsilon(t) &= \sigma_0 \left(\frac{1}{E_0} + \frac{t}{E_0 \tau} \right) + \int_0^{t'} \left(-\frac{\varepsilon_0 E_0}{\tau} \right) e^{-u/\tau} \left[\frac{1}{E_0} + \frac{t-u}{\tau E_0} \right] du \\ &\quad - \varepsilon_0 E_0 e^{-t'/\tau} \left[\frac{1}{E_0} + \frac{t-t'}{\tau E_0} \right] \end{aligned}$$

Recognizing that $\sigma_0/E_0 = \varepsilon_0$, factorization of ε_0 gives

$$\begin{aligned} \varepsilon(t) &= \varepsilon_0 \left[1 + \frac{t}{\tau} - \left(1 + \frac{t-t'}{\tau} \right) e^{-t'/\tau} - \int_0^{t'} e^{-u/\tau} \left(1 + \frac{t}{\tau} - \frac{u}{\tau} \right) \frac{du}{\tau} \right] \\ &= \varepsilon_0 \left[1 + \frac{t}{\tau} - \left(1 + \frac{t-t'}{\tau} \right) e^{-t'/\tau} - \int_0^{t'/\tau} e^{-x} dx - \frac{t}{\tau} \int_0^{t'/\tau} e^{-x} dx + \int_0^{t'/\tau} x e^{-x} dx \right] \\ &= \varepsilon_0 \left[1 + \frac{t}{\tau} - \left(1 - \frac{t-t'}{\tau} \right) e^{-t'/\tau} + e^{-x} \Big|_0^{t'/\tau} + \frac{t}{\tau} e^{-x} \Big|_0^{t'/\tau} - e^{-x} (1+x) \Big|_0^{t'/\tau} \right] \\ \varepsilon(t) &= \varepsilon_0 (1 - e^{-t'/\tau}) \end{aligned}$$

2-13. The expressions for the components of the dynamic modulus for a Maxwell model are given in connection with Problem 2-7. It is convenient in view of the problem equation to space the calculated values by factors of 2. A depiction of a typical result, in dimensionless form, is:



2-14. Start with equation (2-51)

$$t = \int_0^t G(s) J(t-s) ds$$

For the first step

$$\Delta t = \int_0^{\Delta t} G(s) J(\Delta t - s) ds \approx \frac{1}{2} \Delta t [G(\Delta t) J(0) + G(0) J(\Delta t)]$$

Solving for $G(\Delta t)$ gives:

$$G(\Delta t) = [2 - G(0)J(\Delta t)]/J_0$$

For the second point at time $2 \Delta t$

$$G(2\Delta t) = [4 - 2G(\Delta t)J(\Delta t) - G(0)J(2\Delta t)]/J_0$$

and, in general,

$$G(n\Delta t) = \frac{1}{J_0} \left[2n - G(0)J(n\Delta t) - 2 \sum_{i=1}^{n-1} G(i\Delta t)J[(n-i)\Delta t] \right]$$

The difficult aspect of this expression is the evaluation of the sum, as there is one forward-running index, and one going backward. However, because of the simplicity of the expression for $J(t)$, we see that the sum can split into two parts to give the working expression

$$G(n\Delta t) = \frac{1}{J_0} \left[2n - G(0)J(n\Delta t) - 2J(n\Delta t) \sum_{i=1}^{n-1} G(i\Delta t) + 2a\Delta t \sum_{i=1}^{n-1} iG(i\Delta t) \right]$$

where $J_0 = a = 10^{-9}$. To control numerical error, the complete answer will vary Δt .

2-15. (a) Shear strain γ is the gradient of displacement. For torsion, the displacement of the material next to the turning disk is in the θ direction and is simply $r\theta$, where r is the distance out from the center of the disk. Assuming that the material in layers below the turning disk displace in a proportional fashion, the displacement in general will be $r\theta z/h$, where z is the distance away from the stationary plate, and h is the gap. The displacement gradient is then just the derivative of this with respect to z , or $r\theta/h$.

(b) Regarding the torque as force times a lever arm, we can equate the force produced by each annular shell at radius r to $\sigma_{21}(r) \times 2\pi r dr$, where σ_{21} is the shear stress produced by the material in that shell. The lever arm is just r . Integrating over r gives:

$$M = 2\pi \int_0^R \sigma_{21}(r) r^2 dr$$

In terms of the shear modulus, $\sigma_{21}(r) = G\gamma(r)$ if the modulus is independent of strain. Substituting this in the previous equation gives:

$$M = 2\pi \int_0^R G\gamma(r) r^2 dr = 2\pi G \int_0^R (r\theta/h) r^2 dr = 2\pi G\theta/h \int_0^R r^3 dr$$

Integration of the last expression gives finally $M = \pi R^4 G\theta/2$.

(c) The needed expression can be deduced from above by simply recognizing that $\sigma_{21}(r) = G[\gamma(r)]\gamma(r)$.

(d) The Gaussian integration of a moment expression, such as for the torque as shown above, is of the form:

$$\int_0^1 x^k f(x) dx \approx \sum_{i=1}^n w_i f(x_i)$$

It is necessary to put the equation for the torque in this form; the result is:

$$M = 2\pi \int_0^R \sigma_{21}(r) r^2 dr = 2\pi R^3 \int_0^1 \sigma_{21}(r/R)(r/R)^2 d(r/R)$$

For $k = 2$ and $n = 1$, the weighting factor $w_1 = 1/3$, and the location $x_1 = 3/4$. Thus

$$M \approx 2\pi R^3 \sigma_{21}(3/4)/3$$

Note that $\sigma_{21}(3/4) = G(3/4)\gamma(3/4)$, that is the stress at each radial position is given by the known shear strain at this point times an unknown modulus. If we define $\gamma_R \equiv R\theta/h$ and the apparent modulus as $G_{R,A} \equiv 2M/\pi R^4 \theta$, then

$$M = \pi R^4 G_{R,A} \theta/2$$

Equating these two expressions and recognizing that $\gamma^{(3/4)} = 3\gamma_R/4$, then

$$G^{(3/4)} \approx G_{R,A}$$

In other words, an approximation to the actual modulus at a strain of $3/4\gamma_R$ is simply the apparent linear modulus. By replacing the stress in the integral with the modulus and the strain, then the integral is the type $k = 3$. The first-order approximation to this integral is then $G(0.8) \approx G_{R,A}$, which might be regarded as slightly more accurate for small deviations from linearity.

2-16. We adopt the convention that the sample is clamped at $x = 0$ and is pulled at $x = L(t)$ with velocity v_A , the applied velocity. We can see that the velocity at any place along the sample will then be:

$$v = v_A x / L = v_A x / (L_0 + v_a t)$$

Thus we have a strain rate $\dot{\epsilon} = v_A / L$ that is decreasing with time. For convenience, we also define a nominal strain rate $\dot{\epsilon}_0 = v_A / L_0$. Starting with equation (2-46) and keeping the 3-dimensional aspect of the sample strictly in mind, we have:

$$\sigma_E(t) = \sigma_{xx}(t) - \sigma_{yy}(t) = \int_{-\infty}^t \left(\frac{\partial \gamma_{xx}(s)}{\partial s} - \frac{\partial \gamma_{yy}(s)}{\partial s} \right) G(t-s) ds$$

for the time-dependent stress. As both of these strain derivatives will be zero in the interval from $-\infty$ to 0, the only contribution to the stress will be from deformations from 0 to time t . The values of the strains are given by equation (2-18), whereupon observing the respective subscripts gives

$$\gamma_{xx} = \frac{\partial u_x}{\partial x_x} + \frac{\partial u_x}{\partial x_x} = 2 \frac{\partial u_x}{\partial x_x}$$

The displacement u_x is the amount each original point has moved at time t . This amount of motion will be

$$u_x = \int_0^t v_x(t') dt' = \int_0^t v_A x / L(t') dt' = v_A x \int_0^t dt' / [L_0 + v_A t'] = x \ln(1 + \dot{\epsilon}_0 t)$$

To preserve volume, the displacements in the y (transverse) direction will be $1/2$ this amount. The time-dependent strains then become:

$$\gamma_{xx} = 2 \ln(1 + \dot{\epsilon}_0 t) \quad \text{and} \quad \gamma_{yy} = -\ln(1 + \dot{\epsilon}_0 t)$$

The time derivatives (strain rates) are then

$$\dot{\gamma}_{xx} = 2\dot{\varepsilon}_0 / (1 + \dot{\varepsilon}_0 t) \quad \text{and} \quad \dot{\gamma}_{yy} = -\dot{\varepsilon}_0 / (1 + \dot{\varepsilon}_0 t)$$

When placed in the integral we have the result for stress growth of a viscoelastic sample in a tensile-testing machine.

$$\sigma_E(t) = 3\dot{\varepsilon}_0 \int_0^t (1 + \dot{\varepsilon}_0 s)^{-1} G(t-s) ds$$

While we might integrate this with our chosen relaxation function, it is much easier to simply differentiate the integral directly, using Leibnitz's rule, to get the modulus. This is not difficult because all time dependence can be factored out of the integral. Putting this all into place we have finally:

$$E_y = d\sigma_E[\varepsilon(t)]/d\varepsilon|_{\varepsilon \rightarrow 0} = \frac{d}{dt} \{3\dot{\varepsilon}_0 \int_0^t (1 + \dot{\varepsilon}_0 u)^{-1} G_0 e^{-(t-u)/\tau} du\} / (d\varepsilon/dt)$$

Simplifying gives:

$$E_y = \frac{d}{dt} \{3\dot{\varepsilon}_0 G_0 e^{-t/\tau} \int_0^t (1 + \dot{\varepsilon}_0 u)^{-1} e^{u/\tau} du\} / (d\varepsilon/dt)$$

$$E_y = 3\dot{\varepsilon}_0 G_0 e^{-t/\tau} [e^{u/\tau} (1 + \dot{\varepsilon}_0 u)^{-1}]_{u=t} / \dot{\varepsilon}_0$$

As can be seen, as generates the familiar $E_y = 3G_0$ as t goes to zero. Thus, if one is able to measure accurately the slope at $t = 0$, the result is Young's modulus for this type of test.

CHAPTER 3

3-1. Figure 3-3c is a plot of the relaxation behavior of a Maxwell body on a log-log scale. Thus we want to calculate

$$\frac{d \ln E(t)}{d \ln t}$$

where

$$E(t) = E e^{-t/\tau}$$

However,

$$\ln E(t) = \ln E - \frac{t}{\tau}$$

and since

$$\frac{d \ln E(t)}{d \ln t} = \frac{td \ln E(t)}{dt}$$

$$\frac{d \ln E(t)}{d \ln t} = -\frac{t}{\tau}$$

which approaches $-\infty$ for $t \gg \tau$. This is a characteristic of fluids.

3-2 and 3-3. As an example, we will work with $E'(\omega)$ for a Maxwell body:

(a) Equations (2-56) and (2-57) written for tension give

$$E'(\omega) = \omega \int_0^{\infty} \sin \omega s E(s) ds$$

$$E'(\omega) = \omega \int_0^{\infty} \sin \omega s E e^{-s/\tau} ds$$

which integrates to

$$E'(\omega) = \frac{E \omega^2 \tau^2}{1 + \omega^2 \tau^2}$$

(b) Starting with equation (3-6) we find

$$E \varepsilon_0 \int_{t_1}^{t_2} e^{t/\tau} \cos \omega t dt = \int_{\sigma(t_1)e^{t_1/\tau}}^{\sigma(t_2)e^{t_2/\tau}} d(e^{t/\tau})$$

on assuming that

$$\varepsilon(t) = \varepsilon_0 \sin \omega t$$

This expression integrates to

$$\begin{aligned} \sigma(t_2) - \sigma(t_1) e^{(t_1-t_2)/\tau} &= \frac{E \omega \varepsilon_0}{1/\tau^2 + \omega^2} \left[\frac{1}{\tau} \cos \omega t_2 + \omega \sin \omega t_2 \right. \\ &\quad \left. - e^{(t_1-t_2)/\tau} \left(\frac{1}{\tau} \cos \omega t_1 + \omega \sin \omega t_1 \right) \right] \end{aligned}$$

Because our result must be independent of the starting time t_1 , and the present time t_2 ($E'(\omega)$ is not a function of t) let $t_2 \rightarrow \infty$. Then

$$\sigma(t_2) = \frac{E \omega \varepsilon_0}{1/\tau^2 + \omega^2} \left(\frac{1}{\tau} \cos \omega t_2 + \omega \sin \omega t_2 \right) \quad (1)$$

or

$$E'(\omega) = \frac{E\omega^2\tau^2}{1+\omega^2\tau^2}$$

3-4. Here we can start with equation (1) of the answer for Problem 3-2 with added subscripts.

$$\sigma_i(t_2) = \frac{E_i\omega\varepsilon_0}{1/\tau_i^2 + \omega^2} \left(\frac{1}{\tau_i} \cos \omega t_2 + \omega \sin \omega t_2 \right)$$

This expression can be separated into an in-phase part σ'_i and an out-of-phase part σ''_i , as follows:

$$\sigma'_i(t_2) = \frac{E_i\omega\varepsilon_0}{1/\tau_i^2 + \omega^2} (\omega \sin \omega t_2)$$

$$\sigma''_i(t_2) = \frac{E_i\omega\varepsilon_0}{1/\tau_i^2 + \omega^2} \left(\frac{1}{\tau_i} \cos \omega t_2 \right)$$

Now the total in-phase stress considering all elements is just

$$\sigma'(t_2) = \sum_i \frac{E_i\omega^2\varepsilon_0}{1/\tau_i^2 + \omega^2} (\omega \sin \omega t_2)$$

Here the quantity in parentheses merely expresses the phase of the response (in phase) and we may write immediately:

$$E'(\omega) = \sum_i \frac{E_i\omega^2}{1/\tau_i^2 + \omega^2} = \sum_i \frac{E_i\omega^2\tau_i^2}{1 + \omega^2\tau_i^2}$$

Similarly, for the out-of-phase response,

$$\sigma''(t_2) = \sum_i \frac{E_i\omega\varepsilon_0}{1/\tau_i^2 + \omega^2} \left(\frac{1}{\tau_i} \cos \omega t_2 \right)$$

Here $\cos \omega t_2$ just stipulates out-of-phase response and

$$E''(\omega) = \sum_i \frac{E_i\omega\tau_i}{1 + \omega^2\tau_i^2}$$

Then according to equation (2-22) written for tension:

$$E^*(\omega) = \sum_i \frac{E_i \omega^2 \tau_i^2}{1 + \omega^2 \tau_i^2} + i \sum_i \frac{E_i \omega \tau_i}{1 + \omega^2 \tau_i^2}$$

Clearly such sums are difficult to invert analytically.

3-5. Here we can write

$$\frac{d\varepsilon_1}{dt} = \frac{1}{E_1} \frac{d\sigma_1}{dt} + \frac{\sigma_1}{\eta_1}$$

$$\frac{d\varepsilon_i}{dt} = \frac{1}{E_i} \frac{d\sigma_i}{dt} + \frac{\sigma_i}{\eta_i}$$

$$\frac{d\varepsilon_z}{dt} = \frac{1}{E_z} \frac{d\sigma_z}{dt} + \frac{\sigma_z}{\eta_z}$$

These expressions simplify considerably, since:

$$\sigma_1 = \sigma_2 = \dots = \sigma_i = \dots = \sigma_z$$

and

$$\sum_{i=1}^z \frac{d\varepsilon_i}{dt} = \frac{d\varepsilon}{dt}$$

Thus

$$\frac{d\varepsilon}{dt} = \frac{d\sigma}{dt} \sum_{i=1}^z \frac{1}{E_i} + \sigma \sum_{i=1}^z \frac{1}{\eta_i}$$

Defining

$$\frac{1}{E_h} = \sum_{i=1}^z \frac{1}{E_i}$$

$$\frac{1}{H} = \sum_{i=1}^z \frac{1}{\eta_i}$$

this equation becomes:

$$\frac{d\varepsilon}{dt} = \frac{1}{E_h} \frac{d\sigma}{dt} + \frac{\sigma}{H}$$

which is solvable in the usual way.

3-6. (a) Equation (3-83) can be rearranged to give

$$\rho a^2 z^2 = \frac{36}{N} \eta$$

Since all of the terms on the left side are parameters relating to the model itself and not to the specific experimental conditions, this result may be substituted into the expression for τ_p in the problem to give the desired result.

(b) Table 3-2 gives an expression for the tensile creep compliance of a Voigt-Kelvin Model as

$$D(t) = \sum_{p=1}^z D_p (1 - e^{-t/\tau_p})$$

Comparison of this expression with that in the problem yields the result that

$$D_p = \frac{8}{3NkT\pi^2} \frac{1}{p^2}$$

3-7. First let us investigate the values of $E''(\omega)$ and ω at the maximum of a $\log E''(\omega)$ versus $\log \omega$ curve for a single Maxwell element.

$$\log E''(\omega) = \log E + \log \omega + \log \tau - \log(1 + \omega^2 \tau^2)$$

$$\frac{d \log E''(\omega)}{d \log \omega} = 1 - \frac{2\omega^2 \tau^2}{1 + \omega^2 \tau^2}$$

At the maximum this slope is zero and ω is found to equal $1/\tau$. Substitution of this result into the defining equation for $E''(\omega)$ shows that

$$E''(\omega) = \frac{E}{2}$$

at the maximum. Thus

$$\tau_1 = 10^{-2} \quad \text{and} \quad E_1 = 4 \times 10^6$$

$$\tau_2 = 10^{-9} \quad \text{and} \quad E_2 = 2 \times 10^{10}$$

3-8. From equations (3-90) and (4-7)

$$\eta = \int_{-\infty}^{\infty} t G(t) d \ln t = \int_0^{\infty} G(t) dt \quad (4-7)$$

For a Maxwell-Wiechert model:

$$\eta = \int_0^{\infty} \sum_{i=1}^z G_i e^{-t/\tau_i} dt$$

$$\eta = \sum_{i=1}^z G_i \int_0^{\infty} e^{-t/\tau_i} dt$$

$$= \sum_{i=1}^z G_i \tau_i$$

3-9.

$$E(t) = \sum_{p=1}^z E_p e^{-t/\tau_p}$$

$$\approx E_p \int_{p=1}^z e^{-tp/\tau_{\max}} dp$$

$$\approx E_p \frac{\tau_{\max}}{t} (e^{-t/\tau_{\max}} - e^{-t/\tau_{\min}})$$

If $\tau_{\min} < t < \tau_{\max}$, the quantity in parentheses is close to 1 and relatively constant. Thus

$$\frac{d \ln E(t)}{d \ln t} = -1$$

3-10.

Equation (3-42) defines $H(\tau)$ as

$$E(t) = \int_0^{\infty} \frac{H(\tau)}{\tau} e^{-t/\tau} d\tau = \int_{-\infty}^{+\infty} H(\tau) e^{-t/\tau} d \ln \tau \quad (3-42)$$

For $\tau \ll t$, the exponential is ~ 0.0 whereas for $\tau \gg t$, it is ~ 1.0 . If the exponential is approximated by a step function from 0.0 to 1.0 at $t = \tau$, we have

$$E(t) \approx \int_{\ln t}^{\infty} H(\tau) d \ln \tau$$

Furthermore,

$$E(t + \Delta) - E(t) \approx - \int_{\ln t}^{\ln t + \Delta} H(\tau) d \ln \tau \approx H(t) \Big|_{t=\tau} (\ln t + \Delta - \ln t)$$

or, in the limit $\Delta \rightarrow 0$,

$$\left. \frac{-dE(t)}{d \ln t} \right|_{t=\tau} \approx H(\tau) \equiv H_1(\tau)$$

3-11(a)

$$E(t) = E_0 e^{-t/\tau_m}$$

where the subscript m is included to remind us that the relaxation time is constant:

$$\frac{dE(t)}{d \ln t} = \frac{tdE(t)}{dt} = - \frac{tE_0 e^{-t/\tau_m}}{\tau_m}$$

$$H_1(\tau) \equiv \left. \frac{dE(t)}{d \ln t} \right|_{t=\tau} = \frac{\tau}{\tau_m} E_0 e^{-\tau/\tau_m}$$

which is plotted below.

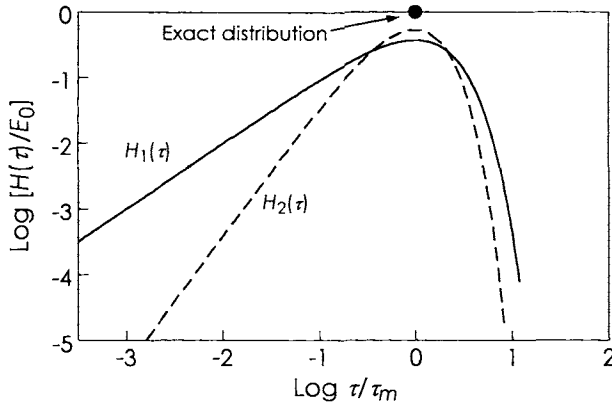
(b) For H_2

$$\frac{d}{d \ln t} \left(\frac{dE(t)}{d \ln t} \right) = \frac{td(dE(t)/d \ln t)}{dt} = t \left(-\frac{E_0}{\tau_m} e^{-t/\tau_m} + \frac{tE_0}{\tau_m^2} e^{-t/\tau_m} \right)$$

$$H_2(t) = \left(E_0 \frac{t}{\tau_m} e^{-t/\tau_m} - E_0 \frac{t}{\tau_m} e^{-t/\tau_m} + \frac{t^2}{\tau_m^2} E_0 e^{-t/\tau_m} \right)_{t=2\tau}$$

$$= 4E_0 \left(\frac{\tau}{\tau_m} \right)^2 e^{-2\tau/\tau_m}$$

which is also plotted in the figure.



3-14. The relationship between viscosity and relaxation modulus is given by equation (3-90) and (4-7). For the latter

$$\eta = \int_0^\infty G(t)dt \quad (4-7)$$

which for the chosen modulus function gives:

$$\eta = G_0 \int_0^\infty \frac{1}{(1+t/\tau)^n} dt$$

For $n = 1$, this gives the log function, which is unbounded, so n must be greater than 1. Substituting $x = (1 + t/\tau)$ gives the form

$$\eta = \tau G_0 \int_1^\infty \frac{dx}{x^n}$$

which can be easily integrated to give:

$$\eta = -\frac{1}{n-1} \tau G_0 \left[\frac{1}{x^{n-1}} \right]_1^\infty$$

Thus, if $n > 1$, the viscosity is finite with a value of

$$\eta = \tau G_0 / (n-1)$$

3-15. The slopes are easily calculated by taking derivatives of the appropriate expressions and examining the limiting behavior. As the Rouse function is a sum of Maxwell elements, it will behave in the same fashion in the limit. For the KWW function

$$G(t) = G_0 \exp[-(t/\tau)^\beta] \quad (3-106)$$

the derivative with time is:

$$\frac{dG(t)}{dt} = -\frac{\beta G_0}{\tau} (t/\tau)^{\beta-1} e^{-(t/\tau)^\beta}$$

which is infinite at $t = 0$ if $\beta < 1$ (the usual situation). However, the slope of the log-log relationship at $t = 0$ will be zero.

3-16. The isochronal stress-strain curve can be found by analysis of the stress-growth function $\sigma(t;\dot{\gamma})$ as given by the Boltzmann superposition relationship of equation (2-46). For a generalized Maxwell model, the result is the familiar

$$\sigma(t;\dot{\gamma}) = \dot{\gamma} \sum_{i=1}^N G_i \tau_i (1 - e^{-t/\tau_i})$$

As the strain rate is constant, we can express the stress as:

$$\sigma(t;\gamma) = \gamma \left(\frac{\sum_{i=1}^N G_i \tau_i (1 - e^{-t/\tau_i})}{t} \right)$$

The quantity in the brackets is a function of time only, so will be a constant for the isochronal stress-strain experiment. Thus the isochronal stress-strain curve for a linear material will be straight.

The isochronal modulus will be the slope of the stress-strain response, and thus equal to the term in the brackets. As $t \rightarrow 0$, the exponential can be expanded to show that the slope is simply:

$$G_0 = \sum_{i=1}^N G_i$$

(b) The stress growth, creep and stress relaxation expressions for the single Maxwell model are:

$$\begin{aligned}\sigma(t) &= G\dot{\gamma}_0\tau(1 - e^{-t/\tau}) = \gamma \frac{G(1 - e^{-t/\tau})}{t/\tau} \\ \gamma(t) &= \frac{\sigma_0}{G}(1 + t/\tau), \quad \text{or} \quad \sigma_0 = \gamma(t) \frac{G}{1 + t/\tau} \\ \sigma(t) &= \gamma_0 G e^{-t/\tau}\end{aligned}$$

It is evident from these expressions that the isochronal stress-strain response depends on the type of experiment. For example, at $t/\tau = 1$, the isochronal stress-strain curves will be $\sigma = 0.632G\gamma$, $\sigma = 0.5G\gamma$ and $\sigma = 0.368G\gamma$ respectively.

CHAPTER 4

4-1(a) Equation (4-6) states

$$\log a_T = \frac{-C_1(T - T_g)}{C_2 + T - T_g} \quad (4-6)$$

The apparent energy of activation for viscoelastic relaxation maybe defined as

$$E^* = R \frac{d \ln a_T}{d(1/T)}$$

which, by simple calculus, is just

$$E^* = -RT^2(2.303) \frac{d \log a_T}{dT} \quad (a)$$

Using equation (a) on equation (4-6) yields

$$E^* = \frac{2.303C_1C_2RT^2}{(C_2 + T - T_g)^2} \quad (b)$$

Since we are interested in the activation energy at T_g , equation (b) is just

$$E^* = 2.303 \left(\frac{C_1}{C_2} \right) RT_g^2$$

Using the universal constants ($C_1 = 17.4$ and $C_2 = 51.6$ K) given in Table 4-1, and for a T_g of 200 K this quantity is about 258 kJ/mol (62 kcal/mol).

(b) As $T \gg T_g$ equation (b) becomes

$$E^* = 2.303RC_1C_2$$

which is equal to 17 kJ/mol (4.1 kcal/mol).

4-2. From Equation (4-19), we have

$$C_1 = \frac{B}{2.303} f_g \quad \text{and} \quad C_2 = \frac{f_g}{\alpha_f}$$

where the reference temperature has been taken as T_g . At any other reference temperature, say T_0 , we have

$$C_1^\circ = \frac{B}{2.303[f_g + \alpha_f(T_0 - T_g)]}$$

and

$$C_2^\circ = \frac{f_g + \alpha_f(T_0 - T_g)}{\alpha_f}$$

where equation (4-16) has been used. Algebraic manipulation of these four equations gives

$$C_1^\circ = \frac{C_1}{1 + (T_0 - T_g)/C_2}$$

$$C_2^\circ = C_2 + T_0 - T_g$$

Utilizing the universal constants, at $T_0 = T_g + 50^\circ\text{C}$ yields

$$C_1^\circ = 8.83 \quad \text{and} \quad C_2^\circ = 101.6^\circ\text{C}$$

4-3. This problem is worked out in references 5 and 9 of Chapter 4.

4-4. Starting with the arbitrary temperature $T = T_g - 5$, substitution into equation (4-6) with the values of C_1 and C_2 from Table 4-1 gives

$$\log a_T = -1.87 \quad \text{or} \quad a_T = 0.0135$$

Thus, at this temperature

$$\tau_i(T_g - 5) = \frac{\tau_i(T_g)}{a_T}$$

and the two relaxation times become

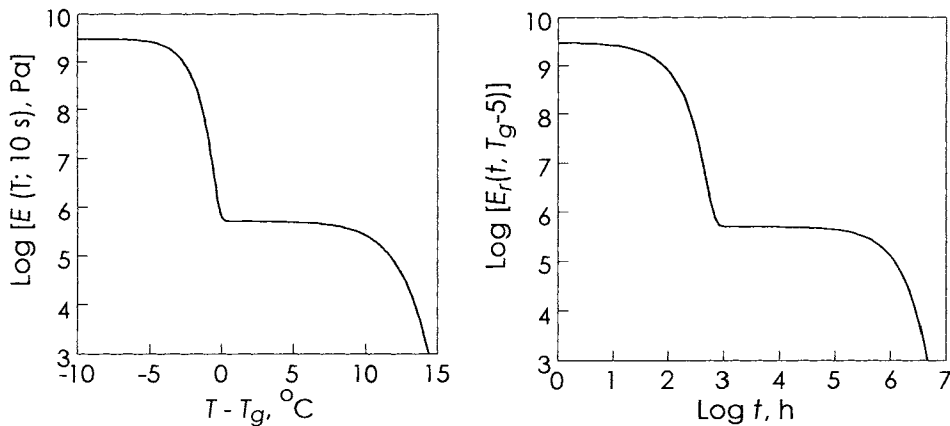
$$\tau_1(T_g - 5) = \frac{1\text{ s}}{0.0135} = 7.4 \times 10^1 \text{ s}$$

$$\tau_2(T_g - 5) = \frac{10^4 \text{ s}}{0.0135} = 7.4 \times 10^5 \text{ s}$$

Thus,

$$\begin{aligned} E(10 \text{ s}, T_g - 5) &= 3.0 \times 10^9 e^{-10 \text{ s}/74 \text{ s}} + 5.0 \times 10^5 e^{-10 \text{ s}/740000 \text{ s}} \\ &= 2.6 \times 10^9 \text{ Pa} \end{aligned}$$

Modulus values at other temperatures are calculated in the same way with the result shown below. For comparison, the relaxation modulus at $T_g - 5$ K is also plotted; the shapes are similar when a log time scale is used.



4-5.

$$G(t, T) = \sum_{i=1}^n G_i e^{-t/\tau_i(T)}$$

$$G(t, T_r) = \sum_{i=1}^n G_i e^{-t/\tau_i(T)}$$

The correspondence principle says

$$G\left(\frac{t}{a_T}, T\right) = G(t, T_r)$$

or

$$\sum_{i=1}^n G_i e^{-t/a_T \tau_i(T)} = \sum_{i=1}^n G_i e^{-t/\tau_i(T)}$$

For this to be true for all values of t , each individual exponent must be equal for all values of t :

$$e^{-t/a_T \tau_i(T)} = e^{-t/\tau_i(T)} \quad 1 \leq i \leq n$$

or

$$\frac{t}{a_T \tau_i(T)} = \frac{t}{\tau_i(T_r)}$$

$$a_T = \frac{\tau_i(T_r)}{\tau_i(T)} = \frac{A_i}{A_i} \frac{e^{H/RT_r}}{e^{H/RT}}$$

$$\ln a_T = \frac{H}{R} \left(\frac{1}{T_r} - \frac{1}{T} \right)$$

$$\log a_T = \frac{H}{2.303R} \left(\frac{1}{T_r} - \frac{1}{T} \right)$$

4-6. From equation (4-6):

$$\log a_T = \frac{-C_1(T - T_g)}{C_2 + T - T_g}$$

which may be rearranged to give

$$\begin{aligned} \log a_T &= \frac{-C_1(T - T_g + C_2)}{T - T_g + C_2} + \frac{C_1 C_2}{T - T_g + C_2} \\ &= -C_1 + \frac{C_1 C_2}{T - T_g + C_2} \end{aligned}$$

If:

$$\beta = C_1$$

$$\alpha = \frac{1}{C_1 C_2}$$

$$T_0 = T_g - C_2$$

we have the Vogel expression.

CHAPTER 5

5-1. Equation (4-16) may be written as

$$f_M = f_g + \alpha_f (T - T_{gM})$$

$$f_\infty = f_g + \alpha_f (T - T_{g\infty})$$

where f_M is the fractional free volume at some temperature and molecular weight. Here we have assumed α_f and f_g are both independent of molecular weight. These relationships may be introduced into the equation given in the problem to yield

$$f_g + \alpha_f (T - T_{gM}) = f_g + \alpha_f (T - T_{g\infty}) + \frac{A}{M_n}$$

$$T_{gM} = T_{g\infty} - \frac{A/\alpha_f}{M_n}$$

which is the same form as equation (5-28).

5-2 (c) The molecular weight of methylene is 14, while that of methacrylate is 84. Thus the weight fraction of methylene is $14n/(84 + 14n)$. Using the hint, we write

$$T_g = T_{g,p} w_p + T_{g,s} w_s + K w_p w_s$$

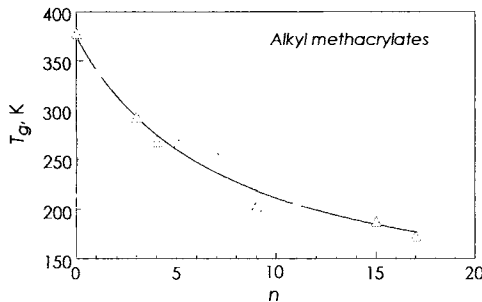
and identify $T_{g,s}$ with the T_g of polyethylene and w_s with its weight fraction in the mixture. (Note: the ends of the methylene sequence are not free ends.) Using equation (5-28) then yields

$$T_g = T_{g,p} (1 - w_s) + T_{g,s} w_s + K w_s (1 - w_s)$$

where

$$w_s = n/(6 + n)$$

Using all three parameters ($T_{g,p}$, $T_{g,s}$ and K), we find that the $T_{g,s} = 94$ K, but with a large error. The graph is shown below with the fitted equation.



5-3. See the answer to Problem 5-10.

5-4 (a) The weight fraction of chain ends, w_e , is just the weight of the ends divided by the total weight of the polymer. If n_i is the number of moles of polymer with molecular weight M_i , w_e is given as

$$w_e = \frac{\text{weight of chain ends}}{\text{total weight}} = \frac{\sum_i n_i M_e}{\sum_i n_i M_i} = M_e \left(\frac{\sum_i n_i}{\sum_i n_i M_i} \right)$$

The term in parentheses, however, is just the reciprocal of the number-average molecular weight of the polymer, M_n , so

$$M_n = \frac{M_e}{w_e}$$

Substitution of this relationship into equation (5-28) yields the desired result.

(b) Rewriting the equation given in terms of relevant parameters, remembering that $w_p + w_e = 1$, gives

$$T_g = T_g^\infty (1 - w_e) + T_g^\infty w_e + Kw_e - K(w_e)^2$$

Since w_e is small for polymers, the last term can be neglected and

$$T_g = T_g^\infty - w_e (T_g^\infty - T_{g_e} - K)$$

This expression is identical to the desired result if we identify the term in the parentheses with c / M_e .

5-5. The reference here should be sufficient.

5-6.

$$\frac{d\delta}{dt} = -\frac{\delta}{\tau} \quad \text{where } \tau \text{ does not depend on } \delta$$

Thus:

$$\frac{d\delta}{\delta} = d \ln \delta = -\frac{dt}{\tau}$$

$$\int_{\ln \delta_0}^{\ln \delta(t)} d \ln \delta = \int_0^t \frac{dt'}{\tau}$$

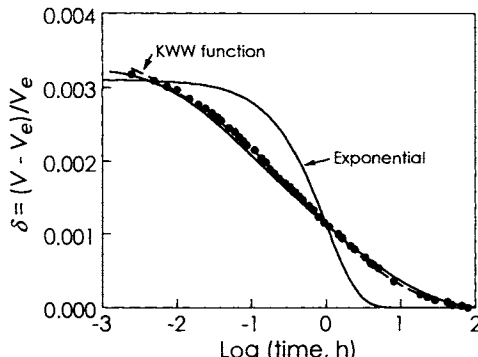
$$\ln \delta(t) - \ln \delta_0 = -\frac{t}{\tau}$$

$$\delta(t) = \delta_0 e^{-t/\tau}$$

where $\delta_0 = 3 \times 10^{-3}$ and $\tau = 1$ h

$$\delta(t) = 3 \times 10^{-3} e^{-t/1.0}$$

This function is plotted in the accompanying figure,* along with the least squares KWW fit for part (b). The parameters for the latter are $\delta_0 = 0.0039$, $\tau = 0.542$ h and $\beta = 0.317$ where $\delta(t) = \delta_0 \exp[-(t/\tau)^\beta]$.



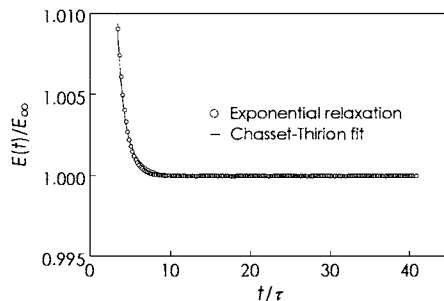
5-11. Solving the equation in the problem for the parameter a gives:

$$a = \frac{E(t)/E_\infty - 1}{\exp(-t/\tau)}$$

which works out to be $0.1/0.368 = 0.271$. Using this value to generate “data” shows that the value of m increases as the data at longer times is used. An example fit using data greater than $t/\tau = 3$ is shown below. The Chasset-

* Data from A. J. Kovacs, *Fortschr. Hochpolym.* 3, 394 (1964), ©Springer-Verlag, 1964. With kind permission of Springer Science and Business Media.

Thirion equation cannot turn as sharply as the exponential in spite of a value of $m = 2.65$.



5-12. The key equation for solving this problem is equation (6-84), which in our case simplifies to

$$G = RT\rho \left(\frac{1}{M_c} - \frac{2}{M} \right)$$

For the general case of network degradation, both M_c and M will change. To see this, consider that $M_c = \rho/2c$ and $M = 2\rho/\text{[ends]}$, where [ends] is the concentration of chain ends. Inverting and taking derivatives of these expressions gives

$$\frac{d(1/M_c)}{dt} = \frac{2}{\rho} \frac{dc}{dt} = -2k_2 c / \rho$$

for the first term and

$$\frac{d(1/M)}{dt} = \frac{1}{2\rho} \frac{d[\text{ends}]}{dt} = \frac{1}{2\rho} \left(-2 \frac{d[L]}{dt} \right) = \frac{1}{\rho} k_1 [L] \approx \frac{k_1}{M_0}$$

for the second, where $[L]$ is the concentration of susceptible linkages of molecular weight M_0 . We have assumed that the concentration of linkages is so large that mild degradation will not change the number appreciably, and thus the reaction is pseudo zero order. Combining these to obtain the rate of change of modulus gives

$$\frac{dG}{dt} = 2RT\rho \left(-\frac{k_2 c}{\rho} - \frac{k_1}{M_0} \right)$$

We can see that both reactions will cause the modulus to decrease, but the concentration of crosslinks c will influence only the first term. Note, however, that the relative change in modulus at the beginning of the process will be:

$$\frac{d \ln G}{dt} = -(k_2 + k_1 \rho / c M_0)$$

showing that an increase in crosslink density will decrease this quantity.

CHAPTER 6

6-1(a)

$$dH = TdS + VdP + fdL$$

Thus:

$$\left(\frac{\partial H}{\partial L} \right)_{T,P} = T \left(\frac{\partial S}{\partial L} \right)_{T,P} + f$$

The Maxwell relation

$$\left(\frac{\partial S}{\partial L} \right)_{T,P} = - \left(\frac{\partial f}{\partial T} \right)_{L,P}$$

gives

$$\left(\frac{\partial H}{\partial L} \right)_{T,P} = -T \left(\frac{\partial f}{\partial T} \right)_{L,P} + f$$

Now

$$\left(\frac{\partial f}{\partial T} \right)_{P,L} = \left(\frac{\partial f}{\partial T} \right)_{P,\lambda} + \left(\frac{\partial f}{\partial \lambda} \right)_{P,L} \left(\frac{\partial \lambda}{\partial T} \right)_{P,L}$$

Evaluating the various coefficients using equation (6-60) gives

$$\left(\frac{\partial f}{\partial T} \right)_{P,L} = \frac{f}{T} - \frac{\alpha f}{3} \frac{\lambda^3 + 2}{\lambda^3 - 1}$$

and

$$\left(\frac{\partial H}{\partial L}\right)_{T,P} = \frac{\alpha Tf}{3} \frac{\lambda^3 + 2}{\lambda^3 - 1}$$

(b) Analogous to part (a) starting with dU instead of dH .

(c)

$$\left(\frac{\partial H}{\partial L}\right)_{T,P} = \frac{T\alpha}{\beta} \left(\frac{\partial V}{\partial L}\right)_{T,P}$$

since

$$\left(\frac{\partial U}{\partial L}\right)_{T,V} = 0$$

Substituting the result of part (a):

$$\left(\frac{\partial V}{\partial L}\right)_{P,T} = \frac{\beta f}{3} \frac{\lambda^3 + 2}{\lambda^3 - 1}$$

Note that since $(\partial H / \partial L)_{T,P} \neq 0$, an ideal rubber has a thermoelastic inversion point.

6-2. Equation (6-11) defines the stress-temperature coefficient in terms of pertinent quantities.

$$\left(\frac{\partial f}{\partial T}\right)_{P,L} = \frac{f - (\delta H / \delta L)_{T,P}}{T}$$

In Problem 6-1a,

$$\left(\frac{\partial H}{\partial L}\right)_{T,P} = \frac{\alpha Tf}{3} \frac{\lambda^3 + 2}{\lambda^3 - 1}$$

So

$$\left(\frac{\partial f}{\partial T}\right)_{P,L} = \frac{f}{T} \left[1 - \frac{\alpha T}{3} \frac{\lambda^3 + 2}{\lambda^3 - 1} \right]$$

6-3. Equation (6-42) in terms of this problem states

$$\Delta A = \frac{1}{3} NkT b^2 r^2 \left(\lambda^2 + \frac{1}{\lambda^2} - 2 \right)$$

Incorporation of (6-44) gives

$$\Delta A = \frac{1}{2} NkT \frac{\overline{r_0^2}}{\overline{r_f^2}} \left(\lambda^2 + \frac{1}{\lambda^2} - 2 \right)$$

Since pure shear is a constant volume process ($\lambda_1 \lambda_2 \lambda_3 = 1$),

$$\alpha^* = \lambda$$

and equation (6-52b) becomes

$$f = \frac{1}{L} \left(\frac{\partial A}{\partial \lambda} \right)_{T,V}$$

Operating with this on the second expression gives:

$$f = \frac{NkT}{L} \frac{\overline{r_0^2}}{\overline{r_f^2}} \left(\lambda - \frac{1}{\lambda^3} \right)$$

or

$$\sigma_E = N_0 k T \frac{\overline{r_0^2}}{\overline{r_f^2}} \left(\lambda^2 - \frac{1}{\lambda^2} \right)$$

6-4. According to equation (6-75)

$$I_1 = \lambda^2 + 1 + \frac{1}{\lambda^2}$$

and

$$I_2 = \lambda^2 + 1 + \frac{1}{\lambda^2}$$

Thus equation (6-80) states:

$$\overline{W} = C_{100} \left(\lambda^2 + \frac{1}{\lambda^2} - 2 \right) + C_{010} \left(\lambda^2 + \frac{1}{\lambda^2} - 2 \right)$$

and using equation (6-79) gives the tensile stress

$$\sigma_E = 2(C_{100} + C_{010}) \left(\lambda^2 - \frac{1}{\lambda^2} \right)$$

6-6. Substitution into equation (6-84) gives

$$G = \frac{(0.95 \text{ g/cm}^3)(8.31 \times 10^7 \text{ erg/mol K})(300 \text{ K})}{5000 \text{ g/mol}} \left(1 - \frac{10^4}{10^5} \right)$$

$$G = 4.3 \times 10^6 \text{ dyne/cm}^2 = 4.3 \times 10^5 \text{ Pa.}$$

Here we have assumed that the front factor $\overline{r_0^2} / \overline{r_f^2}$ is equal to unity.

6-8. Using equation (6-94a)

$$\begin{aligned} E_f &= [1 + 2.5(0.3) + 14.1(0.3)^2] 5 \times 10^7 \text{ dynes/cm}^2 \\ &= 1.5 \times 10^8 \text{ dyne/cm}^2 = 1.5 \times 10^7 \text{ Pa} \end{aligned}$$

If half of the filler particles become ineffective,

$$V_f = 0.15$$

and

$$E_f = 8.3 \times 10^7 \text{ dyne/cm}^2 = 8.3 \times 10^6 \text{ Pa}$$

6-9. Starting with equation (6-66)

$$f = GA_0 \left(\lambda - \frac{V}{V_0 \lambda^2} \right)$$

one can write

$$f = GA_0 \left(\frac{L}{L_0} - \frac{V}{V_0} \frac{L_0^2}{L^2} \right)$$

Differentiation yields

$$\begin{aligned} \left(\frac{\partial f}{\partial T} \right)_{V,L} &= \left(\frac{\partial G}{\partial T} \right)_{V,L_0} A_0 \left(\frac{L}{L_0} - \frac{V}{V_0} \frac{L_0^2}{L^2} \right) \\ &+ \left(\frac{\partial A_0}{\partial T} \right)_{V,L} G \left(\frac{L}{L_0} - \frac{V}{V_0} \frac{L_0^2}{L^2} \right) \end{aligned}$$

$$+ GA_0 \left[-\frac{L}{L_0^2} \left(\frac{\partial L_0}{\partial T} \right)_{V,L} + \frac{V}{V_0^2} \frac{L_0^2}{L^2} \left(\frac{\partial V_0}{\partial T} \right)_{V,L} \right. \\ \left. - 2 \frac{V}{V_0} \frac{L_0}{L^2} \left(\frac{\partial L_0}{\partial T} \right)_{V,L} \right]$$

Grouping terms and using the approximation

$$\frac{1}{V_0} \left(\frac{\partial V_0}{\partial T} \right)_{V,L} = \frac{3}{2} \frac{1}{A_0} \left(\frac{\partial A_0}{\partial T} \right)_{V,L} = 3 \frac{1}{L_0} \left(\frac{\partial L_0}{\partial T} \right)_{V,L}$$

leads directly to equation (6-67).

6-11. Recognizing that for simple extension the only principal stress is in the 1 direction, we have:

$$\bar{W} = \int_1^{\lambda_1} \sigma_{1,0} d\lambda'_1$$

Using Leibnitz's rule to differentiate this integral, keeping in mind that the stress is a function of the dummy variable λ'_1 and not the limit λ_1 gives directly

$$\frac{d\bar{W}}{d\lambda_1} = \sigma_{1,0}(\lambda_1) \frac{d\lambda_1}{d\lambda'_1} = \sigma_{1,0}(\lambda_1) = \sigma_1 / \lambda_1$$

Solving for σ_1 and equating this principal stress to σ_E yields equation (6-79).

6-14. Developing equation (b) in Appendix 1 for $n = 4, p = 1$ yields:

$$\bar{r^2} = \frac{1}{1} \sum_{i=1}^4 (r_i)^2 = (r_1)^2$$

$$\bar{r^2} = \left(\sum_{j=1}^4 I_j \right)^2$$

$$\bar{r^2} = I_1 \cdot I_1 + I_1 \cdot I_2 + I_1 \cdot I_3 + I_1 \cdot I_4 + \\ I_2 \cdot I_1 + I_2 \cdot I_2 + I_2 \cdot I_3 + I_2 \cdot I_4 + \\ I_3 \cdot I_1 + I_3 \cdot I_2 + I_3 \cdot I_3 + I_3 \cdot I_4 + \\ I_4 \cdot I_1 + I_4 \cdot I_2 + I_4 \cdot I_3 + I_4 \cdot I_4$$

6-16. Equation (p), Appendix 1, may be written as

$$\overline{r^2} = \frac{\int_0^\infty r^4 e^{-b^2 r^2} dr}{\int_0^\infty r^2 e^{-b^2 r^2} dr}$$

after using equation (o) to eliminate $\omega(r)dr$. This expression integrates to

$$\overline{r^2} = \frac{3}{2b^2}$$

Since b^2 is $3/2\overline{r^2}$ [equation (m)], we get $\overline{r^2} = \overline{r^2}$.

6-17. Equation (v) of Appendix 1 states

$$n_e = \frac{R^2}{\overline{r^2}} \text{ and } l_e = \frac{\overline{r^2}}{R}$$

If the length of each monomer is 0.46 nm, R must be

$$R = (0.46 \text{ nm}) n$$

where n is the number of monomer units. Thus

$$n_e = (0.46n)^2 / 0.162n = 1.3 n$$

and

$$l_e = 0.16n / 0.46n = 0.35 \text{ nm}$$

6-18. Equation (j) reads

$$\omega(m, n) = \left(\frac{1}{2}\right)^n \frac{n!}{[(n+m)/2]![n-m)/2]!}$$

and if $n \gg m$, we can use the form of Stirling's approximation given in the problem to get

$$\begin{aligned} \ln \omega(m, n) &= \left(n + \frac{1}{2}\right) \ln n - \frac{1}{2}(n+m+1) \ln \left[\left(\frac{n}{2}\right) \left(1 + \frac{m}{n}\right) \right] \\ &\quad - \frac{1}{2}(n-m+1) \ln \left[\left(\frac{n}{2}\right) \left(1 - \frac{m}{n}\right) \right] \end{aligned}$$

$$-\frac{1}{2} \ln 2\pi - n \ln 2$$

However, since $n \gg m$, we can use the series expansion

$$\ln\left(1 \pm \frac{m}{n}\right) = \pm \frac{m}{n} - \frac{m^2}{2n^2}$$

where third-order and higher-order terms of (m/n) are neglected. We now have:

$$\begin{aligned} \ln \omega(m, n) &= \left(n + \frac{1}{2}\right) \ln n - \frac{1}{2} \ln 2\pi - n \ln 2 - \frac{1}{2}(n + m + 1) \\ &\quad \times \left(\ln n - \ln 2 + \frac{m}{n} - \frac{m^2}{2n^2}\right) - \frac{1}{2}(n - m + 1) \\ &\quad \times \left(\ln n - \ln 2 - \frac{m}{n} - \frac{m^2}{2n^2}\right) \end{aligned}$$

Simplifying and taking the antilogarithm of both sides, we obtain

$$\omega(m, n) = \left(\frac{2}{\pi n}\right)^{1/2} \exp\left(-\frac{m^2}{2n}\right)$$

In the simplification we have made use of the fact that $n \gg 1$, so that

$$\frac{m^2}{2n} \left(\frac{1}{n} - 1\right) \approx -\frac{m^2}{2n}$$

6-19. Equation (p) of Appendix 1 is restated in this case as

$$\overline{r^2} = \frac{\int_{1/2b}^{\infty} r^4 e^{-b^2 r^2} dr}{\int_0^{\infty} r^2 e^{-b^2 r^2} dr}$$

where $\overline{r^2}$ indicates a particular average quantity. Our problem then becomes one of evaluating the definite integrals given. This equation may be rewritten as

$$\bar{r^2} = \frac{\int_0^\infty r^4 e^{-b^2 r^2} dr - \int_0^{1/2b} r^4 e^{-b^2 r^2} dr}{\int_0^\infty r^2 e^{-b^2 r^2} dr - \int_0^{1/2b} r^2 e^{-b^2 r^2} dr}$$

Now consider the second term in both the numerator and the denominator of this expression. If r is between 0 and $1/2b$, the exponential is quite close to 1. Thus we may approximate this expression as

$$\bar{r^2} = \frac{\int_0^\infty r^4 e^{-b^2 r^2} dr - \int_0^{1/2b} r^4 dr}{\int_0^\infty r^2 e^{-b^2 r^2} dr - \int_0^{1/2b} r^2 dr}$$

which is integrated to give

$$\bar{r^2} = \frac{3}{2b^2} \left[\frac{\sqrt{\pi} - \frac{1}{60}}{\sqrt{\pi} - \frac{1}{6}} \right]$$

Since the expression in brackets is greater than 1.0, $\bar{r^2} > r^2$. This result is clearly expected since conformations with small r^2 have been excluded in calculating $\bar{r^2}$.

6-20. Once again equation (p) of Appendix 1 is the starting point.

$$\bar{r} = \frac{\int_0^\infty r^3 e^{-b^2 r^2} dr}{\int_0^\infty r^2 e^{-b^2 r^2} dr}$$

In this case the variable transformation

$$y = b^2 r^2$$

is helpful. This yields

$$\bar{r} = \frac{1}{b} \frac{\int_0^\infty y e^{-y} dy}{\int_0^\infty y^{1/2} e^{-y} dy}$$

Both of these integrals are complete gamma functions so that

$$\bar{r} = \frac{1}{b} \frac{\Gamma(2)}{\Gamma(\frac{3}{2})} = \frac{1}{b} \frac{1 \cdot \Gamma(1)}{\frac{1}{2} \Gamma(\frac{1}{2})}$$

or

$$\bar{r} = \frac{2}{b\sqrt{\pi}}$$

In comparing the text with the results of this calculation we see that

$$(\bar{r}^2)^{1/2} \neq \bar{r}$$

In addition, one should recall that \bar{r} for a Gaussian chain is zero. These results are not inconsistent, since what makes the vector average zero is its sign: just as many \mathbf{r} 's are positive as are negative along any axis. In this problem, we have calculated the average of the radius of a spherical shell, a scalar quantity that cannot take on negative values.

6-21(a) From equation (i) in Appendix 2

$$\mathbf{f} = 2kTb^2 \mathbf{r}$$

As we are discussing only directions along the box, $f = 2kTb^2 r$, where r is the length $L = 1/b$ of the box. Thus:

$$P = \frac{f}{A} = \frac{2kTb^2 r}{A}$$

In our case,

$$P = \frac{2kTb^2 \cdot 1/b}{S^2} = \frac{2kTb}{S^2} = \frac{2kT}{S^2 L} = \frac{2kT}{V}$$

(b) Solving for the temperature gives $T = PV/2k$, where $k = 1.381 \times 10^{-23}$ J/molecule K. Thus:

$$\begin{aligned} T &= 100 \text{ atm} (1.013 \times 10^5 \text{ Pa/atm}) \times 1 \text{ nm}^3/\text{molecule} (10^{-27} \text{ m}^3/\text{nm}^3) / \\ &\quad (2 \times 1.381 \times 10^{-23} \text{ J/molecule K}) \\ &= 367 \text{ K} \end{aligned}$$

CHAPTER 7

7-1. For an electrical circuit of the type pictured, the charges in the two branches add:

$$Q = Q_1 + Q_2$$

From equation (7-9)

$$Q_1 = C_1 V_0 (1 - e^{-t/\tau})$$

and

$$Q_2 = C_2 V_0$$

Therefore:

$$Q(t) = C_1 V_0 (1 - e^{-t/\tau}) + C_2 V_0$$

or:

$$C(t) = C_1 (1 - e^{-t/\tau}) + C_2$$

Using the definitions of C_R and C_u and substituting

$$C(t) = (C_R - C_u)(1 - e^{-t/\tau}) + C_u$$

7-2(a) This is entirely analogous to the derivation of the mean square end to end distance of the freely jointed chain given in Chapter 6, Appendix 1. The result is:

$$\langle \mu^2 \rangle = N\mu_0^2$$

(b) Following the argument for the dimensions of a chain with tetrahedral angles given in Chapter 5, Section C, the result is:

$$\langle \mu^2 \rangle = 2N\mu_0^2$$

Since the bonds of this chain are free to rotate about one another (bond rotational potentials are zero), $g = 1$.

(c) If the chain possesses barriers to rotation about backbone bonds, g will take on a value different from 1 since the cosine averages in equation (7-59) are now different from 0.

(d) We must calculate the cosine averages for the angles of each bond with respect to the first. Since we are given that the rotation potentials of each bond are independent and each bond can only assume the angles $\pi/2$, π , and $3\pi/2$ with respect to the first, we have:

$$\langle \cos \gamma_{1j} \rangle = \frac{\cos \pi/2 + \cos \pi + \cos 3\pi/2}{3} = -\frac{1}{3}$$

Thus $g = 0.67$

$$\langle \mu^2 \rangle = 2gN\mu_0^2 = 1.34N\mu_0^2$$

7-3. Let $a = \varepsilon_R - \varepsilon_u$; $b = \varepsilon_R + \varepsilon_u$; $X = \omega\tau$

$$\begin{aligned} \left(\varepsilon_u + \frac{a}{1+X^2} - \frac{b}{2} \right)^2 + \left(\frac{aX}{1+X^2} \right)^2 &= \frac{a^2}{4} \left(\frac{1-X^2}{1+X^2} \right)^2 + a^2 \left(\frac{X}{1+X^2} \right)^2 \\ &= a^2 \frac{(1-X^2)^2 + 4X^2}{4(1+X^2)^2} = \left(\frac{\varepsilon_R - \varepsilon_u}{2} \right)^2 \end{aligned}$$

7-4.

$$q^* = C^* V^*, \quad C^* = C_0 \varepsilon^*$$

$$V^*(t) = V_0 \exp(i\omega t), \quad \varepsilon^* = \varepsilon' - i\varepsilon''$$

$$I^* = \frac{dq^*}{dt} = C^* \frac{dV^*}{dt} = (i\omega C^*) V^* = Y^* V^*$$

Y^* (admittance) = $i\omega C^* = \omega C_0(\varepsilon'' + i\varepsilon')$. For a series of R 's and C 's,

$$Y^* = \frac{1}{R_s - i/\omega C_s}$$

By comparing real and imaginary terms one has:

$$\varepsilon'' = \frac{R_s \omega C_s^2}{C_0(R_s^2 \omega^2 C_s^2 + 1)} \quad \varepsilon' = \frac{C_s}{C_0(R_s^2 \omega^2 C_s^2 + 1)}$$

7-5. Consider only that part of I^* which is in phase with V^* . From Problem 7-4 one has: $I^* = i\omega C^* V^* = \omega C_0 V^* (\varepsilon'' + i\varepsilon')$

$$\text{Power} = V^* \cdot I^* = C_0 \omega \varepsilon'' |V^*|^2 = C_0 V_0^2 \omega \varepsilon''$$

Since

$$\varepsilon'' = \frac{(\varepsilon_R - \varepsilon_u)\omega\tau}{1 + \omega^2\tau^2},$$

$$P = \left[C_0 V_0^2 (\varepsilon_R - \varepsilon_u) \right] \frac{\omega^2 \tau}{1 + \omega^2 \tau^2}$$

7-6. As can be shown by methods of Chapter 3,

$$\left. \begin{aligned} D'' &= \frac{\omega \tau}{E_2 (1 + \omega^2 \tau^2)} \\ D' &= \frac{1}{E_1} + \frac{1}{E_2 (1 + \omega^2 \tau^2)} \end{aligned} \right\} \quad \begin{aligned} \text{where } t &= \eta/E \\ E_1 &= \text{separate spring} \\ E_2 &= \text{Voigt spring} \end{aligned}$$

To complete the analogy,

$$\frac{1}{E_2} = \varepsilon_R - \varepsilon_u ; \quad \frac{1}{E_1} = \varepsilon_u$$

7-7. From problem 7-4, the admittance for a resistance and capacitor in series is

$$Y^* = \frac{1}{R_s - i/\omega C_s}$$

As $Z^* = 1/Y^*$ we have

$$Z^* = 1/Y^* = R_s - i/\omega C_s$$

which gives directly the Nyquist plot. For the Bode plot, the magnitude of Z^* is calculated as:

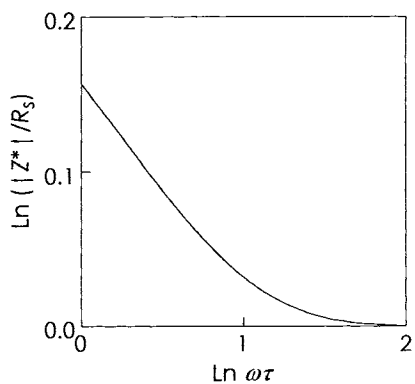
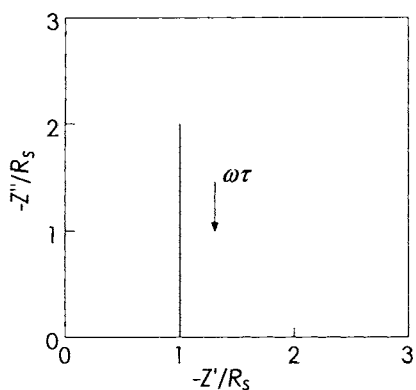
$$|Z^*| = \sqrt{(Z')^2 + (Z'')^2} = \sqrt{R_s^2 + 1/(\omega C_s)^2} = R_s \sqrt{1 + 1/(\omega \tau)^2}$$

where $\tau = C_s R_s$. The Nyquist and Bode plots, respectively, are shown below.

The relationship between, Z^* and ε^* can be easily seen by comparing the results above with those of Problem 7-4, and defining $\tan \delta = Z''/Z'$. The resulting equations are:

$$\varepsilon' = \frac{C_s}{C_0} \frac{(\tan \delta)^2}{1 + (\tan \delta)^2} \quad \text{and} \quad \varepsilon'' = -\frac{C_s}{C_0} \frac{\tan \delta}{1 + (\tan \delta)^2}$$

Note that in contrast to Z^* , ε^* is dimensionless.



List of Major Symbols

In certain instances, symbols in this book are used to denote different meanings to preserve conformity with those commonly accepted in the literature. Those symbols whose usage is restricted to certain chapters are so indicated. Some minor symbols are defined in the text where applicable and are not included in this list. In designated sections, nomenclature has been simplified to avoid complicated formatting.

A	Helmholtz free energy
A	normalization constant (Chapter 7)
A_0	unstretched cross-sectional area
$[A]$	Zimm matrix
a	entanglement parameter
a	atomic radii (Chapter 7)
a^2	mean square end-to-end distance of submolecule
a_s	radius of the dielectric sphere
a_T	shift factor
B	$3kT/a^2\rho_s$ (Chapter 3)
b^2	$3nl^2/2$
C	capacitance (Chapter 7)
C_0	capacitance in vacuum
C_P	constant pressure heat capacity
C_V	constant volume heat capacity
C_r	reference capacitance
C_s	sample capacitance
C_1, C_2	WLF parameters

294 LIST OF MAJOR SYMBOLS

C_1, C_2	Mooney–Rivlin parameters (Chapter 6)
c	mass concentration
c	Fox–Flory constant (Chapter 5)
D	diffusion constant (Chapter 7)
D	tensile compliance
$D(t)$	tensile creep compliance
d	capacitor plate spacing (Chapter 7)
E	electric field (Chapter 7)
E, E_0	tensile modulus
$E(t)$	tensile relaxation modulus
E^*	complex tensile modulus
$E^*(\omega t)$	time-dependent periodic electric field (Chapter 7)
E'	dynamic storage tensile modulus
E'	internal electric field (Chapter 7)
E''	dynamic loss tensile modulus
E_e, E_∞	equilibrium tensile modulus
E_f	tensile modulus of a filled rubber
E_l	glassy tensile modulus
E_2	rubbery tensile modulus
e	charge of the electron
F	Gibbs free energy
F	general function (Chapter 2)
F, f	force
f	fractional free volume (Chapter 4)
f_e	energetic force
f_g	fractional free volume at glass transition
f_s	entropic force
G, G_0	shear modulus
$G(t)$	shear relaxation modulus
G^*	complex shear modulus
G'	dynamic storage shear modulus
G''	dynamic loss shear modulus
G_1	glassy shear modulus
G_2	rubbery shear modulus
g	Kirkwood correlation factor
H	enthalpy
H_a	activation energy
$H(\tau)$	distribution of relaxation times
I	current
I_1, I_2, I_3	strain invariants

$[I]$	identity matrix
I_0	initiator concentration
i	$\sqrt{-1}$
J	shear compliance
$J(t)$	shear creep compliance
J^*	complex shear compliance
J'	dynamic storage shear compliance
J''	dynamic loss shear compliance
J_r	recoverable compliance
K_A, K_B	Gordon–Taylor parameters
k	Boltzmann constant
k	K_A/K_B (Chapter 4)
L	tube length (Chapter 7)
L	length of strained sample
L	Laplace transform
L_0	length of unstrained sample at V_0
L'	length of unstrained sample at V
L_s	new unstrained length
L_u	original unstrained length
L_x	strained length
$L(\tau)$	distribution of retardation times
l	length of a chain link
\vec{l}	vectorial length of a chain link
M	modulus (Chapter 1)
M	molecular weight
M_c	molecular weight of network chain (Chapter 6)
M_c	critical entanglement molecular weight (Chapter 3)
M_n, M_w	number and weight average molecular weights
M_s	total electric moment in a dielectric sphere
m	difference between positive and negative steps (Chapter 6)
N	number of network chains
N_A, N_{Av}	Avogadro's number
N_0	number and molar density of network chains
N_s	number of molecules in a dielectric sphere
n	fixed number of conformations of chain
n	number of links in a polymer chain
n_+	number of positive steps
n_-	number of negative steps
P	pressure
P_D	long-time limit of the polarization

P_R	infinite time polarization
P	instantaneous polarization
$P(t)$	time-dependent polarization
$P_D(t)$	time-dependent portion of the polarization
$P^*(\omega)$	complex dielectric permittivity
p	size parameter
Q	charge (Chapter 7)
$[Q]$	transformation matrix (Chapter 3)
q	elements of $[q]$ matrix (Chapter 3)
\dot{q}	time derivative of q
$[q]$	normal coordinate matrix
R	resistance (Chapter 7)
R	extended chain length (Chapter 6)
R	ideal gas constant
R_r	reference resistance
R_s	sample resistance
r	charge separation (Chapter 7)
$\overline{r^2}$	mean square end-to-end distance
\vec{r}	vectorial length of chain ends
$\overline{r_f^2}$	mean square end-to-end distance of a free chain
$\overline{r_0^2}$	mean square end-to-end distance of a real chain
S	entropy
T	temperature
T_g	glass transition temperature
T_i	inflection temperature
T_m	melting temperature
T_{ref}, T_R	reference temperature
T_2	second-order transition temperature
t	time
t_{ref}, t_R	reference time
U	internal energy
u_0	hole-formation energy
u_i	displacement in i th direction
V	volume
V	voltage (Chapter 7)
V_c	capacitive potential
V_d	volume fraction of diluent
V_f	free volume
V_f	volume fraction of filler (Chapter 6)
V_0	initial volume

V_p	volume fraction of polymer
V_R	resistive potential
V_r	volume fraction of rubber
V_s	voltage across a sample
V_∞, V_f	equilibrium volume
v	velocity
\overline{W}	work
W_A, W_B	strain energy density
X	weight fraction of comonomers
X	calculational variable (Chapter 7)
X_A, X_B	time derivative of displacement
x	mole fractions
x	number of segments per chain
x	diffusion distance (Chapter 3)
x_i	distance in the i th direction
Y	calculational variable and reactance(Chapter 7)
Z	number of primary valences of chain atom
z	number of mechanical elements or submolecules
α	thermal expansion coefficient
α	effective polarizability (Chapter 7)
α_f	thermal expansion coefficient of free volume
α_g	thermal expansion coefficient of glass
α_0	molecular polarizability
α_s	polarizability of a dielectric sphere
α_r	thermal expansion coefficient of rubber
β	isothermal compressibility
β_f	isothermal compressibility of free volume
Γ	gamma function
γ	shear strain
$\vec{\gamma}$	complex strain vector
γ'	in-phase component of strain vector
γ''	out-of-phase component of strain vector
γ_{ij}	component of infinitesimal strain tensor
$\dot{\gamma}_{ij}$	component of strain rate tensor
γ_{ij}	angle between i th and j th chain segment (Chapter 3)
Δ	logarithmic decrement
δ	loss angle
δ	normalized volume departure from equilibrium (Chapter 5)
ε	tensile strain, du_1/dx_1

298 LIST OF MAJOR SYMBOLS

ε	dielectric constant (relative permittivity) (Chapter 7)
$\varepsilon, \varepsilon_A, \varepsilon_B$	flex energies (Chapter 4)
ε_R	long time limit of the dielectric constant
ε_u	instantaneous dielectric constant
ε'	real part of the complex dielectric constant
ε''	imaginary part of the complex dielectric constant
$\varepsilon^*(\omega)$	complex dielectric constant
ϕ	volume fraction
ϕ_f	volume fraction filler
η	shear viscosity
η_E	tensile viscosity
θ	$\pi - \psi$
Λ	extension ratio including strain amplification factor
$[\Lambda]$	diagonalized Zimm matrix
λ	extension ratio
λ_c	extension ratio of dry rubber
λ_p	elements of $[\lambda]$ matrix
λ_s	extension ratio of swollen rubber
$\lambda_1, \lambda_2, \lambda_3$	principal extension ratios
μ	Poisson ratio
μ	molecular mobility (Chapter 3)
μ	dipole moment (Chapter 7)
π	180° angle or 3.1416
ρ	mass density
ρ_s	segmental friction factor (Chapter 3)
ρ_0	segmental friction factor at short times
σ	shear stress
σ	charge density (Chapter 7)
$\vec{\sigma}$	principal stress vector
$\vec{\sigma}'$	in-phase component of stress vector
$\vec{\sigma}''$	out-of-phase component of stress vector
σ_E	tensile stress
$\sigma_{E,0}$	engineering tensile stress, i.e., f/A_0
$\sigma_{i,j}$	component of total stress tensor
σ_0	charge density in vacuum
$\sigma_1, \sigma_2, \sigma_3$	principal stresses
τ	relaxation or retardation time
τ^*	effective relaxation time
τ_c	critical relaxation time
τ_{min}	minimum relaxation time

τ_p	relaxation time of Rouse model
τ_{ij}	component of extra (deviatoric) stress tensor.
τ_1	maximum relaxation time
$[\Phi]$	transformation matrix
ψ	bond angle
Ω	number of conformations
ω	angular frequency (Chapters 2, 3)
ω	probability (Chapter 6)
ζ	ordering parameter

List of Files on CD

INTRODUCTION

The accompanying CD contains data files that are useful or necessary for several of the exercises. Most are text files and thus should be readable by most computer application software.

While the data have been gathered from standard published sources, they have not been checked number for number against the original publications. Indeed, some of the data were acquired by digitizing published figures. Other sets have been transformed, e.g., from the original units to SI units. They should not be used as a fundamental source of information for anything other than their intended purpose.

LIST OF FILES

The table below lists the file name, the problem requiring the data and the nature of the information in the file. The data sources are also listed.

Included on the CD is the free-ware program TRACER.EXE, which can be useful for digitizing data from published graphs for additional analysis.

302 LIST OF FILES ON CD

File name	Problem	Description	Reference
BPA-PC- Rel.TXT	4-3	Stress relaxation data for polycarbonate, 40 kDa, at various temperatures	J. P. Mercier, J. J. Aklonis, M. Litt, and A. V. Tobolsky, <i>J. Appl. Polym. Sci.</i> , 9 , 447 (1965)
Butyl-Rel.TXT	5-11	Physical stress relaxation data for a swollen PIB network.	Unpublished data, M. T. Shaw
Film-Tg.TXT	5-7	Glass transition temperatures (T_g) of thin iPMMA films as a function of film thickness	Digitized from Fig. 4 (p. 6) of F. Kremer and L. Hartmann, Dielectrics Newsletter, September 2001, p. 4-6.
Glucose.TXT	5-6	Volume relaxation data for glucose sugar at 24.9 °C	Digitized from Fig. 3 in A. J. Kovacs, <i>Fortschr. Hochpolym.</i> , 3 , 394 (1964)
MW-Blend.TXT	3-13	Stress relaxation of a PS blend of two narrow fractions of different molecular weights	Digitized from data in Figure 4 of D. Soong, M. Shen, and S. D. Hong, <i>J. Rheol.</i> , 23 , 301 (1979).
NR-Mod.TXT	6-12, 6-13	Stress strain data (reduced) for an NR elastomer	Digitized from M. Shen and P. J. Blatz, <i>J. Appl. Phys.</i> , 39 , 4937 (1986)
PC40kDa.TXT	4-10	10-s creep data for polycarbonate	J. P. Mercier, J. J. Aklonis, M. Litt, and A. V. Tobolsky, <i>J. Appl. Polym. Sci.</i> , 9 , 447 (1965)
PIB-Rel-1.TXT	3-18	“Standard” NBS stress relaxation data for polyisobutylene at 25 °C	J. D. Ferry, <i>Viscoelastic Properties of Polymers</i> , 3rd ed., Wiley, New York, 1980, p. 213, Table 6, Appendix D
PIB-Rel-2.TXT	3-18	Stress relaxation master curve for PIB at 25 °C spaced at 0.2- decade intervals	E. Catsiff and A. V. Tobolsky, <i>J. Colloid Sci.</i> , 10 , 375 (1955).

File name	Problem	Description	Reference
PMMA45 . TXT	2-19	Dynamic modulus master curve for PMMA of 45 kDa molecular weight at 180 °C	Personal communication, Prof. A. Schausberger, Linz University, Austria
Tg-Alkyl-MA . TXT	5-2	Glass transition temperatures (T_g) of poly(alkyl methacrylates)	P. Peysel "Glass Transition Temperatures of Polymers," in <i>Polymer Handbook</i> , 3rd ed., J. Brandrup and E. Immergut eds., Wiley Interscience, New York, pp. VI 209-VI 277
Tg-PDMS . TXT	5-9	Glass transition temperatures (T_g) of PDMS of various molecular weights.	S. J. Clarson, K. Dogson, and J. S. Semlyen, <i>Polymer</i> , 26 , 931-934 (1985)
Tg-PVC . TXT	5-9	Glass transition temperatures (T_g) of PVC of various molecular weights.	G. Pezzin, F. Zilio-Grandiadn and P. Sanmartin, <i>Eur. Polym. J.</i> , 6 , 1053-1061 (1970)
TRACER . EXE TRACER . HLP	7-8	Program to aid in the digitizing of graphs. ^a	Freeware written by Marcus Karolewski, karolewski@alum.mit.edu , 1999.

^aThis program requires distortion-free bitmapped file of the image. Quick instructions: Double click on TRACER . EXE to run. Maximize window. Go to File/Open image and type in bitmapped file path and name. Go to Set-up/Stretch image to fit image to window, if necessary. Double click on reference location near one corner of graph and enter known values of x1 and y1. Lock and click OK. Repeat for second reference location x2, y2 in diagonally opposite corner of graph. Go to Trace/Manual. Click on each point to digitize. Copy file of data points from the Data tab and paste into spread sheet.

Author Index

- Abramowitz, M., 50, 105
Adamson, A. W., 106
Aklonis, J. J., 105, 110, 128, 164, 302
Alfrey, T., 6
Anderson, E. W., 245
Andrews, R. D., 157, 164
Anthony, R. L., 211
Aoki, Y., 234
Bagley, E. B., 50
Baschnagel, J. 105
Beatty, C. L., 147, 164
Belcher, H. V., 136
Bianchi, U., 211
Binder, K., 105
Blatz, P. J., 184, 212, 302
Blythe, A. R., 245
Boo, K., 113, 239
Boob, S., 233
Bovey, F., 245
Boyer, R. F., 163
Breuer, H., 234
Brittain, J. O., 234
Bueche, F., 6, 70, 75, 93, 105, 136, 198, 212, 229
Burlet, H., 105
Carlson, D. W., 211
Catsiff, E., 128, 302
Chasset, R., 93, 105, 155, 163-164, 277
Christensen, R. M., 6
Christianson, D.D., 50
Ciferri, A., 199, 212
Cirlin, E. H., 185
Clarke, D. R., 245
Clarson, S. J., 303
Cole, K. S., 50, 230-231, 244
Cole, R. H., 50, 230-231, 244
Curro, J.G., 92, 105, 164
Daniel, V. V., 244
De Gennes, P. G., 93-94, 105
Debye, P., 212, 220-221, 224, 226-229, 244
DeMallie, R. B., 81, 105
Des Cloizeau, J., 97, 106
Desper, C.R., 50
DeWames, R. E., 105
DiMarzio, E. A., 139-142, 147, 149-150, 159, 163
Dogson, K., 303
Doolittle, A. K., 121, 123, 127-128, 134
Doolittle, D. B., 121, 123, 127-128, 134
Dougherty, T. S., 212
Duffrène, L., 105
Ehrenfest, P., 137, 163
Eirich, F. R., 6
Farris, R. S., 50
Ferry, J. D., 6, 35, 50, 68, 81, 83-88, 92, 105, 119, 122, 128, 153, 164, 302
Flory, P. J., 149-150, 162, 211-212, 244, 294
Flannery, B. P., 105
Frederick, J. E., 105
Frölich, H., 227, 229, 244

- Gebhard, H. M., 185
 Gee, G., 211
 Gibbs, J. H., 137-142, 147, 149-150, 159,
 162-163, 168, 294
 Gold, O., 212
 Goldman, S., 50
 Goodier, J. N., 6
 Gordon, G. V. 50, 118, 128, 212
 Gordon, M., 136-137, 148, 164, 295
 Green, M. S., 211
 Greene, A., 199, 212
 Griswold, P. D., 11, 50
 Gross, B., 68, 105
 Guth, E., 195, 211-212
 Guttman, C. M., 142
 Gy, H., 105
 Hadzioannou, G., 164
 Hall, W. F., 105
 Hamming, R. W., 50
 Hanson, E. E., 157, 164
 Hartmann, H., 161, 302
 Hedvig, P., 245
 Heijboer, J., 153-154, 164, 236
 Hermans, J. J., 211
 Hewitt, F. G., 211
 Hild, G., 164
 Hill, N. E., 244
 Hong, S. D., 302
 Hopkins, I. L., 50
 Hutchinson, J. M., 164
 Illers, K., 234
 Indictor, N., 211
 Inoue, Y., 50
 Ishida, Y., 234
 Kip, A. D., 217
 Kremer, F., 161, 302
 Jackson, J. L., 167, 211
 James, H. M., 211
 Johnson, G. E., 231, 245
 Johnson, J. F., 163
 Karasz, F. E., 147, 164
 Karolewski, M., 303
 Kauzmann, W., 138-139, 163
 Kip, A. D., 217
 Kirkwood, J. G., 227, 229, 294
 Kohlrausch, F., 91, 105
 Kopatake, Y., 50
 Kovacs, A. J., 130, 143, 164, 277, 302
 Kremer, F., 161, 302
 Krieger, I. M., 195, 212
 Kuhn, W., 211-212
 Kwei, T. K., 242
 Lacabanne, C., 234, 245
 Landel, R. F., 6, 83- 88, 105, 119, 128
 Larson, R.G., 95, 105
 Lavergne, C., 234, 245
 Leal, L.G., 95, 105
 Levitt, M. H., 245
 Likhtman, A.E., 95, 105
 Link, G. Z., 245
 Litt, M., 110, 128, 302
 Lutz, P., 164
 MacKnight, W. J., 164
 Malvern, L., 50
 Marau, P., 245
 Mark, H. F., 6, 50, 211
 Marvin, R. S., 136
 Matsuoka, S., 136, 234
 Maxwell, B., 136
 Maxwell, J. C., 52-64, 66, 76-78, 83, 86,
 91, 102-104, 168, 183, 215, 227, 244, 258,
 262-263, 266-267, 269-270, 279
 McBrierty, V. J., 245
 McCall, D. W., 245
 McCrum, N. G., 6, 147, 153, 164, 236-7,
 244
 McKenna, G. B., 133, 164
 McKinley, G. H., 95, 105
 McKinney, J. E., 136
 McLeish, T. C. B., 95, 105
 McQuarrie, D. A., 167, 211
 Mercier, J. P., 110, 126, 128, 302
 Middleman, S., 6
 Mooney, M., 189-190, 193-197, 199, 208-
 210, 212, 294
 Mopsik, F., 245
 Mullins, L., 191, 194-198, 209, 212
 Nielsen, L. E., 6, 132, 152
 Nishi, T., 242
 Okun, K., 92, 105
 Onsager, L., 226, 229, 244
 Ouijada-Garrido, I. 241
 Packer, K. J., 245
 Pascal, B., 8
 Peticolas, W. L., 69, 105
 Peyser, P., 164, 303
 Pezzin, G., 164, 303
 Pignes, R., 105
 Pincus, P., 92, 105, 164
 Pipkin, A. C., 6

- Plazek, D. J., 116, 128
Plumb, R. C., 125
Porter, R. S., 50, 163
Press, W. H., 105
Price, C., 211
Provencher, S. W., 105
Raleigh, Lord, 212
Ramos, A. R., 164
Randall, J. C., 163
Read, B. E., 6, 147, 153, 164, 237, 244
Rehner, J., 212
Rempp, P., 164
Rivlin, R. S., 189-190, 193-194, 196-197,
199, 208, 210, 212, 290
Rose, J., 158
Rouse, P. E., 69-70, 77, 79-81, 83, 86-93,
97, 99, 104-105, 229, 269, 299
Sanmartin, R., 164, 303
Schatzki, T. F., 153, 164
Schmidt-Rohr, K. 245
Schmieder, K., 113, 128
Schwarzl, F. R., 6, 50
Semlyen, S., 303
Shaw, M. T., 50, 118, 128, 212, 239, 302
Shen, M., 105, 167, 184-185, 211-212, 302
Shishkin, N., 136
Sillars, R. W., 227, 244
Simha, R., 163, 212
Sims, D., 136
Sittel, K., 79-80, 105
Smallwood, H. M., 195, 212
Smith, K. J., 199, 212
Smith, T. G. 136
Smith, T. L. 122, 124, 128
Smyth, C. P., 244
Soong, D., 302
Spiess, H., 241, 245
Sridhar, T., 95, 105
Stegun, I. A., 50, 105
Stern, J., 211
Stockmayer, W. H., 212
Straupe, C., 164
Strazielle, C., 164
Suresh, S., 245
Takahashi, Y., 156
Taylor, J. S., 136-137, 148, 164, 295
Teukolsky, S. A., 105
Thirion, P., 93, 105, 155, 163-164, 278
Timoshenko, S., 6
Tobin, N. R., 195-196, 212
Tobolsky, A. V., 6, 50, 68, 88, 91, 105,
110, 122, 128, 156-157, 164, 211, 302
Tolman, R. C., 200
Treloar, L. R. G., 6, 182, 211-212
Tschoegl, N. W., 6, 50, 105
Van der Hoff, B. M. E., 212
Vetterling, W. T., 105
Volkenstein (Vol'kenshtein), M. V., 212
Wall, F. T., 211-212
Ward, I. M., 6, 245
Wilhelm, M., 241
Williams, G., 6, 91, 104, 146-147, 153,
164, 237, 244
Williams, M. L., 83-88, 105, 119, 128
Wilson, G. J., 136
Wolf, K., 113, 128
Wolgardt, M., 105
Wood, L. A., 141, 147, 163
Zilio-Grandi, F., 164, 303
Zimm, B. H., 70, 80-81, 93, 105, 212, 293,
298

Subject Index

- Activation energy, 271
for crankshaft and Heijboer mechanisms, 153
for viscoelastic relaxation, 125
- Admittance, 290
- Affine deformation, 174, 178
- Arrhenius
equation, 127, 154
plot, 125
- Atactic polymer, 112, 139, 149
- Bead-and-spring model, 71, 76, 82, 83, 102
- Block copolymer
elasticity of, 173
- Boltzmann
constant, 95, 181
relationship, 175, 207, 223
superposition principle, 27, 30, 32, 35, 37, 48, 255, 257, 270
- Bond angle
in polyethylene, 204
restriction in chain, 200
restrictions in chain, 204, 206
- Borel's theorem, 36, 37
- Box-and-wedge distribution, 68
- Broadline NMR, 240
- Brownian motion
and chain conformation, 206
and relaxation, 173, 236
in elastomers, 173, 200
of dipoles, 223
- Calorimetry
- as method for measuring T_g , 130
- Capacitance/Capacitor
in analog for dielectric relaxation, 243, 244
in complex impedance spectroscopy, 233, 290
in dielectric bridge, 232
in Maxwell-Wagner-Sillars effect, 227
role in analog for dielectric relaxation, 214
- Chain
force produced by stretching, 207
in flexible-chain models, 89
polarization of, 229
side chain rotation, 236
- Chain conformation, 173, 210
- Chains
and chemical stress relaxation, 158
and Gibbs-DiMarzio theory, 139
as Hookean entropy springs, 70
dipole moment of, 229
entanglements between, 192
equivalent random, 200, 210
extension of, 173, 175, 178, 183, 207
Gaussian, 88, 93, 210
ideal, 200
in elastomer network, 92
in flexible-chain models, 78, 79
in reptation model, 93
in semicrystalline polymers, 114
influence of chain ends on network, 191

- influence of chain ends on relaxation, 155
- influence of side groups on T_g , 159
- interchain interaction, 186
- length of, 202, 206, 210
- motions in main chain, 151
- network, 208
- segmental relaxation, 108, 111, 125
- statistics of, 199, 203
- stiffness of, 147
- vs. rings, 142
- Charge**
 - additivity in parallel circuit, 287
 - analog to strain, 215
 - and interfacial polarization, 227
 - and polarization, 213
 - density, 217
 - in a capacitor, 214
 - motion in TSC/TSD, 234
 - separation in dipole, 220
- Chasset-Thirion equation**, 155, 163, 278
- Chemical stress relaxation**, 156, 157, 158, 163
- Cis** and **trans** geometrical isomers, 148
- Clapeyron equation**, 141
- Clausius-Mosotti equation**, 221
- Cole-Cole plot**, 230
- Complex dielectric constant**
 - and Clausius-Mosotti equation, 225
 - and Maxwell-Wagner-Sillars dispersion, 228
 - as analog to complex compliance, 220
 - behavior through T_g , 133
 - relationship to polarization, 219
- Computer problems**, 49, 104, 126, 127, 159, 209
- Cone and plate geometry**, 43
- Configurational entropy**, 174
- Conformational entropy**
 - and chain stretching, 174, 183, 187, 208
 - and Gibbs-DiMarzio theory, 139
- Continuum mechanics**
 - of rubber elasticity, 187
 - of three-dimensional bodies, 9
- Copolymer**
 - relaxations in, 131
 - secondary relaxation phenomena, 153
- T_g according to Gordon-Taylor equation, 148
- T_g of random, 141
- treatment with Gibbs-DiMarzio theory, 147
- Correlation map**
 - for secondary relaxations, 237
- Couette geometry**, 44
- CP-MAS NMR**, 238, 243
- Crankshaft motion**, 153
- Creep compliance**
 - change at T_g , 131
 - definition, 20
 - of bead-spring model, 102
 - of Maxwell element, 55
 - of Voigt element, 60
 - of Voigt-Kelvin model, 266
 - relationship to stress relaxation, 32
 - time dependence, 30
- Creep experiment**, 20, 22, 27, 55, 59, 216, 248
- Critical molecular weight**
 - for entanglement, 85
 - for viscosity, 97
- Crosslink/Crosslinking**
 - affine motion of, 174, 179
 - and chemical stress relaxation, 158, 163
 - and phantom-chain approximation, 178
 - and rubbery state, 92
 - and swelling of networks, 192
 - and trapping of network imperfections, 192
 - basis for elastomers, 165
 - crystallites as crosslinks, 111, 198
 - degree of crosslinking, 190
 - influence on chemical stress relaxation, 279
 - influence on modulus-temperature curve, 108
 - influence on physical relaxation, 34, 93, 154
 - influence on T_g , 150, 163
 - mechanical analog, 63
 - schematic representation, 173
- Crystallization**, 183
- Cure kinetics of a thermoset**, 159
- Dashpot element**
 - in mechanical model, 51, 56, 59, 60
 - resistance as electrical analog, 214
- Debye**
 - dielectric dispersion, 220, 244
 - equations, 226

- modification of Clausius-Mosotti equation, 221, 224
- Density**
 - as concentration variable in bulk material, 77
 - charge, 217
 - correction in time-temperature superposition, 117
 - effect on T_g , 149
 - mass, 82
 - number, of chains, 87
 - of crosslinks, 150, 155, 163, 279
 - probability, 66, 175
 - strain energy, 187
- Deviatoric stress**, 12
- Dielectric constant**
 - behavior near T_g , 133
 - complex. *See* Complex dielectric constant
 - definition, 213
 - molecular interpretation, 220
 - relationship to permittivity, 215
 - temperature dependence, 214
 - time/frequency dependence, 216, 218, 221, 223, 227
- Diffusion**
 - as fundamental relaxation process, 108
 - via reptation, 91
- Dilatometric method for measuring T_g** , 6, 119, 129, 138
- Diluent**
 - influence on viscoelastic properties, 114, 135, 149
 - See also* Plasticizer, 114
- Dirac delta function**, 48, 254
- Distribution of/Distribution function for charge**, 220
- dielectric dispersion, empirical, 231
- end-to-end distance, 80, 203
- number of conformations, 175, 177, 203
- relaxation/retardation times, 66, 81, 86
- Doolittle equation for viscosity**, 121, 127
- Double reptation**, 97, 104
- Dynamic mechanical behavior through T_g** , 163
- Cole-Cole plot, 231
- material functions, 26, 33, 35, 47, 67, 83, 116, 258
- material functions, conversion to transient, 49
- measurements, 23, 39, 57, 107, 131, 151, 157, 158, 234, 235, 253
- measurements, fixtures for, 43
- Elastomer**
 - and Mullins effect, 198
 - change of T_g on stretching, 162
 - continuum-mechanical description for, 187
 - energy lost in, 92
 - equation of state, 178
 - ideal, 183, 190, 208, 211
 - influence of filler, 195
 - Mooney-Rivlin equation, 209
 - network properties, 165
 - relaxation behavior, 5
 - relaxation, chemical, 156
 - relaxation, physical, 92, 154
 - swelling of, 192, 208
 - thermodynamic properties, 167
 - thermoelastic properties, 185
 - WLF constants for, 119
- Electric circuits**
 - as analogs for dielectric behavior, 214
 - distributed, 235
 - equivalent, for complex impedance, 233
 - lumped, 235
 - RC, 215, 216, 219, 244
 - resonance, 231
- End-to-end distance, 71, 78, 88, 125, 177, 186, 192, 200, 203, 211
- Entanglement**
 - role in relaxation, 111
- Entanglements**
 - and critical molecular weight, 86
 - and reptation, 93
 - in networks, 158, 192
 - role in relaxation, 84, 109, 125
- Entropy**
 - and Kauzmann paradox, 139
 - and rubber elasticity, 166, 168, 172
 - role in Gibbs-DiMarizio theory, 139
 - role in glass transition of mixtures, 160
- Entropy spring. *See* Hookean entropy spring**
- Equation of state**
 - for chain, 200, 206
 - for elastomer, 180, 186, 208
 - for swollen elastomer, 193
- Equilibrium modulus, 93, 155

- Equivalent random chain, 200, 205, 210
- Expansion
 - binomial, 181
 - coefficient of, 6, 121, 130, 134, 150, 162, 171
 - series (log), 285
 - Taylor, 188
- Extra stress, 12
- Filler
 - and Mullins effect, 209, 282
 - crystallites as, 113
 - influence on elastomer properties, 195
- First-order reaction, 156, 163
- First-order relaxation of polarization, 220
- First-order transition
 - definition, 137
 - pressure dependence via Clapeyron equation, 141
- Fixtures for mechanical tests, 20, 44
- Flex energy, 141, 162
- Flexural mechanical test, 44
- Flow region
 - and KWW expression, 92
 - and reptation, 91
 - and Rouse theory, 83
 - effect of diluent, 114
 - effect of molecular weight, 69, 110
- Fourier transform, 34, 231
- Fox equation, 161
- Fox-Flory equation, 149, 162
- Free volume
 - and glass transition, 111, 121, 134, 144
 - influence of chain ends on, 149, 159
 - influence of free surface on, 160
 - influence of plasticizer on, 149
 - of activation for bond rotation, 153
 - of diluent, 135
- Freely orienting chain, 201, 203, 206
- Front factor, 178, 282
- Gaussian chain, 174, 207, 210, 211, 287
- Gaussian distribution function, 80, 175, 203, 205
- Gaussian free energy function, 188
- Gibbs free energy, 137, 168
- Gibbs-DiMarzio theory, 139, 147, 159
- Glass transition
 - and change of coefficient of expansion, 6
 - and modulus change, 5, 109
 - and segment rotation, 108
 - and segmental motion, 109
 - as a rate-dependent process, 130, 132
 - behavior of viscoelastic properties, 131
 - breadth, influence of plasticizer, 113
 - free volume theory for, 135
 - free-volume theory for, 111, 121
 - Gibbs-DiMarzio theory for, 142
 - influence of structure, 145
 - kinetic theory for, 142
 - phenomena of, 129
 - segmental motion in, 125
 - Smith empiricism for, 124
 - theories of, 133
- Glass transition temperature
 - and free volume, 121
 - as reference for time-temperature shifts, 119
- influence of crosslinking on, 150
- influence of diluent, 159
- influence of molecular weight, 111
- influence of plasticizers, 114
- influence of pressure, 135
- isoviscous state, 133
- measurement using dielectric methods, 236
- molecular weight influence, 142
- of compatible polymer blends, 160
- of polyethylene, 112
- of sucrose, 143
- of various polymers, 145
- Glassy modulus, 108, 111
- Glassy state
 - heat capacity in, 160
 - nonequilibrium aspects, 139
 - partial modulus of chains in, 88
 - relaxations in, 129, 151
 - spin relaxation in, 242
 - stretched exponential relaxation in, 91
- Gordon-Taylor equation, 137, 148
- Guth-Smallwood equation, 195
- Heijboer mechanism, 153
- Helmholtz free energy, 170, 175, 180, 187, 206
- Hooke's law, 14, 18, 52, 60, 208
- Hookean behavior, 18, 52, 172, 183
- Hookean elastic solid, 18, 52
- Hookean spring, 51, 52, 55, 70
- Inflection temperature
 - influence of plasticizers, 161

- of modulus-temperature curve, 114
- Intermolecular energy
 - due to hydrogen bonding, 149
 - in elastomers, 172
 - in Gibbs-DiMarzio theory, 140, 149, 150
 - influence on T_g , 147
- Intramolecular energy
 - in Gibbs-DiMarzio theory, 140
- Isoviscous state, 133
- Junction in networks. *See* Crosslinks
- Kauzmann paradox, 138
- Kinetic theory
 - of rubber elasticity, 76, 208
 - of the glass transition, 138, 142, 160
- Kirkwood-Frölich equation, 227, 229
- Laplace transform, 35, 250, 256
- Leibnitz's rule, 254, 262, 283
- L'Hopital's rule, 141
- Linear polymers
 - compared to cyclic, 142
 - glass transition temperature, 147
 - viscoelastic response, 61, 70, 91, 108, 152
- Linear regression, 210
- Linear viscoelastic response, 270
 - and Boltzmann superposition principle, 32
 - experiments to measure, 44
 - $G(t)$ as core material property, 35
 - mechanical analogs for, 51
- Loss compliance, 57, 131
- Loss modulus, 26, 131
- Loss tangent, 26, 133, 236
- Macroscopic polarization, 221
- Master curves for time-temperature
 - superposition
 - basic premise, 120
 - preparation, 117, 123
 - relationship to modulus-temperature curves, 124
- Material-generated stress, 14
- Maxwell model, 53, 56, 61, 83, 102, 258
 - generalized, 61, 76, 86, 270
 - vs. KWW model, 91
- Maxwell's relations, 168
- Maxwell-Wagner-Sillars (MWS) effect, 227
- Maxwell-Wiechert model, 64
- Mean square end-to-end distance, 71, 78, 177, 192, 200, 203, 205
- Melting point, 112, 113, 162
- Modulus. *See also* modulus-temperature curve
 - according to reptation theory, 96
 - complex, 27
 - conversion of dynamic to transient, 34
 - definition, 1, 7
 - dynamic, 23
 - equilibrium in elastomers, 93
 - instantaneous, 76
 - isochronal, 104
 - measurement of, 19, 39
 - partial values in distribution, 66
 - partial, from Rouse theory, 90
 - partial, from Zimm theory, 80
 - relationship to compliance, 33, 35
 - relaxation, 21, 47
 - relaxation for PIB, 68
 - ten-second, 107, 110
 - tensile vs. shear, 13
 - Young's, 39, 43, 52
- Neo-Hookean solid, 189
- Nernst-Einstein equation, 95
- Network
 - affine deformation of, 178
 - and two-network hypothesis, 157
 - chemical stress relaxation of, 154, 156, 278
 - conformational entropy, 175
 - conformations of, 174, 175, 186
 - crosslink density, 93
 - crosslink vs. main-chain scission, 158, 163
 - crystallization on stretching, 198
 - effect of fillers, 195
 - effect of temperature, 109
 - elastic force, 183
 - elastic properties of, 173
 - entanglement, 111, 125
 - entanglements in, 192
 - entropy of, 186
 - exchange reactions in, 158
 - formation by chemical crosslinking, 173
 - formation during cure of thermoset, 158
 - Helmholtz free energy of, 176
 - imperfections in, 93, 191, 192
 - modulus of, 116, 191
 - phantom chains in, 178
 - relaxation of, 92, 154

- treatment of relaxation in linear polymers, 91
- Network chains**
 - and Gibbs-DiMarzio theory, 150
 - behavior at high strains, 183
 - chemical scission, 155
 - crystallization of, 198
 - definition, 174
 - end-to-end distance, 177
 - exchange reactions of, 158
 - finite extensibility, 199
 - formation of new, 157
 - isolated, 178
 - molar density, 181
 - molecular weight of, 191
 - motions, 92
 - number density, 180
 - number density of, 156, 163, 192
 - number of conformations, 174
 - restrictions due to entanglements, 192
- Newton's law of viscosity, 48, 52, 54
- Nomenclature, standard, 2**
- Nominal stress, 181, 184, 194, 210
- Nonlinear regression, 190
- Nuclear magnetic resonance (NMR)
 - and detection of molecular motion, 213, 237
 - and sub- T_g relaxations, 151
 - broadline technique, 240
 - change in line width at T_g , 133
 - CP-MAS, 238
 - Larmor frequency, 238
 - line width through T_g , 235
 - relaxation map, 237
 - spin-spin and spin-lattice relaxation processes, 242
 - time scale of, 238
- Ohm's law, 214
- Onsager equation, 226, 229
- Ordering parameter, 144, 160
- Out-of-phase component, 26, 33, 47, 48, 237, 250
- Permanent dipole moment
 - alignment in electric field, 221
 - definition, 220
- Phantom chain approximation, 93, 178
- Plasticizer
 - effect on glass transition, 113, 135, 149, 161
 - effect on NMR line width, 240
 - phase separation of, 114
- Plateau region. *See* Rubbery plateau
- Poisson's ratio, 18, 43
- Polarization**
 - and dielectric constant, 213
 - and internal field, 222
 - in TSC method, 234
 - interfacial, 227
 - molecular origin, 220
 - of nuclear spins, 238
 - physical origin, 217
 - time dependence, 218
- Pressure**
 - and permanent set, 158
 - application to elastomer to control volume, 179
 - developed by elastic chain, 211
 - effect on a glass, 144
 - effect on bond rotation, 153
 - effect on second-order transition temperature, 141
 - effect on T_g , 135, 136, 162
 - in a balloon, 17
 - in a deformed sample, 11
 - influence on free volume, 135
- Pressure-volume work, 167
- Primary transition. *See* glass transition**
- Principal stresses, 16**
- Pure shear, 208, 281
- Radial distribution function, 203, 206, 210
- Random flight problem, 202
- Reference temperature**
 - effect on shift factor, 119
 - effect on WLF constants, 124, 126, 134
 - for time-temperature superposition, 117
- Regions of viscoelastic behavior, 107
- Relative permittivity, 215
- Relaxation time**
 - and breadth of NMR absorption peak, 240
 - and friction factor, 84
 - Chasset-Thirion equation, 155
 - dielectric, Debye and Onsager treatments, 229
 - distribution in glass transition region, 89
 - distribution of, 66
 - distribution of, box-wedge model, 68

- Ferry, Landel and Williams
 modification of Rouse theory, 86
 for Maxwell model, 54, 104
 for molecular rotation, 226
 generalized Maxwell model, 76
 KWW equation, 104
 KWW modification of Rouse theory,
 92
 multiple, 66
 Rouse model, 69
 spin-spin, 240
 tube models, 94
 Zimm model, 80
- Reptation model, 92, 93
 and Chasset-Thirion equation, 155
 constraint release, 97
 path retracement, 92
- Resistance as analog element in model
 for dielectric response, 215, 233
- Retardation time
 distribution of, 66
 for bead-spring model, 102
 in glassy state, 144, 160
- Root mean square length. *See* Mean square end-to-end distance
- Rouse matrix, 99
- Rouse mode, 77
- Rouse theory, 69, 79, 81, 104, 229
 applied to KWW equation, 92
- Rubber elasticity. *See also* Elastomer
 and degree of crosslinking, 191
 and degree of crosslinking, 178
 effect of crystallization on, 199
 energy contribution, 185
 equation of state, 182
 filler effects, 195
 Gaussian theory, 183
 phenomenological treatment, 187
 statistical treatment, 174
 stress softening of, 198
 swollen networks, 192, 208
 thermodynamic treatment, 166
- Rubber plateau, 69, 83, 109, 111, 161
- Secondary relaxation, 151, 235
- Second-order transition, 124
 and Clapeyron equation, 141
 applicability to glass transition, 138
 definition, 137
 Gibbs-DiMarzio theory, 139
- Segmental friction factor, 72, 78, 82, 84
- Shear modulus
 and rubber elasticity, 181
 complex, 27
 definition, 9
 dynamic, 26
 from Rouse theory, 77
 in rubber elasticity, 157, 191
 measurement of, 43
 relationship to relaxation modulus, 34
 relationship to tensile modulus, 13
 strain dependent, 49
 temperature dependence, 110, 116
- Shear strain
 and rubbery elasticity, 211
 definition, 9
 in creep experiment, 20
 in parallel-plate geometry, 49
 in three dimensions, 14
- Shear viscosity, 53, 78, 82, 104, 120
 relationship to relaxation modulus, 120
- Shift factor
 for secondary relaxations, 154
 temperature dependence according to
 Arrhenius equation, 154
 temperature dependence according to
 WLF equation, 119, 127
 time-temperature superposition, 118
- Side chain/group
 influence on dielectric response, 236
 influence on T_g , 147, 159
 source of secondary relaxations, 153
- Simple shear
 and shear viscosity, 53
 definition, 9, 11
 of elastomer, 182, 211
- Sinusoidal deformation
 and dynamic properties, 23, 34
 applied to generalized Maxwell
 model, 102
 applied to Maxwell model, 102
 complex variable notation, 64
 definition, 25
- Sinusoidal stress, 47, 57
 application to Voigt model, 61
 as analog to sinusoidal voltage, 220
- Spring. *See* Hookean spring
- Spring and dashpot, 53, 59
- Statistical theory of rubber elasticity. *See*
 Rubber elasticity, statistical
 treatment

- Steady flow viscosity. *See* shear viscosity
- Steric isomerism
role in chain stiffness and T_g , 148
- Stirling's approximation, 284
- Stirling's approximation, 210
- Storage modulus. *See* Complex modulus
- Strain. *See* Shear strain and Tensile strain
- Strain history
and Boltzmann superposition principle, 29, 31, 47, 249
and Mullins effect, 197
- Strain invariants, 188, 193
- Strain-induced crystallization, 158, 169, 195, 197, 198
- Stress
definition, 8
extra and deviatoric, 12
in balloon, 17
material, 11
relationship to pressure, 12
sign of, 16
tensile, 8
total, 13
uniaxial. *See* Tensile stress
units for, 8
- Stress relaxation
and time-temperature superposition, 115, 116
chemical, 156
definition, 20, 21
experiment, 22, 39, 56
for measuring high viscosity, 133
master curve, 68, 84
modulus, 32, *See* Stress relaxation modulus
molecular interpretation of, 124
of bead-spring model, 76
of generalized Maxwell model, 62
of Maxwell body, 55
of network, 155, 166
of polycarbonate, 126
of polyisobutylene, 68
of Voigt element, 60
recovery after, 109, 257
slope in glass transition region, 89, 103
- Stress relaxation modulus. *See also* Modulus, relaxation
and distribution of relaxation times, 66
- behavior in the glass transition, 130
conversion to modulus-temperature curve, 126
definition, 22
during chemical stress relaxation, 157
of generalized Maxwell model, 62
of polyisobutylene, 68
predicted by Rouse model, 82
relation to creep compliance, 32, 37, 49
relation to dynamic modulus, 33
relationship to creep compliance, 47
ten-second, 107
- Stress softening (Mullins effect), 198
- Stress-strain relation
and work, 206
at constant velocity, 49
at various temperatures, 184
for elastomers in shear, 211
for elastomers in tension, 182
from phenomenological theory of rubber elasticity, 188
isochronal, 104
relation to stress-relaxation modulus, 48
- Submolecule (subunit), 70, 76, 78, 82, 87, 90
- Sulfur, T_g of, 146
- Sulfur-sulfur bonds, 158
- Superposition
Boltzmann, 27, *See also* Boltzmann superposition principle
time-temperature, 114
- Syndiotactic polymer, 149, 174, 236
- Temperature
influence on viscoelastic properties, 3
- Tensile properties. *See also* extensional properties
and Young's modulus, 39
compliance, 20
dynamic, 57
measurement of, 39
modulus, 8, 13, 15, 53, 76, 77, 116, 209
modulus, equilibrium, 181
of a Maxwell body, 54
of a Mooney elastic material, 190
of a neo-Hookean solid, 189
of a Voigt body, 59
of elastomers, 166
of filled elastomers, 197

- of swollen elastomers, 193
- relationship to shear properties, 15
- sensitivity to environment, 156
- viscosity, 53
- Tensile strain
 - definition, 8
 - geometries for, 20
 - in elastomers, 181
 - in three dimensions, 15
 - instantaneous, 107
 - rate, 48, 53
- Tensile stress
 - and creep experiment, 20
 - definition, 15
 - in bending, 40
 - in three dimensions, 8
 - influence on T_g , 159
 - nomenclature convention, 54
 - nominal, 182
 - relationship to shear modulus, 15, 157
 - relaxation, 22, 48, 115
 - sign convention, 16
- Thermal expansion, 21, *See also* expansion, coefficient of
- Thermally stimulated current (TSC), 233
- Thermodynamic activity, 114
- Thermodynamic identities
 - Maxwell equations, 183
- Thermodynamic measurements, 130
- Thermodynamic theory
 - for single chain, 206
 - of elastomers, 165
 - of glass transition, 137
 - see also* Second-order transition, 141
- Thermodynamic transition
 - first-order. *See* First-order transition
 - second-order. *See* Second-order transition
- Thermoelastic inversion phenomenon, 168
- Time-temperature superposition. *See also* Vogel equation and WLF equation
 - master curves, 115, 116
 - shift factor, 118, *See also* Shift factor
- Torsional flow, 248, 260
- Torsional pendulum, 131
- Transform. *See* LaPlace and Fourier transforms
- Transform methods, 35, 231
- Transition region. *See* Glass transition
- True stress vs. nominal stress, 181
- Two-network theory, 157
- Uniaxial stress. *See* Tensile stress
- van der Waals bond energy, 140
- Viscosity. *See* Tensile properties, viscosity, *See* Shear properties, viscosity, *See* Newton's law of viscosity
 - application in three dimensions, 52
 - at T_g , 120
 - definition, 48
- Viscous dissipation of energy, 27
- Vogel equation, 124, 127, 275
- Vogel temperature, 124
- Voigt element, 59
 - analogy with RC circuit, 216
 - in Voigt-Kelvin model, 64
 - summary of properties, 61, 102
- Voigt-Kelvin model, 64
- Volume dilation, 167, 179
- Volume relaxation
 - near T_g , 138
- Water
 - and Maxwell-Wagner-Sillars effect, 227
 - as plasticizer, 149
 - dielectric constant, 215
- WLF equation
 - and Doolittle equation, 121
 - and iso-free-volume theory, 134
 - and second-order transition
 - temperature, 140
 - finding parameters from data, 127
 - for describing temperature shift, 119
 - relationship to Vogel equation, 127
 - use below T_g , 123
 - vs. Arrhenius equation, 154
- WLF parameters, 119
- Wood's equation, 141, 147
- Young's modulus, 2, 39, 43, 49, 262
- Young's modulus, 52
- Zimm theory, 80